



**THE DEVELOPMENT OF NOVEL
ELECTROCHEMICALLY DEPOSITED
POLYMERS FOR SENSING APPLICATIONS**

Submitted by

Zuzana Vobecká

A thesis submitted in fulfilment of the requirements for the degree of Doctor of
Philosophy in Department of Pure and Applied Chemistry, University of Strathclyde

2013

This thesis is the result of the author's original research. It has been composed by the author and has not been previously submitted for examination which has led to the award of a degree.

The copyright of this thesis belongs to the author under the terms of the United Kingdom Copyright Acts as qualified by University of Strathclyde Regulation 3.50. Due acknowledgement must always be made of the use of any material contained in, or derived from, this thesis.

Signed:

Date:

Acknowledgement

I would like to thank Prof. Peter Skabara for giving me the opportunity to be part of his group and complete my Ph.D. at the University of Strathclyde. I would also like to thank my former supervisor Prof. Ivan Stibor for his help, support and advice throughout my whole University studies and the great opportunities he has provided me with. My big thanks also belong to Prof. Deepak Uttamchandani and Dr. Robert Blue from the Electronic and Engineering Department for their help, advice, support and cooperation throughout the whole project.

I would like to thank to the post-doctorate researchers from PJS group, Dr. Neil Findlay, Dr. Filipe Vilela and Dr. Alexander Kanibolotsky for their advice and supervision throughout my studies, and also all current and former members of the group for the friendly, supportive and fun environment in the laboratory. Certainly, all the help from the technical staff within the Department should not be forgotten and I am thankful for all the useful advice I have been given, namely Denise Gilmour for Elemental analysis, Pat Keating for Mass Spectroscopy and Lindsay McCulloch for TGA measurements. Also, thanks to Dr. Ashleigh Fletcher from the Chemical Engineering Department who was responsible for assistance with the BET measurements.

However, my biggest thanks belong to my closest friends and family. A PhD can sometimes be very stressful and frustrating and I only managed to overcome these difficult moments because I received huge support and understanding. Without you I would not be where I am right now. Thank you very much!

Děkuji mami, tati a Kájo.

Eskerrik asko Clara.

Thaan vaadh Sandie.

Obligada Filipe.

Merci Jules.

Abstract

The development of sensors capable of detecting explosives is an important task needed to protect citizens and infrastructure. The success of such sensors requires progress in materials chemistry and transducer technology to deliver compact, low-cost, stand-alone devices that can be widely deployed. Interdigitated electrodes (IDEs) are viewed as a ubiquitous and low-cost platform for delivering this type of sensor technology. IDEs can be transformed into chemical sensors by depositing or growing sensing materials whose material properties are modified in the presence of the target chemicals. Organic semiconductors offer unique characteristics such as tunability of electronic properties *via* chemical synthesis, compatibility with mechanically flexible substrates, low-cost manufacturing, and tailoring to attain specific chemical and biological functionalities. The concept of combining such functional organic semiconductor films with IDEs presents a technically and economically viable route to sensors having low power consumption, high sensitivity and selectivity to target molecules, reversibility and finally affordability.

Chapter 1 summarizes an overview of polymeric sensors, state of the art of explosive detection and current progress in porous polymeric materials.

Chapter 2 describes the chemical synthesis of novel monomers based on ProDOT (1,3-propylenedioxythiophene) and bisalkylsulfanyl-terthiophenes. These polymers are halogen-functionalised to be selectively sensitive towards nitro-containing compounds related to explosives such as TNT or DNT, based on the halogen-nitro association. The key feature in this work is the localised electropolymerisation of the synthesised monomers directly onto the device; an inexpensive and fast fabrication method.

The development of a suitable testing system, sensor fabrication and its performance are described in Chapter 3. These sensors have been tested under controlled conditions for their sensitivity to vapours of nitro-bearing compounds, and also a range of other volatile chemicals commonly found in the atmosphere. Vapours

of 1-nitropropane, nitrobenzene and 2-nitrotoluene were used in sensor testing as proxies for nitro vapours, which are also present in explosives.

Chapter 4 summarizes the synthesis of new materials, which will provide cross-linked polymers with high porosity and enhanced surface area, thus enhancing the sensitivity and response speed of the previously electrochemically polymerised thin films. The large surface area over volume of such porous films is expected to greatly increase the sensitivity and significantly reduce response times of the sensors.

Symbols and Abbreviations

<i>A</i>	absorbance
Å	angstrom
<i>a,b,c</i>	Antoine coefficients
AC	alternating current
Bu	butyl
BCMA	bis(chloromethyl)anthracene
BCMBP	bis(chloromethyl)biphenyl
BDDT	Brunauer, Deming, Deming and Teller
BET	Brunauer-Teller-Emmet
<i>c</i>	speed of light (constant)/ concentration
<i>C</i>	capacitance
°C	degrees centigrade
CMOS	complementary metal-oxide semiconductor
COF	covalent organic frameworks
CP	conjugated polymers
CPP	conjugated porous polymers
CV	cyclic voltammetry
CVD	chemical vapor deposition
<i>d</i>	doublet
DC	direct current
DCM	dichloromethane
DCX	dichloroxylene
DIBAH	diisobutylaluminium hydride
DMF	dimethylformamide
DMNB	2,3-dimethyl-2,3-dinitrobutane
DNT	dinitrotoluene
DSC	differential scanning calorimetry
<i>e</i>	charge of an electron (constant)
<i>E</i>	potential
<i>E</i> [°]	standard electrode potential
<i>E_a</i>	acceptor band
<i>E_d</i>	donor band

E_g	band gap
EDOT	3,4-ethylenedioxythiophene
eq	equivalents
Et	ethyl
EtOAc	ethyl acetate
eV	electronvolt
F	Faraday constant
fF	femtoFarad
Fc / Fc ⁺	ferrocene / ferrocenium
fF	femtoFarrad
g	gram
GC	gas chromatography
h	Planck's constant
h	hours
ΔH	heat of adsorption
HCP	hypercrosslinked polymer
HDME	hanging drop mercury electrode
HOMO	highest occupied molecular orbital
Hz	hertz
I	current / intensity of light
IDE	interdigitated electrode
IMS	ion-mobility spectroscopy
IR	infrared
iR	internal resistance
ITO	indium tin oxide
J	coupling constant
K	Kelvin
LB	Langmuir-Blodgett
LBL	layer-by-layer
LEDs	light emitting diodes
LIBS	laser induced breakdown spectroscopy
LUMO	lowest unoccupied molecular orbital
M	molar (mol/liter)

MALDI-TOF	matrix-assisted laser desorption/ionisation – time of flight
Me	methyl
MeCN	acetonitrile
MEMS	microelectromechanical system
MHz	megahertz
mL	milliliter
mM	milimolar
mmol	millimole
mmHg	millimeters of Mercury
mol	mole
M.p.	melting point
MS	mass spectrometry
n	non-bonding orbital
<i>n</i>	number of moles
NB	nitrobenzene
n-BuLi	n-buthyllithium
NBS	<i>N</i> -bromosuccinimid
n-doped	negatively doped
NIS	<i>N</i> -iodosuccinimid
nm	nanometre
NMR	nuclear magnetic resonance
NT	nitrotoluene
OFET	organic field effect transistor
OLED	organic light emitting diode
Ox	oxidation
<i>p</i>	<i>para</i> - / pressure
Pa	Pascal
PA	polyacetylenes
PAF	porous aromatic framework
PANI	polyaniline
p-doped	positively doped
PES	polyethersulphone
pF	picoFarad

PF	polyfluorene
PEDOT	poly(3,4-ethylenedioxythiophene)
PIM	polymers of intrinsic microporosity
PMMA	poly(methyl methacrylate)
ppm	parts per million
PPP	poly- <i>para</i> -phenylene
ppth	parts per thousand
PPV	poly- <i>para</i> -phenylene-vinylene
PPY	polypyrrole
ProDOT	3,4-propylenedioxythiophene
PSS	polystyrenesulfonic acid
PT	polythiophenes
PVC	polyvinyl chloride
Q	charge
R	gas constant
R_f	retardation factor
Red	reduction
RT	room temperature
s	second/singlet
SAW	surface acoustic wave
SCE	saturated calomel electrode
SHE	standard hydrogen electrode
SPR	surface plasmon resonance
T	transmittance / temperature
TBAPF ₆	tetrabutyl ammonium fluoride
t-Buli	tert-buthyllithium
TFA	trifluoroacetic acid
TGA	thermogravimetric analysis
THF	tetrahydrofuran
TLC	thin layer chromatography
TMS	trimethylsilyl
TNT	trinitrotoluene
UV	ultraviolet

V	volt
V	volume
V_m	monolayer capacity
vis	visible
vs.	versus
VOC	volatile organic compound
VTC	vinylene trithiocarbonate
<i>Greek</i>	
α	vapour pick-up efficiency
π	pi bonding orbital
π^*	pi anti-bonding orbital
δ	chemical shift
ε	molar extinction coefficient / permittivity
λ	wavelength
σ	sigma bonding orbital
σ^*	sigma anti bonding orbital

Contents:

1 INTRODUCTION	1
1.1 ORGANIC SEMICONDUCTORS	2
1.1.1 Band Theory	3
1.1.2 Conjugated polymers	6
1.2 ANALYTICAL METHODS USED	7
1.2.1 Cyclic voltammetry	7
1.2.2 Electropolymerisation of thiophene derivatives	10
1.2.2.1 Effect of reaction conditions	12
1.2.3 UV-vis absorption	13
1.2.4 Calculation of energy levels and band gap	16
1.3 CHEMICAL SENSORS	17
1.3.1 Polymeric sensors	20
1.3.1.1 Challenges in polymer sensing technology	21
1.3.1.2 Types of polymeric sensor devices	22
1.3.1.3 Deposition techniques of polymer films	25
1.4 INTRODUCTION TO CAPACITORS	26
1.4.1 Chemicapacitive sensors	29
1.4.2 Polymer-coated interdigitated electrodes as chemicapacitors	29
1.4.3 Polymer deposition via electropolymerisation	31
1.5 EXPLOSIVES DETECTION	32
1.5.1 Classification of explosives	32
1.5.2 Detection of explosives	34
1.5.3 Commercially available explosive detectors	35
1.5.4 The development of explosive sensors	36
1.6 POROUS POLYMERS	38
1.6.1 Preparation of porous polymers	40
1.6.2 Organic nanoporous materials	42
1.6.3 BET surface area determination	49
1.6.3.1 Adsorption of gases	49
1.6.3.2 The adsorption isotherms	50
1.6.3.3 BET Instrumentation	54
1.7 AIM OF THE PROJECT	55
2 ELECTROPOLYMERISED HOMOPOLYMERS FOR EXPLOSIVE DETECTION	56
2.1 PRODOT DERIVATIVES	57
2.1.1 Synthesis of ProDOT derivatives	60
2.1.2 Electrochemistry of ProDOT derivatives	63

2.2	<i>BISALKYLSULFANYL-TERTHIOPHENES</i>	70
2.2.1	<i>Synthesis of Bisalkylsulfanyl -terthiophenes</i>	71
2.2.2	<i>Electrochemistry of Bisalkylsulfanyl -terthiophenes</i>	72
2.3	<i>CONCLUSION</i>	77
3	<i>SENSOR FABRICATION AND EVALUATION</i>	79
3.1	<i>SENSORS FABRICATION</i>	80
3.2	<i>PRELIMINARY SENSOR TESTING – STATIC CHAMBER</i>	85
3.3	<i>SENSORS EVALUATION - DYNAMIC SYSTEM</i>	90
3.4	<i>COMPARISON OF SYNTHESISED HOMOPOLYMERS IN SENSOR PERFORMANCE</i>	93
3.4.1	<i>ProDOTs comparison</i>	93
3.4.2	<i>Terthiophenes comparison</i>	98
3.4.3	<i>In-depth characterisation of poly(ProDOT-Br) as a sensor for nitroaromatics</i>	99
3.5	<i>CONCLUSIONS AND FURTHER WORK</i>	105
4	<i>CROSS-LINKED POLYMERS WITH ENHANCED SURFACE AREA</i>	107
4.1	<i>INTRODUCTION TO CROSS-LINKED POROUS POLYMERS</i>	108
4.2	<i>SYNTHESIS OF CROSS-LINKED POLYMERS</i>	109
4.2.1	<i>Polymers prepared via Stille coupling</i>	109
4.2.2	<i>Polymers prepared via Sonogashira-Hagihara cross-coupling</i>	112
4.2.3	<i>Tailoring the structure of porous polymers</i>	115
4.2.4	<i>Polymers prepared via oxidative polymerisation</i>	122
4.3	<i>ELECTROCHEMISTRY</i>	126
4.3.1	<i>Spirocore – EDOT</i>	126
4.3.2	<i>Tetrafunctional Spirocore – alkynyl EDOT</i>	132
4.3.3	<i>Trifunctional core–alkynylEDOT</i>	139
4.4	<i>BET SURFACE AREA MEASUREMENTS</i>	145
4.4.1	<i>Bulk powder polymers</i>	145
4.4.2	<i>Electropolymerised thin films</i>	147
4.5	<i>CONCLUSION</i>	150
5	<i>EXPERIMENTAL</i>	151
6	<i>APPENDIX</i>	195
7	<i>REFERENCES</i>	211

Chapter 1

1 INTRODUCTION

1.1 ORGANIC SEMICONDUCTORS

Organic semiconductors are materials either based on polymers or "small-molecule" structures with semiconducting properties, which offer exciting new possibilities for fundamental research and applications. They electrically conduct upon excitation caused by, for example, an applied voltage or solar/UV irradiation. Organic semiconductors have been used in many novel applications, for example in electronic devices such as organic light-emitting diodes (OLEDs),¹ organic solar cells,²⁻⁴ organic field-effect transistors (OFETs)⁵ and sensors.⁶

The properties of organic semiconductors are based on the properties of carbon-carbon double bonds, within which the carbon atom has a sp^2 hybridisation. The sp^2 -orbitals form a triangle within a plane while the p_z -orbitals are located perpendicular to this plane. A σ -bond between the two carbons can then be formed through an orbital overlap of two sp^2 -orbitals. The p_z -orbitals can then form the additional π -bond (Figure 1-1).⁷

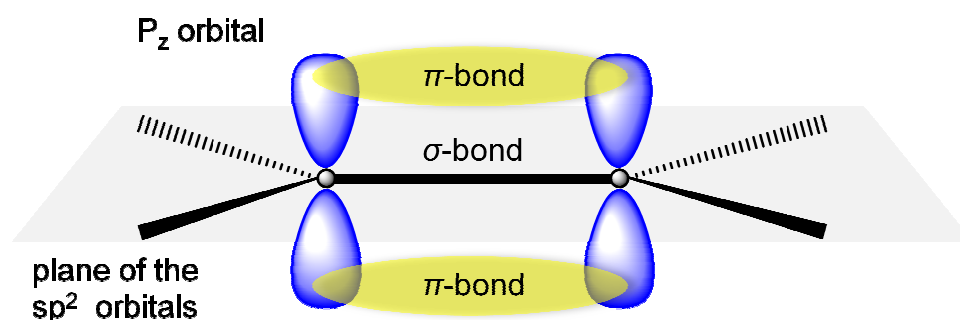


Figure 1-1: Depiction of the orbitals and bonds for two sp^2 -hybridised carbon atoms forming a double bond.

If a long chain of carbon atoms is formed and especially if the multiple and single bond alternate along the chain, the π -bonds become delocalised and form a one-dimensional conjugated electronic system.⁷ This extensive delocalisation of π -electron density within the framework provides organic conducting materials with remarkable abilities such as charge-carrier generation and transfer, light absorption and emission or electroluminescence.⁸⁻¹¹ π -Bonds have a much smaller energetic difference between the HOMO and LUMO (highest occupied molecular orbital and

lowest unoccupied molecular orbital, respectively), leading to strong absorption in or near the visible spectral range and to semiconducting properties.⁷

The ability to conduct lies in the ability of the material to transfer electrons or holes (positive charge created after electron ejection). The extent of conductivity depends on the energy level of the HOMO and LUMO, and on the gap and interaction between them. Organic semiconductors have great advantages over their inorganic counterparts. The ability to tune electronic properties *via* chemical synthesis, their solubility and processability alongside low-cost preparation make them ideal candidates for the fabrication of the next generation of electronic devices.¹²

1.1.1 Band Theory

Band theory describes the electronic structure of a material. There are three different bands; the filled, valence and conduction bands and, according to the energy level of these bands, materials can be classified as metals, semiconductors or insulators, which are depicted in Figure 1-2.^{13, 14} An additional type are superconductors - material that show no resistance at their critical temperature and therefore exhibit no energy loss.¹⁴

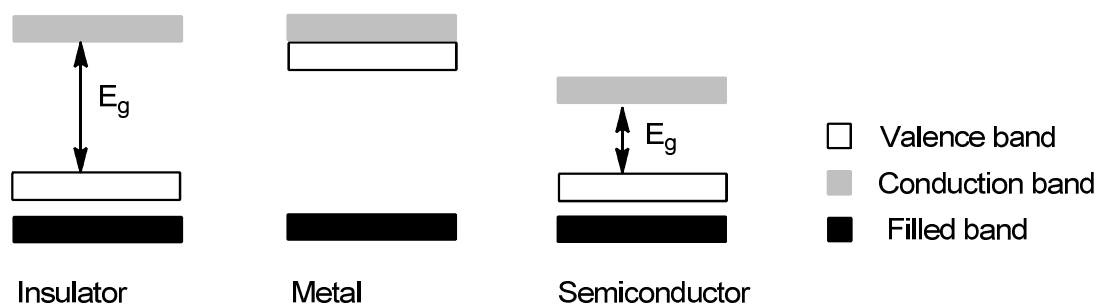


Figure 1-2: Band theory diagram.

The valence and conduction bands are derived from the HOMO and LUMO of the material, respectively. The energy gap between them is known as the band gap (E_g). If the electrons are able to overcome the energy gap between the valence and the conduction band, the material will conduct.^{7, 13-15} Electrical conductivity is

temperature dependent and, according to this dependence, the conductors can be divided into two main groups; (i) a metallic conductor in which the conductivity decreases with an increase in temperature and (ii) a semiconductor where conductivity is directly proportional to the temperature. In the case of an insulator, the band gap is too high and it does not conduct. In metals there is an overlap of the conduction and valence bands, this allows valence electrons to pass through the bulk material and thereby sustain electrical conductivity.⁷

In order to find practical application in an electronic device, an organic material must be accessible for reversible redox processes. When oxidation of a material occurs, an electron is removed from the HOMO, whilst an electron is injected into the LUMO when a material is reduced.¹⁶ These two processes can be observed by electrochemical experiments such as differential pulse voltammetry or cyclic voltammetry. The HOMO and LUMO orbitals can be determined from the energy level of the electrons in the working electrode (Figure 1-3). For oxidation, the increasing positive potential is applied to the working electrode. When the energy level of the electrons becomes lower than that of the HOMO level of the oxidising material, an efficient electron transfer can occur and the electrons from the material (A) will transfer to the electrode which results in an anodic current. In the case of reduction, a negative potential is applied until the electrons from the electrode will transfer to the material, resulting in a cathodic current.¹⁶

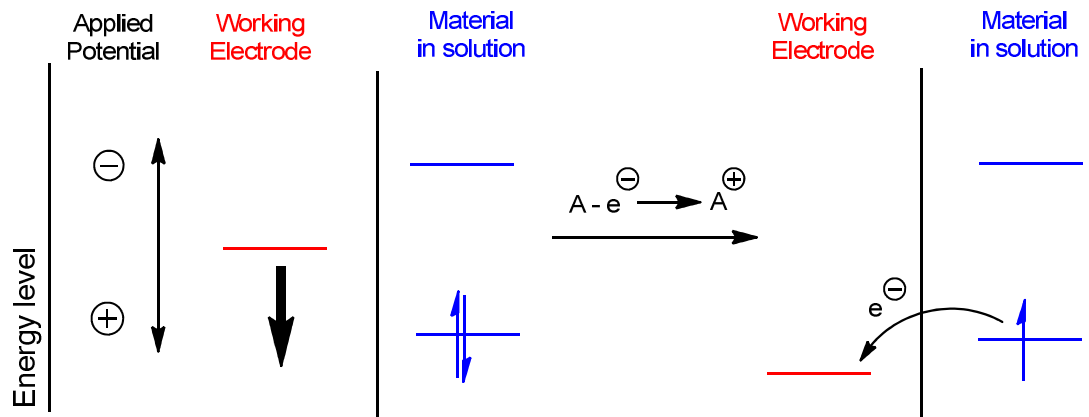
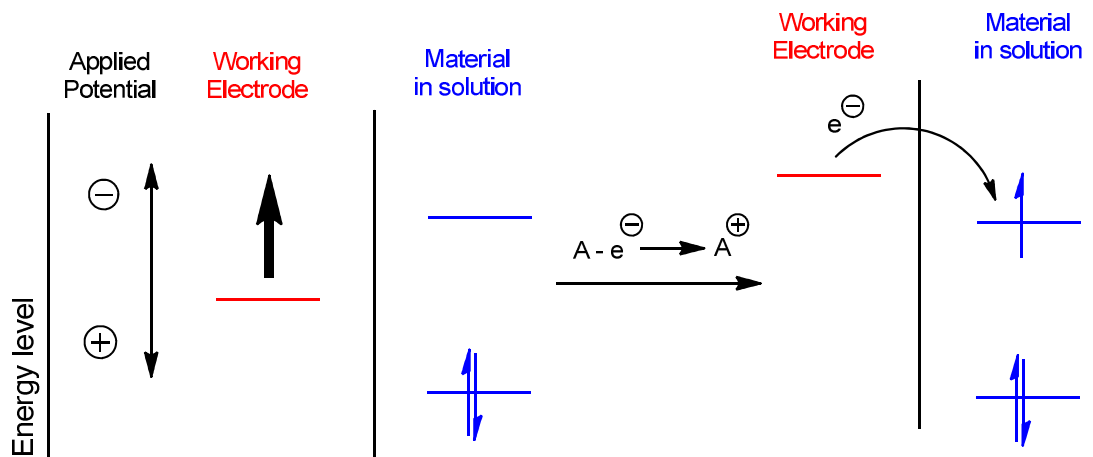
Oxidation:**Reduction:**

Figure 1-3: Illustration of oxidation and reduction in an electrochemical cell.

Semiconductivity depends on the number of charge carriers within the material and can be achieved by p- or n-doping. Doped semiconductors have an additional energy level that provides electron and hole transport and hence increases conductivity (Figure 1-4). In the case of p-doping, the material is oxidised, the electrons are removed, resulting in positive charges or holes in a newly created level just above the valence band, the so called acceptor band (E_a). Subsequently, a neighbouring electron can move into this newly created hole forming another hole in its place; every electron in the valence band can now move, providing a semiconductor with conductivity. n-Doping occurs when the material is reduced and

extra electrons are added to the donor band (E_d), which is formed just below the conduction band and provides a supply of mobile electrons.^{7, 13, 14, 16}

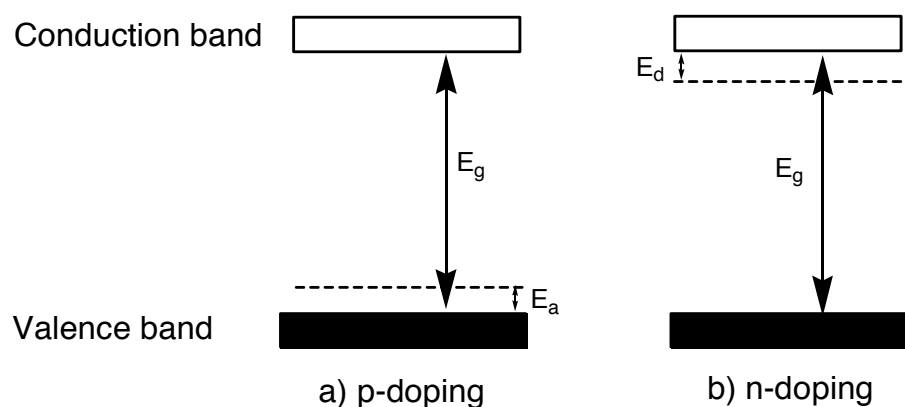


Figure 1-4: P- and n-doping.

1.1.2 Conjugated polymers

Besides small molecules with delocalised π -orbitals, conjugated polymers (CPs) present another large family of organic semiconductors. CPs have a conjugated double bond framework – the π -system extends throughout the whole polymeric chain. This means that the π -electrons are delocalised and form a conductive electronic system.^{7, 17, 18} Undoped polymers usually possess low conductivity, but this can be increased by up to several orders of magnitude by appropriate doping.^{17, 18} CPs have attracted much attention in recent decades and have been used in a range of applications. Amongst their many advantages the most attractive are: diversity in terms of chemical structure and physical behaviour, electronic properties that can be synthetically tailored according to the targeted application and ease of deposition as thin films.^{3, 4, 19, 20}

The most commonly used conjugated polymers are shown in Figure 1-5. These include linear backbone polymers such as polyacetylenes (PA), heterocyclic compounds such as polythiophenes (PT) and polypyrroles (PPy), and incorporation of the phenyl moiety, *e.g.*, poly-*para*-phenylenes (PPP), polyfluorenes (PF), poly-*para*-phenylene-vinylenes (PPV) and polyanilines (PANI).^{21, 22}

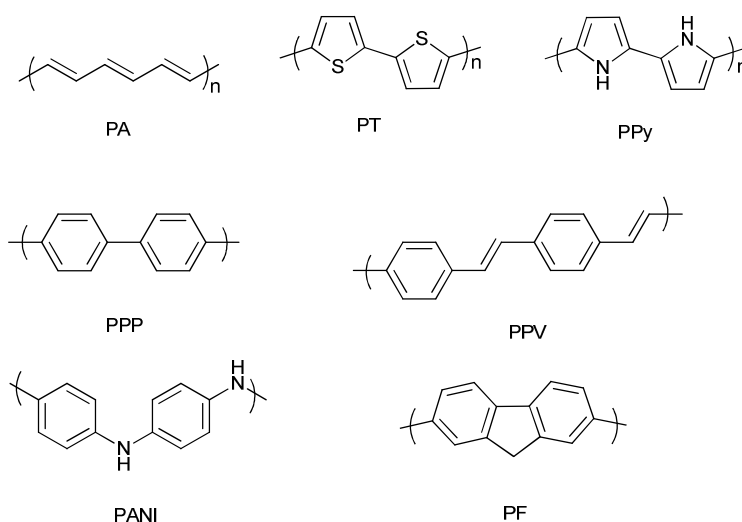


Figure 1-5: Common types of conjugated polymers.

1.2 ANALYTICAL METHODS USED

1.2.1 Cyclic voltammetry

Cyclic voltammetry (CV) is an electrochemical technique commonly used to measure the redox properties of materials, which can be carried out in solution or the solid state. Two different redox reactions can occur upon applying the potential to the material. Positive potential causes an oxidation and the analyte loses n electron(s). A negative potential causes a reduction and the analyte gains n electron(s).²³



The Nernst equation (1-1) describes the relationship between electrode potential and concentration for the above redox reactions,

$$E = E^0 + \frac{RT}{nF} \ln \frac{[Ox]}{[Red]} \quad (1-1)$$

where E° is the standard electrode potential, which is equal to the individual electrode potential in the standard state. R is the gas constant ($8.314 \text{ J mol}^{-1} \text{ K}^{-1}$), T is the temperature, F is the Faraday constant ($9.648\,534 \times 10^4 \text{ C mol}^{-1}$), n is the number of moles of electrons transferred in the cell reactions and $[Ox]$ and $[Red]$ are the concentration of the species in the oxidised and reduced state, respectively.^{13, 16, 23}

CV is the potential sweep technique commonly employed for examination of electronic properties of materials including its HOMO and LUMO levels. The technique uses a working electrode, counter electrode and a reference electrode; each electrode has a different purpose. The working electrode is the electrode where the redox processes are examined. The counter electrode, with an opposite polarity to the working electrode, acts as a supply of current required and ensures that current does not flow through the reference electrode. The current response is measured between the working and the counter electrodes and the applied potential is measured and controlled between the working and reference electrodes. The reference electrode should remain at a fixed potential during the experiment and should be independent of current density. Glassy carbon, platinum or gold are commonly used as working electrodes; alternatively ITO (indium tin oxide) coated glass slides can also be used.^{16, 23, 24} To examine a material in the solid state, it needs to be grown or cast directly onto the working electrode surface. Highly conducting metals such as platinum or silver wire are usually used as the counter electrode. Examples of reference electrodes are the Ag/AgCl electrode, hanging drop mercury electrode (HDME), standard hydrogen electrode (SHE) and the saturated calomel electrode (SCE).^{16, 24, 25} Pseudo reference electrodes are often used when one needs to avoid an aqueous solution, but has to be calibrated to a well known redox couple. A platinum or silver wire is usually used as a pseudo reference.

To allow a reliable comparison, the electrochemical results are referenced against a stable ferrocene/ferrocenium (Fc/Fc^+) redox couple as recommended by IUPAC (Figure 1-6), as it matches almost all of the required criteria:²⁵

- (i) the molecule is spherical and has a large radius (not fulfilled in the case of Fc/Fc^+);

- (ii) the charge carried by the ions is low;
- (iii) the equilibrium between the two redox states is reversible and fast;
- (iv) both the oxidised and reduced forms are soluble;
- (v) there is no geometry change of the molecule or ligands in the two redox forms;
- (vi) the redox potential is accessible in a wide range of solvents;
- (vii) both redox forms are stable.

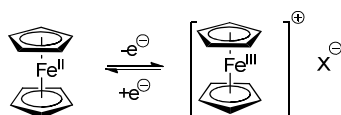


Figure 1-6: Ferrocene / ferrocenium redox couple ($X =$ counter anion).

The electrodes are connected to a potentiostat and suspended in a solution. To allow good conductivity throughout the solution and to reduce the resistance, a soluble electrolyte is added. Despite that, some internal resistance may remain due to insufficient conductivity between the electrodes. Thus, a potential drop between the applied voltage measured at the reference electrode and the observed voltage on the working electrode may occur and cause a serious error. This is usually corrected before each experiment by applying internal resistance (iR) compensation.^{26, 27}

Cyclic voltammetry is a sweep technique in which a potential is increased to a certain voltage and subsequently reversed back to the initial value whilst the current response is recorded. This results in a typical CV graph in which the output is in the form of a smooth wave in a current vs. potential plot (Figure 1-7).^{16, 24}

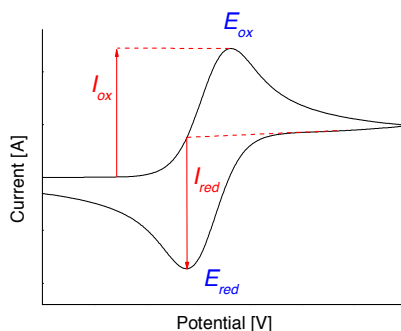


Figure 1-7: A typical CV graph of current vs. potential.

Curves in the positive direction represent the oxidation, whereas the reduction curves are those in the reverse direction. The change of the current response is a result of the electron transfer of the analysed material in the solution or on the electrode surface. In the case of oxidation, the current increases up to a current equal to I_{ox} , reached at voltage E_{ox} (the oxidation potential). Then the concentration of the material at the electrode surface diffuses back into the solution and the current again diminishes. In the case of a fully reversible redox process, a peak of opposite current but similar size and shape should be observed at the reduction potential (I_{red} , E_{red}). When the process is partially or completely irreversible, the reversed peak might have smaller current density and shifted potential peak.^{16,24}

1.2.2 Electropolymerisation of thiophene derivatives

Thiophene based polymers are usually electropolymerised by anodic oxidative polymerisation.²¹ This can be done *via* either a potentiostatic regime, which is essentially imposing a positive potential on the material for a certain amount of time or by cyclic voltammetry (CV). CV is perhaps most commonly used and is a straightforward technique to achieve electropolymerisation. The experiment set up is a three electrode system, which includes a working, reference and counter electrode. The potential is measured between the working and reference electrodes, which are placed close together in order to minimise the ohmic (iR) potential drop. The current response is measured between the working and counter electrodes. The resulting current is monitored as a function of applied potential to give the I - E curve, which is called a cyclic voltammogram. Electrodeposition of a substrate on the working electrode surface (anode if the polymer is grown by oxidation of the monomer), involves immersing a conducting substrate into a monomer solution, then sweeping the voltage at a fixed rate over the first oxidation wave of the monomer. The monomer is dissolved in a suitable solvent and a supporting electrolyte is added in order to achieve homogenous and sufficient conductivity throughout the solution.

The formation of a polymer chain is achieved through the combination of cation radicals created during the process of oxidation. The reaction proceeds with electrochemical stoichiometry, where the stoichiometric coefficient falls in the range

of 2.07-2.5 Faradays per mole. Reversible oxidation (or doping) of the polymers is caused by an excess of the charge, thus more than 2 electrons per molecule²⁸ (Figure 1-8).

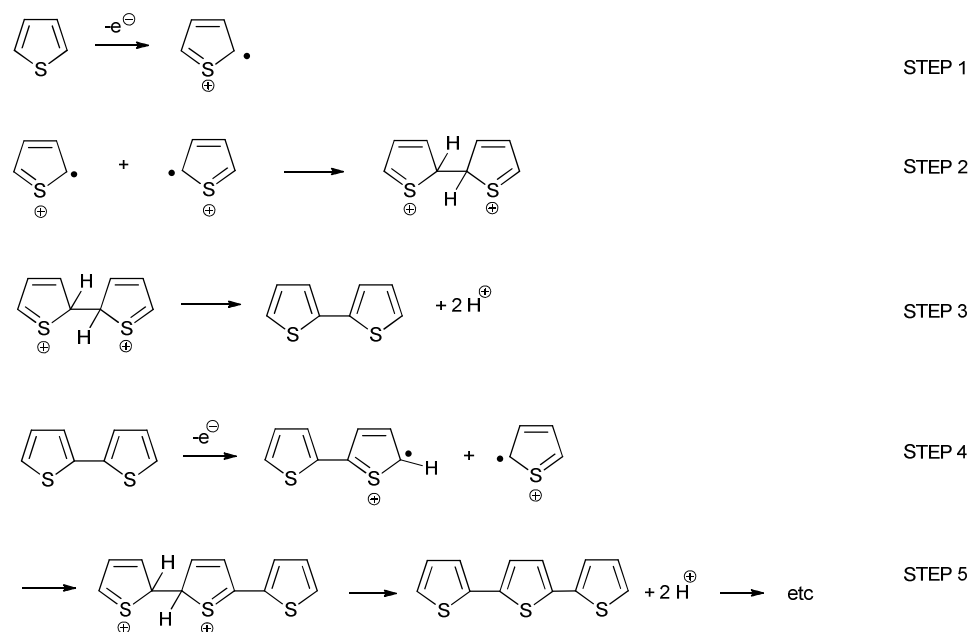


Figure 1-8: Mechanism of polythiophene chain growth *via* electrochemical oxidation.

In STEP 1, the thiophene loses an electron at the electrode surface as the voltage is applied and forms a radical cation. As the diffusion process of the radical cation back to the bulk solution is slower than the electron transfer, a high concentration of radical cations exists around the electrode surface. Therefore two radical cations can easily dimerise in STEP 2.^{21, 29} This dication dimer can subsequently rearomatise through the loss of two protons to form a neutral dimer (STEP 3), that has an oxidation potential lower than the monomer. In STEP 4, an oxidation of the dimer occurs and creates a new radical cation, which can combine with another radical cation (of the monomer) to give a trimer. STEP 5 involves another rearomatization and gives terthiophene. This process repeats many times until the polymer becomes insoluble and forms a film on the electrode surface.^{21, 29}

As the polymer grows, a new reversible peak with an increased current response emerges at a lower potential than that of the associated radical cation. At the same time the polymer formation will cause a bathochromic shift in the

absorption spectrum in comparison to the solid-state spectrum of the monomer. In both cases the shift in values is due to the increased conjugation length of the polymer.²⁹

In many cases when the polymer is grown, it exists in its doped state; p-doped in the case of oxidative polymerisation. Positive charges are trapped throughout the polythiophene chain and balanced with counter anions from the electrolyte. To reduce the polymer back to its neutral state, the film is immersed into monomer free solution and is subjected to cycling in a region where the polymer shows no electroactivity; this is termed the dedoping process (Figure 1-9).

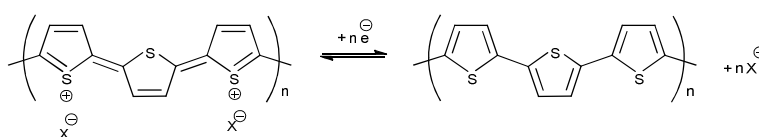


Figure 1-9: Dedoping process.

Due to the presence of radical cations and dications (polarons and bipolarons) in doped polymers, new bands occur in the UV-Vis spectrum, so these species can be easily identified.

1.2.2.1 Effect of reaction conditions

The structure and properties of the resulting polymers are largely influenced by the conditions applied during the electropolymerisation.³⁰ This can be a complex problem due to the fact that there are many experimental variables such as the solvent, concentration of reagents, temperature, cell geometry, nature and shape of the electrodes, and applied electrical conditions.²¹

The best choice for successful polymer growth are solvents that offer very good solubility of the monomer, but poor solubility of the polymer in order to avoid undesirable polymer diffusion away from the electrode surface. Also, the solvent should present good electrochemical resistance against decomposition at the potentials required to oxidise the thiophene ring (generally no more than +2.3 V) and have a high dielectric constant to ensure the ionic conductivity of the electrolytic

medium. The nature of the anion in the supporting electrolyte can also strongly affect the morphology and electrochemical properties of grown polymeric films.²¹

The temperature of electropolymerisation has been reported to affect the extent of the conjugated system and hence the optical and electrical properties of the polymer. The general trend is that polymerisations carried out at higher temperatures have a shorter chain length and less conjugation.³¹

The working electrode material is also an important factor since the physicochemical properties of its surface have a significant influence on the nature and strength of the polymer-surface bond. This affects the electropolymerisation process itself as well as the properties of the resulting polymer.²¹ For this project, the well-known sulfur-gold association³² was a major factor for choosing a gold interdigitated electrode sensor platform.

1.2.3 UV-vis absorption

A material can absorb the energy of ultra violet – visible light to excite π , lone and non-bonding electrons, or electrons involved in charge transfer reactions, to an energetically higher anti-bonding orbital. The lower the energy gap between the HOMO and LUMO, the easier it is to excite the electrons and such a transition corresponds to longer wavelengths of the absorbed light.^{33,34}

In a UV-vis spectrometer, a UV cuvette containing a dilute sample is placed into the path of a UV-vis light beam. Once the light passes through the sample the intensity is reduced as some of the light is absorbed. The intensity of light at each wavelength is measured before and after it passes through the sample, I_0 and I , respectively. The ratio of I/I_0 is called the transmittance T (equation (1-2)) and is usually expressed as a percentage. This value can be converted to absorbance A by equation (1-3).³³

$$T = \frac{I}{I_0} \times 100 [\%] \quad (1-2)$$

$$A = -\log(\%T) \quad (1-3)$$

Absorbance is directly proportional to the sample concentration c (mol L^{-1}), the beam path length l (cm) and the molar extinction coefficient ε ($\text{L mol}^{-1} \text{cm}^{-1}$) – this is the Lambert-Beer law (1-4). The Lambert-Beer law is applicable only for concentrations up to *ca.* $10^{-2} \text{ mol L}^{-1}$, thus for practical application the dilution of the sample should be low enough to give an absorbance of maximum one.^{33,35}

$$A = \varepsilon cl \quad (1-4)$$

Electronic absorbance spectra are commonly plotted as absorbance A vs. wavelength λ (Figure 1-10).

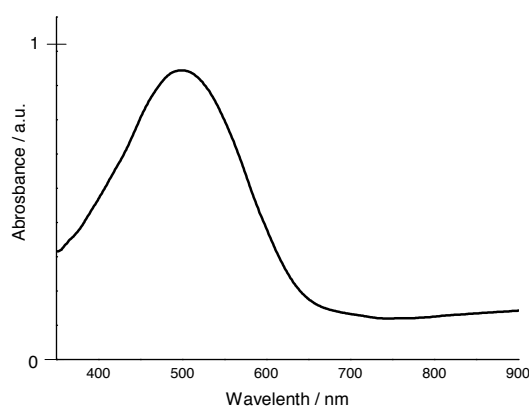


Figure 1-10: An example of UV-vis spectrum.

The internal molecular energy is the sum of the electronic, vibrational and rotational energies. There is a high energy difference between the ground and excited states of a molecule, while there is much smaller difference between neighbouring vibrational and rotational levels. The energy of photons is sufficient enough to excite a molecule to the next electronic energy level. UV-visible radiation can also excite the molecular vibrations and rotations, and so what is observed is the superposition of the electronic absorption in addition to the vibrational and rotational absorption spectra (Figure 1-11). Thus, absorption of photons very similar in energy occurs and this results in broad bands in the UV-vis spectra.³³

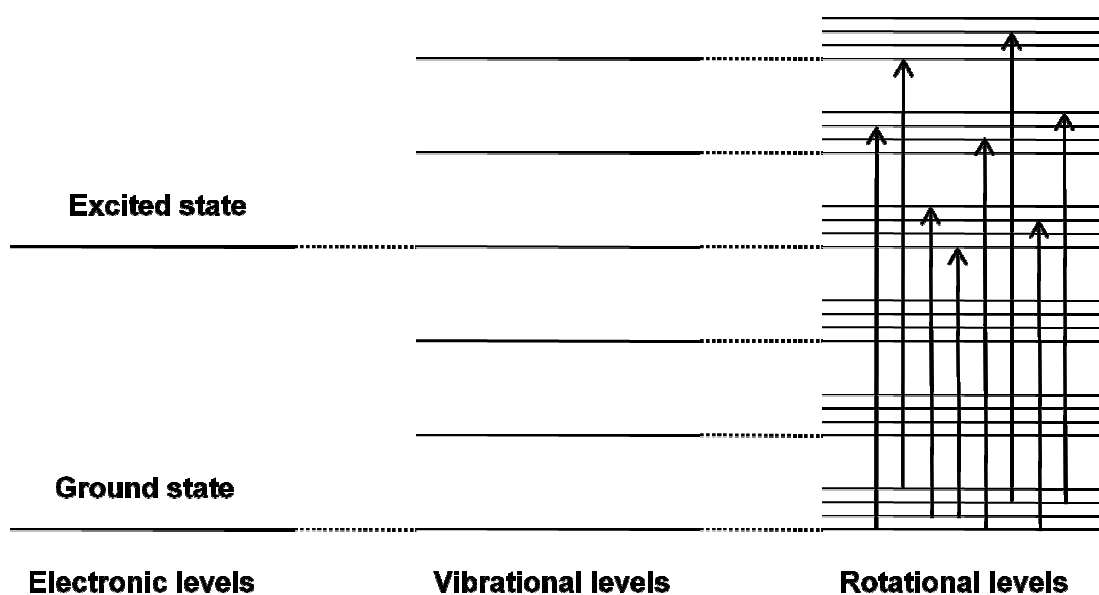


Figure 1-11: Scheme of electron transitions upon absorption of UV-vis light.

Each band in the UV spectra refers to a one-electron transition and is usually described by the maximum wavelength and maximum absorption/extinction coefficient, λ_{max} and ϵ_{max} , respectively. The wavelength is related to the energy of the absorbed light. There are four possible transitions involving σ , π and n-electrons (Figure 1-12).³³

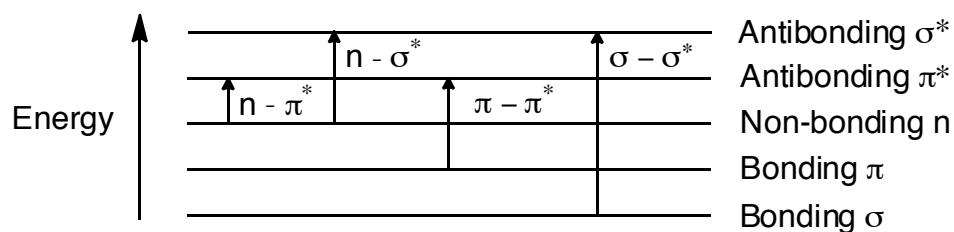


Figure 1-12: Four possible electron transitions.

The $\sigma \rightarrow \sigma^*$ absorption maxima are too low to be observed in UV-Vis spectrum; $n \rightarrow \sigma^*$ results from the lone pair of heteroatoms and usually occurs at 150 – 250 nm, thus is difficult to observe. Usually, $n \rightarrow \pi^*$ and $\pi \rightarrow \pi^*$ transitions are observed in the spectrum, because they occur in the 200-700 nm region. These

transitions occur in molecules containing unsaturated bonds that provide the π -electrons and are called chromophores.³³

Electrons from lone, non-bonding electron pairs on atoms attached *via* a multiple bond provide $n \rightarrow \pi^*$ transition (*e.g.*, a carbonyl group). Increasing the polarity of the substituent attached to the chromophore and increasing the polarity of the solvent will cause a higher solvation of the lone pair, thus decreasing the energy of the n -orbital. This results in a hypsochromic (blue) shift.³³ $\pi \rightarrow \pi^*$ transitions occur at the highest wavelength and the lowest energy, especially those with a high degree of conjugation causing extensive overlap of π -orbitals. This extended delocalisation causes a further reduction of the energy level gap and therefore the absorption maxima are observed at a higher wavelength.³³ Generally, the longer the conjugation in the molecule, the longer the wavelength of the absorption maxima and the smaller the band gap.³⁶ Besides conjugation length, substituent groups are another factor affecting the absorption maxima depending on their electron-donating or withdrawing abilities.³⁷

1.2.4 Calculation of energy levels and band gap

Both, UV and CV can be used as an experimental method to determine the HOMO-LUMO or band gap (E_g) of materials. The HOMO-LUMO gap is considered at the molecular level, whereas the term band gap is used in the case of polymers. Due to the extended π -delocalisation in conjugated systems, both techniques give broader spectra.^{35,36}

The electrochemical band gap is the difference between the onset of oxidation and reduction peaks in the CV. Subtraction of the onset of oxidation and reduction from the HOMO of ferrocene (-4.8 eV) gives the HOMO and LUMO levels of the material, respectively. Similarly the optical band gap can be determined from the UV spectrum as the onset of the longest wavelength absorption edge.^{16,24,36}

The relationship between E and λ is described by equation (1-5)

$$E = \frac{hc}{e\lambda} \quad (1-5)$$

where e is the charge of an electron (1.602×10^{-19} C), h is Planck's constant (6.63×10^{-34} m² kg s⁻¹) and c is the speed of light (3×10^8 m s⁻¹). Therefore, the band gap of a material can be simply estimated by dividing 1242 by the peak onset of the longest wavelength in the UV spectrum (equation 1-6).³³

$$E(\text{eV}) = \frac{1242}{\lambda(\text{nm})} \quad (1-6)$$

In most polymers the optical and electrochemical band gap are of similar values. However, the values can differ in more complicated systems. This may be caused because the redox peaks originate in localised sites within the conjugated backbone, thus representing a cross-section of the larger polymer structure.

1.3 CHEMICAL SENSORS

According to an Analytical division of IUPAC the definition of a chemical sensor is: “*a chemical sensor is a device that transforms chemical information, ranging from the concentration of a specific sample component to total composition analysis, into an analytically useful signal. The chemical information, mentioned above, may originate from a chemical reaction of the analyte or from a physical property of the system investigated.*”³⁸

The main purpose of a sensor is to reliably monitor our chemical, physical and biological environment. Depending on the particular function, sensors can provide information about toxic and explosive gases present in places of public gathering, content of pollutants in waters or soils created by industry or measure the chemical and physical properties of the surrounding environment (such as pH or humidity).³⁹ Current huge demand for environmental, medical and public safety monitoring, the broad possible applications of various detectors and high requirements on their performance has led to a fast developing research field of chemical and biological sensors. A chemical sensor consists of two main parts –

a physical transducer and a chemically selective layer - and gathers information on its environment.^{39, 40} On the contrary, a selective layer in a biological sensor is usually a biological material, such as an enzyme, bacteria or tissue.³⁹

Sensors can be classified according to various criteria, *e.g.*, according to the physical or chemical phenomena they detect, the method of measuring the response, the type of detected analyte or the size and mode of operation of the material in the receptor layer. It is possible to use various classifications as long as they are well and logically defined. IUPAC suggest a classification according to the operating principle of the transducer as shown in Table 1-1.³⁸

Table 1-1: Types of chemical sensors according to the operating principle of the transducer.

Transducer type	General Principle	Specific transducer	Properties measured
Optical	transformation of changes in optical phenomena	Absorbance (transparent medium)	absorptivity of the analyte or an interaction with sensing material
		Reflectance (non-transparent medium)	light reflected by a surface
		Luminescence	intensity of light emitted by an analyte-sensor-intereaction
		Fluorescence	emission effect caused by irradiation, turn on or off effect
		Refractive index	change in solution composition alters angle of passing light may include also a surface plasmon resonance (SPR)
		Optothermal effect	thermal effect caused by light absorption
		Light scattering	light scattering, caused by irregularities in sample shape and size particles

Table 1-1: Continued.

Transducer type	General Principle	Specific transducer	Properties measured
Electro-chemical	electrochemical interaction analyte – electrode	Voltametric & Amperometric	current is measured on chemically inert, active or modified electrodes.
	electrical stimulation or spontaneous interaction at the zero-current	Potentiometric	potential of the indicator electrode (ion-selective electrode, redox electrode, metal oxide electrode) measured against a reference electrode
		Field effect transistor	analyte-sensor interaction transformed into a change of the source-drain current
Electrical	change of electrical properties no electrochemical processes take place	Metal oxide semiconductor	reversible redox processes analyte gas components change conductivity
		Organic semiconductor	formation of charge transfer complexes modify the charge carrier density.
		Chemiresistor	electric conductivity change
		Chemicapacitor	electric permittivity change
Mass sensitive	accumulation of the analyte on a specific surface changes its mass – this is then transformed to a change in a property of the support material	Piezoelectric	voltage is applied to a oscillator adsorption the analyte at the oscillator causes frequency change
		Surface acoustic wave	change of the propagation speed of a generated acoustical wave
Magnetic	change of magnetic properties		
Thermometric	heat effects of a chemical reaction or adsorption of the analyte.		

The active layer of a sensor can be constructed from a variety of materials such as insulators, semiconductors, metals, solid electrolytes, catalytic materials, membranes or polymers. Silicon based field effect transistors have been developed, but usually suffer from low reproducibility, stability and selectivity.³⁹ Semiconducting metal oxide sensors such SnO₂, ZnO₂, TiO₂ and others⁴¹ are based on catalytic reactions of themselves. The reaction between the metal oxide and a gaseous analyte (most often environmental gases such as CO_x and NO_x) produce a change in the semiconductor conductance.³⁹ These types of sensors are robust, low-cost and benefit from relatively long lifetimes and high sensitivity. Ionic rather than electron mobility is the main principle of ionic electrolytes and membranes, where the ionic conductivity is maintained by one type of ion.³⁹ Solid electrolytes such as Y₂O₃, ZrO₂ or LaF₃ have been used for the detection of common gases O₂, NO₂, CO₂ or SO₂.^{39,42}

1.3.1 Polymeric sensors

Organic polymeric materials have several advantages over their inorganic analogues such as compatibility with mechanically flexible substrates, low-cost manufacturing and the possibility of tailoring their chemical and physical properties through modification of their chain structure. Research on the development of polymeric sensors has increased substantially over the last few decades. Most polymeric sensors are based on a change of the properties of the polymeric coatings which are detected and analysed. These changes originate in the interaction of functional groups incorporated within the polymer with the target analytes.^{39,43-47}

Polymers are used either as analytes in specific environments or as sensor arrays for multiple analytes. Each component in the sensor array can be coated by a polymer that shows a different response depending on the analyte. By collecting information from all the units and subsequently interpreting and evaluating the data, an unknown analyte can be identified.⁴⁷ Arrays of polymeric chemical sensors on a single microfabricated chip are known as “electronic noses” and can be combined with various transducer systems.⁴⁷⁻⁵⁰ These electronic noses are often combined with pattern recognition algorithms in order to translate the response from the individual

sensors to an overall sensor output.^{51, 52} The main drawback of these systems is a tendency to drift in the response magnitude after several uses and the need for frequent recalibration, and also the increased cost of the fabrication due to the necessary multiple polymer deposition of each separate material.⁴⁷

As described previously, depending on the doping level, polymers can be conductive or insulating. Both cases present suitable and highly desirable materials for sensing applications. Conductive polymers are usually used as the surface coating of various electrodes, since they conduct an electric charge that can vary upon a contact or reaction of the polymer with an analyte. Insulating polymers are used for adsorption or immobilisation of an analyte on their surface, which results in a physical change of the active layer that is subsequently detected.^{39, 53}

1.3.1.1 Challenges in polymer sensing technology

There are several important issues and requirements that should be addressed and carefully considered before designing a new sensor device, including:

- miniaturisation and portability of the devices, as well as minimum power consumption;
- fast response with low rates of false positives;
- enhanced sensitivity at low concentrations of the analyte;
- long life time and a high degree of reproducibility, without a need for frequent recalibration;
- the possibility for simultaneous separation and detection;
- improved recognition mechanisms that will result in reduced cross-sensitivity and therefore simplified software relating to the device.

Even though many efforts have been invested in addressing the above points, scientists have so far only succeeded in a few cases. The main drawback of these sensors is non-uniformity of the deposited polymers causing poor unit-to-unit reproducibility.⁴⁷ In addition, due to incomplete reversibility of the analyte-sensor interaction frequent recalibration is required.

Cross-sensitivity in particular remains a huge issue in polymeric gas sensors because it is a difficult task to design a material that has a specific reversible interaction with only one analyte. Transfer of a prototype sensor from a controlled laboratory environment to the real world complicates the detection capabilities.⁵⁴ A true sensing environment is a complex mixture of many possible interferents, such as industrial solvents, diesel fuel, gasoline, lighter fluid, bleach, cleaning products, insect repellent, perfumes, deodorants and other cosmetic products, paints, food and drink. However, humidity represents the most common chemical interferent with the highest concentration in the real environment. Removal of a water signal from almost all sensors remains the largest challenge for practical use, even if pattern recognition algorithms in arrays of sensors are utilised.⁵⁴

Nevertheless, whether each attempt fails or is successful, it provides a useful guide for further research. Therefore, the development of new sensing materials and transducer systems remains an important task in sensors research. The successful collaboration of polymer chemists and device engineers may accelerate the development of low-cost artificial sensors for human practical use.

1.3.1.2 Types of polymeric sensor devices

Polymers can be used in wide range of sensing devices, most commonly as pH, ions, gas, volatile organic compounds (VOCs) or water vapour sensors in combination with several different transduction schemes.

pH sensors: pH is an important characteristic in chemical reactions and one which needs to be reliably controlled. The most widely used polymer in pH sensors is polyaniline.^{39, 55} Several others have also been used in pH sensing in a variety of forms and transducer systems, *e.g.*, polypyrrole,⁵⁶ polystyrene⁵⁷ and polythiophene.⁵⁸

Ion sensors: Cations and anions play a fundamental role in biological and chemical processes therefore ionsensors have a wide range of applications. The function of polymers in ionic sensors is mainly as the conductive component or as a matrix for the conductive system. After the ion-sensor interaction or exchange, a change in electronic signal is detected, often on the ion selective electrode (ISE). The

ISE is the most commonly used device for ion sensing and consists of a composition of typical ion-selective membranes including a polymer (entrapping the sensing ions), a plasticizer, an ion carrier and ionic additives.³⁹ The most common material used in these membranes is polyvinyl chloride (PVC).⁵⁹ However, other cationic sensors are based on polymethacrylate,⁶⁰ polyaniline, polypyrrole and other conducting polymers.⁶¹

Humidity sensors: Humidity sensors are useful for monitoring food processing, textile manufacturing, storage areas, computer rooms, hospitals, museums and other environments that require a consistently low water content. The control of humidity therefore becomes an important task. The polymers used as humidity sensors include polyelectrolytes containing electrolytic group (salts, acids, and bases). Conjugated conducting polymers such as polyaniline or poly(*p*-diethynylbenzene), where the released proton from the water molecule can react with conjugated C=C double bonds, were also reported.⁶² Commonly, chemiresistors and chemicapacitors are typical sensing mechanisms in polymeric humidity sensors. PEDOT has been incorporated in a resistive type of sensor,⁶³ whereas, poly(methyl methacrylate) (PMMA) or polyethersulphone (PES) have been used in capacitive sensors.⁶²

Gas sensors: Gas sensors present an affordable and suitable solution to problems with pollutants in the environment and the overall health and safety of citizens. Gaseous pollutants such as NO_x, CO_x, SO_x, HCl, NH₃ and toxic gases from industry represent a huge environmental concern. Therefore, research investigating polymeric gas sensors is a growing field. Sensors based on tetraphenylporphyrin–polymer composite films detecting sub-ppm levels of HCl were previously reported.⁶⁴ Mizutani *et al.* prepared an amperometric sensor for dissolved oxygen using a polydimethylsiloxane (PDMS) membrane.⁶⁵ An electrochemical sensor for SO₂ was developed by Shi *et al.*,⁶⁶ NO₂ sensors based on changing conductivity of polystyrene⁶⁷ and other polymers⁶⁸ were developed. CO₂ sensors were constructed from a variety of polymers and working principles.⁶⁹

Conducting conjugated polymers (CPs), such as polyacetylene, polypyrrole (PPy), polyaniline (PANI), polythiophene (PT) and their derivatives have been widely used as the active layers of gas sensors.^{39, 53} Sensors fabricated from these polymers offer low power consumption, fast response (depending on analyte concentration) and good reversibility of the adsorption/desorption process. Additionally, they can perform at ambient temperature.³⁹ The intrinsic conductivity of these materials is rather low and can be increased by doping. Doping can be achieved *via* chemical or electrochemical oxidation and reversed by reduction.⁵³ The sensing capability of conducting polymers lies in the electrical and/or optical property changes when they are doped upon the sensor-analyte interaction.^{39, 53} It was reported that nucleophilic gases (*e.g.*, NH₃, vapours of MeOH and EtOH) change the conductivity of CPs in the positive direction, whereas electrophilic gases (NO_x, SO₂) have the opposite effect.^{39, 70} The effect of changing conductivity due to the doping of polyacetylene upon exposure to iodine vapour has been known for over 30 years and was used to construct iodine sensitive sensors.⁷¹

VOC sensors: Materials which are gases under standard conditions are more difficult to detect due to a lower absorption into polymers, whereas volatile liquids such as industrial solvents, fuels,⁷² chemical warfare agents^{46, 73} or toxic industrial waste liquids are the most common analytes.⁴⁶ VOC sensors are widely used in industry to monitor possible VOC leaks, but are also useful in civil and military defence to detect chemical warfare agents and explosives.⁴⁷ The absorption of a VOC into a polymer depends on the chemical properties of the VOC and polymer, their interaction character and strength and on the VOC concentration. In general, these types of sensors are based on changing the chemical, physical or structural properties of the polymer when a VOC is absorbed and various different transducer systems can be used.^{39, 47} For example, researchers have used polymeric sensors with resistive sensors,⁴⁵ micro-cantilever based sensors,⁷⁴ surface acoustic wave (SAW) devices,⁷⁵ capacitive sensors,⁴⁷ surface plasmon resonance (SPR) sensors⁷⁶ or various sensors based on an optical output.⁴⁴

1.3.1.3 *Deposition techniques of polymer films*

In order to transform a polymer into the active layer of a sensor, it needs to be selectively deposited onto the surface of the device, often in the form of a thin film. To do this, with various types of sensor structure, several different methods have been developed.

Dip-coating: Immersing a suitable substrate into a solution of the polymer will result in the formation of a thin layer on the substrate surface. The substrate is then removed from the solution at a constant rate. The rate and the time of contact determine the thickness of the coated layer. Once the substrate is withdrawn, excess liquid will drain from the surface and, after evaporation of the solvent, a thin layer of polymer is created.^{77,78}

Spin-coating: Spin-coating produces a thin film on the surface of flat substrates. The polymer is dissolved in a volatile solvent and placed on the substrate, which is then rotated at high speed in order to spread the fluid by centrifugal force. The fluid spins off the edges of the substrate and the solvent is evaporated. The final film thickness and properties will depend on the nature of the polymer and solvent, principally the viscosity and concentration, as well as the parameters chosen for the spin process such as rotation speed and acceleration.⁷⁹

Langmuir-Blodgett (LB) technique: Thin films of polymer and surfactant are produced by the LB method. The solid substrate is vertically immersed then removed from a liquid containing the coating material. The liquid is compressed at constant pressures towards the substrate. This results in adsorption of a vertically assembled monolayer of known size onto a surface. Repetition of this process results in multilayer adsorption and thickness control of the resulting film.^{80,81}

Layer-by-layer (LBL) self-assembly technique: In a way, LBL is similar to the LB and dip-coating techniques. The substrate is alternatively immersed into two solutions of polymers possessing opposite charge. This results in electronic attraction of the alternating layers forming a film. The thickness of the films depends on the number of repetitions.^{82,83}

Thermal evaporation: Thermal evaporation involves high temperature heating of a polymer under vacuum and its subsequent evaporation and deposition onto the substrate surface. The time of the evaporation determines the film thickness.⁸¹

Chemical vapour deposition (CVD) polymerisation: The principle of CVD lies in evaporation or sublimation of a chemical species, which is subsequently transported into a deposition chamber. There the absorption on to the substrate surface takes place, followed by a polymerisation on the surface and formation of a thin film. This technique is used for the preparation of a pure conducting polymer film or composite films consisting of a variety of polymers.⁸⁴

Inkjet-printing: Inkjet-printing is another convenient method for polymer deposition where ink jet technology, very similar to the method used in standard paper printing, is used to deposit materials onto substrates.⁸⁵

Electrochemical deposition: When compared to all of the above methods, electrochemical deposition is the most convenient method to deposit polymeric thin films as it does not require the polymer to be soluble. The growth is performed from a monomer solution and is localised only where the current flows; the deposition can only be carried out on a conducting substrate. Hence, the film can be deposited on patterned microelectrodes of only a few microns in size. However, the growing polymer can bridge the insulating gap between two conducting electrodes, if they are close enough to one another, which is an important feature when fabricating chemiresistors.⁶³ For its numerous advantages, this method has been chosen for this project and is therefore discussed in greater detail later in this chapter (1.4.3).

1.4 INTRODUCTION TO CAPACITORS

A capacitor is a passive electrical element which is used to store energy, in the form of an electrical charge, in an electrostatic field between two separated plates. The structure of a capacitor consists of two or more conductive metal parallel plates separated by a non-conducting substance such as air, paper, ceramic or plastic, which is called a dielectric (Figure 1-13).⁸⁶

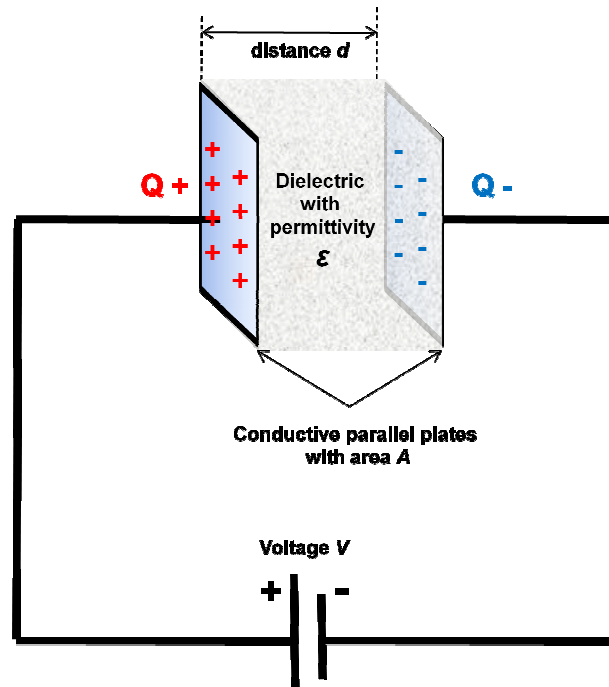


Figure 1-13: Schematic drawing of a circuit containing a capacitor.

The ability of the capacitor to store charge on its plates in the form of an electrostatic field developed across the dielectric is called the capacitance C , which has its unit named after the British physicist Michael Faraday - Farad (F). Capacitance is determined as the ratio of the charge Q measured on the plates and the voltage between them V (equation (1-7)).⁸⁶

$$C = \frac{Q}{V} \quad (1-7)$$

The dimensions of the capacitor also influence the resulting capacitance according to equation (1-8).⁸⁶

$$C = \frac{\varepsilon_0 \varepsilon_r A}{d} \quad (1-8)$$

Thus, the larger the area of the plates (A) and the smaller the distance between them (d), the greater is the capacitance. Another factor affecting the capacitance is the dielectric material and its absolute permittivity ε (equation (1-9))

$$\varepsilon = \varepsilon_0 \times \varepsilon_r \quad (1-9)$$

ϵ_0 is the vacuum permittivity and ϵ_r is a relative permittivity, also known as the dielectric constant of a material (dimensionless). The permittivity of a medium describes how much electric field is generated per unit charge and determines the effect of the electric field on the dielectric and *vice versa*.⁸⁷ Dielectrics differ in their ability to block or permit an electrical charge; the higher the dielectric constant, the more insulating are its properties. Typical values of permittivity for common materials are summarised in Table 1-2.⁸⁶

Table 1-2: Permittivity of selected materials.

Material	Permittivity
vacuum	1.0000
air	1.0005
paper	2.5 – 3.5
glass	3 -10
wood	3 – 8
Metal oxide powders	6 - 20

A capacitor can be used with both direct and alternating current, shortened to DC and AC, respectively. In a DC circuit, the capacitor is charged up positively on one plate and (equally) negatively on the other. The maximum voltage is equal to the supply voltage and the non-conductive dielectric between the plates blocks any further current flow. The capacitor is now a temporary storage device that holds this charge until the supply voltage is turned off. On the contrary, in an AC circuit, the current will pass through the capacitor with little or no resistance. Thus, in an AC circuit, the capacitor will alternately charge and discharge and the capacitance would therefore vary depending on the frequency of the supply.⁸⁸

The function of capacitors is similar to batteries. The difference between them is the ability of the capacitor to release its entire charge in a fraction of second, whilst batteries will release charge over an extended period of time.⁸⁶ An illustrative

example is the flash of a camera; within a few seconds the battery charges up the flash's capacitor, with this energy being evolved in a fraction of second. Lightning is an example of a capacitor in Nature. A storm cloud and the Earth's surface represent the two capacitor plates that become charged up during the storm. Eventually the difference in potential between them becomes great enough that the air dielectric starts to break down, providing a necessary path for the charge. This results in short-circuiting of this natural capacitor, initiating a flash of lightning.

1.4.1 Chemicapacitive sensors

A chemicapacitive sensor is a capacitor coated with a selectively absorbing material such as a polymer. These sensors rely on a combination of swelling and a change of dielectric permittivity of the polymer when a specific analyte is absorbed into the polymeric layer due to a specific chemical or physical interaction. This will result in alteration of the capacitance that is subsequently detected. Polymer-coated chemicapacitors offer a promising platform for low-cost, low-maintenance sensors because no heating, mechanical excitation or light sources are required.⁴⁷

Chemicapacitors can be constructed in two geometries - parallel-plate sensors or interdigitated electrodes (IDE).⁸⁹ Parallel plate capacitive sensors^{46, 47, 90} consist of a layer of metal with a deposited polymer, which is coated with another layer of metal, which in turn is porous to allow penetration of the analyte to the sensing layer. The drawback of this technology is the difficulty in depositing the final metal layer, which can often destroy the polymer.⁴⁷ On the other hand, IDEs are inert, array microelectrodes formed from patterned metal conductors on an insulating substrate chip. A layer of polymeric substrate is deposited on top of the metal conductors creating the sensing layer.

1.4.2 Polymer-coated interdigitated electrodes as chemicapacitors

An interdigitated electrode is a periodic pattern of electrodes deposited on an insulating substrate. IDEs are one of the possible solutions to achieve a low-cost

platform for delivering inexpensive, easy to fabricate sensors with low power consumption (Figure 1-14).⁹¹

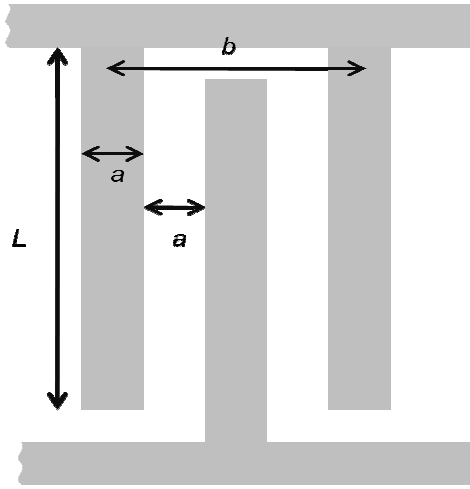


Figure 1-14: Interdigitated electrode format.

IDEs can be fabricated by processes such as patterning or etching and can be produced at low-unit-cost. To create a chemical sensor based on an IDE, a sensing material, *e.g.*, a polymer, has to be deposited on the surface. Combining functional organic polymers with IDEs offers a new method of fabricating affordable, sensitive and selective sensors.⁹¹

A typical IDE consists of N fingers of width and gap a and thickness t . A unit cell b is the distance between the centrelines of the adjacent fingers belonging to the same electrode. By applying a potential on the IDE, the resulting electric field travels from one electrode through the dielectric film to the other electrode. The unit cell capacitance per length is given by equation (1-10):⁹²

$$C_{uc} = \varepsilon_o (\varepsilon_r + \varepsilon_k) \frac{K(\sqrt{1 - (\frac{a}{b})^2})}{K(\frac{a}{b})} + 2\varepsilon_o \varepsilon_k \quad (1-10)$$

All three terms a , b and t are constants. ε_o and ε_r are the relative permittivity of free space and the substrate kind (also constants) and K is the complete elliptic integral of

the first. The total capacitance of the IDE device is given by equation (1-11) where $N-1$ is the number of unit cells and L is the length of the electrode fingers.⁹²

$$C_{TOTAL} = C_{uc}(N-1)L \quad (1-11)$$

Therefore, the response of an IDE chemicapacitor is only dependent on the variation in the capacitance. This originates from the change of the relative permittivity of the polymer upon an interaction with the targeted analyte as all the other parameters are constants.

1.4.3 Polymer deposition via electropolymerisation

In order to achieve integration of polymers with IDEs, it must be possible to selectively deposit the polymeric material onto the patterned microelectrode surface. In this project, the IDE surface was made of gold and localised electrochemical polymerisation of the synthesised monomers directly onto the device was the chosen method of deposition.

Compared to other deposition methods, electrodeposition is a fast and low-cost method, that provides a high level of reproducibility between samples.⁹³ The synthesis of the polymers *in situ* is clean and high-yielding, whilst using minimal amounts of monomer and no costly catalysts or other reagents. By varying the conditions of the experiment such as the number of redox cycles, monomer concentration or scan rate, different film thicknesses can be achieved with a high degree of reproducibility.^{21, 29, 93} The deposition is specifically localised only where the electric current flows - in this case through prototype interdigitated gold electrodes that constitute the sensor platform. Thus, on a single sensor substrate, it is possible to grow a polymer film on one IDE and another, different film on the neighbouring IDE, simply by flowing current through one while keeping the other one open-circuited in the electrochemical cell.⁹⁴ The fabrication of polymeric sensors is usually a time-consuming and costly procedure, demanding sophisticated equipment that increases overall cost.⁴⁷ However, in the case of electrodeposition, the overall number of steps required for sensor fabrication is reduced to just one

processing step as the polymerisation and the generation of the active area of the sensor occurs at the same time. Thus, the simultaneous coating of a large area substrate containing multiple IDEs can be achieved in a single electropolymerisation experiment.

Previously, in an initial proof-of-concept experiment, commercially available 3,4-ethylenedioxythiophene (EDOT) was electrochemically grown across a 12 μm gap between two nickel pads. The resulting chemiresistor was exposed to changing humidity and a variation of its resistivity was monitored to form a discrete, miniaturised humidity sensor.⁶³ This opened up a new and exciting opportunity of combining organic semiconductors with MEMS (microelectromechanical system) sensors as a feasible and affordable prospect. Potential applications for conjugated polymers go beyond humidity microsensors, and sensors that can monitor gases,⁹⁵ (bio)chemical analytes,⁹⁶ and volatile organic chemicals (VOCs).^{97, 98} Electrochemical polymerisation of conducting polymers on interdigitated electrodes has been used to form sensors to measure organic vapours such as alcohols and toluene,^{98,99} or olive oil vapours.¹⁰⁰

1.5 EXPLOSIVES DETECTION

1.5.1 Classification of explosives

An explosion is a process when a local accumulation of energy causes a sudden release of a large amount of energy from an explosive material. There are three main types of explosions.

- Physical explosions occur when a compressed material undergoes a rapid physical transformation.
- Chemical explosions are caused by chemical reactions and generate large amounts of heat and hot gas.
- Atomic explosions are similar to chemical explosions, with the main difference being their potency. This type of explosion is up to a billion

times stronger, lasts longer and the presence of radiation produced would kill all surrounding life.¹⁰¹

A chemical explosive is a substance that contains a great amount of stored energy that can produce an explosion - a sudden expansion of the material after initiation, usually accompanied by the production of light, heat and pressure. The decomposition results in the formation of a more stable material. Explosives can be classified according to different aspects such as power, performance, uses, transport, applications and chemical structure. Explosives are divided into two main groups, low and high explosives, which are further classified into different types.^{101, 102}

Low explosives burn at relatively low rates (cm s^{-1}), whilst high explosives detonate at significantly higher velocities (km s^{-1}). Low explosives include propellants such as smokeless powder, black powder, pyrotechnics, blasting powder *etc.* Propellants are combustible materials that only burn and do not detonate; they produce flames, sparks and cracking sounds. High explosives include two groups according to their function, primary and secondary explosives. Primary explosives, which include lead azide (PbN_6), lead styphnate (lead 2,4,6-trinitroresorcinate), lead mononitroresorcinate (LMNR), potassium dinitrobenzofuroxan (KDNBF) *etc.*, rapidly develop from burning to detonation and are often referred to as ‘initiating explosives’ because they can be used to transmit the detonation to the secondary, more stable explosives. Primary explosives can be initiated through shock, electric spark or high temperature and explode whether they are confined or not. Secondary explosives are mostly organic compounds containing nitro (NO_2) groups. The three major classes of these energetic materials are nitroaromatics (*e.g.*, trinitrotoluene (TNT)), nitramines (*e.g.*, trinitro-triazacyclohexane (RDX)) and nitrate esters (*e.g.*, nitrocellulose and nitroglycerine (NG)), and are often used as the main charge or supporting explosives because they detonate only under specific circumstances. They cannot be detonated as easily as primary explosives by heat or shock, but they need the explosion of a primary explosive to detonate them.^{101, 102}

According to their chemical nature, explosives can be further divided into two groups; explosive substances (TNT, RDX, *etc.*) and explosive mixtures (black

powder). Chemical explosives generally contain nitrogen, oxygen, carbon and hydrogen and can be divided into six main categories with respect to their chemical functional groups (see Table 1-3).¹⁰²

Table 1-3: Chemical categories of explosives.

Compound class	Example	Symbol
Aliphatic nitro	Nitromethane Hydrazine nitrate 2,3-Dimethyl-2,3-dinitrobutane	DMNB
Aromatic nitro (C-NO ₂)	Nitrobenzene	NB
	Nitrotoluene	NT
	2,4,6-Trinitrotoluene	TNT
	2,4-Dinitrotoluene	DNT
	2,4,6-Trinitrophenol (Picric acid)	TNP
Nitrate ester (C-O-NO ₂)	Nitroglycerine	NG
	Ethylene glycol dinitrate	EGDN
	Pentaerythritol tetranitrate	PETN
	Nitrocellulose	
Nitramines (C-N-NO ₂)	Trinitro-triazacyclohexene	RDX
	Tetranitro-tetrazacyclooctane	
Acid salts (NH ₄ ⁺)	Potassium nitrate	
	Ammonium nitrate	
Peroxides (C-O-O-C)	Hexamethylene triperoxide diamine	HMTD
	Triacetone triperoxide	TATP

1.5.2 Detection of explosives

The detection of explosives has received much attention in the last few years.¹⁰²⁻¹⁰⁵ The increasing number of terrorist attacks in the past two decades have led scientists to develop efficient sensors for explosives and therefore ensure safety in public facilities. There are national and international security requirements for the fast and sensitive detection of commercial and homemade explosives at airports and other public transport places. Therefore the detectors need to be miniaturised, low-

cost, user-friendly, with fast response times and offer a very low rate of false positives.¹⁰⁴ On the other hand explosive detectors are highly desirable in environmental applications such as analysing debris at post-explosion sites and for the analysis of contaminated areas. Nitro-aromatic compounds may cause pollution of an environment and health problems in humans and animals. The by-products of common explosives are toxic and carcinogenic even after degradation.¹⁰⁶ Therefore, there is still a growing interest amongst scientific and security specialists to develop increasingly more reliable and efficient explosive detectors.

While designing a new device, it is vital to think of the basis for its use, whether to determine explosive pollutants in soil, in the marine environment or screening luggage at airports. In other words, whether they will be detected in the solid, liquid or gaseous phase. Soils are generally very complex and the formation of adsorbates on the detection electrode surfaces occurs, leading to time dependent effects. Therefore it is difficult to employ reliable and fast detection methods. Detection of explosives in a marine environment is extremely challenging also, as the targeted material can easily disperse in the water and such high dilution levels are difficult to detect.^{102, 103} The explosive composition of many different chemicals and their low vapour pressures (*e.g.* 4.8×10^{-6} Torr at 20 °C for TNT)¹⁰⁵ brings difficulties in gaseous determination, especially since terrorists usually pack them in plastic covers hence adsorbing any vapours.^{102, 103, 105} However, commercial explosives usually contain detection agents with a higher vapour pressure, particularly 2,3-dimethyl-2,3-dinitrobutane (DMNB) to facilitate vapour detection. Another example is the presence of DNT in TNT samples as an impurity resulting from the manufacturing process. The higher vapour pressure of DNT often makes it the target molecule for detection.¹⁰³

1.5.3 Commercially available explosive detectors

Current sensing methods for all molecular classes include the following main types of detectors; spectroscopic methods - ion-mobility spectroscopy (IMS), mass spectrometry (MS) and gas chromatography (GC), trained canine teams, metal detectors or X-ray dispersion.

Whilst each method has some advantages, none is ideal. IMS is used for explosives detection and identification in clothes, skin and other objects. The analysis is based on molecular mass and comparison with a library of standards. This technology is accurate only for clean samples and only for common explosives. IMS and MS/GC are not suitable for broader use due to the necessity of instrumental calibration and a trained operator. X-ray screening employs high-energy X-rays that penetrate luggage and clothing, hence can be used for screening at airports. However, they may only identify higher amounts of explosive, such as large bombs, and not explosive residues. Similarly, metal detectors were used to detect older mines in fields as they used to be made of metal. Due to the availability of plastic packaging for mines, metal detectors are outdated for practical, modern day use.^{107, 108}

Even though significant effort has been devoted to the investigation and development of accurate and sensitive sensors, the most effective and efficient method in current use is through trained canine teams. These sniffer dogs react either to a particular chemical smell or to a combination of many smells that make up an explosive or narcotic.¹⁰⁹ Dogs, however, also suffer from some limitations like the need for constant care and training. They require a skilled handler, cannot work unlimited hours and could be affected by changes in mood or behaviour.^{107, 110}

1.5.4 The development of explosive sensors

So far, many devices have been developed and patented for vapour and liquid detection, which nowadays are commonly used in everyday life.^{103-105, 107, 108, 111, 112} However, there are still many possibilities to improve the quality, sensitivity and selectivity of sensors, whilst simultaneously lowering the production and operating costs. The development of new devices still remains one of the most challenging tasks and the majority of common sensors that are being investigated nowadays can be classified as mass sensors, optical sensors, receptor based sensors and electrochemical sensors.^{107, 108}

Mass sensors: Mass sensor devices adsorb the target analyte onto the surface and the detector records a change in mass.¹¹¹ The detection is either made by changes

in acoustic waves – surface acoustic wave sensors (SAW)¹¹³ or a change in the shape as a mass is collected – microcantilever devices.¹¹⁴ Several types of polymers have been used as coatings for explosives detection, such as polymer coated SAW sensors.¹¹⁵ Microcantilevers have been used in the detection of plastic explosives¹¹⁶ or TNT¹¹⁷ and their main advantage is a greater mass sensitivity, smaller size, low cost and compatibility with large multisensor arrays.

Optical sensors: Optical sensors include inorganic and organic fluorescent polymers and are based on the reaction between the explosive analyte and an indicator. Optical sensors include methods such as colourimetric and fluorometric detection, fluorescence, laser induced breakdown spectroscopy (LIBS) and terahertz spectroscopy.^{103, 107, 111, 118}

Fluorescence based methods include either fluorescence quenching or fluorescence turn-on. Semiconducting polymers are the perfect candidate for use as fluorescent sensors as they can be electron-rich, allowing for electron-poor nitro containing explosives to bind to them and influence the fluorescence. Examples of such materials are organic polymers such as polyacetylenes, poly(p-phenylenevinylenes), poly(p-phenyleneethynylenes), polymeric porphyrins or inorganic polymers such as polysilanes and polymetalloles.^{103, 107}

The colourimetric method involves analyte binding or reaction with an indicator, which results in the absorption of visible light and a colour change. These types of sensors have been commercialised for detecting explosives in soil, water, and on surfaces.¹⁰³

LIBS is a method based on a short laser pulse that is focused on the sample. Laser energy heats, vaporises, atomises and ionises the sample material, generating a small area of plasma. Excited atoms and ions in the plasma emit a secondary light, which is collected and spectrally resolved by the spectrophotometer then analysed by a light detector. Each chemical element has its unique spectral signature, which results in the determination of the composition of the multi-elemental sample.^{111, 118}

The terahertz (THz) explosive sensor is based on differential absorption. The analysed material is irradiated by THz radiation containing at least two frequencies. The frequencies of radiation are chosen according to the targeted explosives and are meant to maximise the contrast between the presence and absence of explosives. It is not only useful for broad detection, but the specific type of explosive can be determined because each material has its own terahertz spectral fingerprint.^{111, 118}

Receptor-based sensors: Receptor-based sensing achieves selectivity through the specific interaction between the receptor molecule and the explosive analyte. A change in mass, conductivity, or absorbance is then used to quantify the interaction. To obtain reversible detection, an explosive must bind to the receptors with weak chemical interactions such as van der Waals interactions or hydrogen bonding.¹⁰⁵ There are a number of coatings that can be used for imparting partial selectivity, such as conducting polymers,¹¹⁹ or molecularly imprinted polymers (MIPs).¹²⁰

Electrochemical sensors: Electrochemical sensors are based on passing electric current through the electrode interacting with explosives, which causes a change in the detected signal. Electrochemical sensors involve the electronic modification of explosives or their degradation products based on the redox properties of the analyte.^{104, 111} The nitro group is an electron acceptor and the reduction process forms an amine or nitroso group *via* a hydroxylamine; reduction of nitro-esters forms nitrite and alcohol functionalities.¹²¹ Electrochemical detection is also suitable for peroxide explosives, because they do not fluoresce and do not exhibit UV absorption.¹²²

There are several examples of electrochemical sensors for explosives such as a remote-controlled sensor for TNT in water¹²³ or improved coatings of working electrodes with various polymers.¹²⁴

1.6 POROUS POLYMERS

Porous polymers are materials containing numerous pores of various dimensions. Porosity is the ratio of empty volume of the material over the whole

volume. Porous materials can be classified according to the IUPAC recommendation¹²⁵ as microporous (pore diameter less than 2 nm), mesoporous (pore diameter 2–50 nm) and macroporous (pore diameter larger than 50 nm). When describing porous material, one should bear in mind several attributes of the pores such as geometry, size, functionality, and characteristics of the polymeric framework such as composition, topology, and functionality. Porous materials exhibit an enhanced surface area compared to their non-porous counterparts with the general trend being that (for a fixed pore volume) the smaller the pores, the larger the surface area.¹²⁶

Porous polymers have received much attention in the past two decades because they offer several advantages over well known, traditional porous materials such as zeolites, activated carbons and porous silica. They have the potential to combine the highly desired properties of polymeric and porous materials in one defined structure.¹²⁶ The superiority of polymers lies mainly in the following factors:

- Their possibility to be chemically engineered and tuned either *via* chemical synthesis from various monomers or *via* post-modification processes to achieve high surface area and well-defined porosity.¹²⁷⁻¹³⁰
- Their pore size, shape and other parameters can be designed and tailored to specific needs. A wide range of synthetic methods enables incorporation of various functionalities into the pores or at the pore surface.¹³¹⁻¹³³
- In general they can be easily processed *via* many different techniques and therefore incorporated in wide range of devices.
- Their organic networks usually consist of light elements providing a low density material.¹³⁴⁻¹³⁶

Due to their outstanding properties, porous polymers have found use in a wide range of applications. Depending on each individual application, different aspects need to be controlled - high surface area is required for gas storage^{128, 133, 137} and sensors,^{138, 139} while the pore dimensions are important in gas separation.^{140, 141} In applications such as catalysis,^{142, 143} media for trapping and release of drugs^{144, 145}

and filtration/separation/exchange membranes,^{146, 147} both of these characteristics play an important role. The main issue for soft polymeric materials is the stability of the pores in the dry state. Therefore, there is a high demand on the further development of suitable and reliable preparation techniques providing polymeric frameworks possessing rigid, non-collapsing pores with a suitable functionality and dimensions.

1.6.1 Preparation of porous polymers

Many different synthetic techniques for the preparation of stable frameworks with well-defined pore structures and customised functionalities have been developed over the last few years. These include three main methods – templating, self-assembly and direct synthesis – which offer both advantages as well as several limitations.¹²⁶

The templating methodology is based on the synthesis of materials around a certain template. The synthesised material is attracted to the template molecule(s) *via* reversible, weak chemical interactions. Once the reaction is finished, the desired product is achieved by removal of this template, retaining its shape and thus generating the porosity (Figure 1-15).

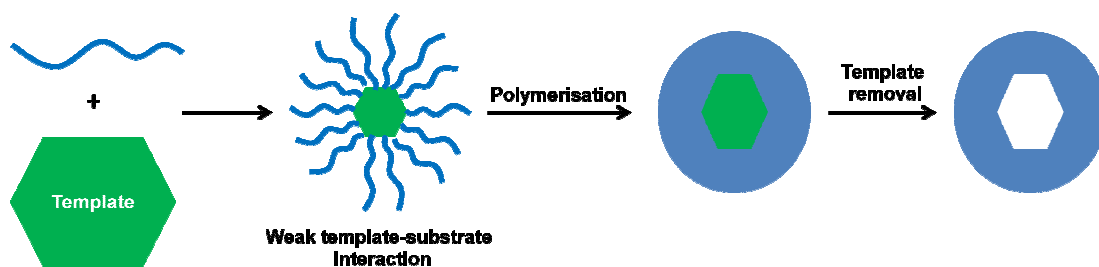


Figure 1-15: Schematic representation of the templating methodology.

Template assisted synthesis is a straightforward and versatile method for the preparation of porous polymers.^{148, 149} Its main benefits include ease of synthetic procedures with a variety of template choice, precise and predictable pore dimensions and the possibility to functionalise the porous network. However, the

template surface must be compatible with the selected synthetic material to ensure a high-yielding and reliable template replication. The compatibility requirement might therefore lead to a necessity of costly template synthetic modification. Additionally, the template must be easily removed without damaging the polymer structure, meaning the “used” templates are usually sacrificed, resulting in a waste of expensive synthetic components, increasing the overall cost of the process. Finally, due to the molecular size of the templates, the as-formed structures lack micropores and therefore this technique is only useful for meso- and macropores.¹²⁶

The raw materials in template synthesis can be premade polymers coated onto the template surface, or monomers that are polymerised *in situ*. An interesting technique that falls within this subcategory of templating methods is electrochemical polymerisation.¹²⁶ Commonly, this method is used to prepare conducting polymers derived from polyaniline, polypyrrole and polythiophene. The numerous advantages of electrochemical polymerisation mentioned previously (Chapter 1.4.3) can be exploited beyond the deposition of simple conducting thin films and can be used for the fabrication of porous polymeric coatings directly onto electrical devices, resulting in well-defined pore sizes and morphology. The polymer is grown on the specifically shaped conducting electrode from the monomer solution and once the growth is completed, the electrode is removed. An example is polypyrrole grown between TiO₂ nanotubes, which are then dissolved in hydrofluoric acid, thus yielding porous polypyrrole.¹⁵⁰ The formation of the porous structure is based on the specifically grown template. The polymerisation rate can be controlled and optimised by several different factors such as the potential scan rate, time, applied, potential, monomer concentration, shape and the electrode materials.

The self-assembly methodology is, alongside templating, useful for creating structures with larger pores - mesoporous or macroporous polymers. This technique is based on block copolymers containing two or more chemically and thermodynamically incompatible components. The microphase separation occurs due to the self-assembly of the covalently linked incompatible segments that are forced to undertake the lowest energy geometry. The composition and architecture of individual blocks can be controlled and adjusted, which opens up a possibility to

create a variety of nanoscale materials.¹²⁶ The role of the block copolymer can be two-fold – it can either act as a sacrificial template for other polymers to form a framework¹⁵¹ or it can itself create the porous scaffold (Figure 1-16).¹⁵² This type of synthesis can provide well-defined, sophisticated structures, but the synthetic steps often include expensive amphiphilic copolymers.

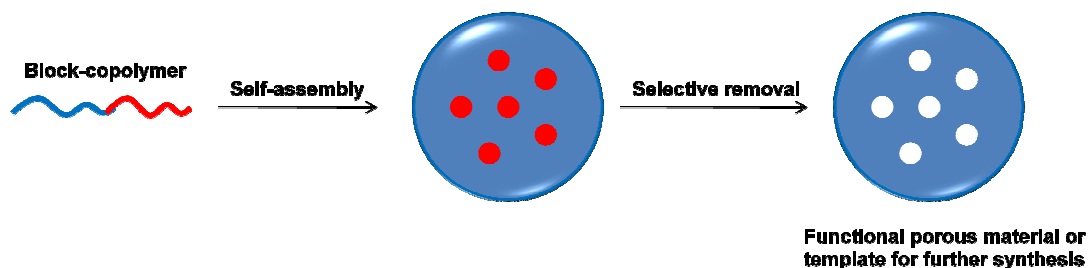


Figure 1-16: Depiction of a self-assembly mechanism for block-copolymers.

The direct synthesis method is the only technique that can create micropores. The porous materials are prepared directly *via* conventional chemical polymerisation, which is followed by solvent removal. The main concern in this type of synthesis is maintaining a permanent porosity in the dry state. To achieve that, rigid and contorted monomer building blocks that inhibit space-efficient packing are commonly used.^{109, 127, 153} The main advantage of this method is the possibility to precisely control the pore size by incorporation of different functional groups, which allows formation of a variety pore sizes within one structure, so called hierarchical porous polymers. However, this method often includes complex multistep synthesis starting from expensive precursors and with poor yields of polymers.^{134-136, 154}

1.6.2 Organic nanoporous materials

Organic nanoporous materials with high surface area include materials composed entirely from light elements of the periodic table (*e.g.* C, H, N, O, S, Si, P, halogens) with a pore size in the nanorange. They are prepared mainly by direct synthesis. The starting materials are usually polymerisable monomers and cross-linkable polymers. Depending on the synthetic strategy, nanoporous polymers can be prepared in a wide range of architectures such as linear polymers, dendrimers,

hyperbranched polymers and networks.^{135, 136} In order to create such a porous structure that is accessible to gases or other guest molecules, it is necessary to create a network of interconnected channels. This can be created by polymerising a monomer containing connectivity in at least three positions (the node), together with a linking monomer with at least two connecting functionalities (the strut), as represented in Figure 1-17.

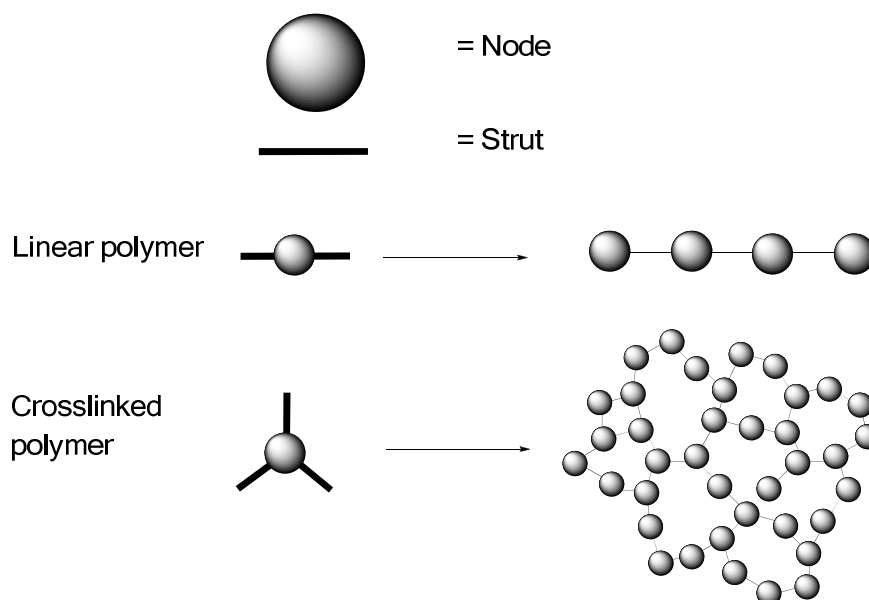


Figure 1-17: Schematic representation of the difference between linear and cross-linked polymers.

For such a network to retain its porosity and high surface area in the dry state, the polymers require rigid linkers to stay locked in the permanent interconnected geometry that prevents the network from collapsing and filling the pores.¹³⁶ Several different methodologies to prepare nanoporous materials have been developed including Sonogashira-Hagihara cross coupling, Gilch coupling, Suzuki cross coupling, Yamamoto coupling, oxidative polymerisation, various cyclotrimerisations, click chemistry, amidation, imidation, Friedel-Crafts reaction and many others.^{126, 140, 143}

Organic nanoporous polymers include four main types of architecture - hypercrosslinked polymers (HCPs), polymers of intrinsic microporosity (PIMs), covalent organic frameworks (COFs) and conjugated porous polymers (CPPs).

According to their morphology, they can be classified as crystalline with ordered structures and uniform pore size related to the strut length (COFs), or amorphous disordered structures with wider pore distribution (CPPs, HCPs and PIMs).^{126, 136, 143} Huge interest in the field of nanoporous organic materials has given rise to a large amount of reported materials. Here, only a few selected examples and their surface areas are mentioned. For further details, the reader is referred to recently published reviews in this field.^{126, 136, 143}

COFs: Covalent organic frameworks are crystalline networked materials prepared from organic monomers linked by reversible covalent bonds, for example strong B-O bonds.^{155, 156} The first COFs were reported in 2005 by Yaghi *et al.*¹⁵⁶ (COF 1 and 2, Figure 1-18). Increased surface areas were observed in COFs with three-dimensional cores reported in 2007 by the same group (COF 3 and 4, Figure 1-18).¹⁵⁷

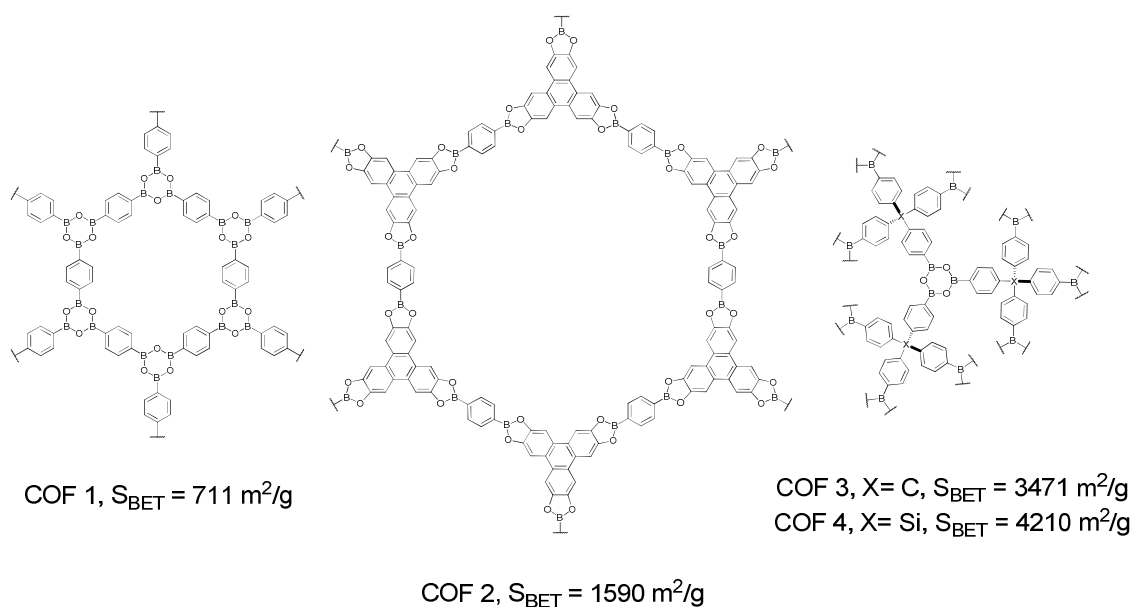
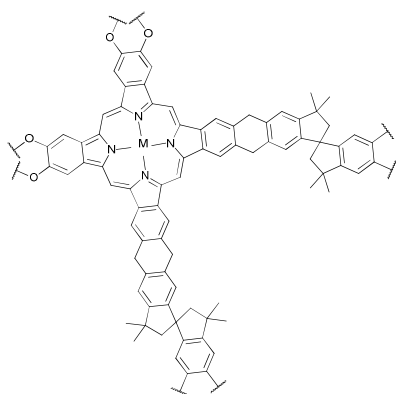


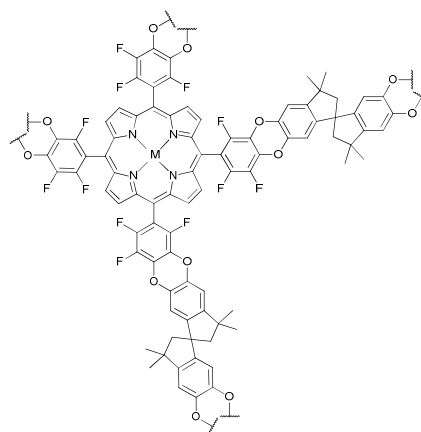
Figure 1-18: Examples of COFs and their surface areas.

PIMs: Polymers of intrinsic porosity are synthesised by non-reversible condensation of monomers containing tetrahedral carbon. The resulting polymer is then rigid and contorted causing ineffective packing of the polymer in the solid state and enhancing porosity. The first PIMs were prepared from phthalocyanines¹⁵⁸ and

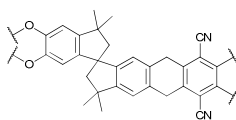
porphyrins¹⁵⁹ (PIM 1 and 2, Figure 1-19). The main benefit of PIMs is the possibility to create a linear structure that is soluble in common solvents and therefore can be simply fabricated into a functional device. The highest surface area of linear PIM was reported in to be 860 m²/g (PIM 3, Figure 1-19).¹⁶⁰ A PIM based on a tryptacene core was reported with the highest surface area of all PIMs (PIM4, Figure 1-19).¹⁶¹



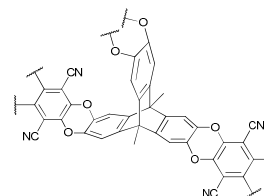
PIM 1, M = Zn²⁺, Cu²⁺, Co²⁺, 2H⁺
S_{BET} = 450 - 950 m²/g



PIM 2, M = H₂, FeCl
S_{BET} = 910 - 980 m²/g



PIM 3, S_{BET} = 860 m²/g



PIM 4, S_{BET} = 1760 m²/g

Figure 1-19: Structure of selected PIMs and their measured surface areas.

HCPs: Hypercrosslinked polymers were one of the first known organic microporous materials with a rigid network structure, small pores and high surface areas. HCPs are prepared by the hypercrosslinking of linear precursors (*e.g.*, polystyrene, polyaniline or polypyrrole), which are dissolved or swollen and then quickly cross-linked to be locked in place. After solvent removal, they maintain their stable porous structure (Figure 1-20).¹²⁶

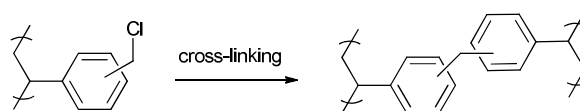


Figure 1-20: Cross-linking of polystyrene.

Polystyrene is the most common precursor for the preparation of HCPs and the highest surface area was achieved by Sherrington and co-workers (HCP 1, Figure 1-21).¹⁶² Other precursors that were polymerised by self-condensation include dichloroxylene (DCX), bis(chloromethyl)biphenyl (BCMBP), and bis(chloromethyl)anthracene (BCMA), which when hypercrosslinked exhibited surfaces area up to almost 1900 m²/g (HCP 2-4, Figure 1-21).¹⁶²

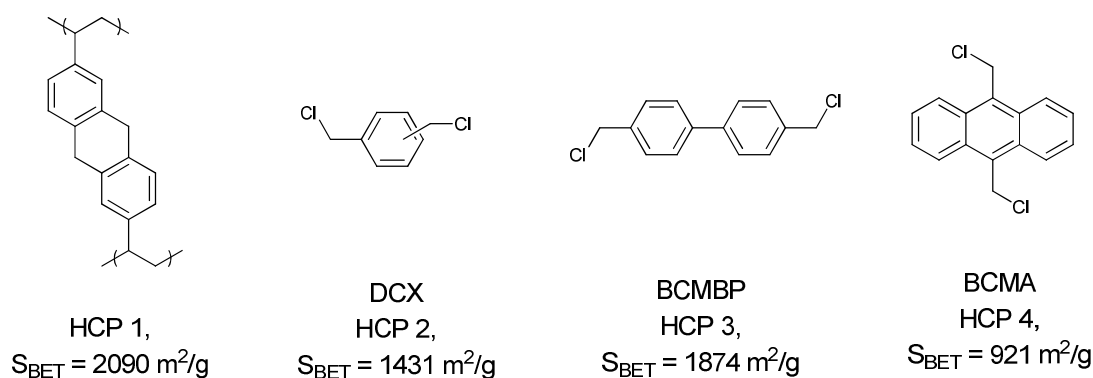


Figure 1-21: Precursors for cross-linking to achieve HCPs.

CPPs: Conjugated porous polymers consist of a conjugated backbone and as such combine the well-known advantages of conjugated polymers and nanoporosity. In addition, due to the wide range of applicable synthetic methods, various chemical functional groups can be incorporated. CPPs based on poly(aryleneethynylene) (PAE) networks were firstly reported in 2007 by Cooper *et.al.*¹⁶³ It has been shown that varying the strut length can influence the pore size and surface area; the polymer possessing the shortest strut exhibited the highest surface area of over 1000 m²/g (Figure 1-22).¹²⁹

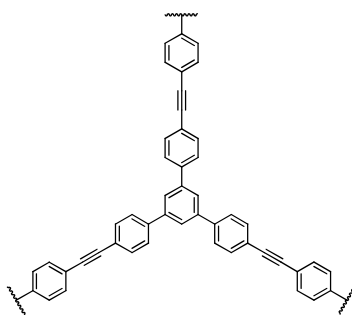
CPP 1, $S_{\text{BET}} = 1018 \text{ m}^2/\text{g}$

Figure 1-22: CPP based on PAE with shortest strut length and highest surface area.

The chemistry used to prepare CPPs is very diverse and it is well-known that the monomer choice and reaction conditions can dramatically influence the surface area of the resulting polymer.^{164, 165} For example, insertion of certain functionalities reduced the surface area compared to the non-functionalised analogues. Also solvent choice can have a dramatic effect on the porosity in CPP networks.^{164, 165}

Spirobifluorene and benzene are the two cores most often applied in the synthesis of CPPs. These can be combined with different struts by various synthetic routes resulting in a variety of polymers with a range of surface areas; various examples of these monomers and the synthetic methods used to synthesise their corresponding polymers are summarised in Table 1-4, entries 1 to 9. The highest ever surface areas achieved in organic polymeric networks were reported as $5600 \text{ m}^2/\text{g}$ and $6461 \text{ m}^2/\text{g}$ (Table 1-4, entries 10 to 11). These materials contained tetrahedral cores based on tetraphenylmethane and tetraphenylsilane. However, the presence of the tetrahedral centre in the monomer breaks the conjugation and therefore some authors avoid referring to these type of polymers as “conjugated” and rather call these type of materials as porous aromatic frameworks (PAFs).¹²⁶

Table 1-4: Several examples of different nodes and struts used for synthesis of CPPs and their surface areas.

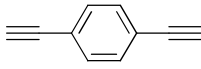
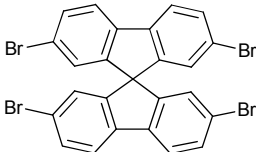
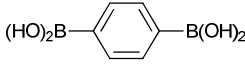
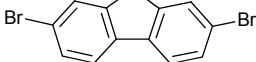
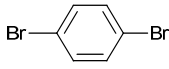
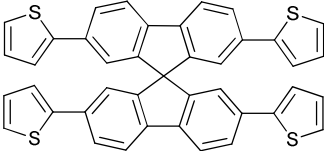
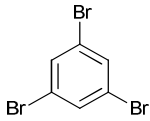
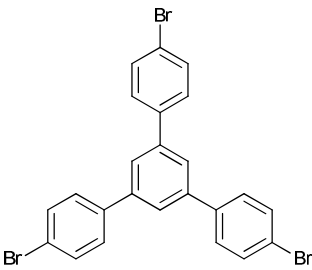
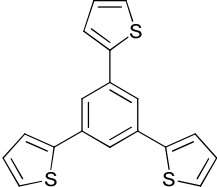
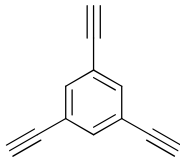
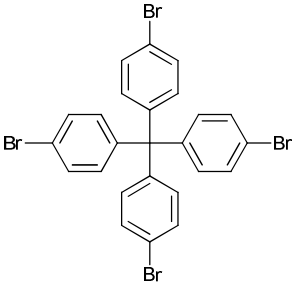
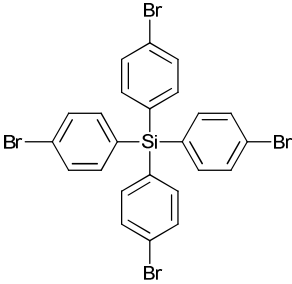
Entry	Core	Strut / Method	S_{BET} [m ² /g]	Ref.
1		 Sonogashira-Hagihara	510	109
2		 Suzuki	800	166
3		 Yamamoto	887	167
4		Yamamoto Homocoupling	1275	167
5		Oxidative polymerisation	577	154
6		Yamamoto Homocoupling	1255	167
7		Yamamoto Homocoupling	1503	168
8		Oxidative polymerisation	1060	154

Table 1-4: Continued.

Entry	Core	Strut / Method	S_{BET} [m ² /g]	Ref.
9		Cyclotrimerisation	1246	137
11		Yamamoto Homocoupling	5600	169
12		Yamamoto Homocoupling	6461	170

1.6.3 BET surface area determination

1.6.3.1 Adsorption of gases

Adsorption of gases is the most common technique of surface area measurement in polymeric networks. An incomplete saturation of the surface of the solid (adsorbent) offers the possibility to attract gaseous molecules (adsorptive) and adsorb them. There are two types of such adsorption: physisorption and chemisorption. Physisorption is dependent on pressure and is fully reversible since it is caused by van der Waals forces, ionic forces or hydrogen bonds. Chemisorption is pressure independent and is caused by actual chemical interaction; therefore it is stronger and may be irreversible.¹⁷¹ The amount of gas adsorbed by the solid depends on the

pressure of the gas, the system temperature and the area of the solid, which is principally defined by its degree of porosity.¹⁷² Determination of the extent of the adsorption can be calculated either by measuring manometrically the volume of the adsorbed gas or gravimetrically by determining the mass adsorbed. The volumetric method is most widely used and is usually performed at low temperatures (-196 °C for nitrogen), where the otherwise weak gas-solid interaction is enhanced and hence makes the measurement much easier.¹⁷²

1.6.3.2 The adsorption isotherms

Adsorption isotherms represent the relationship between the amount of adsorbed gas and the pressure at a fixed temperature.¹⁷³ The isotherms of physical adsorption can be divided into the main groups proposed by Brunauer, Deming, Deming and Teller (BDDT) (Figure 1-23).¹⁷³

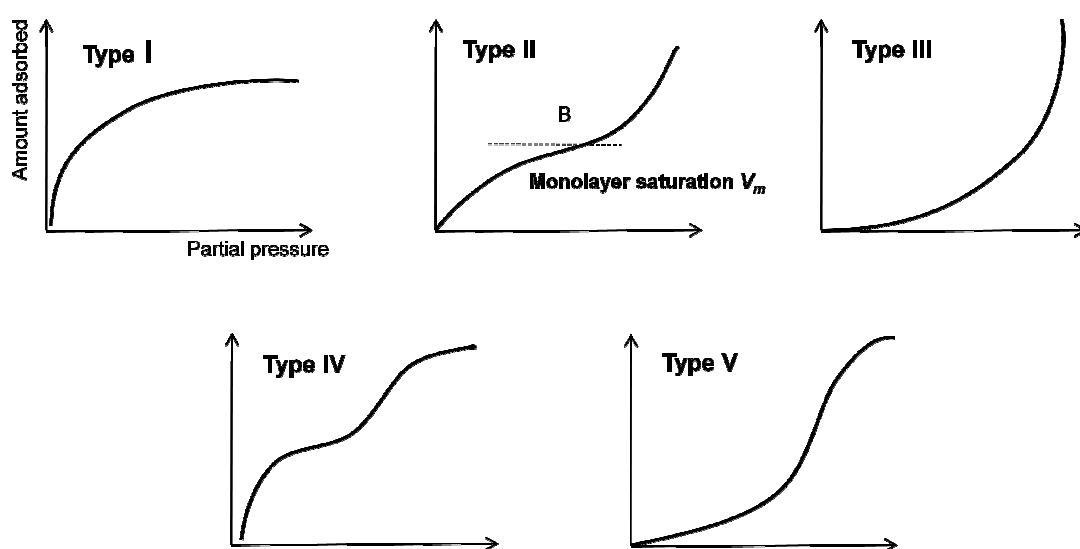


Figure 1-23: Types of adsorption isotherms according to BDDT.

Many theories have been expressed to quantitatively interpret the isotherms. The most well-known and perhaps the most accurate are the Langmuir and Brunauer-Emmett-Teller (BET) theories.¹⁷³ Both of these methods rely on a number

of assumptions made by Langmuir that might lead to an imperfect interpretation such as:

- All adsorption sites on the homogenous adsorbent surface are equal in energy;
- there is a constant ΔH_{ads} in the monolayer;
- the adsorbates do not interact with each other once they have been adsorbed into the localised sites.

The Type I isotherm represents adsorption limited up to a few layers of microporous solids, which have a pore size not greater than a few molecule diameters of adsorbate. At higher pressures, the pores are filled up leading to a plateau and not allowing any further adsorption. Type I represents a Langmuir isotherm described by equation (1-12)

$$\frac{V_{ads}}{V_m} = \frac{KP}{1+KP} \quad (1-12)$$

Where V_{ads} is volume of adsorbed gas, V_m is volume of adsorbed gas in complete monolayer, K is the equilibrium constant and P is adsorbate pressure. Langmuir proposed that at equilibrium the amount gas molecules being adsorbed on the surface are equal to the amount of molecules leaving the sorbent. This only takes place in one layer as the adsorption forces become saturated when the entire monolayer is created.¹⁷⁴

The BET model invented in 1938,¹⁷⁴ is basically an extension of the Langmuir method and takes into account the existence of multiple layers during absorption since the van der Waals forces are strong enough to attract another layer after saturation of the first. Thus, capillary condensation inside the pores can take place. BET is generally plausible for Type II isotherms, its application to Type III isotherms is unsuccessful and cannot be used to calculate the specific surface area.

Both Type II and III best describe non-porous material or materials possessing pores larger than micropores. The point of the inflexion “B” in Type II represents the monolayer saturation which is subsequently followed by capillary

condensation. The Type III curve is convex to pressure axis, which represents that the greater the number of molecules that are adsorbed, the easier the further adsorption gets. This states that attraction of the gaseous molecules to each other is greater than the gas-solid interaction, which is not in agreement with the basic BET assumption.

Type IV and V are modifications of II and III, respectively, and are applicable for solids with pores in the range of 15-1000 Å. The increase at higher pressure indicates higher uptake after the pores have been filled.¹⁷⁵

There are a number of other proposed assumptions associated with this BET method, including:^{173, 174}

- multilayer formation is unlimited, when the partial pressure equals 1;
- adsorption and desorption can only occur on or from the exposed sites, which are energetically uniform;
- the enthalpy of adsorption in the second and subsequent layers equals the enthalpy of condensation, ΔH_L ;
- evaporation – condensation constants above the first layer are equal.

The following equation was derived by Brunauer, Emmet and Teller for multilayer adsorption, for a volume of adsorbed gas V_m (1-13)¹⁷⁴

$$\frac{P}{V_{ads}(P-P_0)} = \frac{1}{V_m C} + \frac{(C-1)}{V_m C} x \frac{P}{P_0} \quad (1-13)$$

where V_m is the monolayer capacity at standard pressure and temperature, V_{ads} is the amount of adsorbate adsorbed at pressure P , P_0 (Torr) is the vapour pressure of adsorbate that can be calculated from the Antoine equation (1-14), C is dimensionless unit often used for the calculation of the net heat of adsorption ($\Delta H_{ads} - \Delta H_L$) expressed as equation (1-15).¹⁷³

$$\log_{10} P_0 = a - \frac{b}{T+c} \quad (1-14)$$

where T is temperature in °C and a , b and c are Antoine coefficients, for nitrogen at -196 to 100 °C, these values are $a = 6.49457$, $b = 255.68$ and $c = 266.550$ ¹⁷⁶

$$C = \exp \left[\frac{\Delta H_{ads} - \Delta H_L}{RT} \right] \quad (1-15)$$

where ΔH_{ads} is the heat of adsorption of the first layer (J mol^{-1}), ΔH_L is the heat of adsorption of the second and subsequent layers (J mol^{-1}), T is temperature (K) and R is gas constant ($8.314 \text{ J K}^{-1} \text{ mol}^{-1}$). C value has a great influence on the shape of the BET isotherm, when $C > 2$ giving Type II, whereas $0 < C < 2$ giving Type III isotherms.¹⁷³

V_m and C are characteristic for each adsorbent/adsorptive system and therefore are constants. Plotting $P/(V_{ads}(P_0 - P))$ against P/P_0 gives a straight line, where the intercept and slope of this line are represented by equations (1-16) and (1-17) (Figure 1-24).¹⁷¹

$$\text{Slope} \quad b = \tan \varphi = \frac{C-1}{V_m C} \quad (1-16)$$

$$\text{Intercept} \quad a = \frac{1}{V_m C} \quad (1-17)$$

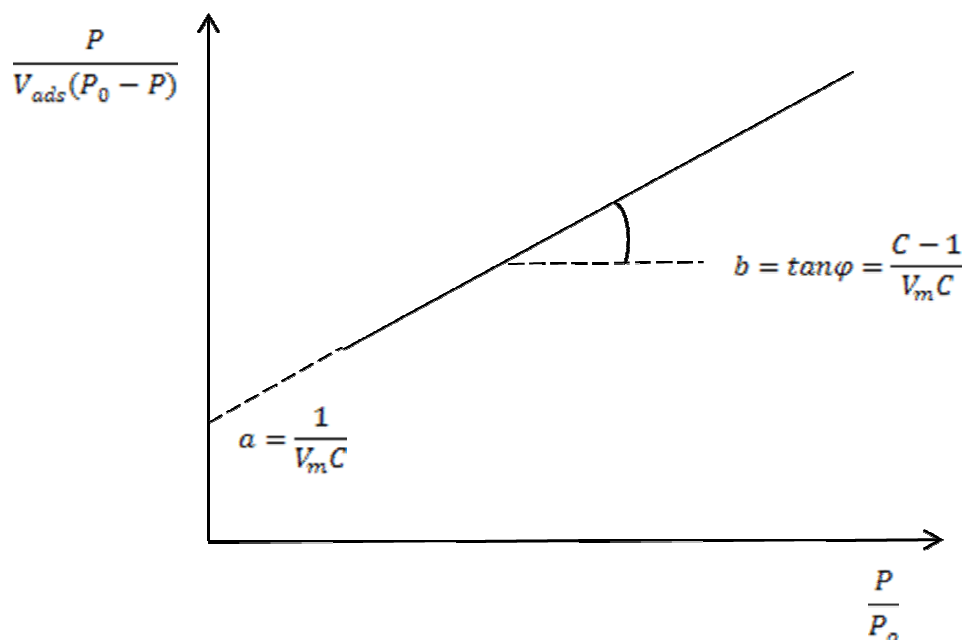


Figure 1-24: BET isotherm transform into a straight line.

From the equations above one can derive the equation for calculating V_m and C (1-18) and (1-19).

$$V_m = \frac{1}{a+b} \quad (1-18)$$

$$C = 1 + \frac{b}{a} \quad (1-19)$$

The specific surface area is the surface area per unit of material, commonly given as m^2 per gram.¹⁷¹ The BET surface area can be calculated from the monolayer capacity V_m , and the cross-sectional area of the adsorbate A_m , (0.162 nm^2 for nitrogen at $-195 \text{ }^\circ\text{C}$)¹⁷³ according to equation (1-20).

$$S = \frac{V_m}{M} \times N \times A_m \quad (1-20)$$

Where M is the molecular volume of adsorbate ($22.4 \text{ dm}^3/\text{mol}$) and N is the Avogadro constant ($6 \times 10^{23} \text{ mol}^{-1}$).

BET is the most commonly reported method, although one should always bear in mind its limitations. The major drawback of the BET equation is that it is only linear over a narrow P/P_o range of $0.05 - 0.35$.^{171, 172} It is found that at lower relative pressures, lack of surface energetic homogeneity causes the model to fail, and interactions between neighbouring adsorbate molecules result in the model failing at $P/P_o > 0.35$.¹⁷³ Also, phenomena such as pore-filling or polymer swelling may invalidate the theory. However, as long as the results obtained are considered carefully and one bears in mind all the factors of limitations, the BET serves as a good method of measuring the specific surface area of polymeric networks.¹³⁶

1.6.3.3 *BET Instrumentation*

At first, the materials are degassed under high vacuum, usually with heating, to expel any guest species for several hours. The analysis is subsequently performed by introducing the sorbing gas into the sample, which is adsorbed onto the surface. Commonly, nitrogen gas is used as the adsorbate at $-196 \text{ }^\circ\text{C}$ as it is readily available at low cost and offers the largest number of models to choose from, although it is also

possible to use other gases such as Ar, H₂, CO₂, SO₂ or *n*-alkanes.^{136, 172, 173} The isotherms obtained are then analysed by programs associated with the equipment.

1.7 AIM OF THE PROJECT

The aim of the project is to develop microsensors for nitroaromatic compounds related to explosives such as TNT or DNT. The key feature is using electropolymerisation to selectively deposit a polymeric material onto the patterned surface of an IDE, thus creating a discrete microsensor. This method offers fast, high-yielding and *in situ* polymer synthesis whilst using minimal amounts of monomer, and is compatible with producing structures on the nanoscale.

The properties and requirements for this type of sensor are as follows:

- The production of the material is to be accomplished with low unit manufacturing equipment and in high yield and can ultimately be integrated with CMOS circuitry to enable on-chip signal processing;
- the functionality of the polymer is to be tailored for sensing of specific target analytes;
- the sensors should retain their sensitivity and reproducibility with low power consumption.

To achieve these aims, the synthesis of functionalised monomers that bear a nitro-selective group will take place. Subsequently, their electropolymerisation onto IDE will be performed, allowing the determination of the most responsive polymer. Optimisation of the electrodeposition chemistry and process conditions in order to achieve good uniformity and reproducibility will then be undertaken. The next step will include evaluation of the performance of the microsensors. The sensors will be used as chemicapacitors for the detection of target analytes in the vapour phase. The interpretation of results and evaluation of devices will focus on selectivity, sensitivity, noise performance and reproducibility. Depending on the outcome of these preliminary studies, the strategy for improving any unsatisfactory parameters will be developed.

Chapter 2

**2 ELECTROPOLYMERISED HOMOPOLYMERS
FOR EXPLOSIVE DETECTION**

2.1 *PRODOT DERIVATIVES*

The first objective was to synthesise the monomers, which are designed to be selective to analytes bearing the nitro groups present in explosives such as TNT or DNT. To create suitable candidates for this desired application, the synthesised monomer has to comply with two main requirements:

- (i) it has to be easy to electropolymerise;
- (ii) it should bear a nitro selective group to provide an anchor point for the analyte.

3,4-Ethylenedioxythiophene (EDOT) (Figure 2-1) and its derivatives are well-known because of their facile electropolymerisability and reactivity.^{37, 177, 178} Compared to thiophene, EDOT derivatives are oxidised at a lower potential because of the strong electron donor effect of the ether groups that stabilises the radical cation during the electropolymerisation process and gives increased reactivity to the α -positions. Also, the formation of undesirable α - β and β - β linkages during the polymerisation is avoided due to the blockage of β -positions of the thiophene ring. Poly(3,4-ethylenedioxythiophene) PEDOT (Figure 2-1) based polymers are known to have high levels of conductivity in their doped state (up to 550 S cm^{-1}),^{37, 179, 180} low band gaps¹⁸¹ and thermal¹⁸² and chemical stability.¹⁸³ They have been widely used in sensing applications,^{63, 96-99} as well as in organic photovoltaics,^{181, 184} electrochromics,¹⁸⁵ and light emitting diodes.³⁷ In its oxidised state, PEDOT is very stable and almost transparent as a thin film and has a positive charge, thus conductivity is produced through hole transport.³⁷ A counter-anion is used to neutralise the overall charge and its nature and amount present in the polymer backbone greatly influence the conductivity.¹⁸⁰ In the reduced state, the polymer is neutral and is non-conductive. The issue of insolubility of PEDOT polymers was overcome by adding water-soluble poly(styrene sulfonic acid) (PSS) as the charge-balancing anion during the polymerisation to obtain a very stable, conductive polymer.³⁷ The specific electronic properties of EDOT/PEDOT and its derivatives represent an interesting tool for the design of precursors suitable for the desired purpose.

is a function of the intrinsic electronic properties of the nitro group itself and the nature of the hydrogen bond donor.

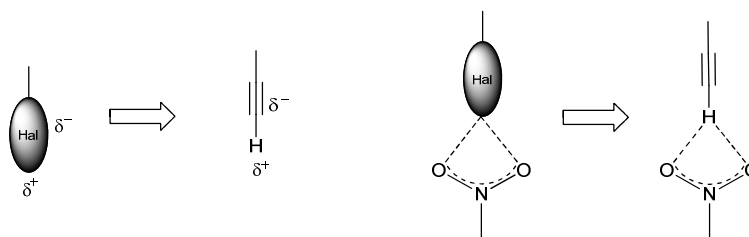


Figure 2-3: Models of alkynyl...nitro interactions.¹⁸⁸

3,4-Propylenedioxythiophene (ProDOT) (Figure 2-4) and its derivatives,^{189,190} which are most commonly used in electrochromic applications,¹⁹¹ retain the ease of electropolymerisability of EDOT^{192,193} and offer a free position in the propylene bridge that can be functionalised by a nitro recognition group, leading to a symmetrical derivative. Therefore, ProDOT derivatives are proposed as ideal candidates to develop for this application. The monomers chosen to meet the project aims are halogen- or alkynyl-functionalised ProDOT derivatives (Figure 2-4). Non-substituted phenyl ProDOT and commercially available EDOT were used as references for comparison (Figure 2-4). These type of materials also offer an advantage of simplicity and relatively low cost synthesis, including few synthetic steps and simple purification, which is highly desirable for industrial applications.

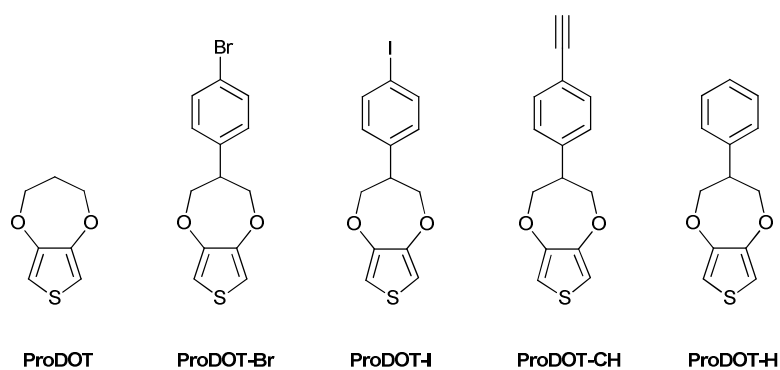
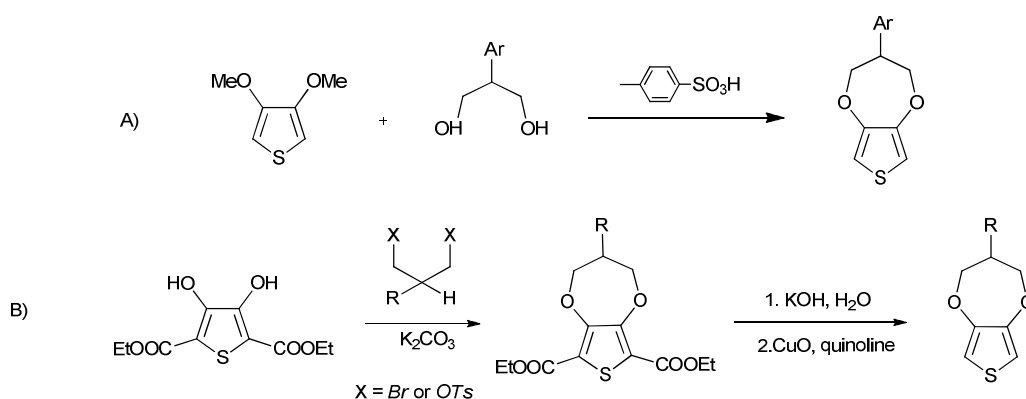


Figure 2-4: Chemical structures of ProDOT and target ProDOT derivatives

Functionalised ProDOT derivatives can be synthesised *via* two routes, either transesterification of 3,4-dimethoxythiophene with 1,3-substituted diols (with the

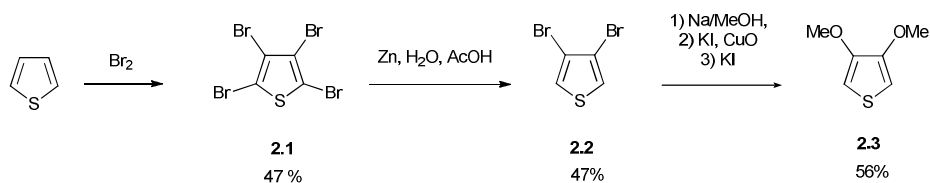
desired aromatic ring in the 2-position) in the presence of *para*-toluenesulfonic acid (Scheme 2-1A),¹⁹⁰ or *via* Williamson etherification between diethyl 3,4-dihydroxythiophene-2,5-dicarboxylate and the appropriate dibromo- or ditosyl-compound (Scheme 2-1B).¹⁹⁴ However, the latter is not suitable for neopentyl-type structures as reactions of this type were observed to be difficult or not to proceed.¹⁹⁴ Also, in the case of additional halogen functionality (such as in this case), this type of reaction could produce undesirable by-products. Therefore, route A was chosen to be a suitable method for the synthesis of the desired materials.



Scheme 2-1: General procedures for synthesis of functionalised ProDOT derivatives.

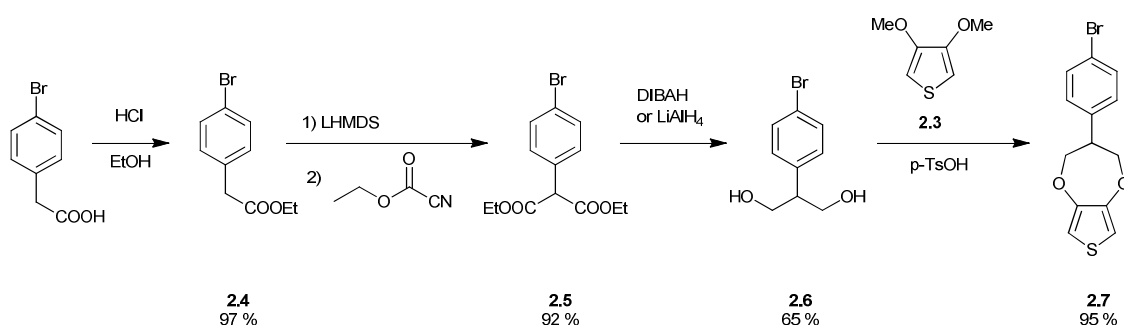
2.1.1 Synthesis of ProDOT derivatives

3,4-Dimethoxythiophene (**2.3**) was prepared from thiophene by following a well-known procedure starting with tetrabromination of thiophene with bromine, followed by selective removal of the bromines in the 2- and 5-position using zinc and acetic acid.¹⁹⁵ The final step was aromatic nucleophilic substitution of the bromines to achieve the product in moderate yield¹⁹⁶ (Scheme 2-2).



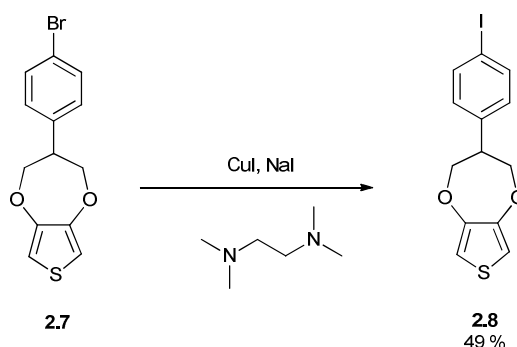
Scheme 2-2: Synthesis of 3,4 –dimethoxythiophene **2.3**.

2-(4-Bromophenyl)propane-1,3-diol was synthesised according to a previously reported procedure¹⁹⁷ (Scheme 2-3). Esterification of *para*-bromobenzoic acid was followed by condensation of ethyl cyanofornate at the α -position of the ester **2.4** to obtain 2-substituted malonate **2.5**. The yield for the reduction of the diester **2.5** was improved by using LiAlH_4 instead of the reported DIBAH. The desired final product *p*-bromophenyl-3,4-propylenedioxythiophene **2.7** was obtained by the transesterification of 3,4-dimethoxythiophene described above with 2-(4-bromophenyl)propane-1,3-diol in the presence of *para*-toluenesulfonic acid. At first only very low yields (less than 10 %) were achieved. However, optimisation of the reaction conditions, such as choice of solvent, stoichiometric ratio of the reagents, reaction temperature and duration, were investigated. The optimised conditions consist of refluxing in toluene for six days, adding a second portion of *para*-toluenesulfonic acid on the second day and using high dilution of reagents with a concentration of no more than 10 mM and a stoichiometry of 2:1 (diol:thiophene). The product was obtained in a very good yield of 95 % (equal to 47 % conversion of the diol). However, diol **2.6** is a more precious material compared to 3,4-dimethoxythiophene **2.3** in this transformation due to a higher price of reagents and the nature of synthetic steps required to make this compound. Therefore another attempt was made using 1:1 stoichiometric amounts (**2.6:2.3**) rather than 2:1 as previously reported for similar transesterification.¹⁵³ Higher conversion of the diol **2.6** is actually achieved using this method giving a yield of 69%. Therefore, this set of conditions is considered the most economical option and should be used for future synthesis.



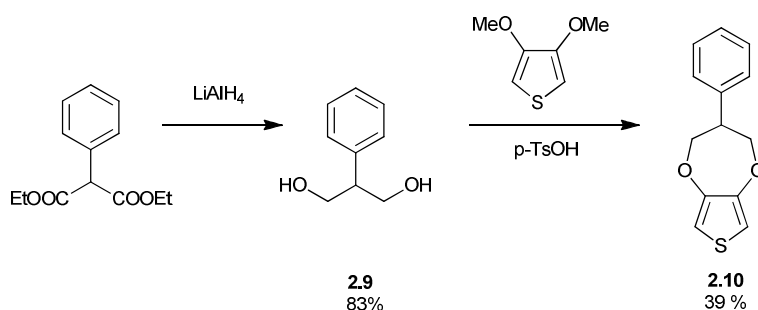
Scheme 2-3: Synthesis of ProDOT-Br **2.7**.

Iodine derivative ProDOT-I (**2.8**) was prepared from compound **2.7** via aromatic Finkelstein transhalogenation as described by Klapars and Buchwald,¹⁹⁸ using sodium iodide, copper iodide and *N,N'*-dimethylethylenediamine (Scheme 2-4). The iodinated derivative 3-(4-iodophenyl)-3,4-dihydro-2H-thieno[3,4-b][1,4]dioxepine (**2.8**) was achieved in one step in moderate yield.



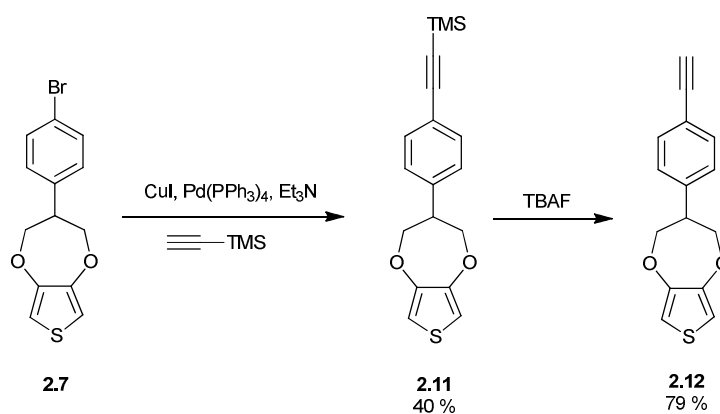
Scheme 2-4: Synthesis of ProDOT-I **2.8**.

In order to be able to investigate the strength of the proposed aryl halogen-nitro interaction and compare it to the possible π - π interaction caused by the phenyl ring itself, the reference monomer ProDOT-H **2.10** was synthesised following the procedure¹⁹⁷ for ProDOT-Br **2.7** described above (Scheme 2-5).



Scheme 2-5: Synthesis of ProDOT-H **2.10**.

The synthesis of the alkynyl derivative **2.12** is depicted in Scheme 2-6. Sonogashira coupling¹⁹⁹ of **2.7** with trimethylsilyl ethylene following by deprotection of the TMS (trimethylsilyl) group gave compound **2.12** in good yield.



Scheme 2-6: Synthesis of ProDOT-CH **2.12**.

2.1.2 Electrochemistry of ProDOT derivatives

The redox properties of monomers **2.7**, **2.8** and **2.10** in dichloromethane solution (1 mM) were assessed using cyclic voltammetry, with the oxidation and reduction of the systems shown in Figure 2-5 (a) and (b). The compounds undergo irreversible oxidations at +1.19, +1.23 and +1.30 V for **2.7**, **2.8** and **2.10**, respectively, which are attributed to the formation of a radical cation. The reductions occur approximately between -2 and -2.3 V for all three compounds, corresponding to the formation of a radical anion. The values are quoted vs. ferrocene in dichloromethane solution (1 mM), using a gold disk working electrode, silver wire as pseudoreference electrode and platinum wire as counter electrode and TBAPF₆ (*n*-tetrabutylammonium hexafluorophosphate) as the supporting electrolyte (0.1 M).

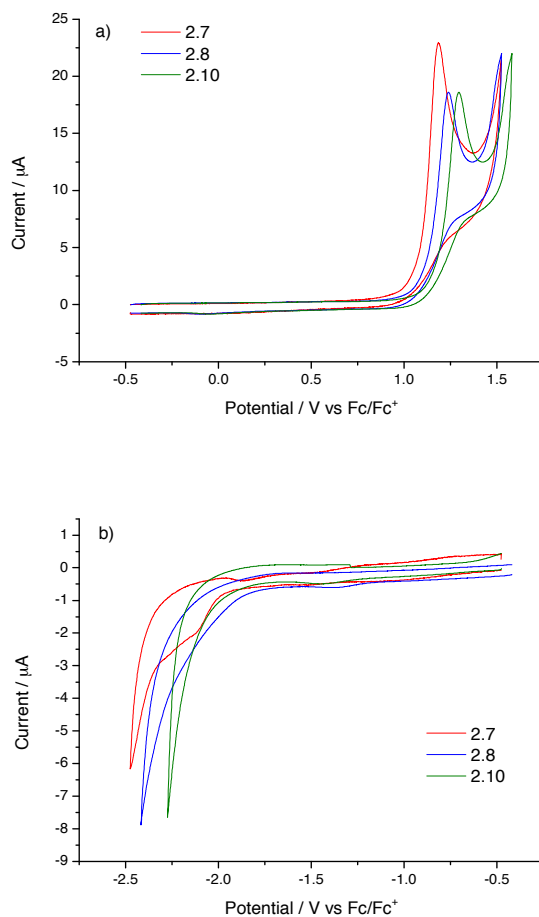


Figure 2-5: Cyclic voltammograms for the (a) oxidation and (b) reduction of monomers **2.7**, **2.8** and **2.10** in CH₂Cl₂ (1 mM), using a gold disk working electrode, Pt wire counter electrode, Ag wire pseudoreference electrode, TBAPF₆ as the supporting electrolyte (0.1 M), scan rate 100 mV/s. The data are referenced to the Fc/Fc⁺ redox couple.

Alkynyl derivative **2.12** was not suitable for our application, because it does not electropolymerise. This could be due to the presence of the terminal alkyne or poor adhesion of the compound to the electrode surface that does not allow further chain growth or deposition. The cyclic voltammogram for the oxidation of compound **2.12** in comparison to **2.7**, **2.8** and **2.10** is shown in Figure 2-6. It is observed that a new peak occurs in the cyclic voltammogram compared to the other ProDOT analogues (**2.7**, **2.8**, **2.10**), which might be attributed to the oxidation of the phenyl acetylene.

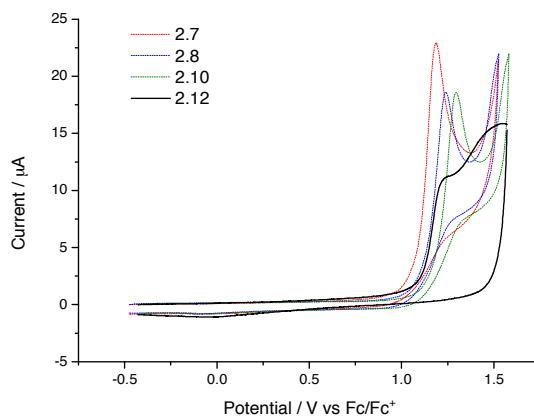


Figure 2-6: Cyclic voltammogram for the oxidation of **2.12** in comparison to **2.7**, **2.8** and **2.10**.

Compounds **2.7**, **2.8** and **2.10** were polymerised *via* electrochemical oxidation by repetitive cycling over the first oxidation wave from a dichloromethane solution of the monomer. As the conjugation increases when forming oligomers and polymers, the oxidation potentials shift to a lower value and the current increases due to the deposition of the polymer on the electrode surface. It was observed that in the case of ProDOT derivatives the polymerisation only occurs at certain concentrations of the monomer solution; this concentration must be higher than 0.5 mM. Similar concentration dependence on the polymer growth efficiency was previously observed in a ProDOT related structures.^{96, 190} The growth of the polymers over 40 cycles are presented in Figure 2-7, using a gold disk working electrode. Each polymer was subsequently dedoped by repetitive cycling between -0.2 and +0.2 V (where there is no redox activity) to produce the neutral polymer.

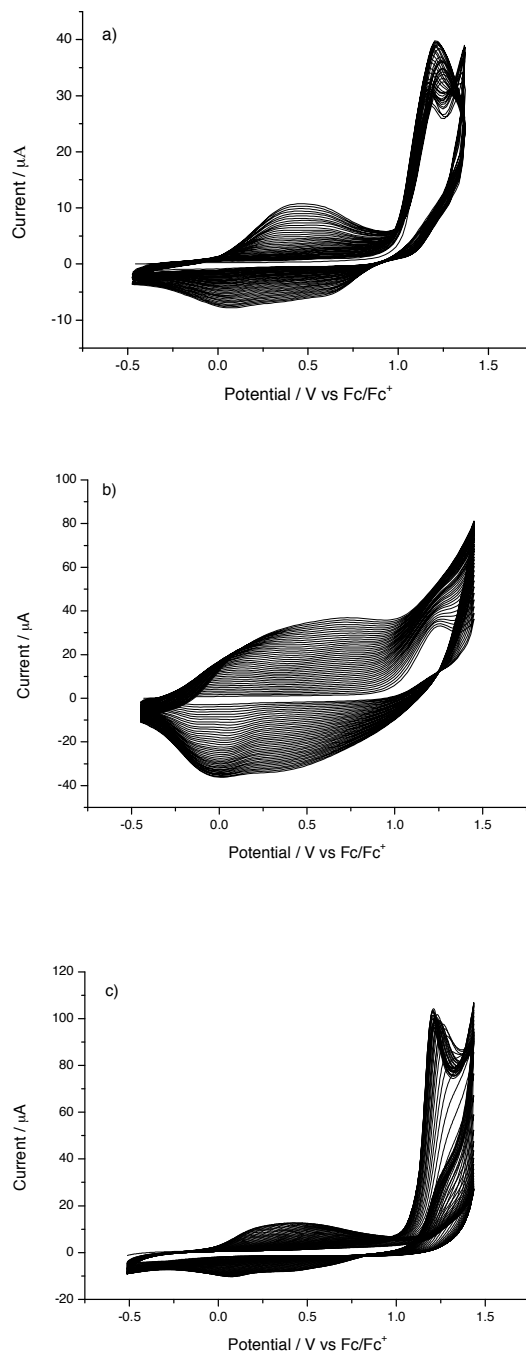


Figure 2-7: Electropolymerisation of monomers (a) **2.7**, (b) **2.8** and (c) **2.10** on a gold disk working electrode from dichloromethane solution (1 mM), using a Pt wire counter electrode, Ag wire pseudoreference electrode, and TBAPF₆ as the supporting electrolyte (0.1 M). The data are referenced to the Fc/Fc⁺ redox couple.

The redox properties of the polymer films grown on the gold electrode were also recorded, using monomer-free acetonitrile solution containing the supporting electrolyte. Fresh films were deposited for each experiment (reduction and oxidation) and the films were dedoped before proceeding. The polymers show reversible oxidation peaks at +0.63, +0.58 and +0.54 V (**2.7**, **2.8** and **2.10**) and irreversible reduction between -2.1 and -2.4 V (Figure 2-8).

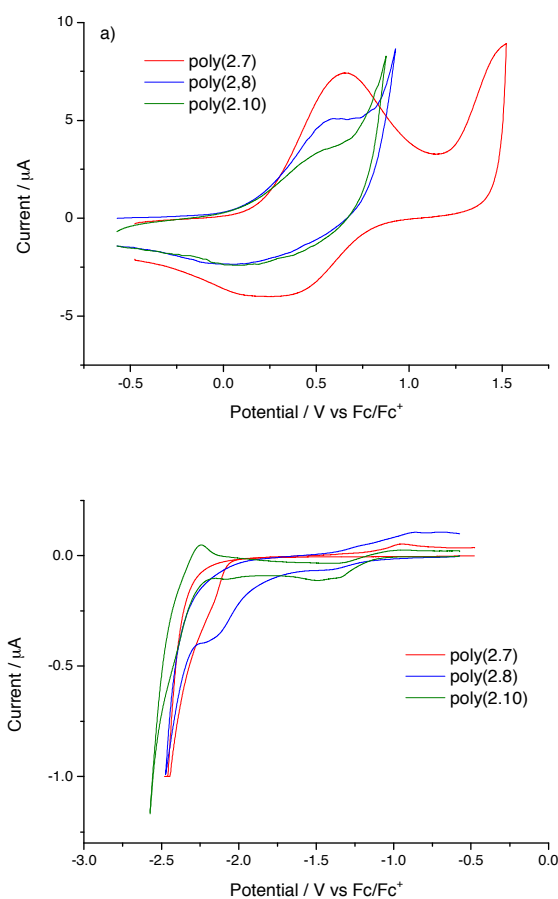


Figure 2-8: Cyclic voltammograms for the (a) oxidation and (b) reduction of poly(**2.7**), poly(**2.8**) and poly(**2.10**) as films on gold disk working electrodes in monomer-free acetonitrile solution using a Pt counter electrode, Ag wire pseudoreference electrode, TBAPF₆ as the supporting electrolyte (0.1 M). The data are referenced to the Fc/Fc⁺ redox couple.

The absorption spectra of compounds **2.7**, **2.8** and **2.10** (dichloromethane solution) and poly(**2.7**), poly(**2.8**) and poly(**2.10**) in the doped and dedoped states (as thin films on an ITO slide) are shown in Figure 2-9 and Figure 2-10.

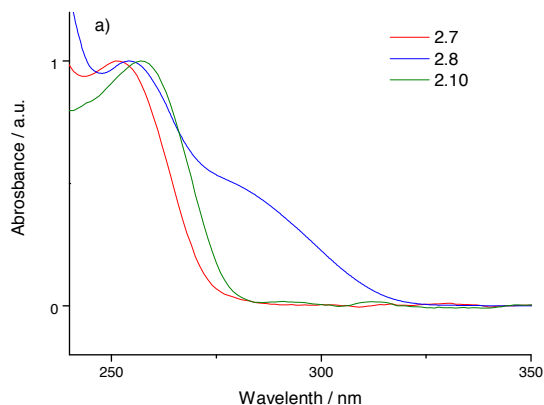


Figure 2-9: Normalised absorption spectra of monomers **2.7**, **2.8** and **2.10** in dichloromethane solution ($c = 5 \times 10^{-5}$ M).

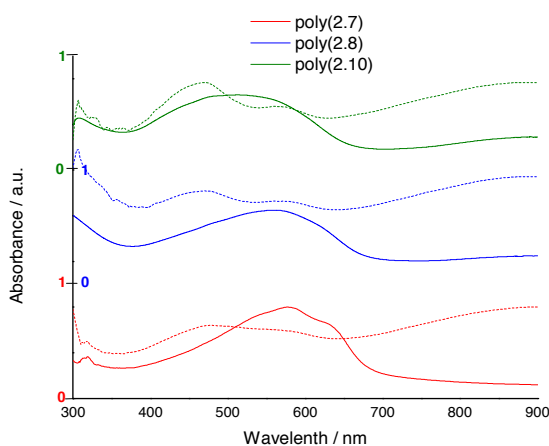


Figure 2-10: Normalised absorption spectra of poly(**2.7**), poly(**2.8**) and poly(**2.10**) as films on ITO slides in the doped (dashed line) and dedoped state (continuous line).

The polymers showed a bathochromic shift of the absorption maxima to *ca.* 580 nm, in comparison with the monomers at *ca.* 255 nm, which corresponds to the increased conjugation length. The shoulder at long wavelength in compound **2.8** can be attributed to an additional transition caused by presence of the heavy iodine atom. The new band present in the doped state of the polymer is due to the presence of polarons and bipolarons and formation of the quinoidal structure, which produce absorption bands at higher wavelengths. The difference can be also observed by the

naked eye as the freshly grown polymers are dark navy blue/black in colour and, after dedoping, turn bright violet.

Even though the band gaps of the polymers have no significant importance for sensing applications, they were calculated for completeness. The electrochemical HOMO and LUMO levels were calculated by subtracting the value of the onset of the first oxidation and reduction peaks, respectively, from the HOMO of ferrocene (-4.8 eV). The electrochemical HOMO-LUMO/band gap is the difference between the HOMO and LUMO. Table 2-1 below summarises the redox potentials and electrochemical HOMO-LUMO gaps of the ProDOT monomers and band gaps of corresponding polymers. These values are in agreement with values which were reported for analogous ProDOT structures.^{96, 189, 191} For example symmetrically substituted ProDOTs bearing hydroxymethyl or phenoxymethyl functionality were reported to have oxidation potential in range of 1.1-1.3 V (for monomers), 0.05-0.5 V (for electrochemically prepared polymers) and λ_{\max} of polymers in range of 540 – 600 nm.⁹⁶

Table 2-1: Electrochemical HOMO-LUMO gaps of ProDOT monomers and polymers.

	Onset of oxidation [V]	HOMO [eV]	Onset of reduction [V]	LUMO [eV]	HOMO-LUMO /band gap [eV]
2.7	+1.06	-5.86	-2.05	-2.75	3.11 / 4.59*
Poly(2.7)	+0.17	-4.97	-2.07	-2.73	2.24 / 1.82*
2.8	+1.02	-5.82	-2.08	-2.72	3.10 / 4.00*
Poly(2.8)	+0.13	-4.93	-2.04	-2.76	2.17 / 1.84*
2.10	+1.16	-5.96	-2.03	-2.77	3.19 / 4.51*
Poly(2.10)	+0.14	-4.94	-2.21	-2.59	2.35 / 1.90*

*Optical HOMO-LUMO and band gap.

The monomers **2.7**, **2.8** and **2.10** have the same electronic properties as there is no huge discrepancy in the recorded values. The non-substituted polymer poly(**2.10**) has a slightly higher band gap due to the higher reduction potential caused

by the absence of the halogen as the effect of this distant substituent from the polymer backbone can have greater effect in the solid state compared to a solution.

2.2 BISALKYLSULFANYL-TERTHIOPHENES

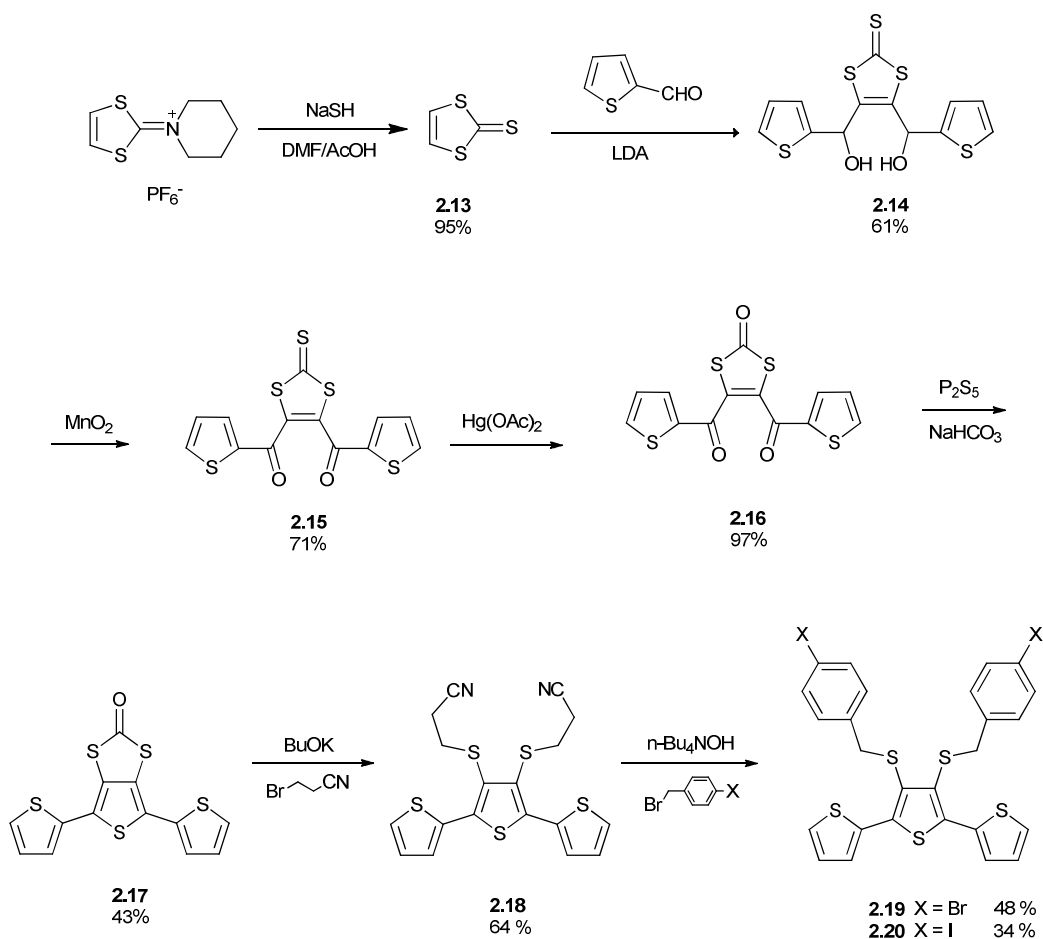
Alkylsulfanyl-terthiophenes were chosen as another suitable candidate for this application for similar reasons as the ProDOT analogues, which are as follows:²⁰⁰

- (i) These derivatives have extended conjugation throughout the terthiophene unit. Compared to alkylthiophenes, alkylsulfanyl-analogues offer greater stabilisation of the radical cation thanks to the electron-donating effect through the π -resonance contribution from the attached sulfurs. Both of these reasons contribute to the low oxidation potential and ease of electropolymerisation.
- (ii) They offer two symmetrical positions for functionalising with an arylhalo moiety, with the synthesis of such units being simple and rich yielding.

In addition to this, these derivatives allow free rotation around the short alkyl chains and are less rigid than ProDOTs. The steric hindrance in the corresponding polymers is diluted since only every third unit contains the bulky functionality. In their polymeric form, they can often be twisted preventing tight packing and therefore forming more porous materials. This is particularly desirable for sensing applications as the increased porosity and/or surface area allows deeper penetration of the analyte and a larger host-guest interface. For this project, the increased surface area is particularly important as this is one of the parameters determining the efficiency of the sensor based on the capacitive transduction scheme. This concept is discussed in detail in Chapter 4, which is devoted to the development of porous polymers.

2.2.1 Synthesis of Bisalkylsulfanyl -terthiophenes

The synthetic route to achieve terthiophene derivatives **2.19** and **2.20** is depicted in Scheme 2-7 and was previously developed and optimised within the Skabara group. First, 2-piperidino-1,3-dithiolium hexafluorophosphate was treated with sodium hydrogen sulphide in a 3:1 mixture of acetic acid and *N,N'*-dimethylformamide to obtain vinylene trithiocarbonate (VTC, **2.13**) in very high yield.²⁰¹ The diol **2.14** was achieved *via* double stepwise lithiation of VTC and subsequent trapping of the carbanion with 2-thiophenecarboxaldehyde.²⁰² The diol was immediately oxidised by manganese(IV) oxide to obtain diketone **2.15**, which was treated with mercury(II) acetate to facilitate transchalcogenation and obtain the oxone derivative **2.16** in almost quantitative yield.²⁰⁰ Paal-Knorr synthesis using phosphorus pentasulfide was applied to yield terthiophene **2.17**. Compound **2.17** reacted with potassium *tert*-butoxide followed by subsequent addition of two equivalents of 3-bromopropionitrile to give derivative **2.18** in moderate yield.²⁰⁰ The final step was electrophilic substitution on the sulfur with the corresponding benzyl halide to achieve the desired bis(alkylsulfanyl)-terthiophenes **2.19** and **2.20** in 34-48% yield.



Scheme 2-7: Synthesis of terthiophene derivatives **2.19** and **2.20**.

2.2.2 Electrochemistry of Bisalkylsulfanyl -terthiophenes

As shown previously in the case of the ProDOTs, the redox properties of monomers **2.19** and **2.20** were assessed using cyclic voltammetry (Figure 2-11). The compounds undergo irreversible oxidations at +0.89 and +0.81 V and an irreversible reduction at -2.25 and -2.27 V for **2.19** and **2.20**, respectively.

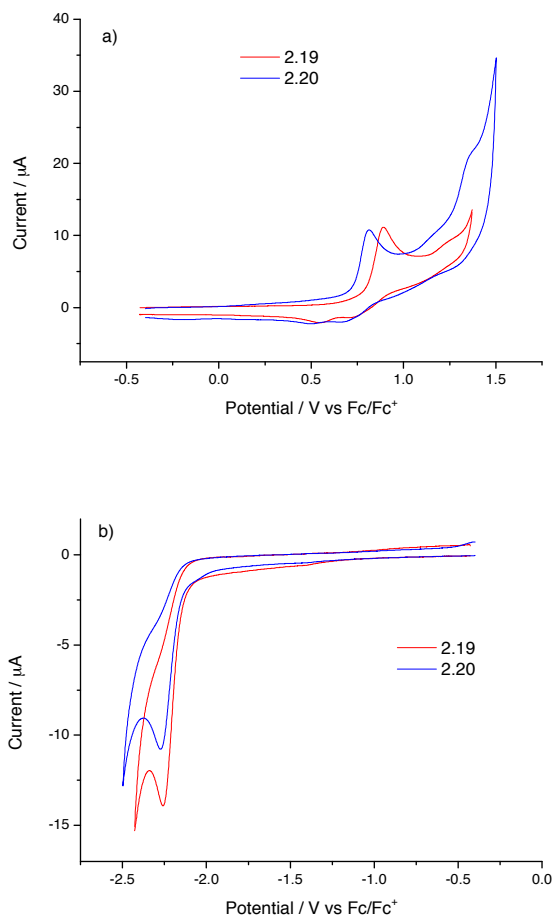


Figure 2-11: Cyclic voltammograms for (a) oxidation and (b) reduction of monomers **2.19** and **2.20** in CH₂Cl₂ (0.5 mM) using a gold disk working electrode, Pt wire counter electrode, Ag wire pseudoreference electrode, TBAPF₆ as the supporting electrolyte (0.1 M), and scan rate 100 mV/s. The data are referenced to the Fc/Fc⁺ redox couple.

As before, the monomers were dissolved in dichloromethane solution (0.5 mM), the values are quoted vs. ferrocene, using a gold disk working electrode, Pt wire counter electrode, Ag wire as the reference electrode and TBAPF₆ (*n*-tetrabutylammonium hexafluorophosphate) as the supporting electrolyte (0.1 M).

Compounds **2.19** and **2.20** were polymerised *via* electrochemical oxidation by repetitive cycling over the first oxidation wave. The solubility of these polymers in dichloromethane proved to be unfavourable for sufficient polymer growth, therefore the solvent choice was altered to dichloromethane/hexane (3/1), which made a

significant difference. The growths of the polymers over 40 cycles are presented in Figure 2-12. The voltammograms show an increase in current with each cycle and the development of a new peak at a lower oxidation potential due to the emergence of the polymer.

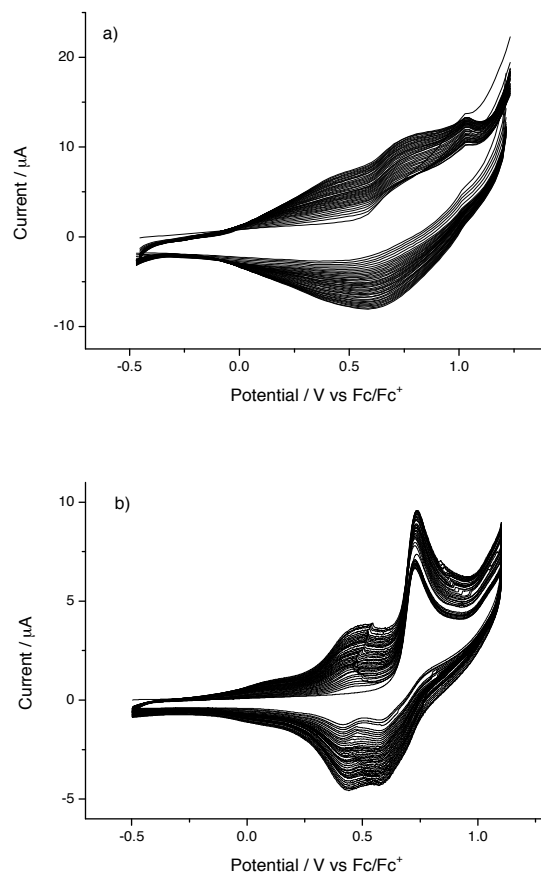


Figure 2-12: Electropolymerisation of compounds (a) **2.19** and (b) **2.20** on a gold disk working electrode from dichloromethane/hexane (3/1) monomer solution, using a Pt wire counter electrode, Ag wire pseudoreference electrode, and TBAPF_6 as the electrolyte (0.1 M).

The redox properties of the polymer were investigated by cyclic voltammetry in monomer-free acetonitrile solution (Figure 2-13). The polymers show a broad reversible oxidation wave at +0.71 and +0.75 V for poly(**2.19**) and poly(**2.20**), respectively, and a reduction onset at *ca.* -1.6 V.

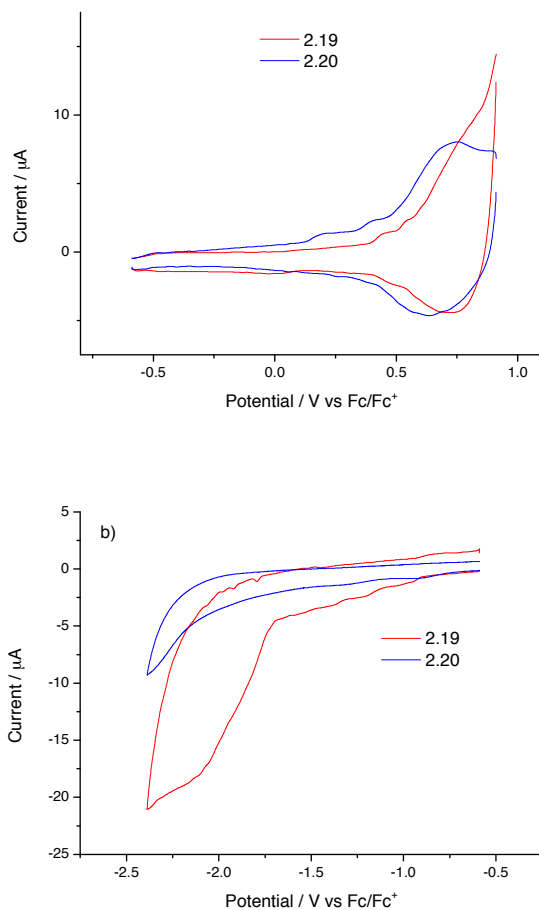


Figure 2-13: Cyclic voltammograms for (a) oxidation and (b) reduction of poly(**2.19**) and poly(**2.20**) as films on a gold disk working electrode in monomer-free acetonitrile solution using Ag wire pseudoreference electrode, TBAPF₆ as the supporting electrolyte (0.1 M). The data are referenced to the Fc/Fc⁺ redox couple.

The absorption spectra of compounds **2.19** and **2.20** (dichloromethane solution) and poly(**2.19**) and poly(**2.20**) in their dedoped state (thin films on ITO slides) are shown in Figure 2-14 and Figure 2-15. The polymers show a bathochromic shift of absorption maxima (528 nm) compared to their monomers (that have absorption maxima at 360 nm).

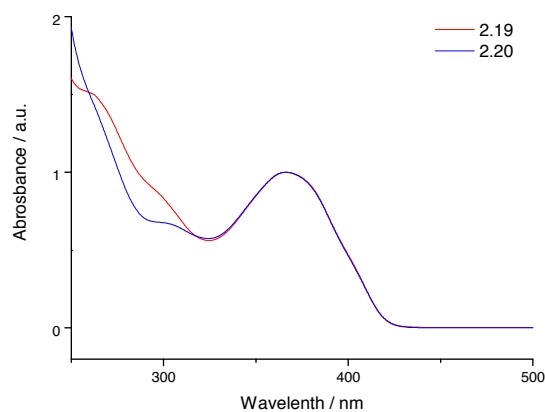


Figure 2-14: Normalised absorption spectra of compound **2.19** and **2.20** in dichloromethane solution.

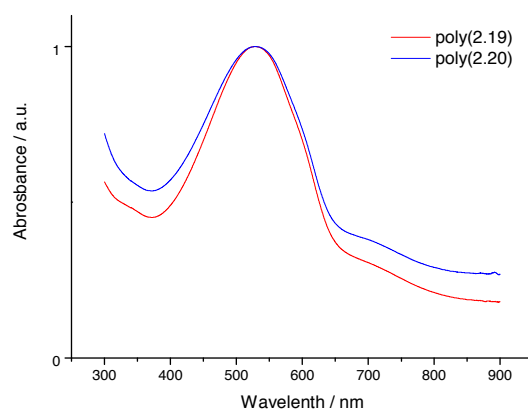


Figure 2-15: Normalised absorption spectra of poly(**2.19**) and poly(**2.20**) as films on ITO slides.

Table 2-2: Electrochemical and optical gaps of monomers **2.19** and **2.20** and corresponding polymers.

	Onset of oxidation [V]	HOMO [eV]	Onset of reduction [V]	LUMO [eV]	HOMO-LUMO/band gap [eV]
2.19	+0.82	-5.62	-2.10	-2.70	2.92 / 2.98*
Poly(2.19)	+0.50	-5.3	-1.65	-3.15	2.15 / 1.90*
2.20	+0.75	-5.55	-2.07	-2.73	2.82 / 2.98*
Poly(2.20)	+0.44	-5.24	-1.69	-3.11	2.13 / 1.93*

*Optical HOMO-LUMO and band gaps.

As with the ProDOTs, the HOMO and LUMO levels were calculated from the onset of the first peak of the corresponding redox waves and referenced to ferrocene, which has a HOMO of -4.8 eV.

Compared to the literature values of similar bisalkylsulfanyl terthiophenes (Figure 2-16, **2.21** – **2.24**),²⁰⁰ the electrochemical band gaps of poly(**2.19**) and poly(**2.20**) are considerably higher. This could be caused by the presence of electron rich moieties such as an aromatic ring which makes the reduction unfavourable and therefore lowers the LUMO level and increases the band gap. The optical band gaps of the polymers are comparable with the most sterically hindered derivative containing a bulky hexyl chain **2.22**. This is in good agreement with the expectation since the aromatic rings in poly(**2.19**) and poly(**2.20**) could increase steric hindrance between the dithio fragment and the two neighbouring thiophene rings, which would affect the donor abilities of the molecules.²⁰⁰

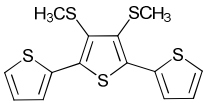
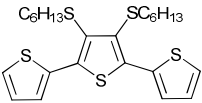
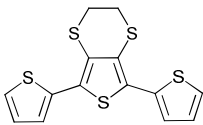
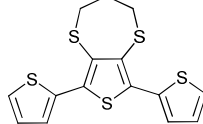
				
	2.21	2.22	2.23	2.24
Optical band gap / eV	1.58	1.97	1.53	1.45
Electrochemical band gap / eV	1.54	1.61	1.44	1.43

Figure 2-16: Electrochemical and optical band gap of other bisalkylsulfanyl terthiophenes **2.21** – **2.24** previously reported within the Skabara group.²⁰⁰

2.3 CONCLUSION

Several novel derivatives of ProDOT (**2.7**, **2.8**, **2.10**, **2.12**) and bisalkylsulfanyl-terthiophenes (**2.19**, **2.20**) were synthesised in good yields. With exception of alkynyl-ProDOT (**2.12**), which does not electropolymerise, all other derivatives and their corresponding polymers were characterised by means of cyclic voltammetry and the absorbance spectra were also recorded. The electrochemical and

optical HOMO-LUMO/ band gaps were determined and found to be in a good agreement with literature values reported for similar compounds.

All the materials were subsequently electrochemically deposited onto a gold interdigitated electrode (IDE) and tested as potential sensors for nitro-containing compounds related to explosives. The sensor performance results are discussed in the next chapter.

Chapter 3

3 SENSOR FABRICATION AND EVALUATION

3.1 SENSORS FABRICATION

To coat the developed monomers onto a viable sensor platform, commercial metallic interdigitated electrodes (IDEs) on glass chips were purchased from Abtech Scientific Inc (USA). Each IDE device consisted of 25 pairs of 100 nm thick gold electrodes, with each digit 15 microns wide and 3000 microns long, and an interdigit space of 15 microns (as shown in Figure 3-1). The IDE device was situated on a borosilicate glass substrate and the chip as a whole contained two IDE devices to allow two different polymers to be electrochemically grown on a single chip. Each IDE device had two gold tracks linked to bonding pads at the top edge of the chip to allow wire bonding and thus electrical connection to each set of electrodes. These tracks were themselves covered in a protective polymer coating (that was resistant to dissolution in dichloromethane) so that polymer growth was localised on the electrode pairs and not on the tracks during electropolymerisation. Such a sensor format we refer to as a *chemicapacitor*.

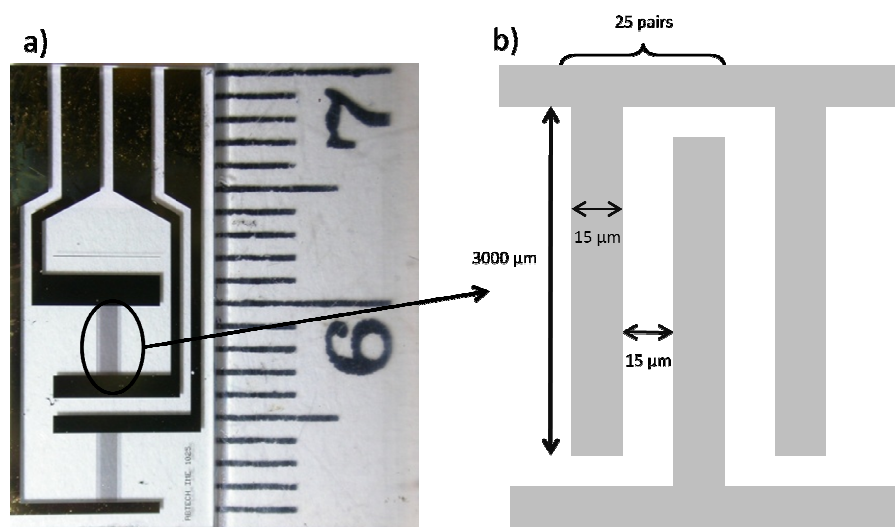


Figure 3-1: a) A chip purchased from Abtech Scientific Inc., (the scale is in cm) b) Detail of the electrode structure.

Growth of the polymer upon these chips was completed using standard cyclic voltammetry apparatus (BAS model CV50W Voltammetric Analyser, Bioanalytical Systems Inc., USA). The configuration is shown in Figure 3-2 where the IDE chip

was used as the working electrode, while platinum wire was the counter electrode, and silver wire was a pseudoreference electrode (referenced to ferrocene). Polymer films were grown on the electrodes *via* electrochemical oxidative polymerisation of the monomers from 1 mM dichloromethane solutions containing *n*-tetrabutylammonium hexafluorophosphate (TBAPF₆) as the supporting electrolyte, by repetitive cycling over the first oxidation wave.

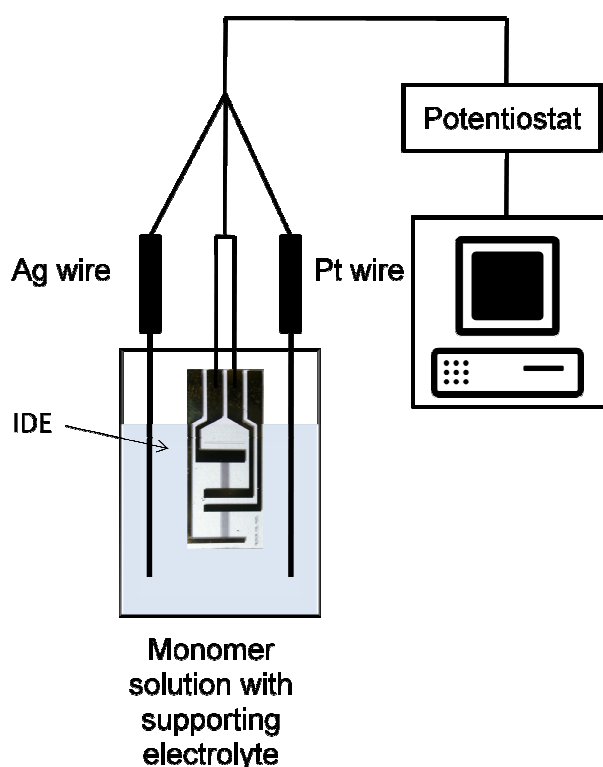


Figure 3-2: Schematic drawing of the three electrode cell system. The synthesised monomers were dissolved in dichloromethane (1 mM).

An example of the growth of ProDOT-Br (**2.7**) on the gold electrode over 40 cycles is shown in Figure 3-3. Since the growth is almost identical to that observed using the standard gold electrode and the gold chips are made of high quality, it is reasonable to assume a high reproducibility of the sensor fabrication.

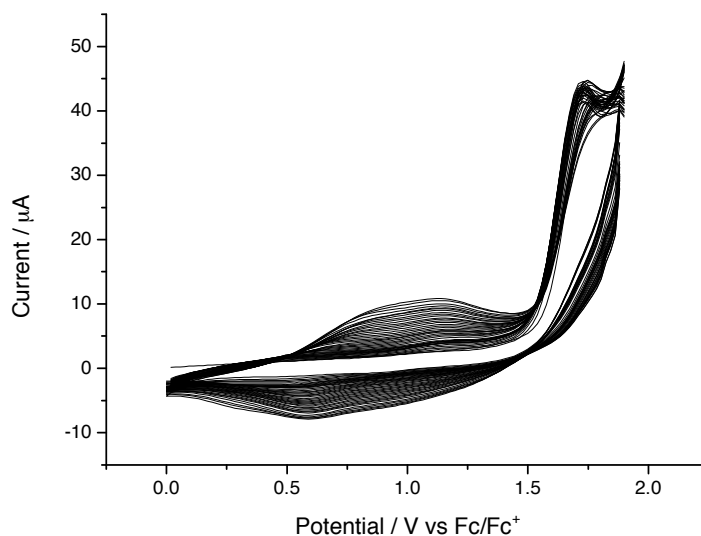


Figure 3-3: Electropolymerisation of **2.7** on a gold Abtech Chip.

During standard growth experiments, electropolymerisation times varied from *ca.* 40 to 60 minutes depending on the number of cycles (usually 20 to 50 cycles). Different polymer types were grown on each of the two IDE devices for comparative experiments. This was achieved by immersing the whole chip into the monomer solution but only connecting one device to the potentiostat. Thus, a sensing and reference polymer could be created on the same chip (Figure 3-4). This is one of the advantages of electrochemical growth in that individual sensors can be formed locally on a substrate by control of the electrical current path. This has a particular commercial application in forming low cost, mass produced sensors on silicon wafers by creating different types of sensors on the same wafer by dipping into different monomer solutions.

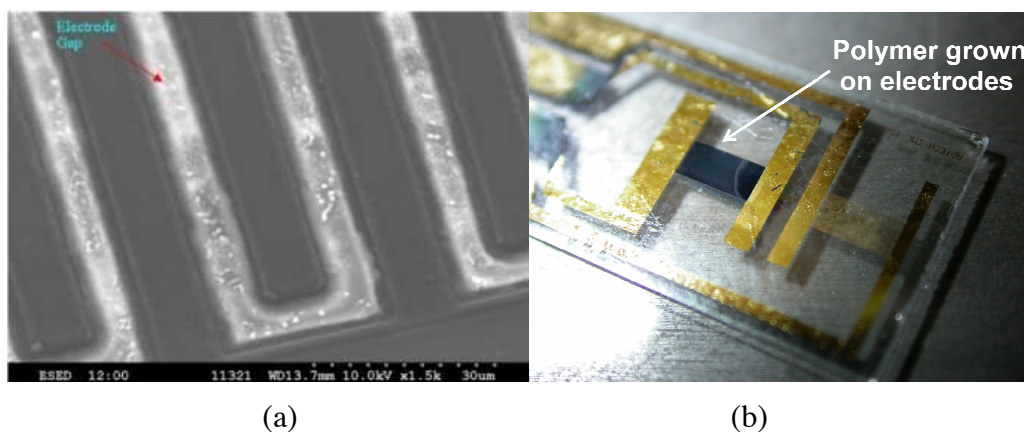


Figure 3-4: a) SEM image of the interdigitated electrodes coated electrochemically with poly(**2.7**) polymer. (b) Glass chip with two IDE devices coated with polymer films. Chip dimension 20×10mm.

The thickness of the films can be altered by changing the concentration of the monomer solution or varying the number of cycles during electropolymerisation. The thickness of polymer films was examined by taking the average of nine thickness measurements on each chip using an Alpha-Step IQ Surface Profiler (KLA Tencor Corp.). A major issue in this assessment is the protective layer around the electrodes, which does not allow a reference measurement. The only position of uncoated substrate is between the electrodes, but this may also be coated with polymer up to a certain unknown level, especially at the edge of the gold substrate. Nevertheless, the thickness determination was carried out assuming that there is an actual “blank” reference point between the electrodes. This assumption is reasonable because the nonconductive glass between the electrodes will not result in polymer growth since it is not a favourable place for the polymer coating to grow laterally and the coatings were intentionally not thick enough to bridge the gap between the electrode fingers. Table 3-1 summarises the results obtained for the thickness measurements on the Abtech chips coated by polymers **2.7**, **2.8**, **2.10**, **2.19** and **2.20**. Each electrode was examined at several different positions and an average value was considered. Also, for reproducibility purposes, each polymer was grown at least twice under the same experimental conditions on different chips and the results were compared and observed to be in good agreement.

Table 3-1: Summary of thicknesses for homopolymers deposited on Abtech IDEs.

Polymer	C_{monomer} [mM]	No. of cycles	Thickness [nm]
poly(2.7)	1	40	310 - 456
poly(2.8)	1	40	219 - 256
poly(2.10)	1	40	454 - 627
poly(2.19)	0.5	50	146 - 177
poly(2.20)	0.5	50	203 - 252

In order to investigate the dependence of the film thickness on the polymerisation conditions, several different films of poly(2.7) were grown and compared (Figure 3-5). The monomer solutions for the individual growths were prepared by dilution from one main monomer stock solution to eliminate experimental weighing error.

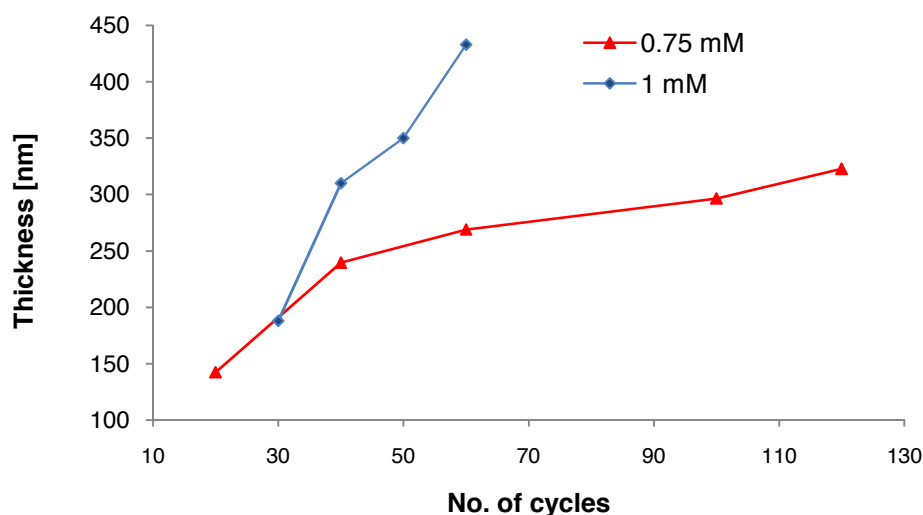
**Figure 3-5:** Graph of thickness of the poly(2.7) film vs. no of cycles applied during electropolymerisation.

Figure 3-5 shows that the thickness is proportional to the number of cycles used during the electropolymerisation process and the higher the concentration of monomer in the solution for polymer growth, the steeper the dependence of thickness on the number of cycles. Also, as could be expected, the dependence is not linear. This may be for two reasons; (i) as the film is being formed on the surface, the resistance builds up, the conductivity of the film diminishes and therefore subsequent growth is partially prevented; (ii) the monomer in solution is consumed and therefore the concentration at the electrode vicinity lessens.

3.2 PRELIMINARY SENSOR TESTING – STATIC CHAMBER

In order to investigate the performance of the fabricated sensors, several initial tests were carried out within a homemade test-bed comparing the behaviour of customised polymer based on ProDOT-Br (poly(**2.7**)) and commercially available PEDOT towards several different analytes.⁹⁴ For this purpose, a sealed temperature and humidity-controlled glass chamber was built (in-house), which is schematically shown in Figure 3-6. The system consist of a thick walled sealed glass container of *ca.* 1L volume equipped with an external water jacket, which regulates the temperature and keeps it stable during the measurement. Inside the chamber, a humidity sensor (HIH-4000, Honeywell) and a temperature sensor (HEL-775-B-T-1, Honeywell) were placed to measure these variables. During the course of a standard experiment, dry nitrogen gas was flowed through the system until the relative humidity was stable at less than 1%, after which the nitrogen flow was reduced to give just a slight positive pressure. Each sensor chip to be tested was mounted in the centre of the chamber on wire clips. BNC (bayonet Neill–Concelman) cables ran from these connectors externally to two instruments for simultaneous measurement of the capacitance of each IDE on the glass chip. An LCR meter (E4980A, Agilent Ltd.) and an Impedance Analyser (4294A, Agilent Ltd.), both operating at excitation frequency of 100 kHz, were connected to the chips in order to measure simultaneously the capacitance changes of the poly(**2.7**) and PEDOT sensor induced

by the interaction of the polymer film with analytes introduced into the atmosphere of the sealed chamber.

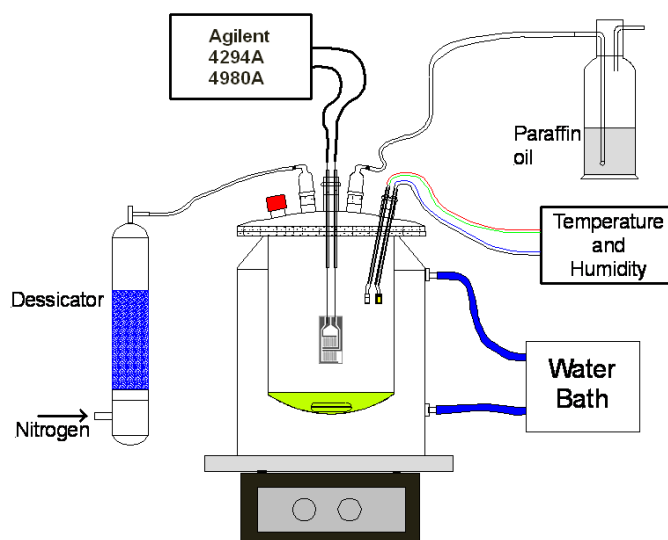


Figure 3-6: Customised test chamber for evaluating polymer sensor performance to different analytes.

It was not possible to use explosives directly in the laboratory for health and safety reasons. Therefore nitrobenzene and 1-nitropropane were used as proxies to explosives to generate nitro vapours to test the polymers as potential explosive detectors. For comparative purposes, other volatile organic compounds (VOC) such as octane, methanol, ethyl acetate, toluene and tetrahydrofuran, analytes commonly found in the atmosphere, were also employed to investigate cross-sensitivity of the sensors. Nitrobenzene was distilled and stored over 4 Angstrom molecular sieves; toluene, tetrahydrofuran and hexane were obtained from a solvent purification system (SPS 400, innovative technologies) using alumina as the drying agent; acetone, ethyl acetate (anhydrous), and ethanol (anhydrous) were purchased from Sigma Aldrich and used as received. The individual solvents were carefully placed at the bottom of the chamber *via* a needle through the septum in the lid and continuously stirred to generate a saturated atmosphere around the sensor and the capacitance reading was subsequently recorded.

Figure 3-7 demonstrates a comparison of the response of the ProDOT-Br (poly(2.7)) sensor and the PEDOT sensor using methanol and 1-nitropropane as

representatives of interfering and targeted analytes, respectively. It was observed that both PEDOT and ProDOT-Br capacitive sensors gave a similar magnitude of response within a methanol vapour atmosphere, showing less than a 1 pF capacitance change. However, when the methanol atmosphere was replaced by a nitropropane atmosphere the response of ProDOT-Br sensor to 1-nitropropane was over 500 pF (7.2–529.8 pF), whereas the PEDOT-based sensor capacitance change remained less than 1 pF (13.0–13.8 pF). This was a very promising result as it showed the high sensitivity of this sensor to target nitro-bearing compounds, as well as a good reversibility of the response since, after withdrawal of the 1-nitropropane vapour, the capacitance quickly returned close to its initial value.

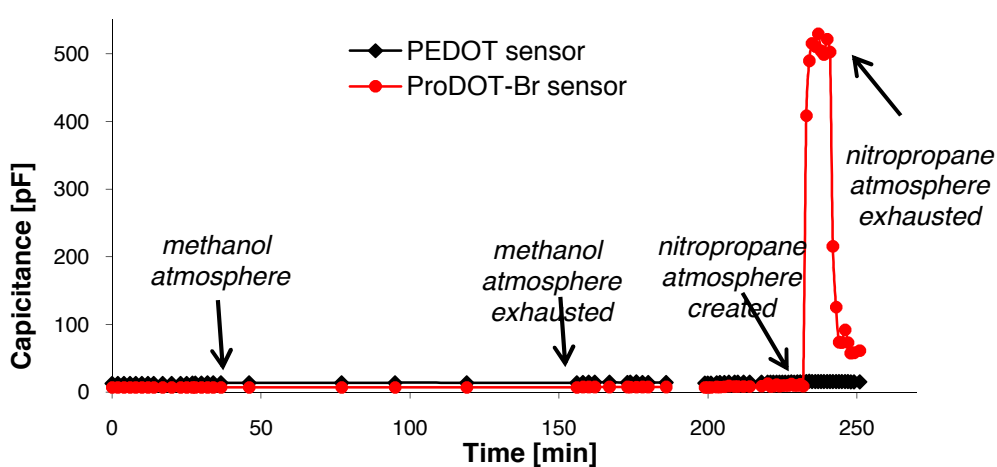


Figure 3-7: Response of PEDOT and ProDOT-Br sensor to methanol and 1-nitropropane.

Other solvents were tested as possible interferences in the same manner. There is a large discrepancy of boiling point and hence vapour pressure in the tested analytes, ranging from 65 °C for methanol, up to 211 °C for nitrobenzene, which caused different concentrations of the saturated vapours inside the chamber. The concentration in parts per million (ppm) is without units and is often quoted either with regards to volume or moles of present gases. 1 ppm is equal to a fraction of 1 unit of calculated gas (moles) over 10^6 inert gas (moles), which is in our case dried nitrogen (equation 3-1).

$$1 \text{ ppm} = \frac{1 \text{ } \mu\text{mole of gas}}{1 \text{ mole of nitrogen}} \quad (3-1)$$

The number of moles of gas in a closed system can be calculated using the ideal gas law (equation 3-2),

$$n = \frac{pV}{RT} \quad (3-2)$$

where p is considered to be atmospheric pressure (101,325 Pa) when calculating nitrogen and the saturated vapour pressure when calculating the inserted volatile, V is the volume of the test chamber (1L), R is the gas constant (8.314 J K⁻¹mol⁻¹) and T is the temperature measured inside the chamber for each experiment (20 - 26 °C). Thus, the number of moles of nitrogen inside the chamber is 0.041 (for the whole temperature range).

The saturated vapour pressure of a volatile (mmHg) can be calculated from the Antoine equation (3-3) for each volatile.

$$\log_{10} p_{sat} = a - \frac{b}{T+c} \quad (3-3)$$

Where T is temperature (°C) and a , b , c are the Antoine coefficients summarised in Table 3-2 for selected volatiles.

Table 3-2: Antoine coefficient for selected volatiles, T is in °C and p in mmHg.

Solvent	a	b	c	T_{min}	T_{max}
Acetone ¹⁷⁶	7.117	1210.595	229.664		liquid
Ethanol ¹⁷⁶	8.321	1718.100	237.520	-2	100
Ethyl acetate ¹⁷⁶	7.102	1244.950	217.880	15	76
Hexane ¹⁷⁶	6.876	1171.170	224.410	-25	92
Methanol ¹⁷⁶	7.897	1474.080	229.130	-14	65
Nitrobenzene ²⁰³	7.545	2064.000	230.000	6	23
1-Nitropropane ¹⁷⁶	7.495	2086.100	230.000	50	222
2-Nitrotoluene ²⁰³	7.114	1467.450	215.230	59	131
Octane ¹⁷⁶	6.909	1340.800	209.385	19	132
Tetrahydrofuran ¹⁷⁶	6.995	1202.290	226.290	23	100
Toluene ¹⁷⁶	6.954	1344.800	219.480	6	137

Thus, for example in the case of the targeted volatile nitrobenzene, the saturated vapour pressure at 23 °C is 0.24 mmHg (or 32.5 Pa), which is equal to 13.2 μmol of nitrobenzene vapour inside the chamber. Therefore, assuming complete saturation and equilibrium, according to equation (3-1) the concentration in a 1L enclosed chamber is 320 ppm (0.320 ppth).

The difference in concentration restricts direct comparison of capacitance change acquired directly from the measurement. Therefore the results obtained were recalculated and normalised to 1 ppth of each vapour, thus allowing a response comparison (Table 3-3).

Table 3-3: Measured and normalised capacitance response of ProDOT-Br and PEDOT sensor to various VOCs.

Chemical	Concentration [ppth]	T [°C]	Observed response [pF]		Normalised response to 1 ppth [pF]	
			ProDOT-Br	PEDOT	ProDOT-Br	PEDOT
1-Nitropropane	15	25	523	0.80	34.840	0.0533
Nitrobenzene	0.320	23	346	0.31	1081.975	0.968
Tetrahydrofuran	170	20	0.534	1.6	0.00313	0.00941
Methanol	170	25	0.456	2.25	0.00268	0.0132
Toluene	30	20	0.208	1.25	0.00693	0.0415
Octane	15	20	0.137	0.15	0.00913	0.00993
Ethyl Acetate	132	26	0.023	0.24	0.000178	0.00184

Finally, Figure 3-8 (with a logarithmic scale) summarises the response of the ProDOT-Br and PEDOT sensors exposed to different VOCs under the same conditions. For ease of presentation, the results are shown as the relative response to

the smallest obtained capacitance change, which is the PEDOT-Ethyl Acetate response, set at 50 units.

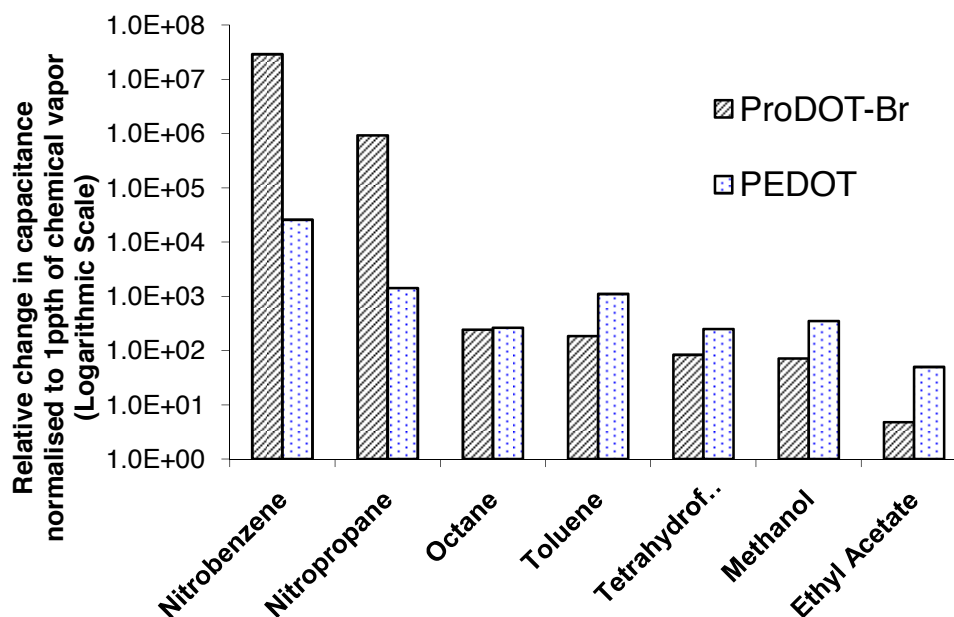


Figure 3-8: Comparison of PEDOT and ProDOT-Br to various VOCs.

These results demonstrate a response up to three orders of magnitude higher towards nitro-containing compounds such as nitrobenzene and nitropropane, than other VOCs. These preliminary results were very encouraging and validated our initial goal of tailoring monomers to target analytes, growing them electrochemically on miniature metallic substrates, and demonstrating a sensitive and selective response to the target analyte. In addition, with this level of discrimination against interfering chemicals in the atmosphere, it may be possible to construct single sensors rather than arrays of sensors that use pattern recognition algorithms to reveal concentration data on the target molecules.⁴⁷

3.3 SENSORS EVALUATION - DYNAMIC SYSTEM

Following these initial results, the experimental test-bed was changed to allow a dynamic flow of vapours of varying concentration. This system consists of

three main parts – a vapour-generating bubbler, the dilution system and the detection chamber (Figure 3-9).

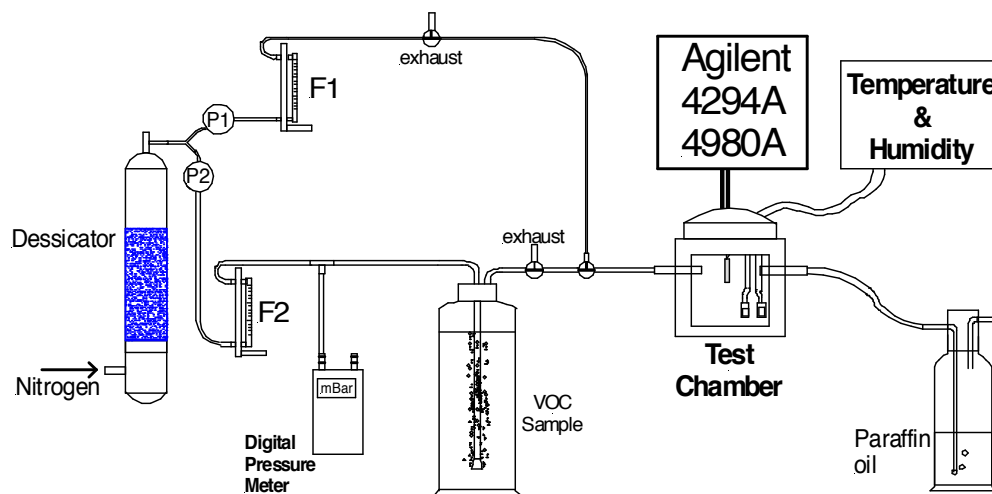


Figure 3-9: In-house made testing chamber using a dynamic flow of VOCs.

The carrier gas (dry nitrogen) was split into two lines - the dilution line with a flow controller (F1, Platon NGX, Roxspur Measurement & Control Ltd., UK) with an adjustable flow rate of between 20 to 250 mL/min and the carrier line with an identical flow meter (F2) and digital pressure meter (Anton APM 1300). The carrier line enters the fritted glass bubbler situated inside a glass tube filled with the individual chemicals and equipped with a water jacket around it to stabilise the temperature throughout the experiment. The glass tube used was 330 mm in length and the glass air stone was situated at the end of an extended (in-house) glass test tube. The bubbler provides a distribution of nitrogen through the liquid and allows uniform and efficient vapour generation. The carrier gas leaves the vapour-generating system enriched by a vapour of the analyte. For simplicity, in the calculations it was assumed that this concentration was equal to the saturated vapour concentration. Avoiding this assumption would be possible only by incorporating an extra instrument that would measure the real concentration generated such as a gas chromatograph (GC), but such equipment was unavailable. However, this assumption is very reasonable as it is the highest possible overestimation; in fact the real concentration is likely to be lower. Therefore the sensor performance is actually

underestimated, because the measured response is in reality likely to be of a lower concentration than the reported value. This concentration can be varied by the dilution line by changing the ratio between the two flow controllers, because the carrier and dilution lines are subsequently connected back together before entering the detection chamber where the polymeric sensor is placed. The concentration of the analyte can be calculated from equation 3-4;²⁰⁴⁻²⁰⁶

$$c_{analyte}(ppm) = \frac{10^6 \alpha}{F_1/F_2 + 1 + \alpha} \quad (3-4)$$

where α represents the vapour pick-up efficiency, F_1 is the dilution flow measured at F1 (sscm, standard cubic centimetres per minute) and F_2 is the carrier flow measured at F2 (sscm). Assuming that the stream leaving the bubbler contains saturated vapour, α can be calculated from equation 3-5;²⁰⁴⁻²⁰⁶

$$\alpha = \frac{p_{sat}}{p_i} \quad (3-5)$$

where p_i is the input pressure to the bubbler that is measured on the digital differential manometer (mbar) and p_{sat} is the saturated vapour pressure, which can be calculated from the Antoine equation (3-3), mentioned above.

The detection chamber was made much smaller than the one used previously. Once again, the chamber was a sealed glass container; however, it was 60 mm in diameter and 55 mm in height, with an in-built water jacket to assure a stable temperature. As previously described, the same commercial humidity and temperature sensors were placed inside the chamber in order to ensure a repeatable environment and the electrical response of these sensors was again recorded with the impedance analyser and LCR meter (excitation frequency 100 kHz). The vapour inlet and outlet pipes were located on opposite sides of the chamber and the fabricated polymeric sensor was placed in front of the inlet tube to interact fully with the vapour stream and minimise any error caused by dispersion inside the chamber. Throughout the apparatus, inert glass tubing was used to avoid any absorption from the vapour stream, which was a problem encountered when using plastic tubing. To allow switching between removal of the vapour out of the system or entering into the test

chamber, an exhaust tap was included after the bubbler. Additionally, a 25 mm long section of SiO₂ glass wool (Sigma Aldrich) was placed inside the glass tubing before the test chamber to increase flow turbulence and maximise mixing of the vapor and diluting nitrogen gas.²⁰⁷

Prior to each experiment, each volatile was bubbled through for at least 2 hours (sometimes overnight in the case of nitrobenzene) in order to achieve stability in the analyte concentration. Also, before each experimental run, pure nitrogen was flowed through the test chamber to purge and maintain the humidity within the chamber at below 5%.

3.4 COMPARISON OF SYNTHESISED HOMOPOLYMERS IN SENSOR PERFORMANCE

3.4.1 ProDOTs comparison

At first, experiments were carried out to compare the influence of different halogen functionalisation at the *para*-phenyl position of the ProDOT derivatives on the sensor performance. Halogenated polymers poly(2.7) and poly(2.8) were grown using the same conditions (40 cycles, 1 mM monomer solution in dichloromethane) and subsequently tested against nitro vapours. From Figure 3-10 and Figure 3-11, it can be seen that ProDOT-Br poly(2.7), in comparison to its iodinated analogue poly(2.8) has at least double the magnitude of capacitance change when exposed to nitropropane and nitrobenzene. In addition, poly(2.7) films generally exhibit much better reproducibility and faster response time. It should be noted that the minimum analyte vapour flow rate available was 20 mL/min and the maximum nitrogen dilutant flow was 250 mL/min, which limited the minimum concentration that could be achieved for the more volatile chemicals to several thousand ppm; such is the case for 1-nitropropane. In order to achieve lower concentration, an extra dilution line would have to be incorporated or a flowmeter with a wider range of flow rates would have to be used. The nitropropane response showed to be nonlinear, especially when

reaching concentrations above 10,000 ppm where the response suddenly increased by a factor of 10.

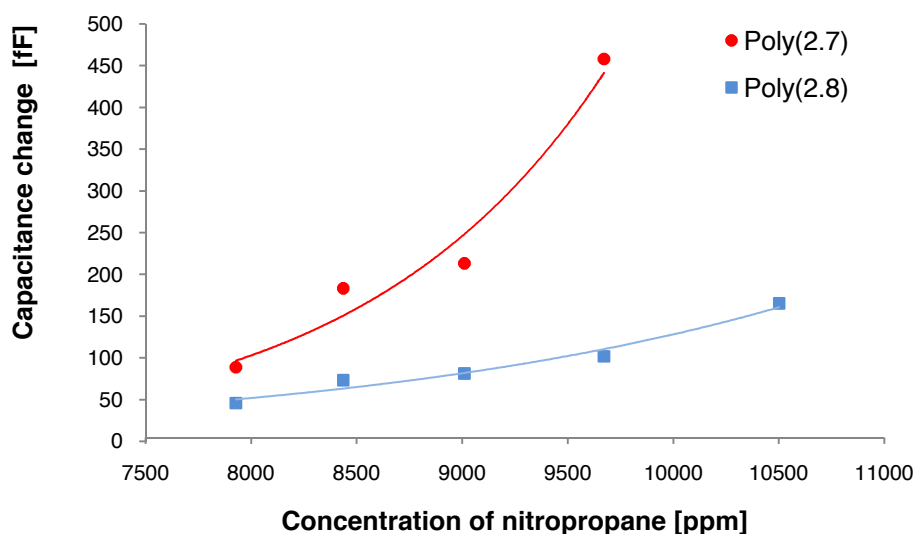


Figure 3-10: Response of poly(2.7) and poly(2.8) to nitropropane at different concentrations. Nitropropane flow set at 250 mL/min and kept constant throughout the measurement.

Nitrobenzene has a higher boiling point of 211 °C and this allowed the vapour concentration to be reduced to around 15 ppm. In this sub-100 ppm region the nitro sensor exhibited a linear response to a change in nitrobenzene concentration but, again, when approaching higher concentrations, the nonlinear response occurred (Figure 3-11).

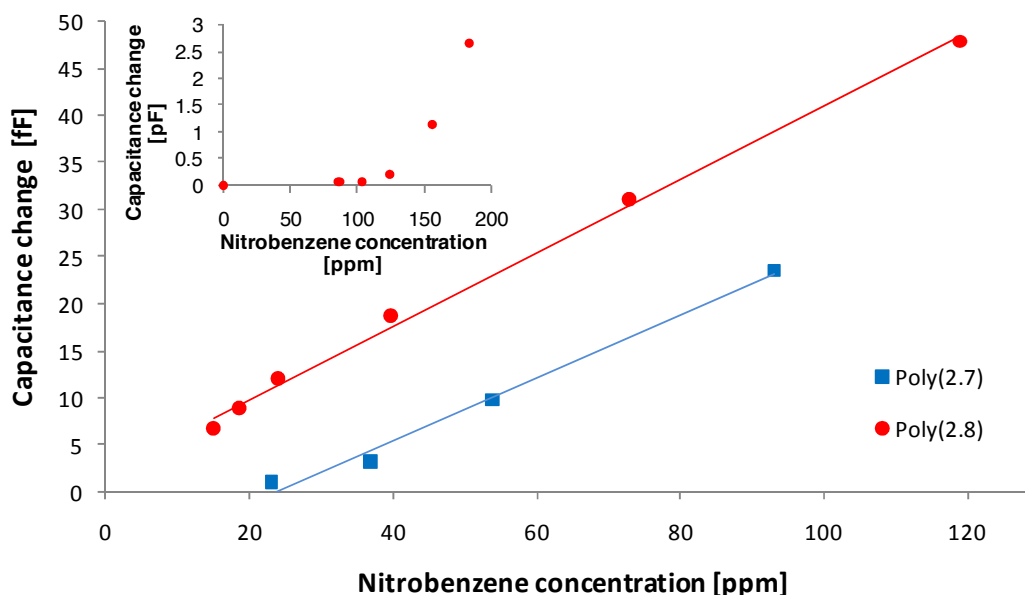


Figure 3-11: Response of poly(2.7) and poly(2.8) to nitrobenzene in sub-100ppm; the insert shows nonlinear response at higher concentrations. Nitrobenzene flow set to 20 mL/min and kept constant throughout the measurement.

This was a rather unexpected result since the association strengths of the halogen-nitro synthon were shown to be increasing in the order of $\text{Cl} < \text{Br} < \text{I}$,¹⁸⁶ therefore iodine should create a stronger sensor.

To further understand the mechanism of the interaction, a response of non-halogenated ProDOT-H poly(2.10) to nitro compounds was compared to the one of poly(2.7). Both films were freshly grown on the same chip (40 cycles, 1 mM monomer solution in dichloromethane). Poly(2.10) did not show a significant response to nitropropane at high concentration (Figure 3-12), which suggests that the halogen-nitro interaction plays an important role in the analyte recognition as we speculated.

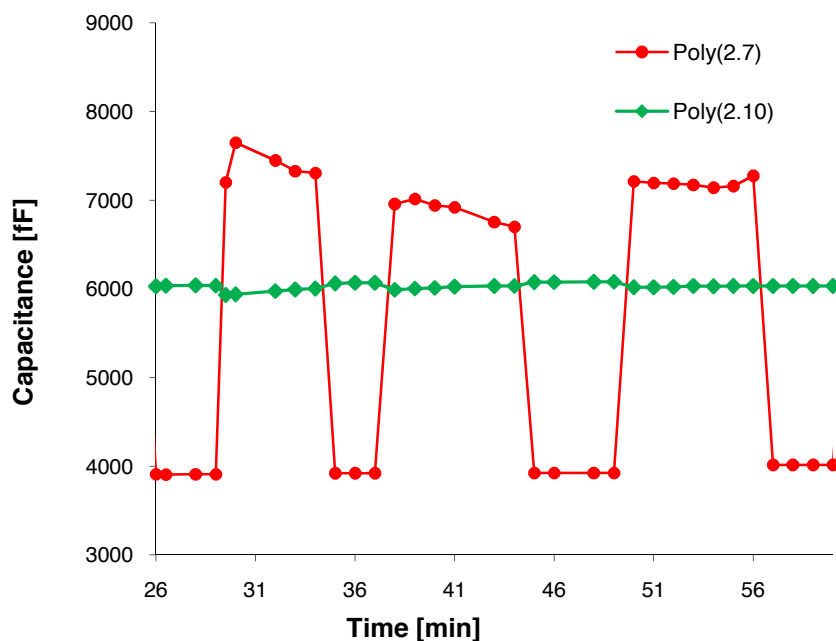


Figure 3-12: Comparison of the response of poly(2.7) and poly(2.10) to 1-nitropropane (10,000 ppm). Nitropropane flow set to 140 mL/min and kept constant throughout.

When testing the same material at a high concentration of nitrobenzene, an unexpected behaviour of poly(2.10) was observed. Poly(2.10) (growth over 40 cycles from 1 mM dichloromethane solution of monomer) showed a slowly stabilising response, but of a similar magnitude as poly(2.7) (Figure 3-13).

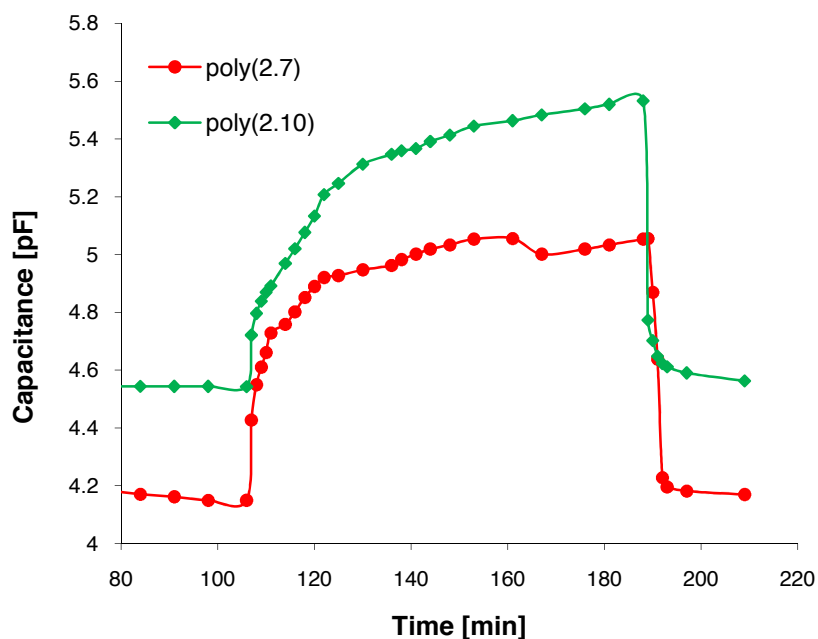


Figure 3-13: Comparison of the response of poly(2.7) and poly(2.10) to nitrobenzene (250 ppm). Nitrobenzene flow set to 250 mL/min switching to nitrogen at 20 mL/min.

This observation suggests that the interaction is not only induced by halogen-nitro interactions since there is a lack of this functionality in poly(2.10). Instead, the sensor response from poly(2.10) may be caused by π - π stacking of the two aromatic rings (nitrobenzene and ProDOT) or charge transfer between the two species. However, it has also been shown that both iodinated and brominated ProDOT derivatives, poly(2.7) and poly(2.8), respond to 1-nitropropane, which strongly supports our expectation of a nitro-halogen interaction in the absence of an aromatic ring.

In conclusion, our overall observations about ProDOT polymers suggest that the interaction is much more complex than just a nitro-halogen recognition and could well be a combination of several additional factors such as π - π stacking of the aromatic rings, charge transfer, steric effects in conformation and shape of the material at the electrode, porosity, surface area, and other properties of the polymer. The determination of mechanism of this interaction was attempted by methods such as UV and NMR titration or computational studies. However, none of these

experiments provided a clear and definite conclusion. Further investigation of the interaction extends beyond the scope of this project and should be considered for future work.

3.4.2 Terthiophenes comparison

In order to also investigate sensor performance based on the synthesised bisalkylsulfanyl-terthiophene polymers, poly(**2.19**) and poly(**2.20**), electrodeposited on the IDE (50 cycles growth from 0.5 mM dichloromethane solutions), were exposed to nitrobenzene vapour. Figure 3-14 and Figure 3-15 shows that both films exhibited very slow response stabilisation with average magnitudes of *ca.* 10 and 25 fF for poly(**2.19**) and poly(**2.20**), respectively.

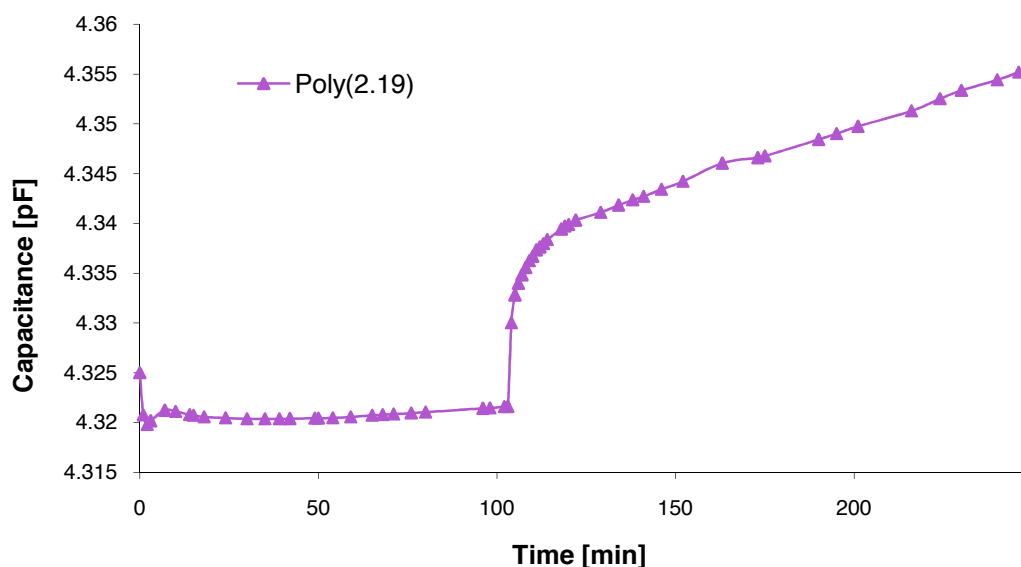


Figure 3-14: Response of poly(**2.19**) to nitrobenzene (140 ppm). Nitrogen flow at 250 mL/min plus nitrobenzene at 50 mL/min.

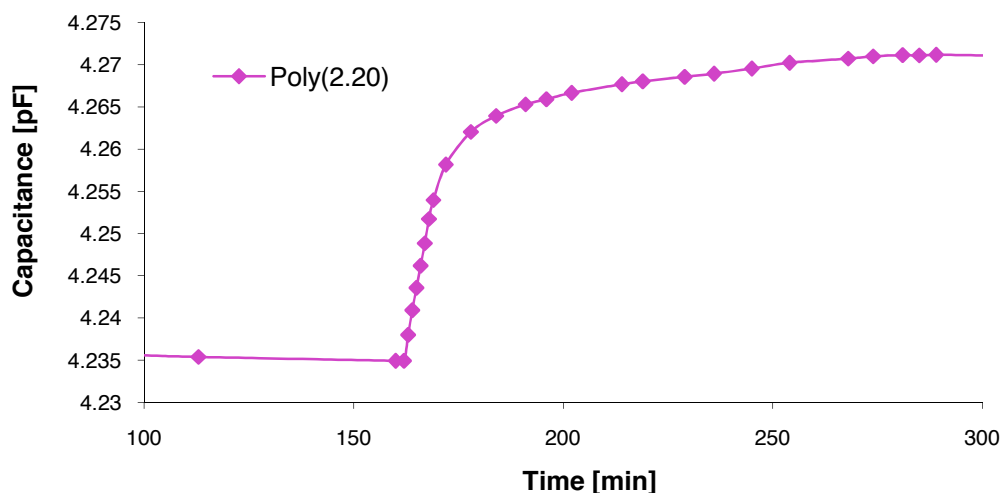


Figure 3-15: Response of poly(2.20) to nitrobenzene (140 ppm). Nitrogen flow at 20 mL/min plus nitrobenzene at 20 mL/min.

These results were inferior to those achieved for ProDOT based polymers. In addition, ProDOT derivatives require less synthetic steps and exhibit better electropolymerisability from a single solvent rather than a solvent mixture, as in the case of terthiophenes. This simplicity can dramatically reduce the time and cost of the overall sensor fabrication, which is desirable for industrial applications. Therefore, the terthiophene materials were not further investigated and the main focus was the development of sensors containing ProDOT-Br (poly(2.7)), which exhibited the best sensor performance.

3.4.3 In-depth characterisation of poly(ProDOT-Br) as a sensor for nitroaromatics

From the previous investigation, it is clear that the ProDOT-Br based polymer poly(2.7) demonstrated the best behaviour as a potential explosive sensor in terms of magnitude, speed, reversibility and reliability of a response towards nitro compounds. Therefore, this candidate has been chosen to be investigated further. It was decided to focus on one particular class of explosives – nitroaromatics. Hence, nitrobenzene (NB) and 2-nitrotoluene (NT) were used as proxies to explosives such as trinitrotoluene (TNT) and dinitrotoluene (DNT) shown in Figure 3-16.

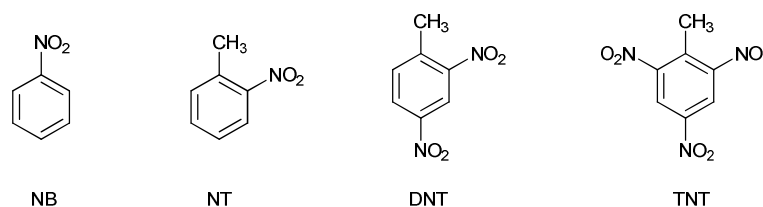


Figure 3-16: Chemical structure of NB, NT, DNT and TNT.

Figure 3-17 demonstrates the capacitance change of a poly(2.7) film to step changes of nitrobenzene concentration. As can be seen, these films exhibit a response time of only a few minutes, which also incorporates the time for the test chamber itself to equilibrate under this low nitrobenzene flow rate.

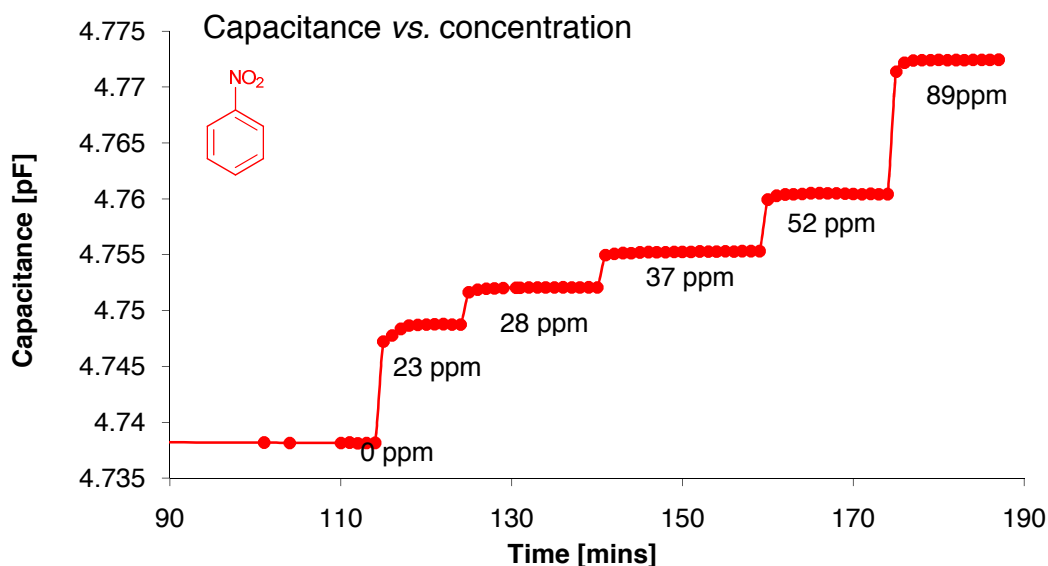


Figure 3-17: Measured change of capacitance of a poly(2.7) film subjected to step changes of nitrobenzene. Constant nitrobenzene flow rate of 20 mL/min, the nitrogen diluent flow rate was varied from 250 mL/min to 50 mL/min.

The reproducibility and reversibility of the sensor response is shown in Figure 3-18. The experiment was carried out with cycling of the vapour concentration from 0 to 50 ppm nitrobenzene (using the exhaust tap after the bubbler) and the sensor exhibited a fast reversible response, which is the characteristic for an alarm sensor.

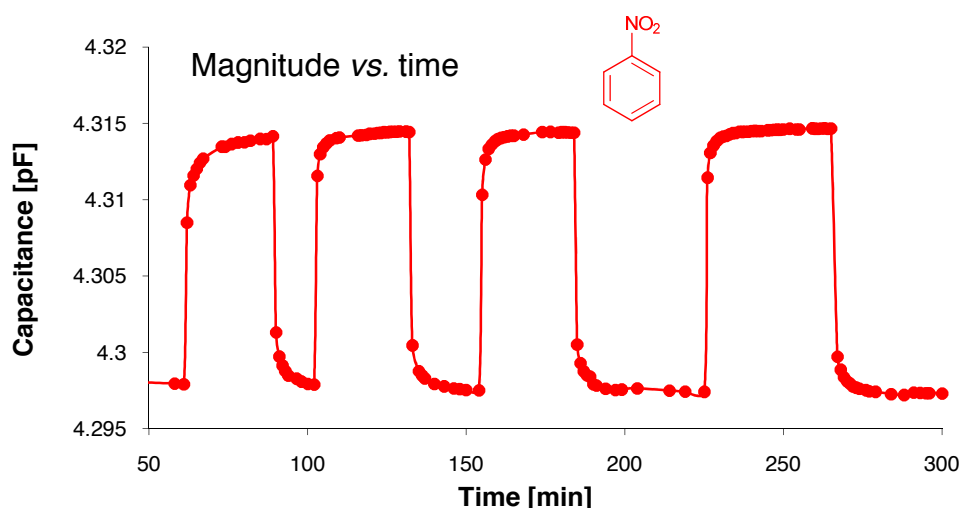


Figure 3-18: Cycling of poly(2.7) sensor several times between 0 and 50 ppm nitrobenzene.

The same test was also repeated after a few weeks of using the chip for different volatiles, and the device exhibited similar results, indicating a long-term stability and lifetime of the sensor. It was also noted that the signal level for vapour concentrations around 20 ppm was found to be well above the noise floor which indicates that the formed sensors could be suitable for measurements at lower concentrations, perhaps sub-ppm. Unfortunately it was not possible to achieve such a measurement with the present set-up. However, future incorporation of a secondary dilutant nitrogen flow and cooling of the VOC samples might allow measurements at these lower concentrations.

It was found that the poly(2.7) film is more sensitive to nitrobenzene compared with nitrotoluene (Figure 3-19). This might be proof that charge transfer between the electron rich polymer and the electron poor nitroaromatics plays an important role in the analyte-sensor interaction since the electron-donating effect of the methyl group in nitrotoluene diminishes its electron deficiency compared to nitrobenzene. As observed in our previous experiments, the capacitance change becomes non-linear for both nitroaromatic compounds at concentrations above around 130 ppm, therefore the data above 150 ppm are not plotted for clarity for presentation.

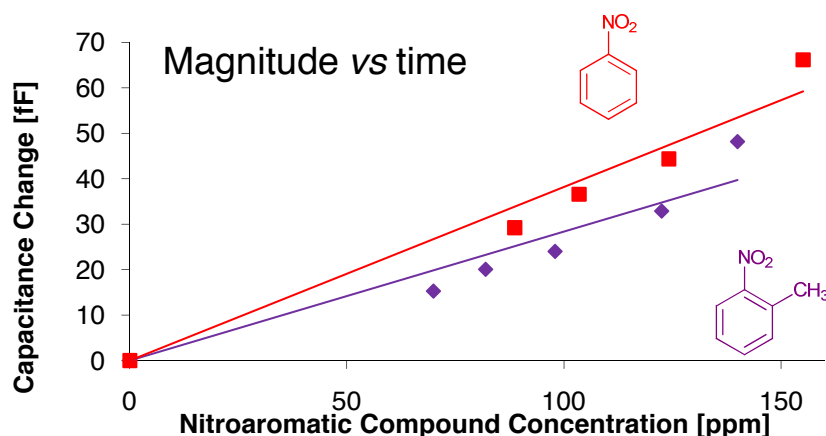


Figure 3-19: Response of a poly(2.7)film to nitrobenzene and nitrotoluene (nitrobenzene and nitrotoluene flow rate of 100 mL/min).

The effect of film thickness on sensor performance was also investigated. Figure 3-20 demonstrates that the thicker the film, the larger the response to nitrobenzene. However, this comes at the expense of an increased stabilisation time (Figure 3-21). Films thicker than 500 nm took considerably longer to stabilise. This is in agreement with results observed in biosensors, where at constant diffusivity the thinner membrane exhibits a smaller time lag.²⁰⁸ From this experiment it can be concluded that the rate of vapour transfer through a polymer film is inversely proportional to the film thickness. As the thickness increases the vapour takes longer to fully diffuse through the thicker polymer film.

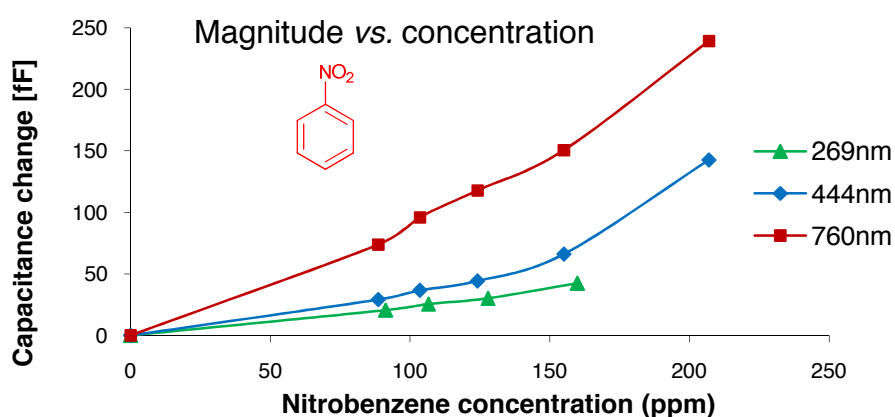


Figure 3-20: Magnitude of sensor response to nitrobenzene for different poly(2.7) film thicknesses.

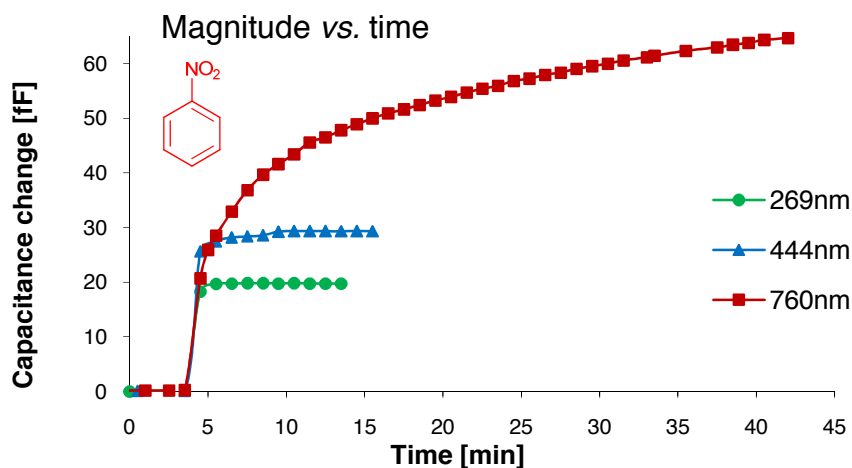


Figure 3-21: Stabilisation time curves versus thickness of poly(2.7) films to a step change of 0 to 90 ppm nitrobenzene.

Taking into account these observations, it was decided to limit the film thicknesses in future experiments to less than 500 nm. Next, the cross-sensitivity with various different volatiles was measured using the new dynamic vapour flow setup. As discussed above, the minimum concentration that could be achieved with the experimental set-up was several thousand ppm for the lower boiling point VOCs. Figure 3-22 represents the sensor response to these chemicals on a logarithmic concentration scale. It can be concluded that, compared to target analytes NB and NT, the response level of toluene, acetone, ethyl acetate, hexane, tetrahydrofurane and ethanol was found to be considerably lower, taking into account the large difference of the concentrations during the measurement.

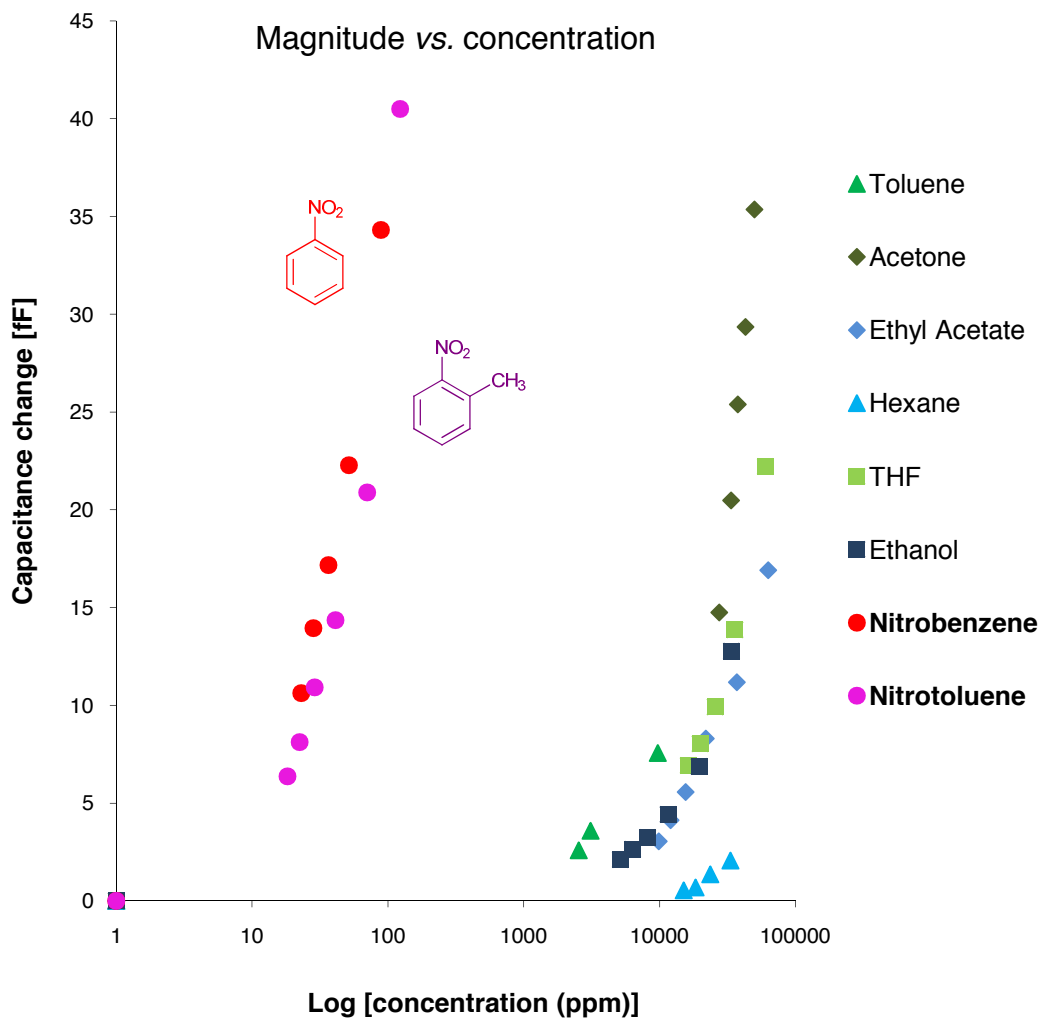


Figure 3-22: Measured capacitance change of a poly(2.7) film (average thickness 444 nm) for changing concentrations of several VOCs and nitroaromatic compounds.

To give a more quantitative indication that the poly(2.7) based sensor exhibits an enhanced response to nitroaromatic compounds compared with other VOCs, the capacitance responses were extrapolated to 100 ppm and the results are shown in Table 3-4.

Table 3-4: Measured response of poly(2.7) film to nitrobenzene and nitrotoluene, and the relative response to other chemical vapours extrapolated to 100 ppm.

Chemical [100 ppm]	Capacitance Change [fF]
Nitrobenzene	46.75
Nitrotoluene	32.50
Toluene	0.102
Acetone	0.0536
THF	0.042
Ethanol	0.041
Ethyl Acetate	0.031
Hexane	0.0035

The sensor based on ProDOT-Br poly(2.7) demonstrated a response over three orders of magnitude higher to nitroaromatics than other volatiles tested at the same concentration. To the best of our knowledge this is the highest reported selectivity of chemicapacitor towards nitro compounds.

3.5 CONCLUSIONS AND FURTHER WORK

It can be concluded that there are three important outcomes from these sets of experiments.

- Polymeric capacitive sensors are often constructed as arrays of sensors and use pattern recognition algorithms to distinguish the different chemicals from each other, resulting in significantly greater cost and complexity. Such complex system can be avoided by designing a custom polymer that has a high sensitivity and selectivity towards a desired analyte. Specifically, a novel ProDOT-Br polymer-based sensor was tested and its performance compared to a commercially available

polymer (PEDOT). The novel sensor demonstrated a higher sensitivity to the target nitro molecules and good reversibility. Additionally, these materials can be prepared by simple and low-cost chemical synthesis in high yields and purity.

- It has been shown that electropolymerisation can be used as an inexpensive and fast method to selectively deposit polymers onto microelectrodes. Two different materials can be grown on a single sensor chip by letting the current flow through one IDE whilst keeping the other one open-circuited in the electrochemical cell.
- The new ProDOT-Br based sensor was tested for its response to a series of VOCs often found in the atmosphere and the device demonstrated a very high selectivity towards nitroaromatics whilst retaining a high degree of reversibility, which presents the highest selectivity of a chemicapacitor towards nitroaromatics reported to date.

Further work will be focused on modifying the experimental apparatus to allow the measurement of developed sensor responses at lower concentrations, ideally below 1 ppm. In addition, electrochemical growth on new sensor platforms upon silicon wafers will be also investigated, which represents a novel route to mass-produced low-cost sensor electronics.

Chapter 4

***4 CROSS-LINKED POLYMERS WITH ENHANCED
SURFACE AREA***

4.1 INTRODUCTION TO CROSS-LINKED POROUS POLYMERS

In order to enhance the sensitivity and response speed of the current electrochemically polymerised thin films, investigations were carried out on synthesising new materials that will provide networked polymers with high-porosity and enhanced surface area. The larger volumetric surface area of such porous films is expected to greatly increase the sensitivity and significantly reduce the response time of the sensors, as the capacitance change of the polymeric coated electrode is proportional to the size of the contact surface of the capacitor and also increases the analyte-sensor interaction area.

Owing to the inherent insolubility of these cross-linked porous structures it is very difficult to fully characterise them. Conventional chemical analysis commonly used for other polymers, such as nuclear magnetic resonance (NMR), gel permeation chromatography (GPC) or matrix-assisted laser desorption/ionisation MALDI-TOF mass spectrometry, cannot be used as they are all analysed in solution. Infrared spectroscopy (IR) is only useful in cases where a specific IR active group is present within the backbone. For example, IR has been used to monitor the completion of the polymerisation by the disappearance of starting material functionalities.¹⁶³ Microanalysis is not suitable since the total mass commonly does not completely match due to incomplete combustion or difficult-to-remove impurities remaining trapped inside the pores, such as entrapped solvent.¹³⁶ It was reported that even hydrophobic structures readily physisorb water vapour from a humid atmosphere.¹³⁷ Therefore, the most widely used technique to characterise a porous network is solid state NMR, where assignment of the different peaks related to ¹³C shifts in different electron cloud environments can provide structural information.^{127, 129, 130}

Overall, the aim of this investigation was to find a material which would fulfil three main requirements:

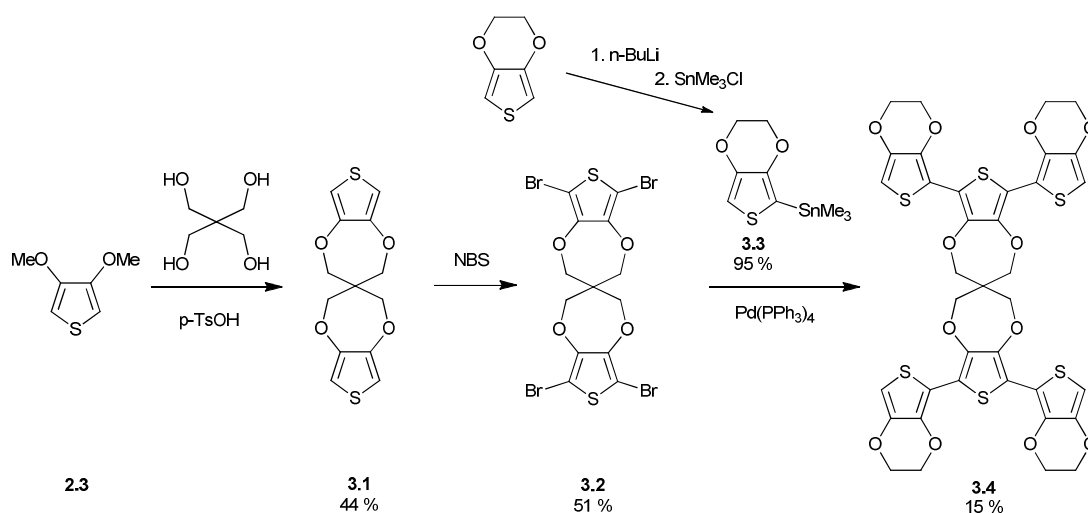
- The polymers should have high porosity and surface area.

- Contain a moiety that can be replaced at a later stage by a nitro sensitive moiety that was discussed in the previous two chapters (e.g., ProDOT-Br (**2.7**) could be incorporated within the structure). As the synthesis of these materials is particularly challenging, commercially available EDOT was used as a strut in these preliminary studies to find an adequate scaffold. Once a high surface area polymer is achieved, this can subsequently be replaced with ProDOT-Br (**2.7**).
- The polymers should retain ease of electropolymerisability since this is the main deposition technique used to fabricate our sensors – the second advantage of EDOT being used as a strut.

4.2 SYNTHESIS OF CROSS-LINKED POLYMERS

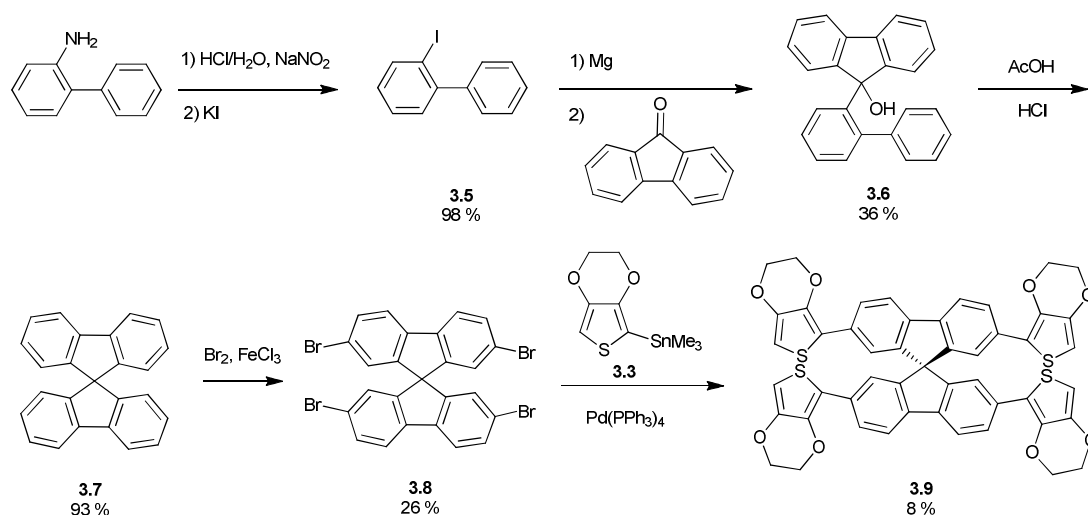
4.2.1 Polymers prepared via Stille coupling

The first objective was the preparation of derivatives containing cores with spiro carbon centres such as spiroProDOT and spirobifluorene. Structures containing these moieties maintain a rigid shape and have been previously reported as being part of CPPs with high surface areas.^{127, 135} SpiroProDOT¹⁵³ (**3.1**) was synthesised *via* transesterification from 3,4-dimethoxythiophene (**2.3**) with pentaerythritol and subsequently brominated using NBS to achieve spiro-bis(2,5-dibromopropylenedioxythiophene) **3.2** in 51 % yield.¹²⁷ Lithiation of EDOT with *n*-butyl lithium and subsequent addition of trimethyltin chloride gave stannylated counterpart **3.3**.^{209, 210} The desired compound **3.4** was prepared *via* microwave assisted Stille coupling of **3.2** with **3.3** and was obtained in a low yield of 15 % (Scheme 4-1).



Scheme 4-1: Synthetic route for spiroProDOT-EDOT derivative **3.4**.

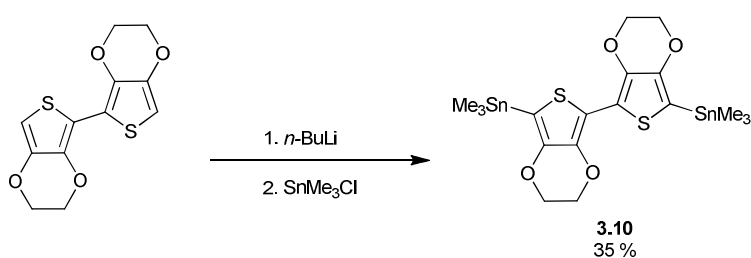
The synthesis of spirobifluorene-EDOT derivative **3.9** is depicted in Scheme 4-2. Firstly, 2-aminobiphenyl was converted to the corresponding 2-iodobiphenyl **3.5** under Sandmeyer conditions. Formation of the corresponding Grignard with magnesium followed by reaction with 9-fluorenone generated tertiary alcohol **3.6**, which was subsequently treated with acetic acid to form the spirobifluorene **3.7** in good yield. Reaction of **3.7** with bromine and FeCl_3 yielded 2,2',7,7'-tetrabromo-9,9'-spirobifluorene **3.8** after difficult separation of a reaction mixture containing multibrominated products. The final compound **3.9** was achieved *via* low-yielding microwave-assisted Stille coupling.



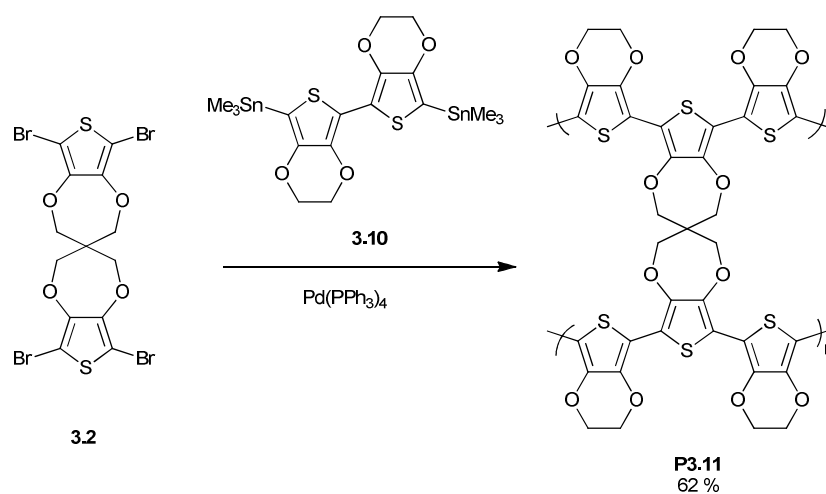
Scheme 4-2: Synthesis of spirobifluorene-EDOT **3.9**.

The corresponding polymers **P3.11** (Scheme 4-4) and **P3.12** (Scheme 4-5) were prepared *via* conventional Stille coupling in toluene from the tetrabrominated species **3.2** and **3.8** and stannylated BisEDOT **3.10**,²¹⁰ synthesised the same way as stannylated EDOT **3.3** (Scheme 4-3). The resulting insoluble polymer was then collected and purified by Soxhlet extraction.

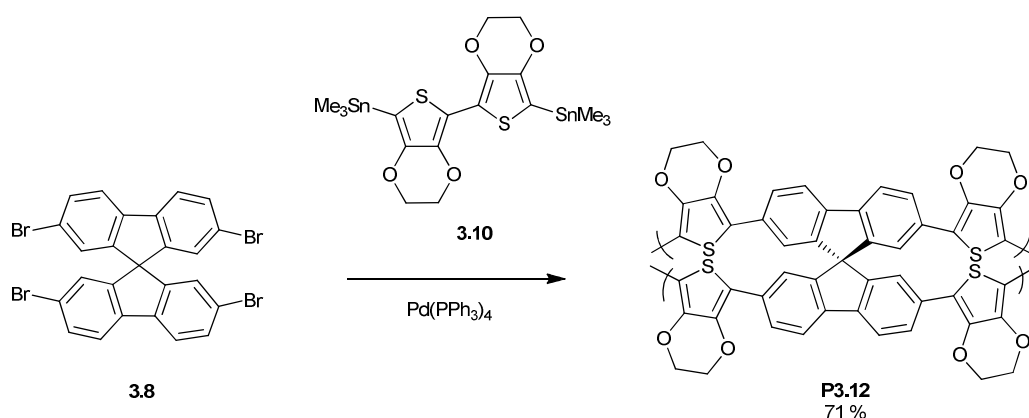
It is important to mention that in order to avoid confusion, the chemically synthesised polymers are labelled with prefix **P**-, whereas electrochemically prepared polymers are labelled **poly**-; the number following the prefix corresponds to the starting monomer.



Scheme 4-3: Synthesis of bisEDOT **3.10**.



Scheme 4-4: Preparation of **P3.11** *via* Stille coupling.

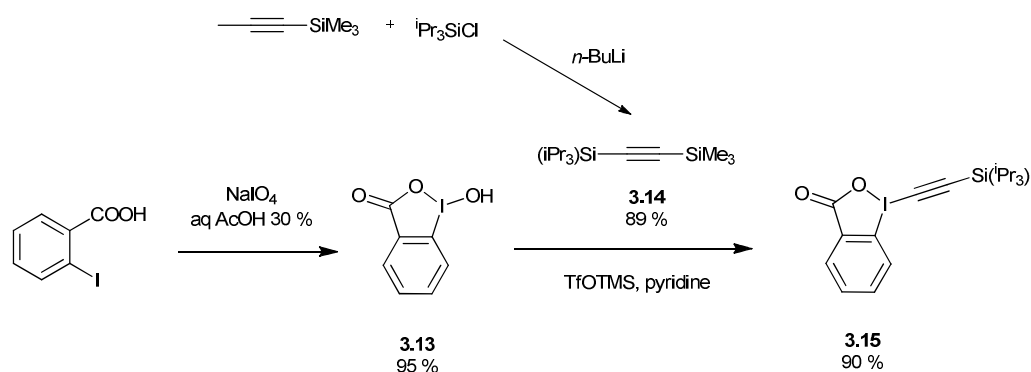


Scheme 4-5: Preparation of **P3.12** *via* Stille coupling.

The BET surface area of the polymers was measured using a porosimeter ASAP2020, which was available within the department; samples were degassed at 50 °C under vacuum for half an hour and then at 100 °C for 4 hours. The apparent surface area was found to be very low; 0.2 m²/g and 0.3 m²/g for **P3.11** and **P3.12**, respectively. It is possible that this could be caused due to high steric hindrance in these crowded structures, and therefore only creating small pores inaccessible to the adsorbed gas. Insertion of a longer spacer strut within the structure could help to overcome this issue. Therefore the alkynyl derivative of EDOT was prepared in order to be subsequently used as an alternative to the simple EDOT strut.

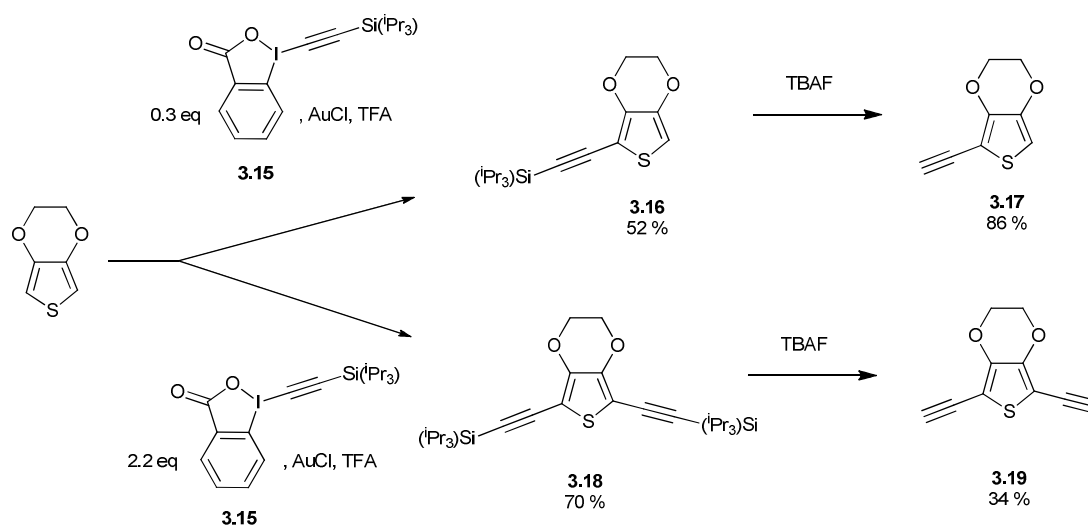
4.2.2 *Polymers prepared via Sonogashira-Hagihara cross-coupling*

The research group of J.P. Brand and J. Waser reported direct alkylation of thiophene derivatives mediated by gold and trifluoroacetic acid (TFA) under ambient conditions.²¹¹ TIPS-EBX (1-[(Triisopropylsilyl)ethynyl]-1,2-benziodoxol-3(1*H*)-one) **3.15** was synthesised following their procedure (Scheme 4-6) and subsequently used to alkylate EDOT. Triisopropylsilyl trimethylsilylacetylene **3.14** was synthesised by reaction of ethynyltrimethylsilane with chlorotriisopropylsilane and then reacted with 2-iodosylbenzoic acid **3.13** which was prepared from 2-iodobenzoic acid in excellent yield. Final attachment of the TIPS group to **3.13** gave **3.15** in good overall yield.



Scheme 4-6: Synthesis of TIPS-EBX **3.15**.

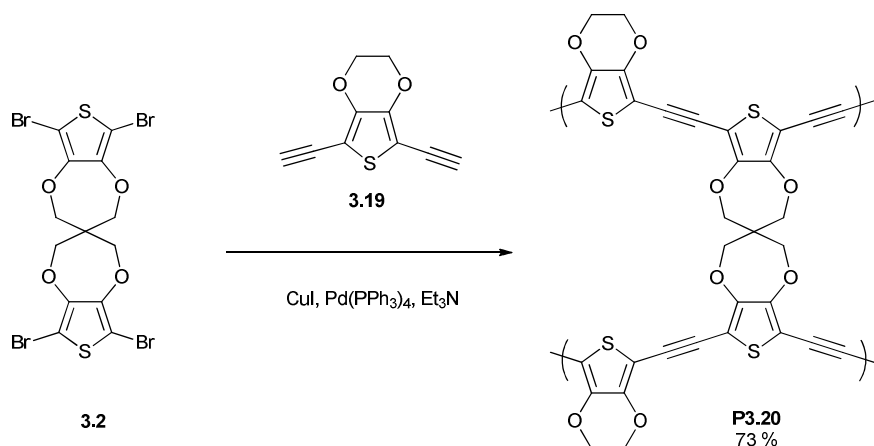
EDOT can be mono- or bifunctionalised depending on the reaction stoichiometry.²¹¹ The silylethynylation step proceeds with cooperative activation of a thiophene ring by gold catalyst (AuCl) and Bronsted acid (**3.15**). The deprotection of derivatives **3.16** and **3.18** gives **3.17** and **3.19** in good/moderate yield (Scheme 4-7). The bisalkynylated product **3.19** proved to be very unstable and turns black in few hours due to a possible rapid polymerisation, so it had to be used immediately for the next step.



Scheme 4-7: Synthesis of mono- and bi-alkynylated EDOT **3.17** and **3.19**.

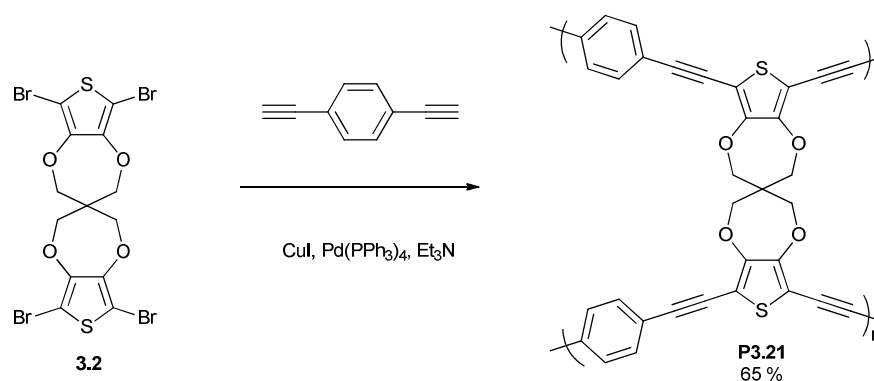
The spiroProDOT–alkynyl EDOT polymer **P3.20** was synthesised *via* Sonogashira-Hagihara cross-coupling using the tetrabrominated spiroProDOT **3.2** and bisethynyl-EDOT **3.19** in the presence of copper iodide, Pd⁰ and triethylamine

(Scheme 4-8). As before, the insoluble polymer was purified by Soxhlet extraction. The surface area of this polymer was measured to be $16 \text{ m}^2/\text{g}$ (Figure 4-1), which is two orders of magnitude higher than that observed for the corresponding polymer without the extended spacer length (**P3.11**). This confirms the assumption that the alkynyl spacer suppresses steric hindrance and is encouraging that the correct hypothesis for creating polymers with an enhanced surface area was taken.



Scheme 4-8: Sonogashira coupling of tetrabromospiroProDOT **3.2** with bisethynyleDOT **3.19** to afford **P3.20**.

Nevertheless, a similar polymer where a phenyl moiety was present instead of the EDOT unit was reported with a surface area of $1600 \text{ m}^2/\text{g}$.¹²⁷ This difference could be caused either by the structure, the polymer synthesis itself or by the BET measurement technique. To clarify this, the reported polymer was reproduced following exactly the same procedure as reported (Scheme 4-9).



Scheme 4-9: Reproduction of reported procedure for polymer **P3.21**.

An insoluble brown polymer was obtained with a measured surface area of $460 \text{ m}^2/\text{g}$ (Figure 4-1). Even though this is a little over a quarter of the reported value, it exhibits a considerably enhanced surface area and therefore the polymerisation and BET technique used were considered to be reliable. Therefore the low values observed for the prepared polymers (**P3.11** and **P3.12** and **P3.20**) seemed to be a consequence of the structure. It could be that the ethylene bridge of EDOT might be causing a deformation of the structure and therefore increases steric hindrance, thus lower the porosity and surface area.

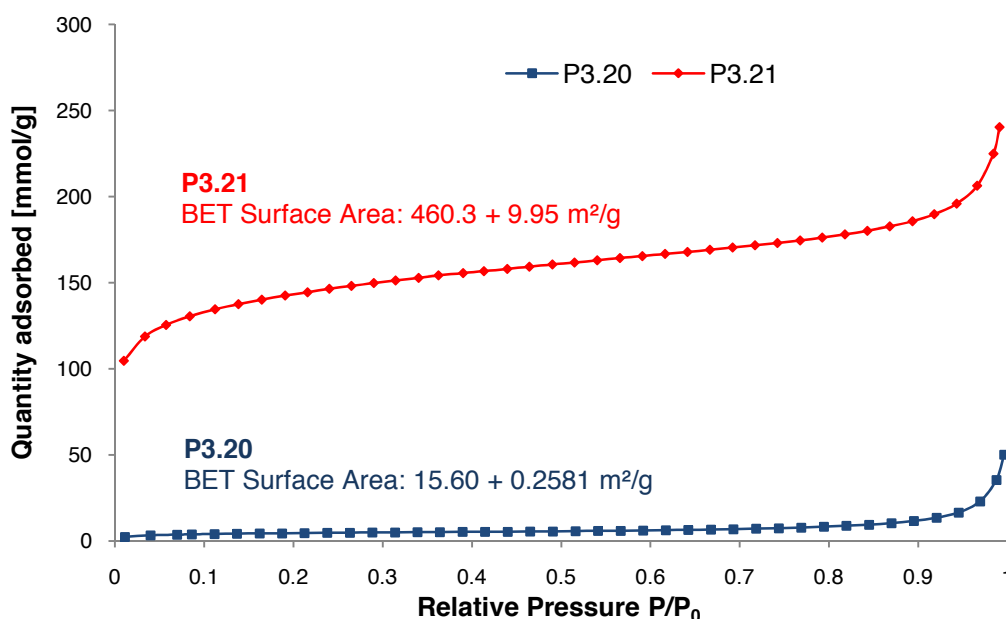


Figure 4-1: Nitrogen uptake measurement to determine the surface area of **P3.20** and **P3.21**. The sample was cooled in the measuring flask using liquid nitrogen.

4.2.3 Tailoring the structure of porous polymers

Following the previous investigation, it was envisaged that it is possible to achieve polymers with enhanced surface area by using alkynylene- EDOT struts and a core that forms a polymeric structure, retaining a high degree of rigidity in a solid state form. To investigate this further, several different cores were suggested as suitable candidates (Figure 4-2).

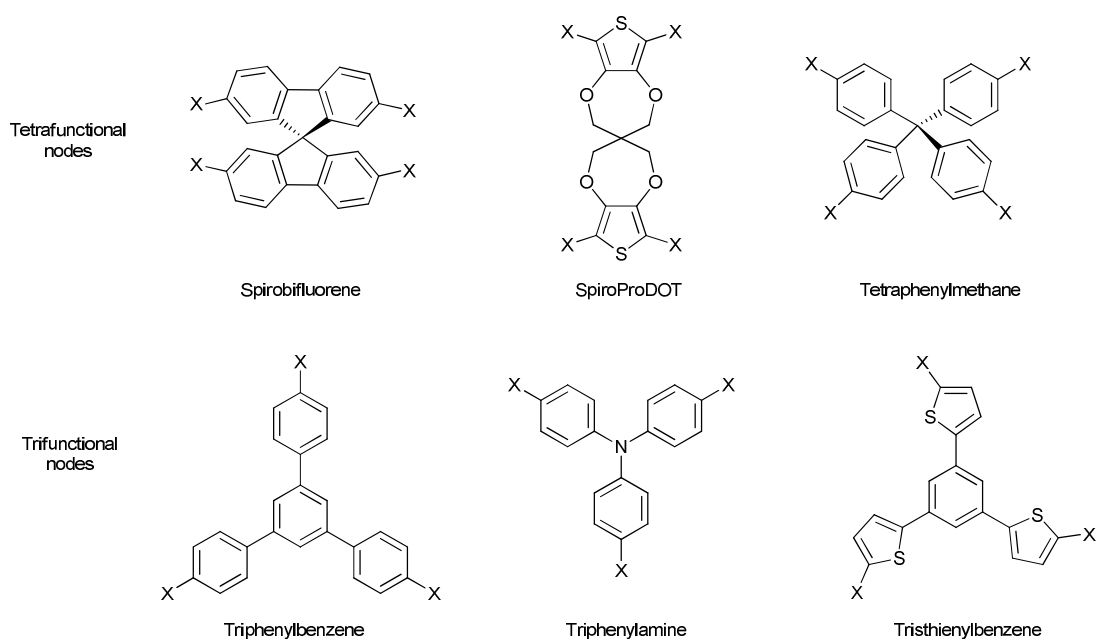


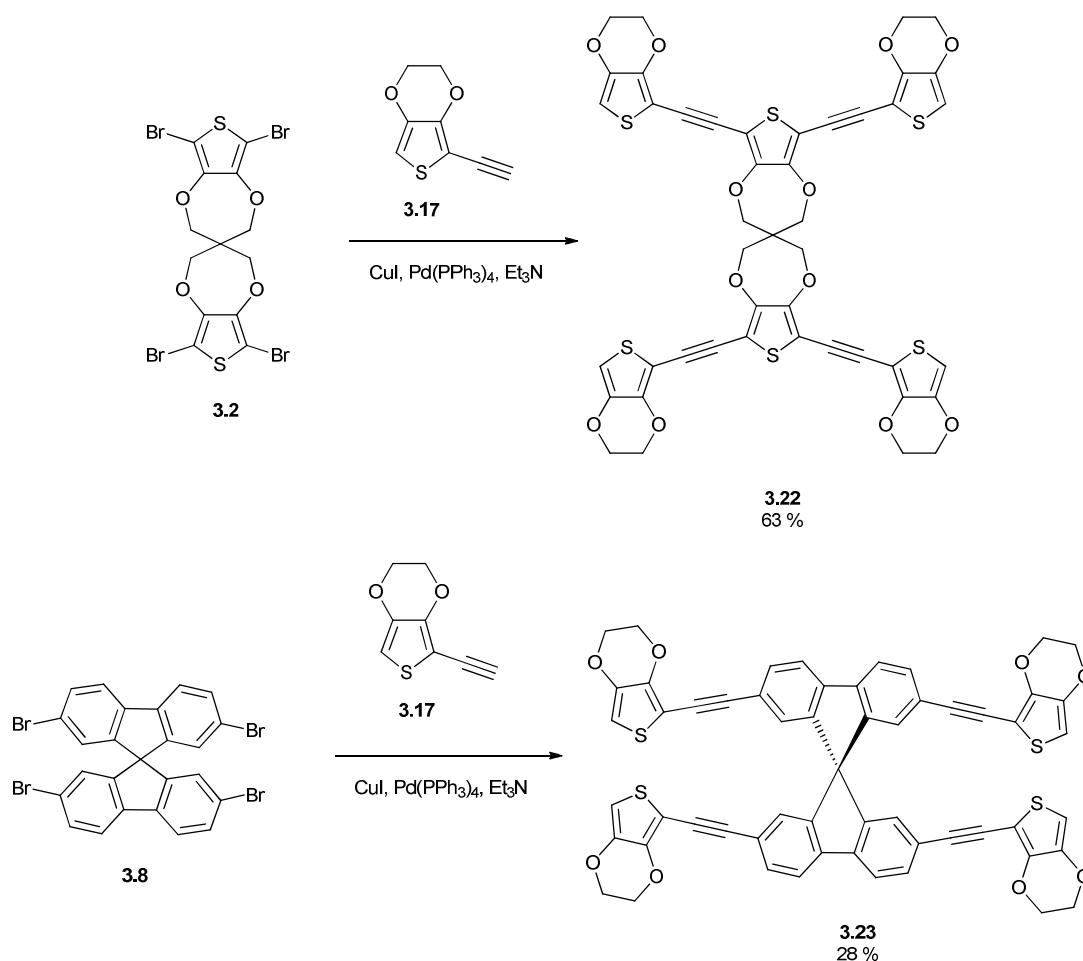
Figure 4-2: Suitable candidates to be investigated as cores for the synthesis of enhanced surface area polymers, where X represents a halogen (Br or I).

Two different families of nodes were investigated, with either a connectivity of three or four. All compounds containing a spiro-carbon are tetrafunctional. The cores are locked in a tetrahedral shape and, depending on the steric hindrance of their surrounding substituents, they can be highly twisted. Additionally, due to electronic repulsion, they remain rigid in a 3D structure.¹²⁸ Using these building blocks resulted in polymers with a BET area of *ca.* 1600 m²/g and *ca.* 500 m²/g for spiroProDOT¹²⁷ and spirobifluorene,¹⁰⁹ respectively. Tetraphenylmethane has been reported as part of an organic framework having an exceptional BET surface area of over 5000 m²/g.¹³⁰

Triphenylbenzene, triphenylamine and trithienylbenzene were chosen as cores bearing a connectivity of three. Cooper and co-workers reported the synthesis of conjugated porous polymers (CPPs) with a triphenylbenzene core and varying lengths of an ethynylene-benzene strut. They showed that the pore size can be controlled by the size of these struts and the structures exhibited BET areas between 500 – 1000 m²/g.¹²⁹ Another publication from the same group compares similar structures, but uses a triphenylamine core as a node gives a calculated S_{BET} of

ca. 1000 m²/g.²¹² The research group of Arne Thomas reported microporous conjugated poly(thienylenearylene) networks having a S_{BET} of 1060 m²/g.

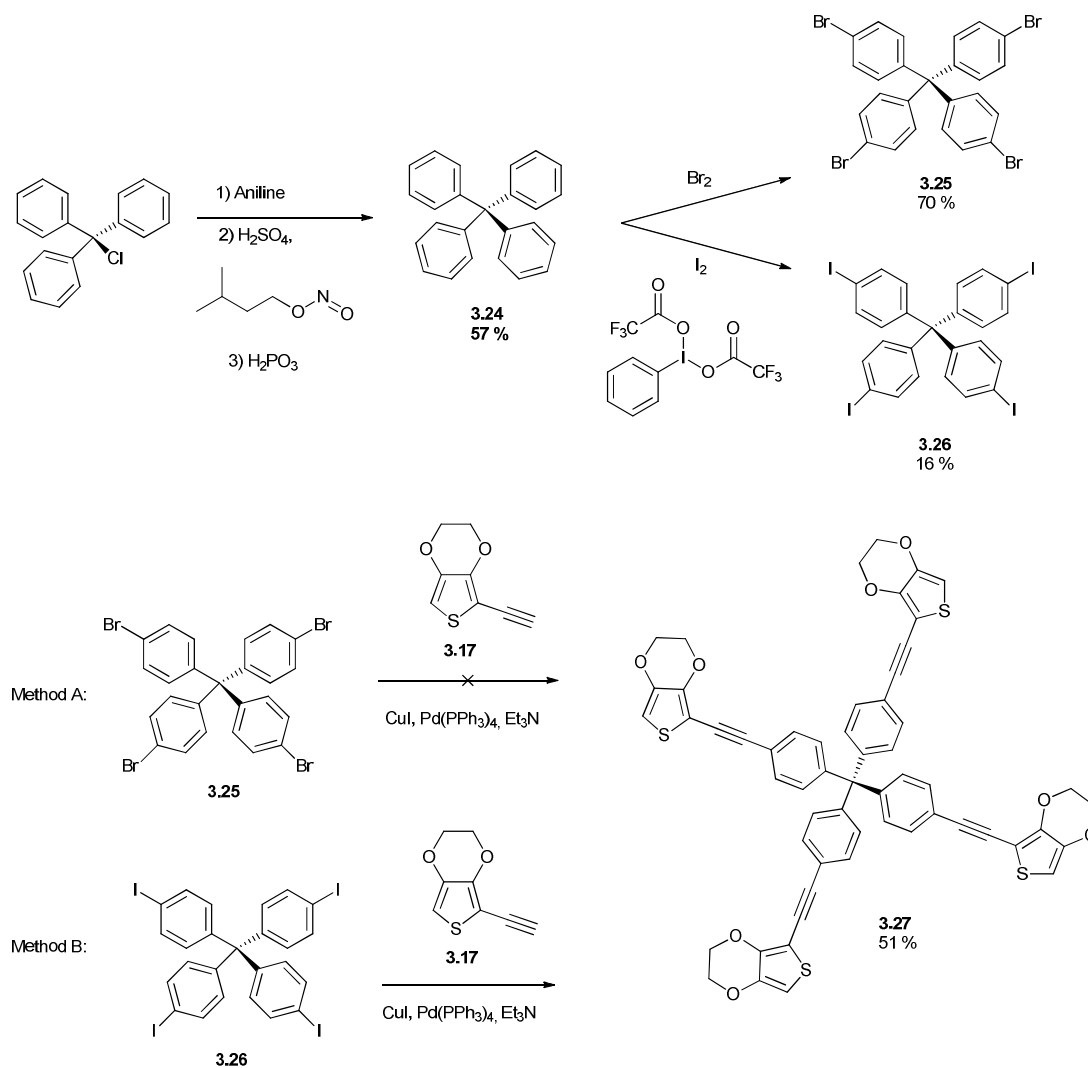
Compounds **3.22** and **3.23** were prepared from previously synthesised tetrabrominated spiro compounds **3.2** and **3.8** *via* microwave assisted Sonogashira cross-coupling with monoalkynyl-EDOT **3.17** (Scheme 4-10). Both compounds were achieved with a maximum purity of 95% and 97% (**3.22** and **3.23**, respectively) after several purification attempts by column chromatography, preparative TLC or reprecipitation, as it was not possible to separate the partial coupling by-product due to it possessing the same retardation factor (R_f) as the main product.



Scheme 4-10: Sonogashira coupling to achieve compounds **3.22** and **3.23**.

Tetraphenylmethane **3.24** was prepared from chlorotriphenylmethane according to a previously described procedure²¹³ and subsequently brominated using

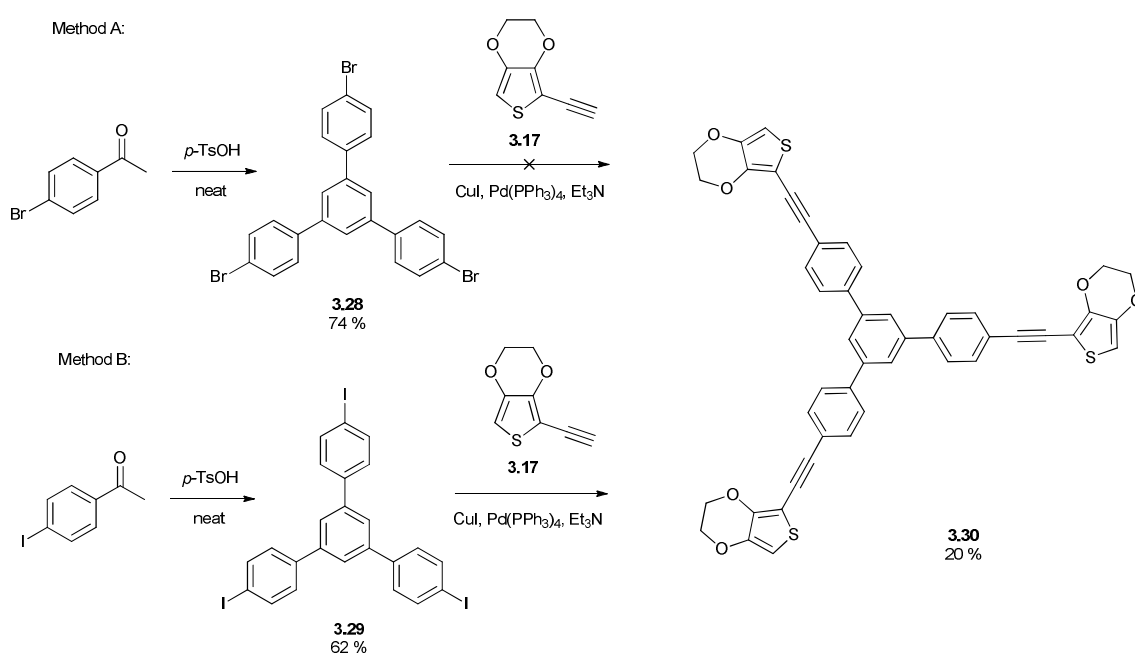
bromine.²¹³ In the complex mixture obtained after the attempted reaction of tetrakis(4-bromophenyl)methane **3.25** with alkynyl-EDOT **3.17** only products were identified as partial coupling, but not the desired product (Scheme 4-11- Method A). However, the final coupling was successful using tetraiodinated derivative **3.26**,²¹⁴ prepared by iodination of **3.24** with iodine and bis(trifluoroacetoxy)iodobenzene; the final compound **3.27** was achieved in a good yield (Scheme 4-11-Method B).



Scheme 4-11: Synthetic route to compound **3.27**.

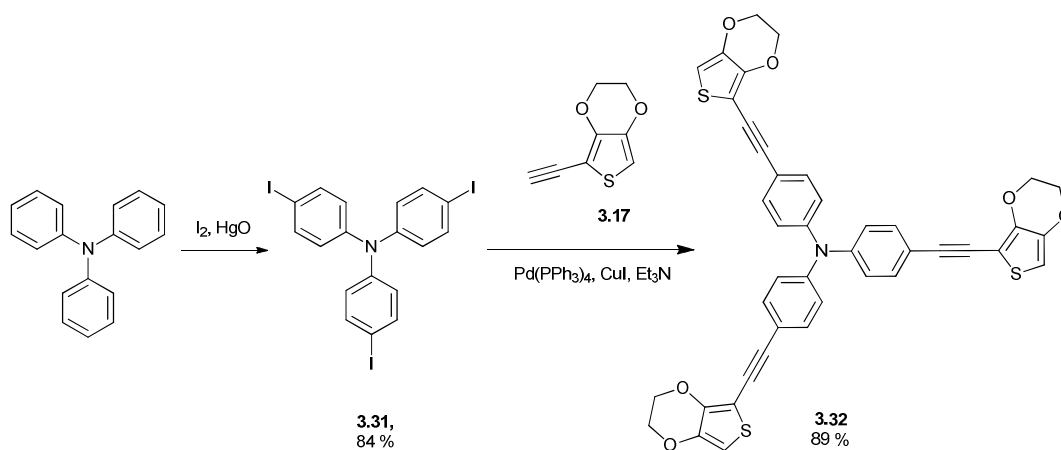
1,2,3-(4-Bromophenyl)benzene **3.28** was synthesised in good yield using green chemistry, according to a solvent-free procedure assisted by *p*-toluenesulfonic acid, described by Jia and his co-workers.²¹⁵ The mixture obtained from the subsequent cross-coupling contained many different by-products, including partial

coupling, and the desired product was not found in any of the collected fractions (Scheme 4-12-Method A). The approach was therefore altered and compound **3.28** was replaced by iodine derivative **3.29**. The general reactivity of sp^2 substrates in Sonogashira coupling follows the order of vinyl iodide > vinyl triflate > vinyl bromide > vinyl chloride > aryl iodide > aryl triflate > aryl bromide > aryl chloride.²¹⁶ Therefore, higher yields are usually achieved when more expensive and more unstable aryl or vinyl iodides are used. Moreover, electron-poor aryl halides make the coupling even more favourable.²¹⁶ Hence, following the same procedure, the desired compound **3.30** was achieved *via* Sonogashira cross-coupling of **3.17** with 1,2,3-(4-iodophenyl)benzene **3.29** (Scheme 4-12– Method B).



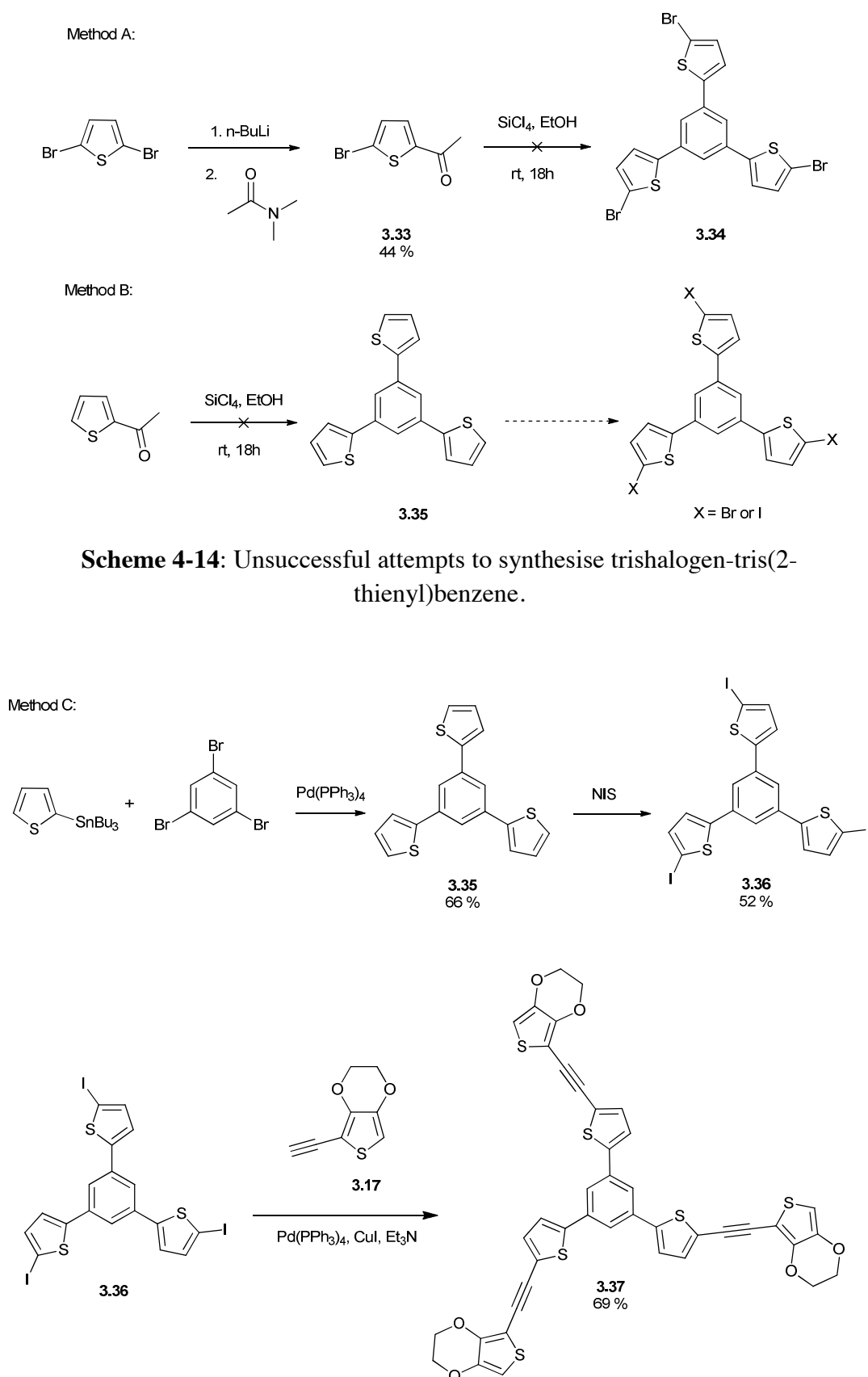
Scheme 4-12: Synthetic route to triphenylbenzene-alkynyl-EDOT **3.30**.

Tri-iodotriphenylamine **3.31** was prepared from triphenylamine using mercury (II) oxide and iodine. The desired product **3.32** was prepared *via* conventional Sonogashira coupling in a good yield of 89% (Scheme 4-13). Microwave conditions were also attempted, but the yield was considerably lower and also resulted in an impurity with the same R_f as the product. This complex mixture was not successfully separated either *via* recrystallisation or by column chromatography.



Scheme 4-13: Preparation of compound **3.32**.

F. Cherioux and L. Guyard described the preparation of 1,3,5-tristhienylbenzenes *via* triple ketolisation and dehydration of the acetyl-aromatic compound with tetrachlorosilane/ethanol (1/1) as a reagent and considered this method to be superior to the Stille coupling of 1,3,5-tribromobenzene with stannylated thiophenes.²¹⁷ 5-Acetyl-2-bromothiophene **3.33** was prepared by nucleophilic attack of *in situ* generated 2-bromothiophene-5-yl lithium salt on *N,N*-dimethylacetamide. The yield of the subsequent ketolisation was expected to be lower than 10 % due to the strong electron-withdrawing effect of the bromine atoms, as described in the original paper. However, the desired product **3.34** was not observed at all (Scheme 4-14 – Method A). The authors claim high yields in the case of 2-acetylthiophenes with an electron-donating group in the 5-position. However, an attempt to reproduce their procedure failed and 1,3,5-tris(2-thienyl)benzene **3.35** was not obtained (Scheme 4-14–Method B). Nevertheless, compound **3.35** was finally synthesised *via* microwave-assisted Stille coupling of stannylated thiophene and tribromobenzene in good yield and subsequently iodinated with NIS under reflux conditions in tetrachloromethane to obtain **3.36**.²¹⁸ The final conventional Sonogashira coupling gave compound **3.37** in good yield (Scheme 4-15- Method C).



In conclusion, it is clear that Sonogashira cross-coupling is a suitable and convenient route for the synthesis of a variety of star-shaped or 3D structures containing different cores and alkynyl-EDOT. Table 4-1 summarises the yields obtained using either microwave or conventional procedures for the reaction of aryl bromides or aryl iodides. It was observed that the cross-coupling of brominated cores is successful only under microwave conditions at high temperatures, with the exception of tetrakis(4-bromophenyl)-methane, but purification of the mixtures proved to be very difficult. Iodinated moieties were coupled in good yields using conventional conditions.

Table 4-1: Obtained yields for Sonogashira cross-coupling of aryl halides and alkynyl -EDOT (**3.17**).

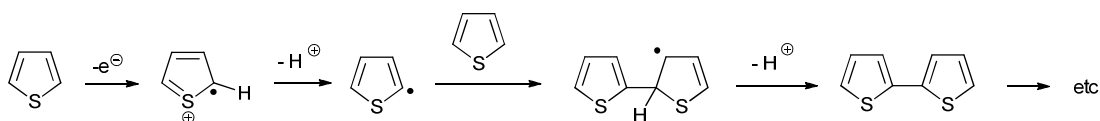
Core	Product No.	Halide	Microwave conditions yield [%]	Conventional procedures yield [%]
SpiroProDOT	3.22	4x Br (3.2)	63, 95% purity	0
Spirobifluorene	3.23	4x Br (3.8)	28, 97% purity	---
Tetraphenylmethane	3.27	4x Br (3.25)	0	---
		4x I (3.26)	---	51
Triphenylbenzene	3.30	3x Br (3.28)	---	0
		3x I (3.29)	---	20
Triphenyl amine	3.32	3x I (3.31)	Impure	89
Trithienylbenzene	3.37	3x I (3.36)	---	69

4.2.4 Polymers prepared via oxidative polymerisation

In order to be able to compare electropolymerised and polymers polymerised by chemical oxidation, a technique that is mechanistically close to electrodeposition has to be used. As depicted in Figure 4-3, oxidative polymerisation is an adequate method since the polymer chain growth forms *via* the same mechanism as

electropolymerisation. There are two proposed mechanisms following radical initiation for oxidative polymerisation, either *via* a radical or cationic route.²¹⁹

Radical route



Cationic route

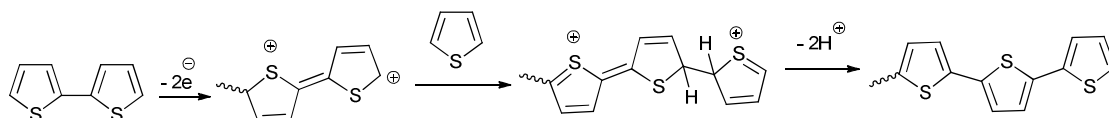


Figure 4-3: Mechanism of the oxidative polymerisation of thiophene.

Therefore it is reasonable to assume that the polymers generated by these two techniques will be similar in their porosity and surface area. There could be some discrepancy in their shape and structure as the electrochemical polymer growth on the slide could create a different polymer (*e.g.* variation in molecular weight and functional group conversion) compared to that which occurs in solution. The aim was to investigate this hypothesis and determine if the polymers generated *via* the above mentioned methods are comparable.

The most common reagents for the oxidative polymerisation of thiophenes are transition metal halides, in particular ferric chloride.²¹⁹⁻²²¹ The main drawback of this reagent is the difficulty in removing the iron salts after polymerisation. These impurities exist as a Fe(III) complex coordinated to the π -system (η^5) of the polymer backbone or S-bonded (η^1) between the thiophene rings.²²⁰ These trace impurities have a great effect on device performance.²²⁰

This issue can be avoided by using nitrosonium salts as the reagent,^{222, 223} where the reaction results in the BF_4^- salt (or other anion depending on the reagent used) of the polymer and evolves NO as a gas, which simplifies further purification. The positively charged polymers can be subsequently dedoped using hydrazine.²²⁴

Monomers **3.22**, **3.23**, **3.27**, **3.30**, **3.32** and **3.37** were chemically polymerised using NOBF_4 . The resulting insoluble black powder was collected and purified by Soxhlet extraction to remove unreacted monomeric residues. These powders were subsequently suspended in chloroform and dedoped using an excess of hydrazine, then purified once more by Soxhlet extraction with chloroform and methanol before being dried under vacuum. Table 4-2 summarises the yields and temperatures for the onset of decomposition (measured by a Perkin Elmer TGA instrument, heating rate $10\text{ }^\circ\text{C}/\text{min}$ under nitrogen atmosphere) of the resulting polymers **P3.22**, **P3.23**, **P3.27**, **P3.30**, **P3.32** and **P3.37**.

Table 4-2: Yields and onset of decomposition temperatures of polymers **P3.22**, **P3.23**, **P3.27**, **P3.30**, **P3.32** and **P3.37**.

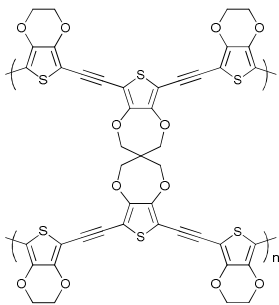
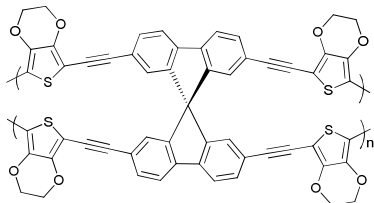
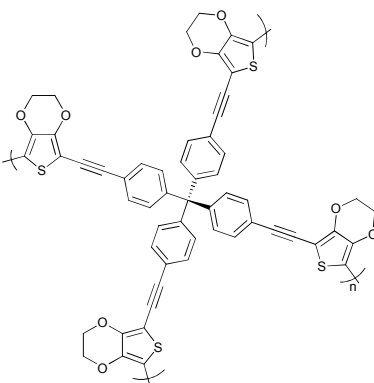
Entry	Expected Structure	Yield [%]	TGA onset [$^\circ\text{C}$]
P3.22		95	334
P3.23		91	366
P3.27		98	336

Table 4-2: Continued.

Entry	Expected Structure	Yield [%]	TGA onset [° C]
P3.30		85	184
P3.32		98	388
P3.37		87	340

The polymers were characterised by cross-polarisation ^{13}C NMR in the solid state (spectra are shown in Chapter 5 Experimental). With the exception of **P3.30**, all the materials exhibit thermal stability over 330 °C. Differential scanning calorimetry (DSC) showed no transition below the decomposition temperature, suggesting a low degree of freedom within the structure and therefore a high degree of cross-linking. Nevertheless, elemental analysis showed an unusually high content of nitrogen (between 5-10%) in all the materials. Due to the electrophilic character of the nitrosonium cation,²²⁵ it is possible that the substitution of some aromatic protons by

the nitrosyl groups may have occurred during the polymerisation, resulting in materials having randomly placed NO-substituents within the backbone. Hence, according to these observations, oxidative polymerisation is not a suitable technique for this desired purpose and these materials are not in agreement with the expected pristine structure, and are thus incomparable with the electropolymerised films.

4.3 ELECTROCHEMISTRY

4.3.1 Spirocore – EDOT

The chemical structures of spirocore-EDOT derivatives are shown in Figure 4-4.

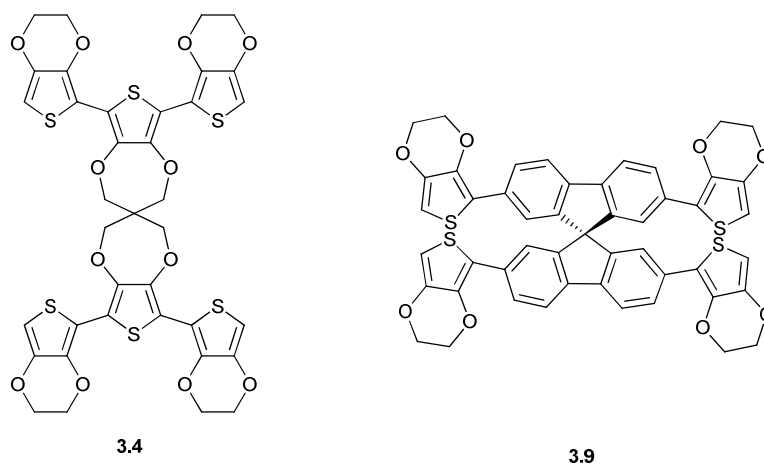


Figure 4-4: Chemical structure of **3.4** and **3.9**.

The redox properties of monomers **3.4** and **3.9** in dichloromethane solution and their corresponding polymers were investigated using cyclic voltammetry. The oxidations and reductions of the monomers are shown in Figure 4-5. Compound **3.4** undergoes a quasi-reversible oxidation at +0.16 V associated with the radical cation, which is efficiently stabilised within the terthiophene unit and therefore allows further oxidation observed as an irreversible peak at +0.78 V. The radical cation is probably located within the central thiophene unit as there was no polymer growth observed when the cycling was performed over the first oxidation wave associated

with it. However, efficient growth was achieved when cycling over the second wave suggesting that the second radical formed is placed on the external thiophene ring of the terthiophene system. An irreversible reduction of **3.4** occurs at -2.1 V. Compound **3.9** shows one quasi-reversible oxidation at +0.55 V and an irreversible reduction at -2.2 V, respectively.

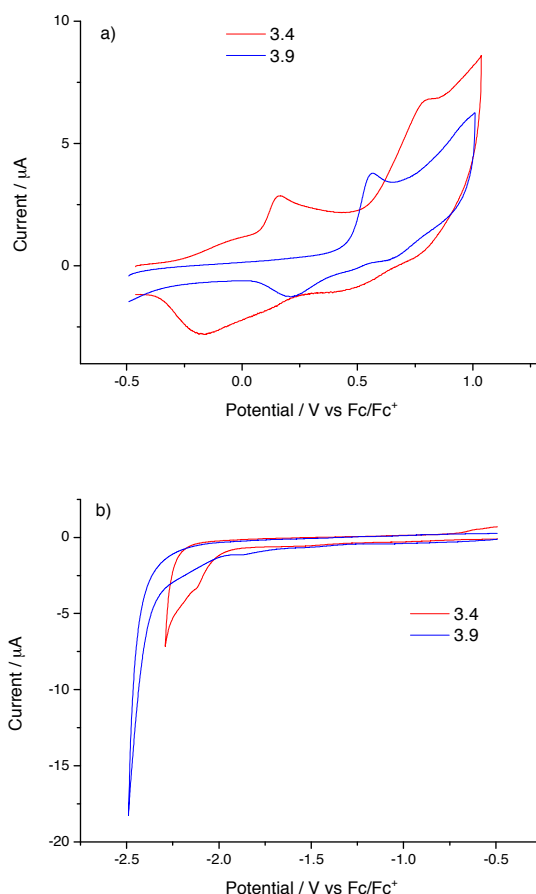


Figure 4-5: Cyclic voltammograms for (a) oxidation and (b) reduction of monomers **3.4** and **3.9** in CH_2Cl_2 (0.1mM), using a gold disk working electrode, Pt wire counter electrode, Ag wire pseudoreference electrode, TBAPF_6 as the supporting electrolyte (0.1 M) and a scan rate of 100 mV/s. The data are referenced to the Fc/Fc^+ redox couple.

Compounds **3.4** and **3.9** were polymerised *via* electrochemical oxidation by repetitive cycling from a dichloromethane solution of the monomer. The growth plots of the polymers over 50 cycles are presented in Figure 4-6 using a gold disk working electrode.

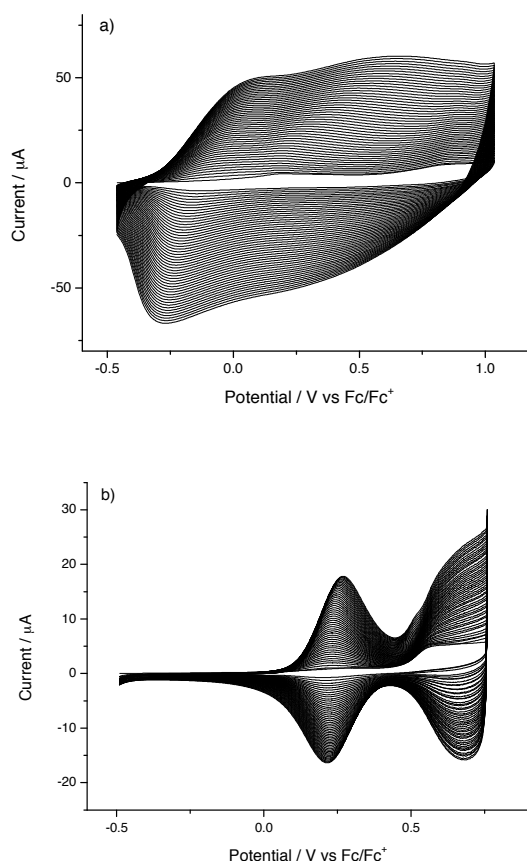


Figure 4-6: Electropolymerisation of monomer (a) **3.4** and (b) **3.9** on a gold working electrode in dichloromethane solution (0.1mM), using a Pt wire counter electrode, Ag wire pseudoreference electrode, and TBAPF₆ as the supporting electrolyte (0.1 M). The data are referenced to the Fc/Fc⁺ redox couple.

The redox properties of the polymer films are presented in Figure 4-7. The polymer poly(**3.4**) shows a reversible oxidation peak at +0.03 V and a quasi-reversible peak at +0.62 V, which correspond to the formation of stable polarons and subsequent formation of bipolarons within the polymer backbone, respectively. Poly(**3.9**) shows a reversible oxidation peak at +0.34 V. Irreversible reduction peaks are observed at -2.22 and -2.38 V for poly(**3.4**) and poly(**3.9**), respectively. Both compounds formed very dark polymers, but poly(**3.9**) showed low current density when performing redox cycles. For a clear comparison, the oxidation and reduction cycles are plotted on a double y-axis.

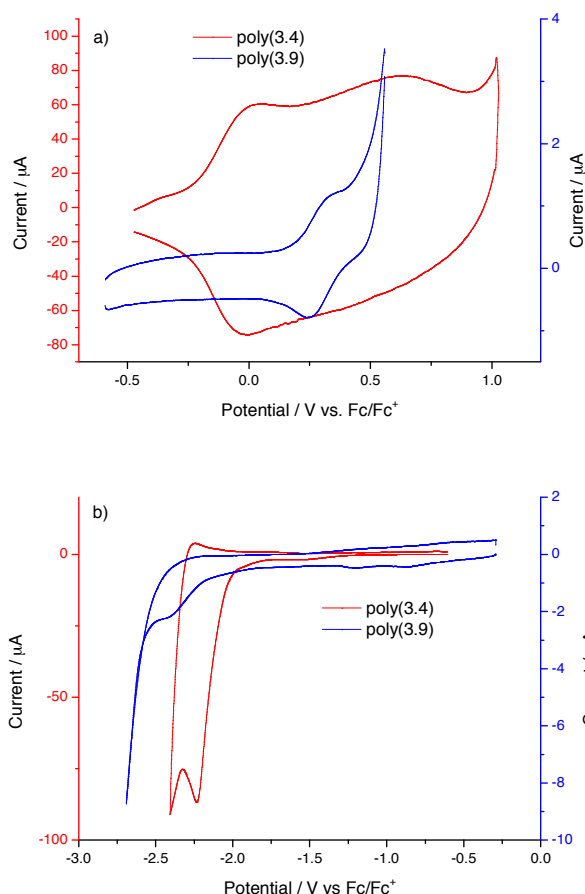


Figure 4-7: Cyclic voltammograms for the (a) oxidation and (b) reduction of poly(**3.4**), poly(**3.9**) as films on a gold disk working electrode in monomer-free acetonitrile solution, using a Pt counter electrode, Ag wire pseudoreference electrode, TBAPF₆ as the supporting electrolyte (0.1 M). The data are referenced to the Fc/Fc⁺ redox couple.

Absorption spectra of the monomers in dichloromethane solution and polymers as films on ITO slides were recorded and are shown in Figure 4-8. The monomers show absorption maxima at 375 and 397 nm for **3.4** and 363 and 380 nm for **3.9**, whereas the corresponding polymer absorption maxima related to the lowest energy transition are bathochromically shifted to 500 and 556 nm for poly(**3.4**) and poly(**3.9**), respectively, due to the increased conjugation.

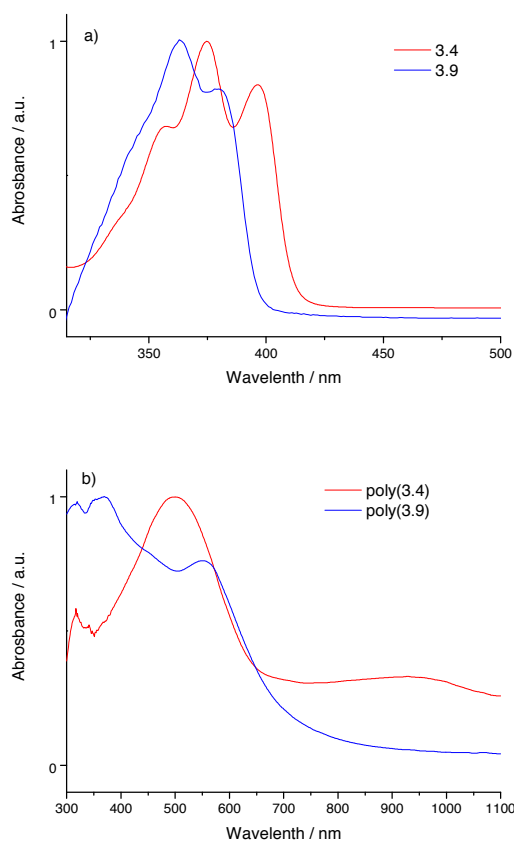


Figure 4-8: Normalised UV-vis spectra of (a) **3.4** and **3.9** in dichloromethane solution and (b) poly(**3.4**) and poly(**3.9**) as films on ITO slides.

Table 4- 3: HOMO-LUMO and band gaps of compounds **3.4** and **3.9** and their corresponding polymers. The electrochemical HOMO and LUMO levels were calculated by subtracting the value of the onset of the first oxidation and reduction peaks, respectively, from the HOMO of ferrocene (-4.8 eV). The electrochemical HOMO-LUMO/band gap is the difference between the HOMO and LUMO.

	Onset of Oxidation [V]	HOMO [eV]	Onset of Reduction [V]	LUMO [eV]	HOMO-LUMO /BAND gap [eV]
3.4	+0.08	-4.88	-2.00	-2.8	2.08 / 3.02*
poly(3.4)	-0.18	-4.62	-1.56	-3.24	1.85 / 1.92*
3.9	+0.46	-5.26	-2.02	-2.78	2.48 / 3.13*
poly(3.9)	+0.20	-5.00	-2.14	-2.66	2.34 / 1.72*

*Optical HOMO-LUMO and band gap.

The values for the electrochemical and optical band gaps of the polymers are lower than the HOMO-LUMO gaps of the associated monomers in both cases, as a result of increased conjugation. The difference between the electrochemical and optical values in poly(**3.9**) can be explained as the redox peaks result from localised sites instead of from the conjugated backbone. As expected, compound **3.4** and poly(**3.4**) exhibit lower electrochemical HOMO-LUMO and band gaps than **3.9** and poly(**3.9**). This is caused because **3.4** retains a planar structure thanks to the sulfur-oxygen interactions within the EDOT-ProDOT chain (Figure 4-9), forcing planarity and therefore possessing greater electron delocalisation. On the contrary, the EDOT-fluorene unit in **3.9** is likely to be contorted out of the plane. In addition, the fluorene has a higher aromatic stabilisation energy compared to thiophene, so the band gap of the polymer is expected to be larger for poly(**3.9**) than it is for poly(**3.4**). The measured optical band gap of poly(**3.4**) might be unreliable due to inefficient dedoping; the anion is trapped within the pores of the three-dimensional structure. The absorbance onset corresponds to partially doped structures and is therefore of a longer wavelength, hence lower band gap, than what is expected for the neutral polymer.

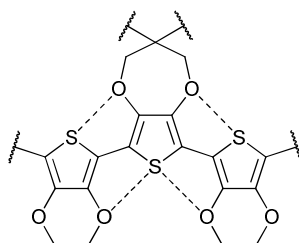


Figure 4-9: Sulfur-oxygen interactions in compound **3.4** and poly(**3.4**).

4.3.2 Tetrafunctional Spirocore – alkynyl EDOT

The structures of the tetrafunctional spirocore – alkynyl EDOT compounds are shown in Figure 4-10.

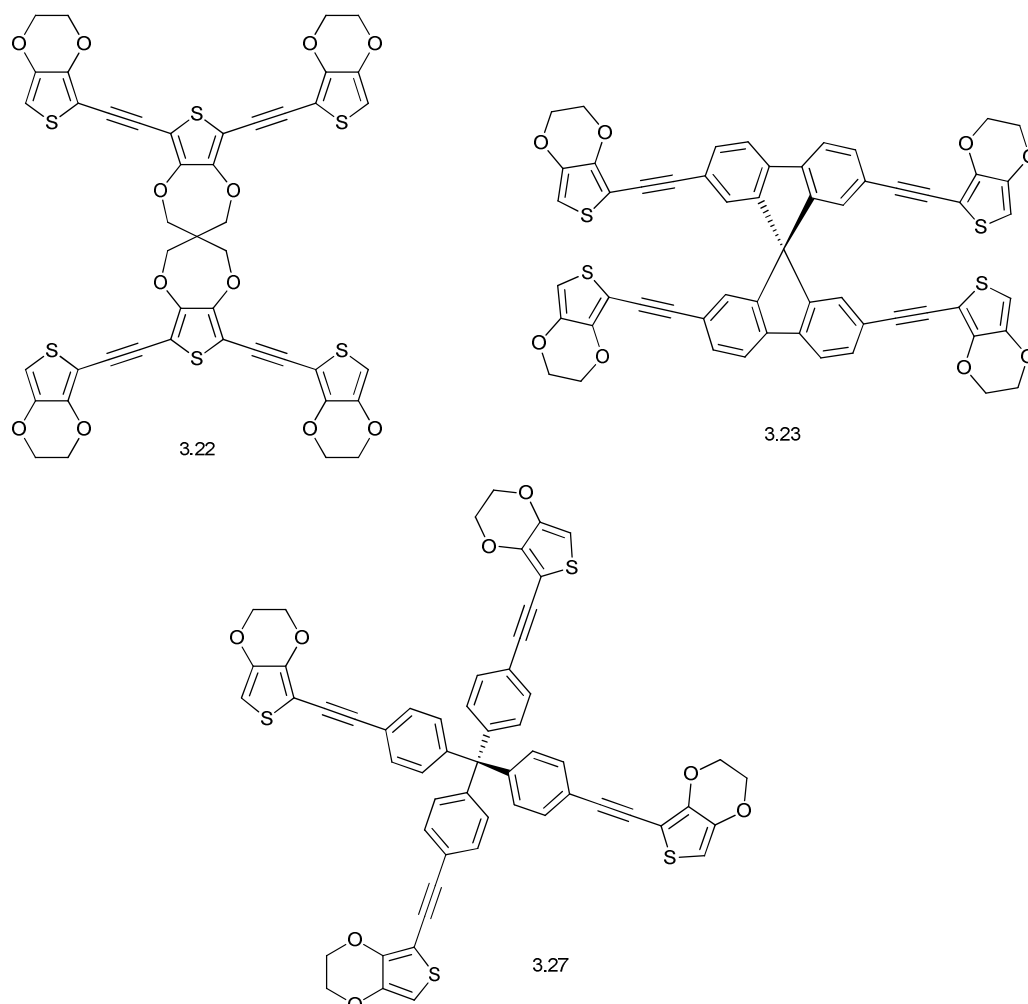


Figure 4-10: Structures of monomers **3.22**, **3.23** and **3.27**.

The redox properties of monomers **3.22**, **3.23** and **3.27**, are shown in Figure 4-11. Compound **3.22** undergoes one quasi-reversible oxidation at +0.41 V, which is over 0.2 V higher compared to the first wave in the analogue **3.4**. This is associated with the formation of a less stable cation radical in **3.22** than that generated in **3.4**, showing that the insertion of an ethyne-1,2-diylspacer between the thiophene rings reduces the stabilisation due to the electron-withdrawing effect of the sp-sp linker group. The same effect is observed for compound **3.23**, which exhibits an irreversible

oxidation peak at +0.77 V (+0.55 V for **3.9**). The chemical structure of monomer **3.27** is close to that of **3.23**, therefore similar redox behaviour is expected and an irreversible oxidation peak occurs at +0.82 V. All the three compound **3.22**, **3.23** and **3.27** are electron rich and not favourable for reductions, therefore they show irreversible processes below -2 V.

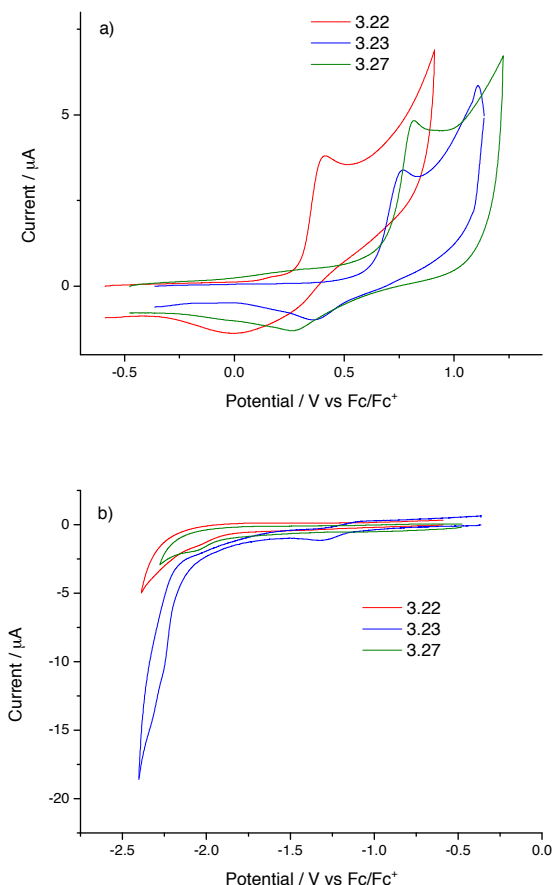


Figure 4-11: Cyclic voltammograms for (a) oxidation and (b) reduction of monomers **3.22**, **3.23** and **3.27** in CH_2Cl_2 (0.1 mM), using a gold disk working electrode, Pt wire counter electrode, Ag wire pseudoreference electrode, TBAPF_6 as the supporting electrolyte (0.1 M) and a scan rate of 100 mV/s. The data are referenced to the Fc/Fc^+ redox couple.

The polymers were grown over 20 cycles for **3.22** and **3.23** and 10 cycles for **3.27** (Figure 4-12). The potential cycling had to be stopped in the case of **3.27** due to a collapse of the current and termination of growth; **3.23** showed the same effect after 20 cycles. This can be caused due to an increased thickness of the polymer layer

and/or resistance built-up, therefore current flow is interrupted and hence depleted. Poly(**3.27**) possesses broken conjugation throughout the backbone, which is likely to result in a polymer with lower conductivity, whereas poly(**3.22**) and poly(**3.23**) have extended conjugation throughout each half unit of the polymer (determined by the spirocarbon). Additionally, this observation is in agreement with the fact that the polymer could grow in three dimensions. Comparing the crystal structure of spiroProDOT (**3.1**) published by Cooper *et al.* (Figure 4-13)¹²⁷ to the structure of compound **3.22**, only a slight contortion from planarity is expected. On the contrary, the spirobifluorene core in **3.23** stays rigid at almost a 90° angle and the tetraphenylmethane core in **3.27** has a very hindered propeller-like structure. The twisted backbone in the latter two is therefore likely to result in a polymer with three dimensions and inhibited packing. These considerations support the ease of electropolymerisation in the order **3.22** > **3.23** > **3.27**.

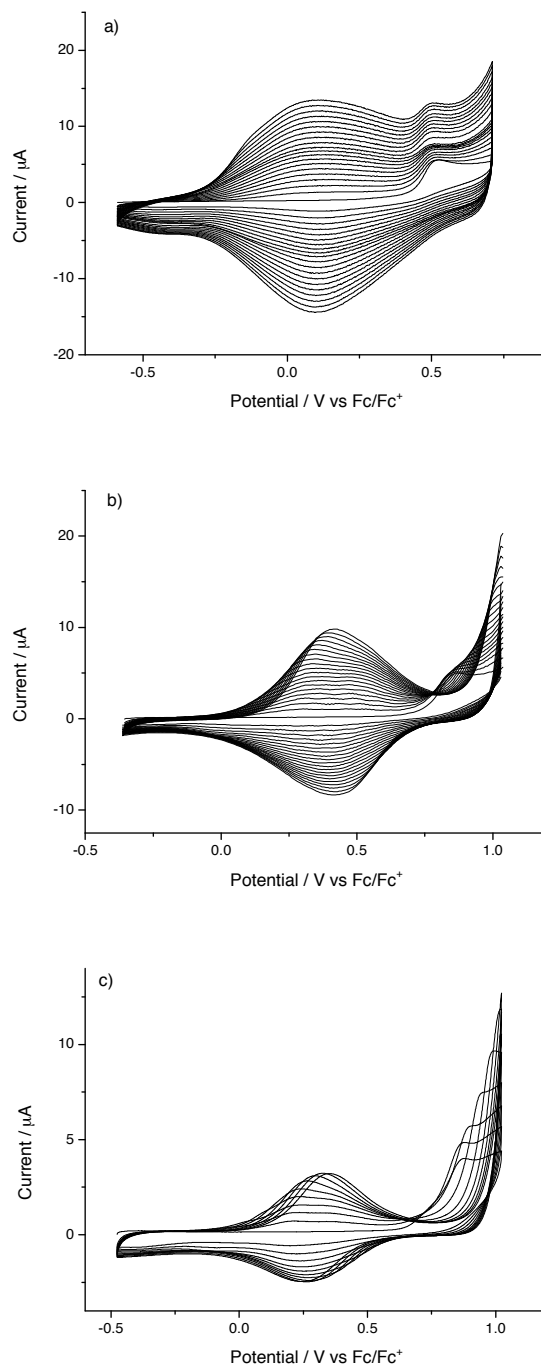


Figure 4-12: Electropolymerisation of monomers: (a) **3.22**, (b) **3.23** and (c) **3.27** on a gold disk working electrode in dichloromethane solution (0.1 mM), using a Pt wire counter electrode, Ag wire pseudoreference electrode, and TBAPF_6 as the supporting electrolyte (0.1 M). The data are referenced to the Fc/Fc^+ redox couple.

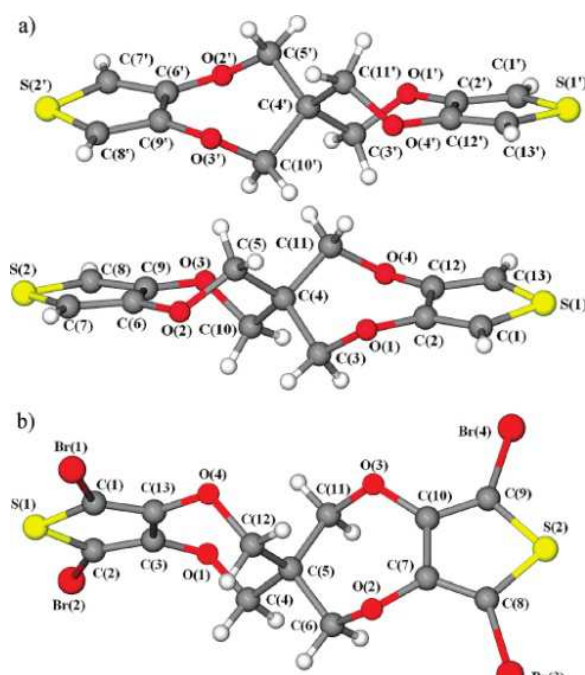


Figure 4-13: Molecular structures of (a) spiroProDOT (**3.1**) and (b) tetrabrominated spiroProDOT (**3.2**) obtained by X-ray crystallography by Cooper *et al*¹²⁷

The redox properties of the polymers are presented in Figure 4-14. Lower oxidation potentials than those associated with the corresponding monomers were observed due to the extended conjugation, but the ease of oxidation of the polymers' oxidation potential stay in the same order (+0.26, +0.47 and +0.58 V for poly(**3.22**), poly(**3.23**) and poly(**3.27**), respectively). Poly(**3.27**) exhibits the smallest current response, which can be caused either due to a lower film thickness or insufficient charge penetration throughout the film. The same phenomena or poorer charge transfer between the aromatic rings in the solid state may be responsible for the deeper reduction potential of poly(**3.27**) (-2.31 V) compared to poly(**3.22**) and poly(**3.23**) (-1.81 and -1.90 V, respectively).

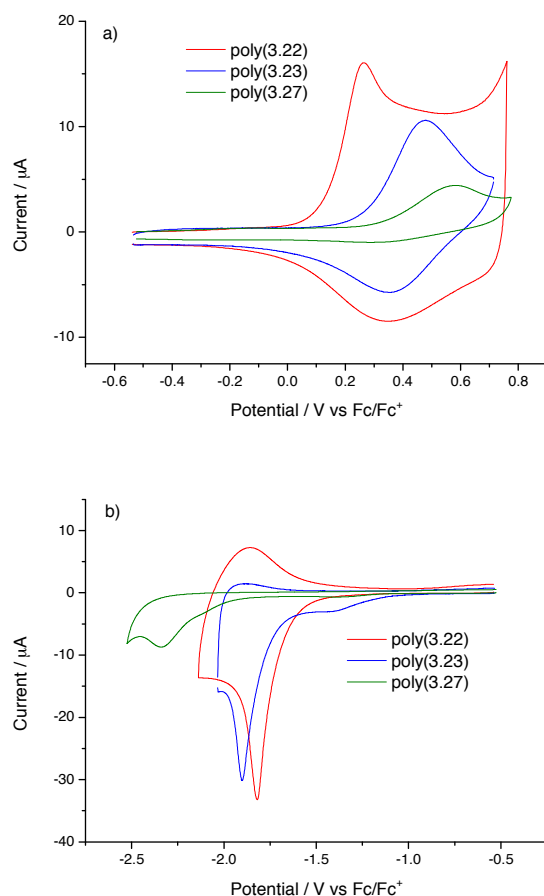


Figure 4-14: Cyclic voltammograms for (a) oxidation and (b) reduction of poly(**3.22**), poly(**3.23**) and poly(**3.27**) as films on gold disk working electrodes in monomer-free acetonitrile solution, using a Pt counter electrode, Ag wire pseudoreference electrode, TBAPF₆ as the supporting electrolyte (0.1 M). The data are referenced to the Fc/Fc⁺ redox couple.

UV spectra of the monomers in dichloromethane solution and the polymers as films deposited on ITO slides are shown in Figure 4-15. The compounds **3.22** (λ_{max} at 385 nm) and **3.23** (λ_{max} at 376 nm) absorb at higher wavelength compared to **3.27** (λ_{max} at 321 and 341 nm), due to the increased conjugation length (trisEDOT or EDOT-fluorene-EDOT vs. EDOT-phenyl for **3.22**, **3.23** and **3.27**, respectively). Owing to the increased conjugation, the onsets of UV absorption for the polymers are bathochromically shifted.

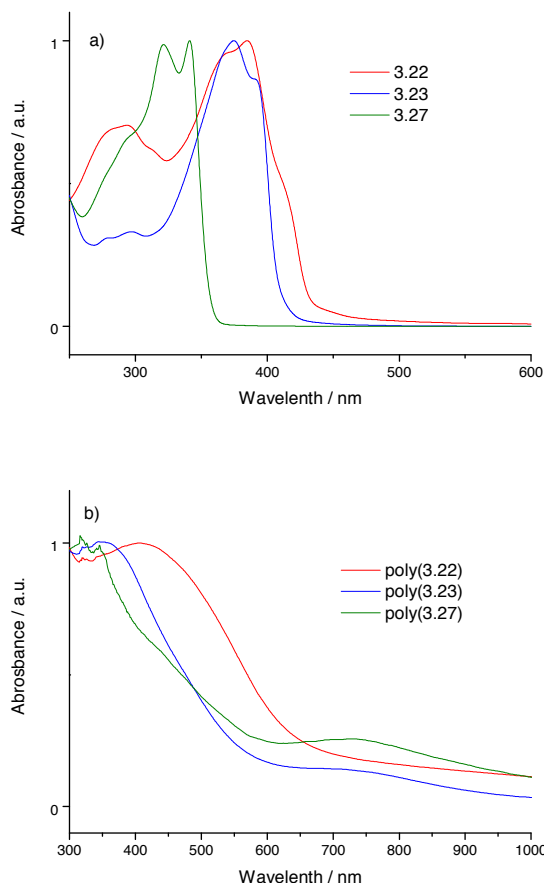


Figure 4-15: Normalised UV spectra of (a) monomers in dichloromethane solution and (b) polymers as films on ITO slides.

The HOMO-LUMO and band gaps are summarised in Table 4-4. The increased stabilisation of the radical cation in **3.22** causes a decrease of the HOMO-LUMO gap when compared to **3.23** and **3.27**. Due to the increased conjugation within the polymeric backbone, the band gaps of all the polymers are decreased compared to their corresponding monomers. The smallest difference of only *ca.* 0.2 V is observed between **3.27** and poly(**3.27**) because these compounds possess a break in conjugation in the backbone. As such, the polymer shows electrochemically similar behaviour to the molecular units. Similarly, as in the case of **3.4**, it is expected that **3.22** and **3.27** create a crowded 3D structure on the electrode surface, entrapping the counter anions and making complete dedoping challenging. This can be observed in the UV spectrum, where the presence of a positive charge in the

quinoidal structure produces absorption bands at higher wavelengths. Hence the optical band gap is not an accurate representation of the neutral polymer HOMO-LUMO gap and the electrochemical value should be considered as the true HOMO-LUMO value.

Table 4-4: HOMO-LUMO and band gaps of **3.22**, **3.22** and **3.27** and their corresponding polymers. The electrochemical HOMO and LUMO levels were calculated by subtracting the value of the onset of the first oxidation and reduction peaks, respectively, from the HOMO of ferrocene (-4.8 eV). The electrochemical HOMO-LUMO/band gap is the difference between the HOMO and LUMO.

	Onset of Oxidation [V]	HOMO [eV]	Onset of Reduction [V]	LUMO [eV]	HOMO-LUMO /BAND gap [eV]
3.22	0.31	-5.44	-2.05	-2.75	2.36 / 2.89*
poly(3.22)	0.11	-4.91	-1.61	-3.19	1.72 / 1.96*
3.23	0.64	-5.44	-2.09	-2.71	2.73 / 3.02*
poly(3.23)	0.27	-5.07	-1.74	-3.06	2.01 / (2.27)*
3.27	0.70	-5.50	-1.95	-2.85	2.65 / 3.48*
poly(3.27)	0.34	-5.14	-2.09	-2.71	2.43 / (2.22)*

*Optical HOMO-LUMO or band gap

4.3.3 *Trifunctional core–alkynylEDOT*

The structures of the trifunctional core–alkynyl EDOT compounds are shown in Figure 4-16.

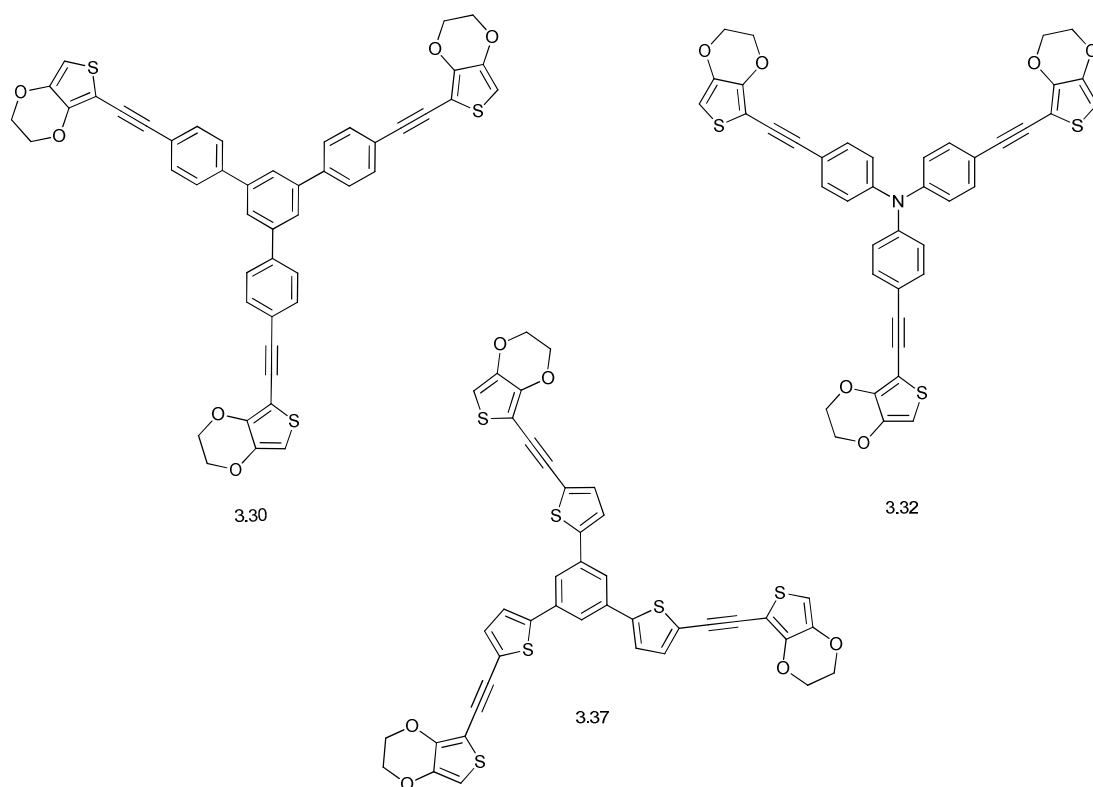


Figure 4-16: Chemical structures of compounds **3.30**, **3.32** and **3.37**.

The redox properties of monomers **3.30**, **3.32** and **3.37** were assessed by cyclic voltammetry (Figure 4-17). Compound **3.30** and **3.37** exhibit oxidation potentials at +0.88 and +0.72 V, respectively, associated with the formation of radical cations within the EDOT moiety. In the case of **3.32**, the formation of a radical cation, which is probably located at the nitrogen atom, is observed at +0.55 V and a radical cation located at the EDOT moiety at +0.83 V. Benzene ring has a higher aromatic stabilisation energy compared to thiophene, therefore the presence of the fully aromatic system in **3.30** destabilise the radical anion and increases its reduction potential (over -2.0 V) compared to **3.32** and **3.37** (observed at ca. -1.6 V).

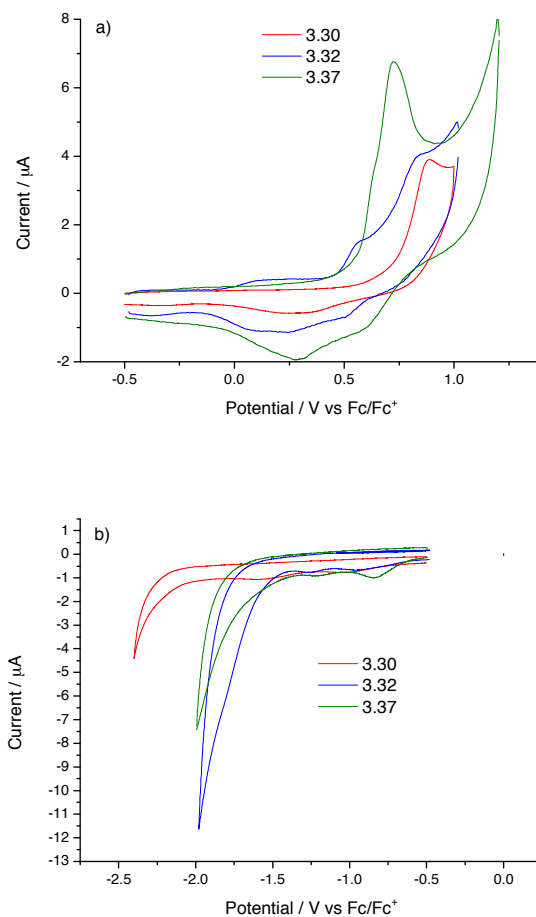


Figure 4-17: Cyclic voltammograms for (a) oxidation and (b) reduction of monomers **3.30**, **3.32** and **3.37** in CH_2Cl_2 (0.1 mM), using a gold disk working electrode, Pt wire counter electrode, Ag wire pseudoreference electrode, TBAPF_6 as the supporting electrolyte (0.1 M) and scan rate of 100 mV/s. The data are referenced to the Fc/Fc^+ redox couple.

The polymers were grown on a gold disk working electrode over 7, 30 and 22 cycles for **3.30**, **3.32** and **3.37**, respectively (Figure 4-18). The growth was stopped in the case of the first two before the current started depleting, which happens due to loss of conductivity within the film and hence prevents deposition of another layer.

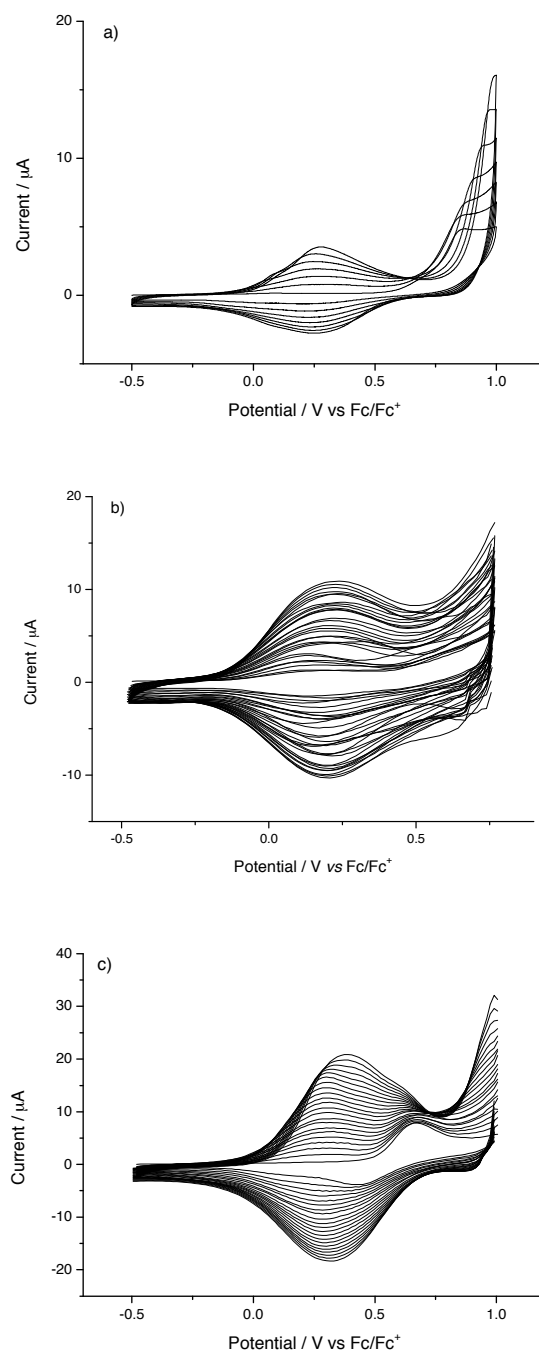


Figure 4-18: Electropolymerisation of monomers (a) **3.30**, (b) **3.32** and (c) **3.37** on gold disk working electrodes in dichloromethane solution (0.1 mM), using a Pt wire counter electrode, Ag wire pseudoreference electrode, and TBAPF_6 as the supporting electrolyte (0.1 M). The data are referenced to the Fc/Fc^+ redox couple.

Oxidation and reduction curves of the polymers are shown in Figure 4-19. The polymers show the formation of a radical cation at +0.38, +0.32 and +0.75 V, and reduction potentials at -2.12, -2.16 and -1.8 V for poly(**3.30**), poly(**3.32**) and poly(**3.37**), respectively.

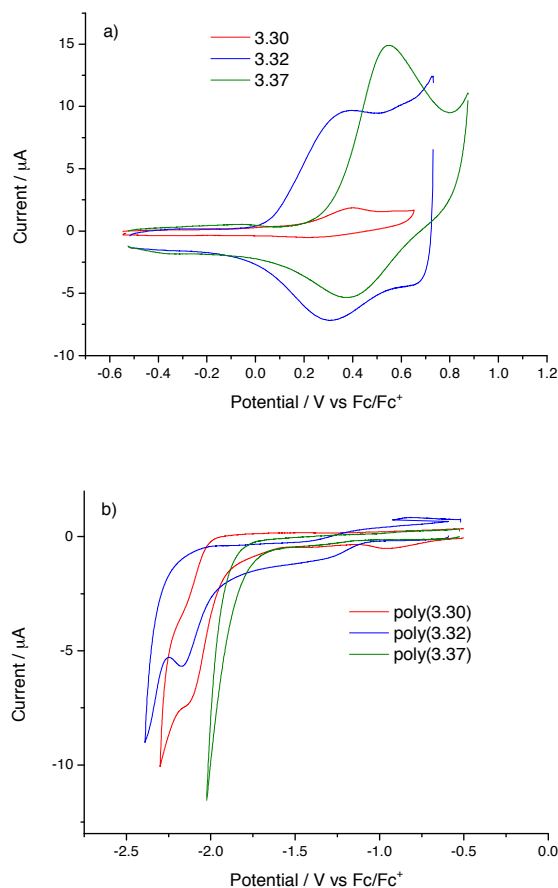


Figure 4-19: Cyclic voltammograms for the (a) oxidation and (b) reduction of poly(**3.30**), poly(**3.32**) and poly(**3.37**) as films on gold disk working electrodes in monomer-free acetonitrile solution, using a Pt counter electrode, Ag wire pseudoreference electrode, TBAPF₆ as the supporting electrolyte (0.1 M). The data are referenced to the Fc/Fc⁺ redox couple.

As expected, the onsets of UV-vis absorption bands of the polymers are bathochromically shifted to *ca.* 600 nm in comparison with their monomers, which have absorption maxima at 379, 334 and 364 nm for **3.32**, **3.30** and **3.37**, respectively (Figure 4-20).

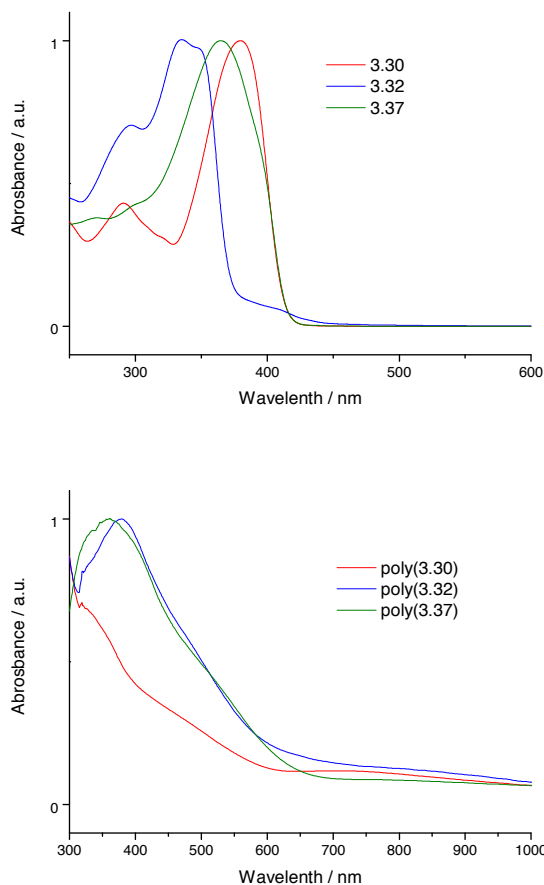


Figure 4-20: Normalised UV-vis spectra of (a) monomers in dichloromethane solution and (b) polymer films on ITO slides.

Table 4-5 summarises the electrochemical and optical gaps of the trifunctional cores **3.30**, **3.32** and **3.37**. The order of the electrochemical HOMO-LUMO gaps of the monomers is in agreement with the electron-withdrawing ability of the central cores. All polymers showed decreased electrochemical and optical band gaps with low discrepancy between poly(**3.30**), poly(**3.32**) and poly(**3.37**) due to the similarity in their chemical structure and conjugation length.

Table 4-5: Electrochemical and optical properties of **3.30**, **3.32** and **3.37** and their corresponding polymers. The electrochemical HOMO and LUMO levels were calculated by subtracting the value of the onset of the first oxidation and reduction peaks, respectively, from the HOMO of ferrocene (-4.8 eV). The electrochemical HOMO-LUMO/band gap is the difference between the HOMO and LUMO.

	Onset of Oxidation [V]	HOMO [eV]	Onset of Reduction [V]	LUMO [eV]	HOMO-LUMO /BAND gap [eV]
3.30	0.74	-5.54	-2.02	-2.78	2.76 / 2.98*
poly(3.30)	0.19	-4.99	-1.91	-2.89	2.10 / 2.11*
3.32	0.47	-5.27	-1.57	-3.23	2.04 / 3.33*
poly(3.32)	0.06	-4.86	-1.98	-2.82	2.04 / 2.09*
3.37	0.56	-5.36	-1.73	-3.07	2.29 / 2.98*
poly(3.37)	0.31	-5.11	-1.77	-3.03	2.08 / 1.96*

*Optical HOMO-LUMO or band gap

4.4 BET SURFACE AREA MEASUREMENTS

4.4.1 Bulk powder polymers

BET measurements were carried out to determine the surface area of the powder polymers, but should be treated with caution due to the high nitrogen content recorded in the elemental analysis. It is possible that the pores may be filled and therefore exhibit a lower uptake. This measurement provides qualitative information to allow a comparison between the chemically and electrochemically prepared polymers to investigate if there is a correlation between the two techniques.

An accelerated surface area and porosimetry system (Micrometrics ASAP 2420), was used to perform N₂ adsorption studies at -196 °C. Samples were out-gassed within the system at 120 °C for 16 hours. Isotherms were obtained *via* nitrogen adsorption, performed on the degassed sample using pressure increments between vacuum and the saturated vapour pressure (a dewar of liquid nitrogen to

hold the sample temperature constant at $-196\text{ }^{\circ}\text{C}$ and zero grade nitrogen with a minimum purity of 99.998% was used, supplied by BOC Polmadie). The data were analysed using application specific software, running in Windows XP. Figure 4-1 shows the isotherms obtained and Table 4-6 summarises the calculated BET surface areas.

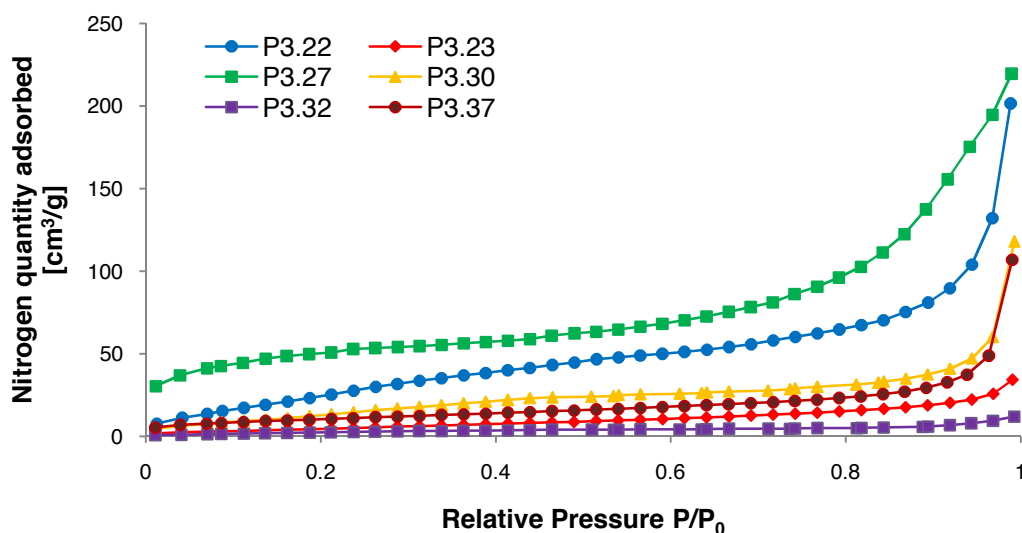


Figure 4-21: Obtained isotherms for **P3.22**, **P3.23**, **P3.27**, **P3.30**, **P3.32** and **P3.37** at $-196\text{ }^{\circ}\text{C}$. The quantity of nitrogen absorbed is shown as an equivalent specific volume of nitrogen at STP (1 atm and 298 K).

Table 4-6: BET surface areas for **P3.22**, **P3.23**, **P3.27**, **P3.30**, **P3.32** and **P3.37**.

	BET	
	Surface. Area	Error
	[m ² /g]	
P3.22	122.0	3.6
P3.23	21.0	0.8
P3.27	171.0	3.2
P3.30	62.0	2.6
P3.32	12.0	0.2
P3.37	39.0	0.1

All isotherms are of Type II, validating the application of the BET method and suggesting either non-porous materials or pores larger than micropores. It was observed that the order of size of the apparent surface area in the examined polymers is **P3.27** > **P3.22** >> **P3.30** > **P3.37** > **P3.23** > **P3.32**. However, in all cases the surface area is much smaller than expected. The reported values for polymers containing the same cores were reported in the range of 500 m²/g for spirobifluorene,¹⁰⁹ and up to 5000 m²/g for tetraphenylmethane,¹³⁰ as discussed at the beginning of section 4.2.3. This difference may originate from the structure, steric hindrance and shape of the polymer or in the fact that oxidative polymerisation using a nitrosonium salt is not a suitable technique to produce high surface area materials. It is well known that apart from the structure itself, there are many additional factors that can influence the surface area of polymeric networks such as the type of synthetic transformation, monomer reactivity or reaction conditions, including solvent, temperature, catalyst, concentration and ratio of reagents.¹²⁶ This is a large number of variables to be examined and optimised in order to find the ideal combination, which was beyond the scope of this project.

The main feature of the project was the electropolymerisation of the monomers directly onto the electrode surface, therefore these materials were not further optimised and the main focus was switched to the investigation of the surface area of the electrochemically grown thin films.

4.4.2 Electropolymerised thin films

The electrochemically prepared polymers poly(**2.7**), poly(**3.4**), poly(**3.9**), poly(**3.22**), poly(**3.23**), poly(**3.27**), poly(**3.30**), poly(**3.32**) and poly(**3.37**) were grown on ITO slides from their respective monomer solutions in dichloromethane using cyclic voltammetry. All the films were subsequently dedoped in a region with no redox activity.

The BET measurements were performed using the same apparatus and procedure as described above for the bulk powders. In each experiment, the surface area of the coated slide was measured in m²/g ($S_{BET\text{measured}}$). The mass of the coated

ITO was recorded ($m_{coated\ ITO}$) on a seven decimal place balance and, after the measurement, the slide was carefully cleaned to remove the thin film, dried under high vacuum and reweighed. Subtracting the two masses gives mass of the thin film itself ($m_{thin\ film}$). The surface area of the blank ITO slide was also measured ($S_{BET-ITO} = 0.524 \pm 0.0568$). It is possible that this value may slightly vary from slide to slide as the surface area is mainly derived from the roughness caused during slide preparation due to a lack of appropriate cutting tools. The BET surface area of the thin film can be calculated from equation (4-1).

$$thin\ film\ S_{BET} = \frac{(S_{BET\ measured} - S_{BET-ITO}) \times m_{coated\ ITO}}{m_{thin\ film}} \quad (4-1)$$

The obtained isotherms are shown in Figure 4-22 and the calculated results are shown in Table 4-7.

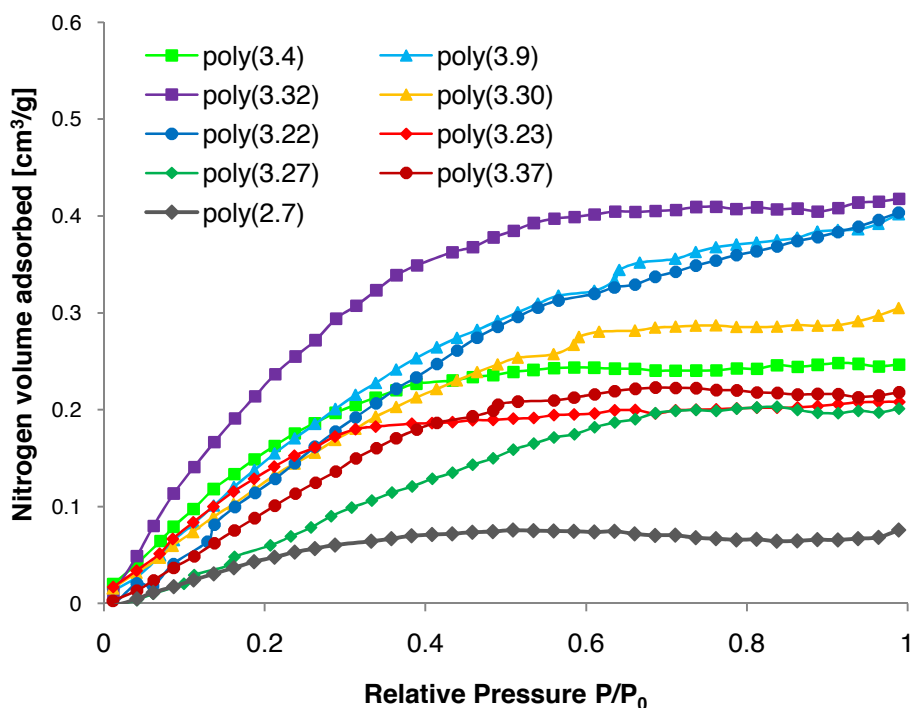


Figure 4-22: The isotherms obtained for electrochemically grown thin films at $-196\text{ }^{\circ}\text{C}$. The quantity of nitrogen absorbed is shown as an equivalent specific volume of nitrogen at STP (1 atm and 298 K).

Table 4-7: Measured and recalculated surface areas for electropolymerised films on ITO.

	S_{BET} measured [m ² /g]	Error [m ² /g]	Mass of coated ITO [mg]	Mass of thin film [mg]	Surface area [m²/g]	Error [m ² /g]
poly(2.7)	0.4752	0.0965	753.9374	0.1538	~ 0	---
poly(3.4)	0.8944	0.0359	739.2984	0.0529	5179	208
poly(3.9)	1.1867	0.0706	753.907	0.1173	4261	253
poly(3.22)	0.8354	0.0319	767.6657	0.1807	1324	51
poly(3.23)	0.8174	0.0456	680.2582	0.1835	1088	61
poly(3.27)	0.9056	0.0842	464.2543	0.1113	1593	148
poly(3.30)	0.861	0.0239	813.773	0.1137	2413	67
poly(3.32)	1.3682	0.0446	872.4512	0.1984	3713	121
poly(3.37)	1.1794	0.1549	809.7535	0.0934	5684	747

The electropolymerised thin films showed very high surface areas, two orders of magnitude higher than the bulk powders. The difference between the bulk polymers and the thin films might be due to a structural instability of the polymeric powders and therefore a collapsing and filling of the pores, or due to an inappropriate synthetic approach towards the bulk powders.

All films exhibit Type I isotherms, suggesting Langmuir-type monolayer adsorption in contrast to multilayer characteristics for the bulk powders. Hence, the reliability of the surface area determined may include a high degree of uncertainty.

The order of the surface area is poly(**3.37**) > poly(**3.4**) > poly(**3.9**) > poly(**3.32**) > poly(**3.30**) > poly(**3.27**) > poly(**3.22**) > poly(**3.23**). Surprisingly, the spirocore-EDOT polymers (poly(**3.4**) and poly(**3.9**)) exhibit higher surface areas than those with alkynyl functionality (with the exception of poly(**3.37**)), which is not in agreement with the very low surface area observed for **P3.11** or **P3.12**. The

tetrafunctional spirocore-alkynyl EDOT show the lowest measured surface areas. In comparison to poly(**2.7**), which showed negligible S_{BET} , all network polymers exhibit a surface area at least 1000times larger. This proves the hypothesis that the electropolymerisation of structures with connectivity higher than two can greatly increase the surface of the deposited thin film, which is highly desirable in sensing applications.

4.5 CONCLUSION

Novel monomers incorporating a node with connectivity higher than two and struts bearing an EDOT functionality were successfully synthesised, polymerised and electrochemically characterised. The electrochemical and optical HOMO-LUMO of monomers and band gaps of their corresponding polymers were determined.

The purpose of this preliminary study was to examine the possibility of enhancing the surface area of the polymers through the use of cross-linked networks. Two important outcomes can be concluded:

- Oxidative polymerisation is not a suitable technique to achieve cross-linked EDOT-based polymers due to the high content of nitrogen determined by microanalysis and the low BET surface areas observed.
- The electropolymerised monomers with connectivity of three or four formed polymeric networks with much higher (over 1000times) surface area than the linear homopolymer based on Poly(ProDOT-Br).

Further work will investigate substitution of the EDOT moiety within the network structures by the nitro-sensitive unit ProDOT-Br (**2.7**). It is envisaged, that such sensors will have greatly increased sensitivity and significantly reduced response times in comparison with the device described in section 3.5. With such enhanced sensitivity, it is possible to create a selective and rapid-response sensor for nitroaromatics, with sensitivity in the sub-ppm region.

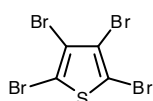
5 EXPERIMENTAL

General

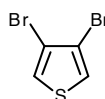
- For all reactions that require anhydrous conditions, glassware was dried in an oven at 120 °C.
- Microwave assisted reactions were performed in a Biotage Initiator microwave oven.
- ^1H and ^{13}C NMR spectra were recorded on a BrukerAvance / DPX400 at 400.13 and 100.61 MHz and a BrukerAvance / DRX500 at 500.13 MHz and 125.75 MHz. Chemical shifts are given in ppm; all J values are in Hz. Solvent residues of CHCl_3 in CDCl_3 were referenced to 7.2700 ppm for proton and 77.1600 for carbon, solvent residues of $(\text{CH}_3)_2\text{SO}$ in $(\text{CD}_3)_2\text{SO}$ were referenced to 2.500 for proton and 39.5200 ppm for carbon. Solid state NMR were obtained at the EPSRC UK national solid-state NMR service at Durham recorded on VNMRS 400 at 100.562 MHz.
- Mass spectra (EI and low-resolution) were recorded on a Micromass Trio 2000, Perkin Elmer AutoSystem XL TurboMass Mass Spectrometer and Kratos Concept spectrometers, respectively. High Resolution mass spectra were obtained at the EPSRC National Mass Spectrometry Service Centre at Swansea University using Orbitrap APCI using the ASAP probe, no solvents were added.
- Infrared spectra were recorded on a Perkin Elmer spectrum One FT-IR spectrometer (thin film deposited onto a diamond plate). Only selected absorptions (ν_{max}) are reported.
- Elemental analyses were obtained on a PERKIN ELMER 2400 elemental analyser.
- Solvents were removed using a rotary evaporator (vacuum supplied by low vacuum pump).
- Column chromatography was performed with commercially available solvents, using VWR silica gel (40-63 μm). For TLC chromatography was used a commercial TLC plates (Silica gel 60 F₂₅₄) were used.
- High vacuum distillations were performed with an Aldrich Kugelrohr fitted with a hot air bath.
- Melting points were recorded using a Stuart Scientific apparatus and are

uncorrected.

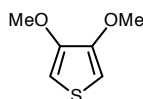
- Dry solvents (tetrahydrofuran, dichloromethane, toluene, diethyl ether and hexane) were obtained from a solvent purification system (SPS 400, Innovative Technologies) using alumina as drying agent, any other dry solvents (DMF, CH₃CN) were commercially available from Aldrich.
- Unless otherwise specified, all the reagents were purchased from Sigma Aldrich and Alfa Aesar and used as received.
- Cyclic voltammetry measurements were performed on a CH Instruments 660A Electrochemical Workstation or BAS model CV50W Voltammetric Analyser, Bioanalytical Systems Inc. with *iR* compensation. Unless stated, the electrodes were gold, platinum wire and silver wire as the working, counter and reference electrodes, respectively. The supporting electrolyte was *n*-Bu₄NPF₆ (0.1 M) for monomer and monomer-free solutions. Every measurement is referenced against the $E_{1/2}$ of the Fc/Fc⁺ redox reaction using a fresh ferrocene solution containing the appropriate solvent and electrolyte. All the monomers were polymerised *via* electrochemical oxidation by repetitive cycling over the first oxidation wave from a dichloromethane or dichloromethane/ hexane (3:1) solution of the monomer (concentration ranging from 0.5 – 1.5 M). The polymers were characterised as thin films grown on the electrode surface in monomer free MeCN solution.
- Thermogravimetric analysis was performed using a Perkin Elmer TGA instrument, heating rate 10 °C/min under nitrogen atmosphere.
- BET surface area measurement was performed using an accelerated surface area and porosimetry system Micrometrics ASAP 2420. Samples were out-gassed within the system at 120 °C for 16 hours. Isotherms were obtained *via* nitrogen adsorption, performed on the degassed sample using pressure increments between vacuum and the saturated vapour pressure (a dewar of liquid nitrogen to hold the sample temperature constant at -196 °C and zero grade nitrogen with a minimum purity of 99.998% was used, supplied by BOC Polmadie). The data were analysed using application specific software, running in Windows XP.

2,3,4,5-Tetrabromothiophene (2.1)¹⁹⁵

Thiophene (30 g, 0.36 mol) and CH_2Cl_2 (100 mL) were added to a 500 mL three-necked flask under nitrogen gas with stirring. Bromine (80 mL, 1.60 mol) was added to a dropping funnel and then added dropwise to the reaction flask. An ice bath was used to cool the solution. After addition (1.5 h), the ice bath was removed and the solution was warmed to 70 °C, and left stirring overnight. The solution was transferred to a beaker, and an ice bath was used to cool the contents for one hour with occasional stirring. During cooling a white solid precipitated. The solid was filtered and washed several times with methanol and water. The crude product was recrystallised from ethanol and then dried under vacuum for several hours until completely dry. The reaction gave a white solid (67 g; 47%); M.p. 113 – 115 °C (Lit.²²⁶ 114 °C).

3,4-Dibromothiophene (2.2)¹⁹⁵

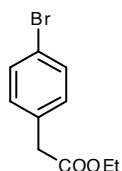
2,3,4,5-Tetrabromothiophene (**2.1**) (36.0 g, 0.09 mol) was added to a 500 mL flask containing zinc (40.0 g, 0.61 mol) and water (150 mL). Acetic acid (36 mL, 0.63 mol) was slowly added to the flask whilst stirring at a temperature of 70 °C. The mixture was stirred for 4h at 70° C and then at RT overnight. The mixture was filtered and the filtrate extracted with diethyl ether (3 × 100 mL). The organic phase was washed with NaHCO_3 solution. The diethyl ether solution was dried over MgSO_4 . Removal of the solvent under reduced pressure yielded a crude oil that was distilled under high vacuum (2×10^{-2} mbar) at 70 °C to yield a colourless oil (10 g; 47%). ^1H NMR (500 MHz, CDCl_3) δ_{H} (ppm): 7.32 (2H, s).

3,4-Dimethoxythiophene (2.3)¹⁹⁶

To the 250 mL flask was added CH_3ONa (62 mL, 25% solution in MeOH) and 3,4-dibromothiophene (**2.2**) (11.0 g; 45.5 mmol), potassium iodide (0.075 g, 4.55 mmol) and copper oxide (3.61 g, 45.50 mmol) were then added. The solution was kept at 0 °C during the addition. The reaction was stirred at 90 °C for 3 days, before cooling the solution to 50 °C and adding a further portion of potassium iodide (0.075 g, 4.55 mmol). The reaction was reheated to 90 °C and left

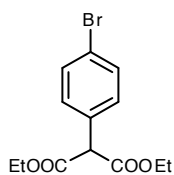
to stir overnight. The mixture was cooled to RT, filtered and the filtrate extracted with diethyl ether (3 × 100 mL). The combined organic phases were washed with water (2 × 100 mL) and then dried over anhydrous magnesium sulphate and filtered. Removal of the solvent under reduced pressure yielded a crude oil. Distillation under high vacuum (60 °C, 2 × 10⁻² mbar) yielded a colourless oil (3.70 g, yield 56%). ¹H NMR (500 MHz, CDCl₃) δ_H (ppm): 6.21 (1H, s), 3.88 (3H, s).

(4-Bromophenyl)acetic acid ethyl ester (**2.4**)¹⁹⁷



NaCl (45.5 g, 0.78 mol) with HCl was added to a 500 mL round bottom flask equipped with a vigreux column and a dropping funnel. H₂SO₄ (20 mL, 0.39 mol) was added dropwise and generating gaseous HCl that was bubbled into a second flask charged with ethanol. (4-Bromophenyl)acetic acid (25.0 g, 0.121 mol) was dissolved in the ethanol saturated with HCl and stirred for 20 h. The reaction mixture was diluted with ethyl acetate, and washed with aqueous NaHCO₃ and then brine. The organic layer was dried over anhydrous sodium sulfate and concentrated, yielding a colourless oil which solidified under vacuum to obtain a white solid with a melting point around RT (28.4 g, 97%). ¹H NMR (500 MHz, CDCl₃) δ_H (ppm): 7.46 (2H, m), 7.17 (2H, m), 4.16 (2H, q, *J* = 7.1 Hz), 3.57 (2H, s), 1.26 (3H, t, *J* = 7.1 Hz).

2-(4-Bromophenyl)malonic acid diethyl ester (**2.5**)¹⁹⁷



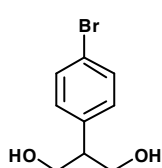
(4-Bromophenyl)acetic acid ethyl ester **2.4** (2.0 g, 8.23 mmol) was dissolved in THF (160 mL, *ca.* 0.05 M), cooled to -78 °C, and subsequently treated with lithiumhexamethyldisilane (LHMDS, 9.1 mL, 9.1 mmol, 1M in THF). The reaction was allowed to stir for 1 h at -78 °C, after which time ethyl cyanofomate (CN-COOEt, 1.22 g, 12.3 mmol) was added. The reaction was stirred for 30 min at -78 °C and allowed to warm to room temperature overnight. The reaction mixture was quenched with aqueous NH₄Cl, allowed to stir for 30 min and then washed with water and brine, dried over anhydrous Na₂SO₄, filtered and concentrated. The resulting dark red oil was purified by column chromatography with ethyl acetate/hexane (1:3) yielding **2.5** as a clear oil

(2.0 g, 77 %). $^1\text{H NMR}$ (500 MHz, CDCl_3) δ_{H} (ppm): 7.50 (2H, m). 7.30 (2H, m), 4.57 (1H, s), 4.22 (4H, m), 1.27 (6H, t, $J = 7.2$ Hz).

Table of yields for synthesis of 2-(4-Bromophenyl)malonic acid diethyl ester (2.5)

Batch Number	2.4	LHMDS	CN-COOEt	Yield
I	2.0 g (8.23 mmol)	9.1 mL (9.1 mmol)	1.2 g (12.3 mmol)	2.0 g, 77 %
II	3.0 g (12.3 mmol)	13.6 mL 1 (13.6 mmol)	1.8 g (18.5 mmol)	3.6 g, 92 %
III	10.0 g (41.1 mmol)	45.2 mL (45.2 mmol)	6.1 g (61.7 mmol)	8.3g, 64 %
IV	5.0 g (20.6 mmol)	23 mL (23 mmol)	3.1 g (30.9 mmol)	5.7g, 88 %
V	5.0 g (20.6 mmol)	23 mL (23 mmol)	3.1 g (30.9 mmol)	5.9 g, 91 %
VI	10.0 g (41.1 mmol)	45.2 ml (45.2 mmol)	6.1 g (61.7 mmol)	7.6g, 59 %

2-(4-Bromophenyl)propane-1,3-diol (2.6)¹⁹⁷



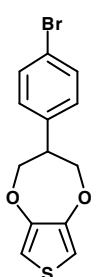
DIBAH reduction¹⁹⁷: 2-(4-Bromophenyl)malonic acid diethyl ester (2.0 g, 6.35 mmol) was dissolved in diethyl ether (50 mL, 0.14 M) and cooled to -78°C . DIBAH (26 mL, 26 mmol, 4.1 equiv, 1 M in hexane) was added and the solution was allowed to stir for 18 h at RT. The solution was combined with an equivalent volume of saturated aqueous sodium potassium tartrate and stirred vigorously for 24 h. The layers, when clear, were partitioned and the aqueous layers extracted with ethyl acetate. The organic layers were dried (Na_2SO_4) and concentrated. The resulting mixture was purified by column chromatography with ethyl acetate/hexane (1:1) to yield the product **2.6** as a clear oil (700 mg, 48 %).

LAH reduction²²⁷: LiAlH₄ (1.8 g, 44.7 mmol) was added to a flask under nitrogen and diethyl ether (60 ml) was added then cooled to 0 °C. A solution of **2.5** in diethyl ether (100 mL) was added and the mixture was left to stir at RT overnight. Water (10 mL) was slowly and carefully added at 0 °C. The mixture was filtered through celite and then washed with water (50 mL) and extracted back with diethyl ether (50 mL). The organic layers were combined and dried over Na₂SO₄, filtered and evaporated. The resulting mixture was purified by column chromatography with ethyl acetate/hexane (1:1) the product as a clear oil (2.65 g, 65 %). ¹H NMR (400 MHz, CDCl₃) δ_H (ppm): 7.47 (2H, m), 7.14 (m, 2H), 4.03 - 3.89 (4H, m), 3.10 - 3.04 (1H, m), 2.00 (2H, br s).

Table of yields for synthesis of 2-(4-Bromophenyl)propane-1,3-diol (2.6)

Batch Number	Diester (2.5)	DIBAH	LiAlH ₄	Yield
I	2.0 g, (6.35 mmol)	26 ml, (26 mmol)	---	700 mg, 48 %
II	3.3 g, (10.2 mmol)	42 ml, (42 mmol)	---	1.1 g, 46 %
III	4.5 g, (14.3 mmol)	59 ml, (59 mmol)	---	1.7 g, 51 %
IV	2.0 g, (6.35 mmol)	26 ml, (26 mmol)	---	370 mg, 25 %
V	3.3 g, (10.5 mmol)	43 ml, (43 mmol)	---	0.9 g, 37 %
VI	5.6 g, (17.8 mmol)	---	1.8 g, (44.7 mmol)	2.7 g, 65 %
VII	6.0 g, (19 mmol)	---	2.17 g, (5.7 mmol)	2.4 g, 55 %

3-(4-Bromophenyl)-3,4-dihydro-2H-thieno[3,4-b][1,4]dioxepine (2.7)

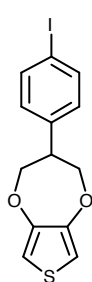


2-(4-Bromophenyl)propane-1,3-diol (**2.6**) (1.5 g, 6.5 mmol, 1 eq), 3,4-dimethoxythiophene (0.94 g, 6.5 mmol, 1 eq) and *p*-toluenesulfonic acid (150 mg, 10 % mass of **2.6**) were added to a 2-necked 1L round-bottom flask and dissolved in dry toluene (10 mM, relative to the diol). The flask was equipped with a Soxhlet extractor containing activated 4 Å molecular sieves. The reaction mixture was refluxed under nitrogen for 6 days; after the second day another portion of *p*-toluenesulfonic acid was added and the solution turned dark purple. When cooled, the mixture was washed with 10 % aq.

NaOH solution and water, then extracted with dichloromethane. The combined organic layers were dried over Na₂SO₄, filtered and evaporated. The crude product was purified by column chromatography, eluting with ethyl acetate/hexane (1:9), afforded the product **2.7** as a white solid (1.4 g, 69 %). M.p. 61-62 °C; ¹H NMR (500 MHz, CDCl₃) δ_H (ppm): 7.48 (2H,d, *J* = 8.5 Hz.), 7.22 (2H, d, *J* = 8.5 Hz), 6.55 (2H, s), 4.39 (2H, m), 4.14 (2H, m) 3.52-3.45 (1H, m); ¹³C NMR (125 MHz, CDCl₃) δ_C (ppm): 149.8, 138.1, 132.2, 129.8, 121.6, 105.8, 74.7, 48.7; MS GC/EI (m/z (%)): 313 (45) [M⁺+H], 311 (45) [M⁺+H], 197 (100) [C₉H₈Br⁺]; Elemental analysis, Found: C, 50.47; H, 3.72; Br, 25.01; S,10.14, C₁₃H₁₁BrO₂S requires: C, 50.17; H, 3.56; Br, 25.68; O 10.28; S, 10.30 %.

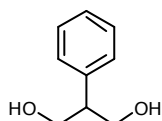
Table of yields for the synthesis of 3-(4-bromophenyl)-3,4-dihydro-2H-thieno[3,4-b][1,4]dioxepine (2.7)

Batch Number	Diol (2.6)	Thiophene (2.3)	<i>p</i> -TsOH	Solvent	Conditions	Yield
I	500 mg (2.16 mmol) 1.5 eq	208 mg (1.44 mmol) 1 eq	50 mg	Tol/CH ₂ Cl ₂ , (2/1) c _{diol} =17mM	3 days	20 mg, 3 %
II	900 mg (3. mmol), 2 eq	280 mg (1.95 mmol) 1eq	90 mg	Tol/CH ₂ Cl ₂ , (2/1) c _{diol} = 20 mM	Very dry conditions, 3 days	420 mg, 35 %
III	380 mg (1.64 mmol) 2 eq	120 mg (0.82 mol) 1 eq	40 mg	Toluene C _{diol} = 30mM	Very dry Mol. sieves 6 days	30 mg, 6 %
IV	1.5 g (6.5 mmol) 2 eq	470 mg (3.25 mmol) 1eq	2 x150 mg	Toluene C _{diol} =10 mM	Big dilution, 6 days at reflux, additional portion of <i>p</i> -TsOH 2 nd day	0.95g, 95% (47 % diol conversion)
V	1.5 g (6.5 mmol) 1 eq	0.94 g (6.5 mmol) 1 eq	2 x150 mg	Toluene C _{diol} =10 mM	Big dilution 6 days at reflux additional portion of <i>p</i> -TsOH 2 nd day	1.4g, 69 % (69 % diol conversion)

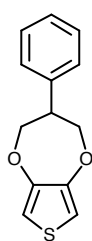
3-(4-Iodophenyl)-3,4-dihydro-2H-thieno[3,4-b][1,4]dioxepine(2.8)

3-(4-Bromophenyl)-3,4-dihydro-2H-thieno[3,4-b][1,4]dioxepine (**2.7**) (300 mg, 0.96 mmol), CuI (10 mg, 0.048 mmol), NaI (570 mg, 3.8 mmol) and *N,N'*-dimethylethylenediamine (10 mg, 0.096 mmol) were dissolved in anhydrous dioxane (10 mL, 1 M) and refluxed for 24 h. The crude mixture was filtered through a short silica plug, washed with diethylether, evaporated and purified by column chromatography (EtOAc/hexane, 1:9).

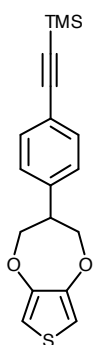
The resulting white solid was recrystallised from hexane to yield white crystals (105 mg, 49 %). M.p. 78-79 °C; ¹H NMR (400 MHz, CDCl₃) δ_H (ppm): 7.68 (2H, d, *J*=8.4 Hz), 7.09 (2H, d, *J*=8.4 Hz), 6.53 (2H, s), 4.39 (2H, m), 4.14 (2H, m), 3.50-3.43 (m, 1H); ¹³C NMR (125 MHz, CDCl₃) δ_C (ppm): 149.8, 138.7, 138.1, 130.1, 105.8, 93.1, 74.7, 48.8; MS GC/EI (m/z (%)): 358 (100) [M⁺], 217 (45) [C₇H₇I⁺]; Elemental analysis, Found: C, 44.25; H, 3.12; S, 9.06, C₁₃H₁₁IO₂S requires C, 43.59; H, 3.10; Br, 35.43; O 8.93; S, 8.95 %.

2-Phenylpropane-1,3-diol (2.9)¹⁹⁷

Suspension of 5.1 g (12.7 mmol) of 95 % pure LiAlH₄ in 250 mL of diethyl ether was cooled to 0 °C. Then 9.3 mL of diethyl 2-phenylmalonate was added dropwise. The mixture was left to stir at RT overnight. The reaction mixture was diluted with 50 mL of diethyl ether and cooled down to 0 °C and 5 mL of water was slowly added. Then 15 mL of 15% aqueous solution of NaOH was added and then again 5 mL of water. The mixture was left to warm up to RT and 4 spoons of MgSO₄ were added and stirred again for 15 min. The mixture was then filtered through celite and evaporated. The resulting crude oil was purified by column chromatography with ethyl acetate/hexane – 1/1 to yield 5.4 g of a white solid (83 %). M.p. 53 – 54 °C (Lit.¹⁹⁷ 53 – 56 °C); ¹H NMR (500 MHz, CDCl₃) δ_H (ppm): 7.37–7.2 (5H, m), 4.01 (2H, dd-roof, *J* = 10.8 and 7.6 Hz), 3.95 (2H, dd-roof, *J* = 10.75 and 5.6 Hz) 3.14 – 3.08 (1H, m), 2.18 (2H, br s).

3-Phenyl-3,4-dihydro-2H-thieno[3,4-b][1,4]dioxepine (2.10)

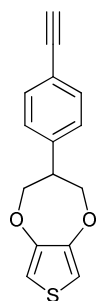
2-Phenylpropane-1,3-diol (**2.9**) (1.5 g, 9.86 mmol), 3,4-dimethoxythiophene (1.42 g, 39.86 mmol) and *p*-toluenesulfonic acid (150 mg, 10 % mass) were added to a 2-neck 1L round bottom flask and dissolved in of dry toluene (600 mL, 10 mM). The flask was equipped with a Soxhlet extractor with 4Å molecular sieves. The reaction mixture was refluxed for 6 days, an extra portion of *p*-TSOH was added on the second day. Once cool, the mixture was washed with 10 % NaOH water solution and water and extract with CH₂Cl₂ (200 mL). The combined organic layers were dried over Na₂SO₄, filtered and evaporated. The crude product was purified by column chromatography eluting with ethyl acetate/hexane (1:9) (*R*_f = 0.4) to achieve **2.10** as a white solid (0.9 g, 39 %). M.p. 85-86 °C; ¹H NMR (500 MHz, CDCl₃) δ_H (ppm): 7.38-7.28 (5H, m), 6.55 (2H, s), 4.42 (2H, m), 4.16 (2H, m) 3.57-3.51 (1H, m); ¹³C NMR (125 MHz, CDCl₃) δ_C (ppm): 150.1, 138.9, 129.1, 128.0, 127.6, 105.8, 75.2, 49.4; MS GC/EI (*m/z* (%)): 232 (100) [M⁺], 117 (100) [C₄H₅O₂S⁺]; Elemental analysis, Found: C, 67.45; H, 5.20; S, 13.74; C₁₃H₁₂O₂S requires C, 67.21; H, 5.21; O, 13.77; S, 13.80 %.

((4-(3,4-Dihydro-2H-thieno[3,4-b][1,4]dioxepin-3-yl)phenyl)ethynyl)trimethylsilane (2.11)

Triethylamine (10 ml) was added to a 50 mL 2-neck round bottom flask and degassed for 15 min. Then CuI (10 mg) and Pd(PPh₃)₄ (20 mg) and **2.7** (400 mg, 1.3 mmol) were added and heated up to 70 °C during which time the solution turned black and then trimethylsilylethylene (130 mg, 1.05 eq, 1.35 mmol) was added. The resulting black mixture was heated at 70 °C overnight. The reaction was followed by TLC (developed in CH₂Cl₂) and once cool, the mixture was filtered through celite, diluted with diethyl ether (50 mL) and then evaporated. The resulting crude oil was purified by column chromatography eluting with ethylacetate/hexane (1:9) to yield yellow oil (170 mg, 40 %), which was used for the next step without further purification.

^1H NMR (400 MHz, CDCl_3) δ_{H} (ppm): 7.44 (2H, d, $J = 8.12$ Hz), 7.26 (2H, d, $J = 8.2$ Hz, CDCl_3 overlap), 6.53 (2H, s), 4.39 (2H, m), 4.15 (2H, m), 3.56 – 4.48 (1H, m).

3-(4-Ethynylphenyl)-3,4-dihydro-2H-thieno[3,4-b][1,4]dioxepine (2.12)

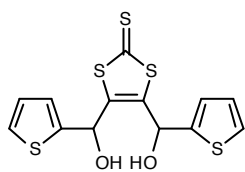


2.11 (170 mg, 0.52 mmol) was dissolved in dry THF (50 mL) and TBAF (0.05 mL, 0.05 mmol) were added and stirred at RT overnight. The reaction was quenched with saturated solution of NH_4Cl , extracted with ethyl acetate (100 mL) and organic layer were dried over Na_2SO_4 , filtered and evaporated and purified by column chromatography eluted with ethylacetate:hexane (1:9) to yield **2.12** as a white solid (90 mg, 68%, purity of 97%) M.p. 59-61 °C, ^1H NMR (500 MHz, CDCl_3) δ_{H} (ppm): 7.48 (2H, d, $J = 8.20$ Hz), 7.29 (2H, d, $J = 8.2$ Hz), 6.54 (2H, s), 4.40 (2H, m), 4.16 (2H, m) 3.55-3.49 (m, 1H), 3.08 (1H, s); ^{13}C NMR (125 MHz, CDCl_3) δ_{C} (ppm): 149.9, 139.8, 132.8, 128.1, 121.5, 105.8, 83.4, 74.8, 49.2, 29.9; MS GC/EI (m/z (%)): 256 (100) [M^+], 141(100) [C_9H_6^+], 115(80) [$\text{C}_4\text{H}_5\text{O}_2\text{S}^+$]; Found: C, 69.58.75; H, 5.26; requires: $\text{C}_{15}\text{H}_{12}\text{O}_2\text{S}$, C, 70.29; H, 4.72 %.

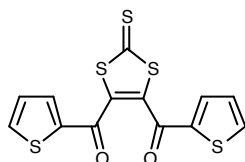
Vinylenetrithiocarbonate (2.13)²⁰¹



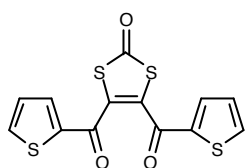
2-Piperidino-1,3-dithiolium hexafluorophosphate (10.0 g, 0.03 mol) was dissolved in dimethyl formamide/AcOH (3:1, 70 mL) while cooling the mixture with an ice bath. Then sodium hydrosulfide (2.5 g, 0.045 mol) was added portion-wise and the mixture was stirred overnight. The reaction mixture was poured into the water (200 mL) and extracted with diethyl ether (4x150 mL). The extracts were combined and washed with water (3x100 mL), saturated NaHCO_3 (3x 100 mL) and water (2x 100 mL), dried over Na_2SO_4 , filtered and evaporated. The product was dissolved in CH_2Cl_2 (100 mL) and stirred with charcoal for 15 min and filtered through a short silica column. Evaporation of solvent gave a yellow solid (3.86 g, 95%). M.p. 49 – 51 °C (Lit²⁰¹ 49 – 50 °C), ^1H NMR(CDCl_3 , 500 MHz) δ_{H} (ppm): 7.11 (s).

***meso*-4,5-Bis(2-thienylhydroxymethyl)-1,3-dithiole-2-thione (2.14)**²⁰²

To a solution of vinylenetrithiocarbonate (**2.13**) (3.5 g, 26 mmol) in dry THF (95 mL), at -55 °C, was added lithium diisopropylamide (LDA) (20 mL, 1.43 M solution in cyclohexanes, 28.7 mmol). The mixture was stirred under nitrogen for 20 min. The reaction was then cooled to -70 °C, 2thiophenecarboxaldehyde (2.9 g, 26 mmol) was added over 1-2 min, and after stirring for 3 min, a second portion of LDA (19 mL, 27.3 mmol) was added. The mixture was stirred at -55 °C for 15 min, after which the 2-thiophenecarboxaldehyde (2.9 g, 26 mmol) was added over 1-2 min. The reaction was heated quickly to -30 °C and poured into saturated NaHCO₃ solution (320 mL), to which KBr (33 g) was added. The product was extracted with ethyl acetate (3 x 150 mL), and the combined organic layers were dried over MgSO₄. The solvent was removed under vacuum and the residue was purified by column chromatography (silica, CH₂Cl₂). On recovery of the top spot (mono-addition product), the eluent was changed gradually to ethyl acetate. Evaporation of solvent gave a brown solid 5.7 g (61 %), which was used for the next step immediately without further purification.

4,5- Bis(2-thienoyl)-1,3-dithiol-2-thione (2.15)²⁰²

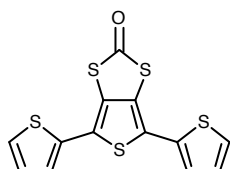
To a solution of *meso*-4,5-bis(2-thienylhydroxymethyl)-1,3-dithiole-2-thione (**2.14**) (5.7 g, 15.9 mmol) in dichloromethane (15 mL) was added MnO₂ (22 g). The mixture was stirred at RT for 2 min and immediately filtered through a layer of silica, while eluting with CH₂Cl₂. The solvent was removed in vacuum to obtain a yellow tar which gradually solidified on standing (4.0 g, 71 %, 44 % for the two steps). M.p. 132 – 133 °C (Lit.²⁰² 130 – 132 °C); ¹H NMR(CDCl₃, 500 MHz) δ_H (ppm): 7.75 -7.70 (m, 4H), 7.12-7.10 (m, 2H).

4,5-Di(2-thienoyl)-1,3-dithiol-2-one (2.16)²⁰⁰

To a solution of 4,5- bis(2-thienoyl)-1,3-dithiol-2-thione (**2.15**) (4.0 g, 11.2 mmol) in dichloromethane–glacial acetic acid (200 mL, 3:1 v/v) was added mercuric acetate (5.6 g, 17.7 mmol).

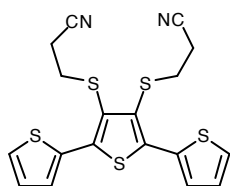
The mixture was stirred at RT for 16 h, filtered and washed with dichloromethane (50 mL). The organic extracts were washed with water and saturated sodium bicarbonate solution, then dried (MgSO_4). The solvent was removed under reduced pressure to afford **2.16** as a pale yellow solid (3.7 g, 97 %). This compound was used for the next step immediately without further purification.

4,6-Di(2-thienyl)thieno[3,4-d]-1,3-dithiol-2-one (**2.17**)²⁰⁰



A mixture of 4,5-di(2-thienyl)-1,3-dithiol-2-one (**2.16**) (3.7 g, 10.2 mmol), P_2S_5 (22.6 g, 50.9 mmol) and NaHCO_3 (3.5 g) in 1,4-dioxane (70 mL) was stirred under nitrogen whilst the temperature was raised from 60–90 °C over 1 h. The mixture was cooled, water was added (400 mL) (caution! H_2S and CO_2 evolution) and the suspension was allowed to reflux for 0.5 h and then stirred at RT overnight. The crude product was filtered, the residue dissolved in CS_2 , dried (MgSO_4) and filtered to remove residues of P_2S_5 and MgSO_4 . The product was stirred with charcoal and filtered through a short silica layer. Evaporation of solvent gave a yellow solid (1.5 g, 43 %). M.p. 170–172 °C (Lit.²⁰² 170–172 °C); ^1H NMR (CDCl_3 , 500 MHz) δ_{H} (ppm): 7.39, (2H, dd, $J = 1.1$ and 5.1 Hz), 7.25 (2 H, dd, $J = 1.2$ and 3.7 Hz), 7.13 (2 H, dd, $J = 3.6$ and 5.1 Hz).

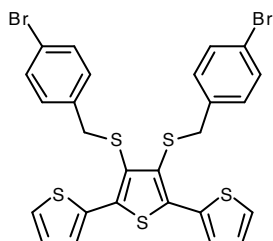
2,5-Di(2-thienyl)-3,4-bis(2-cyanoethylsulfanyl)thiophene (**2.18**)²⁰⁰



A solution of compound **2.17** (1.5 g, 4.43 mmol) in dry tetrahydrofuran (70 mL) under dry nitrogen was cooled to 0 °C. Potassium tert-butoxide (1.1 g, 9.75 mmol) was added and the mixture was allowed to stir at 0 °C for 1 h. 3-Bromopropionitrile (0.8 mL, 9.75 mmol) was added and this was allowed to stir under dry nitrogen for approximately 2 h whilst warming to RT. The reaction was poured into water (50 mL) and the product was extracted into ethyl acetate (3 x 100 mL). The combined organic extracts were washed with water (2 x 100 mL) and dried (MgSO_4). The solvent was removed under reduced pressure and the product was isolated by column chromatography (silica, dichloromethane), to afford **2.18** as a dark yellow solid (1.2 g, 64 %). M.p. 132 – 133 °C (Lit.²⁰² 132 – 134 °C); ^1H NMR (CDCl_3 , 400 MHz) δ_{H}

(ppm): 7.49 (2 H, dd, $J = 1.2$ and 3.7 Hz), 7.44 (2 H, dd, $J = 1.1$ and 5.2 Hz), 7.11 (2 H, dd, $J = 3.7$ and 5.2 Hz), 3.13 (4 H, t, $J = 7.3$ Hz), 2.59 (4 H, t, $J = 7.32$ Hz).

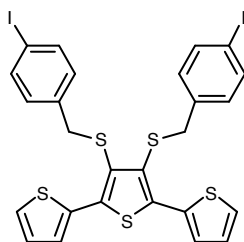
2,5-Di(2-thienyl)-3,4-bis(4-bromobenzylsulfanyl)thiophene (2.19)



To a solution of **2.18** (0.5 g, 1.19 mmol) in dry THF (50 mL) at 0 °C under nitrogen, was added tetrabutylammonium hydroxide (2.63 mL, 1 M solution in methanol, 2.63 mmol). The reaction was allowed to stir at this temperature for 1 h and 4-bromobenzyl bromide (0.65 g, 2.63 mmol) was added.

The reaction was allowed to warm to RT and was stirred for a further 3 h. Water was added (100 mL) and the product was extracted into ethyl acetate (3 x 75 mL). The combined organic extracts were washed with water (2 x 100 mL) and dried (MgSO_4). The product was isolated by column chromatography (silica, CH_2Cl_2 /hexane, 4:6) to give a yellow solid (370 mg, 48 %). M.p. 98 -100°C; ^1H NMR (500 MHz, CD_2Cl_2) δ_{H} (ppm): 7.39 (2H, dd, $J = 2.6$ and 0.6 Hz), 7.30 (6H, m), 7.06 (2H, m), 7.00 (4H, d, $J = 10$ Hz), 3.98 (4H, s); ^{13}C NMR (125 MHz, CD_2Cl_2) δ_{C} (ppm): 139.5, 136.3, 134.7, 131.2, 130.8, 130.4, 127.1, 127.0, 126.6, 120.9, 40.4; MS/MALDI: $m/z = 649$ [M^+]; Elemental analysis, Found: C, 47.73; H, 2.51; S, 24.37 requires: $\text{C}_{26}\text{H}_{18}\text{Br}_2\text{S}_5$, C, 48.00; H, 2.79; S, 24.64 %.

2,5-Di(2-thienyl)-3,4-bis(4-iodobenzylsulfanyl)thiophene (2.20)

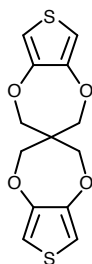


To a solution of **2.19** (0.5 g, 1.19 mmol) in dry tetrahydrofuran (50 mL) at 0 °C under nitrogen was added tetrabutylammonium hydroxide (2.63 mL, 1 M solution in methanol, 2.63 mmol). The reaction was allowed to stir at this temperature for 1 h and 4-iodobenzyl bromide (0.82 g, 2.63

mmol) was added. The reaction was allowed to warm to RT and was stirred for a further 5 h. Water was added (100 mL) and the product was extracted into ethyl acetate (3 x 75 mL). The combined organic extracts were washed with water (2 x 100 mL) and dried (MgSO_4). The product was isolated by column chromatography (silica, CH_2Cl_2 /hexane – (3/7) to give yellow the product **2.20** as a yellow solid (300 mg, 34 %). M.p. 119 -120 °C; ^1H NMR (500 MHz, CD_2Cl_2) δ_{H} (ppm): 7.50 (4H, d, J

= 8.0 Hz), 7.40 (2H, dd, $J = 4.8$ and 1.5 Hz), 7.30 (2H, dd, $J = 3.8$ and 1.3 Hz), 7.06 (2H, m), 6.86 (4H, d, $J = 8.5$ Hz) and 3.95 (4H, s); ^{13}C NMR (125 MHz, CD_2Cl_2) δ_{C} (ppm) 139.5, 137.2, 136.94, 134.7, 131.0, 130.3, 127.1, 127.0, 126.6, 92.5, 40.6; MS/MALDI: $m/z = 744$ [M^+]; Elemental analysis, Found: C, 41.73; H, 2.01; S, 21.71 requires: $\text{C}_{26}\text{H}_{18}\text{I}_2\text{S}_5$, C, 41.94; H, 2.44; S, 21.53 %.

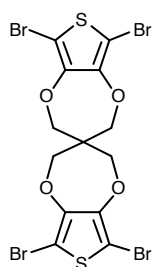
Spiro-bispropylenedioxythiophene) (3.1)¹⁵³



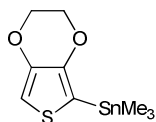
3,4-Dimethoxythiophene (2.0 g, 13.8 mmol) and pentaerythritol (11.33 g, 83.2 mmol) and *p*-toluenesulfonic acid (0.26 g, 1.38 mmol) were added to a 2-necked 1L round-bottom flask and dissolved in dry toluene (250 ml). The flask was equipped with a Soxhlet extractor containing activated 4 Å molecular sieves. The reaction mixture was refluxed under nitrogen for 24 h. When cooled, the black mixture was washed with 10 % aq. NaOH solution and water, then extracted with dichloromethane. The combined organic layers were dried over MgSO_4 , filtered and evaporated. The crude product was filtered through short silica plug and after evaporation of CH_2Cl_2 , the resulting white solid was recrystallized from chloroform yielding **3.1** as white crystals (1 g, 23 %). M.p. 228 – 229 °C (Lit¹⁵³ 226 – 229 °C); ^1H NMR (400 MHz, CDCl_3) δ_{H} (ppm): 6.48 (s, 4H), 4.06 (s, 8H).

Table of yields for synthesis Spiro-Bispropylenedioxythiophene) (3.1)

	3,4-dimethoxy-thiophene (2.3)	pentaerythritol	Yield
I	2.0 g, (13.8 mmol)	11.33 g, (83.2 mmol)	1.0 g, 23 %
II	2.0 g, (13.8 mmol)	11.33g, (83.2 mmol)	1.0 g, 23 %
III	5.0 g, (34.7 mmol)	28.3 g, (207.8 mmol)	2.5 g, 44 %

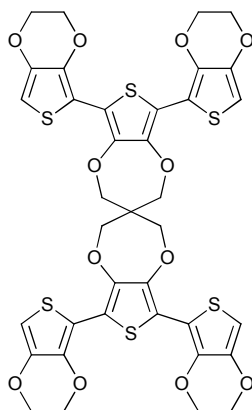
Spiro-Bis(2,5-dibromopropylendioxythiophene) (3.2)¹²⁷

N-Bromosuccinimide (1.3 g, 7.25 mmol) in DMF (40 mL) was added to a solution of spiro-bispropylendioxythiophene (**3.1**) (500 mg, 1.6 mmol) in CHCl₃ (30 mL) over 45 min. The mixture was stirred at room temperature for 6 h and then concentrated under reduced pressure. Water (150 mL) was added into the residue with stirring. The precipitate was filtered and washed with water and methanol, and the crude product was purified by recrystallization from THF/MeOH (1/3, v/v) to give **3.2** as a white crystalline solid (0.5 g, 51%). M.p.: 218 – 220 °C (Lit. not reported), ¹H NMR (500 MHz, CDCl₃) δ_H (ppm): 4.14 (s).

2-Trimethylstannyl-3,4-ethylenedioxythiophene (3.3)²⁰⁹

To a solution of 3,4-ethylenedioxythiophene (2.0 g, 14.1 mmol) in anhydrous THF (40 ml) was added dropwise *n*-butyllithium (6.3 ml, 15.5 mmol, 2.45 M solution in hexane) at -78 °C. The mixture was stirred at -78 °C for 1 h. Trimethyltin chloride (15.5 ml, 15.5 mmol, 1.0 M solution in THF) was added dropwise and the resulting mixture was stirred at -78 °C for 1 h before allowing it to warm to RT overnight. A saturated solution of NH₄Cl was added to the mixture and the product was extracted with CH₂Cl₂. The organic layer was separated, washed with water, dried with Na₂SO₄ and filtered. The solvent was removed by rotary evaporation to afford a brown oil which solidified in the freezer (4.1 g, 95 %). ¹H NMR (400 MHz, CDCl₃) δ_H (ppm): 6.59 (1H, s), 4.18 (4H, s), 0.36 (9H, s).

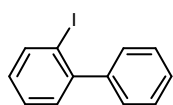
6,6',8,8'-Tetrakis(2,3-dihydrothieno[3,4-b][1,4]dioxin-5-yl)-2,2',4,4'-tetrahydro-3,3'-spirobi[thieno[3,4-b][1,4]dioxepine] (3.4)



Spiro-bis(2,5-dibromopropylenedioxythiophene) (**3.2**) (300 mg, 0.97 mmol), 2-tributylstannyl-3,4-ethylenedioxythiophene (**3.3**) (2.5 g, 5.8 mmol) and Pd(PPh₃)₄ (30 mg) were added to the microwave vial with anhydrous DMF (20 mL) and heated to 160 °C for 2 h in a microwave. The mixture was then filtered through celite and washed with CH₂Cl₂. The resulting solution was washed with water and the organic layer was dried over Na₂SO₄, filtered and evaporated. The remaining DMF was removed by Kugelrohr distillation at 45 °C, 2x10⁻² mbar and the resulting orange solid was purified by column chromatography in CH₂Cl₂/hexane (3/1) R_f = 0.2. The product was reprecipitated with CH₂Cl₂/hexane to yield 3.4 as green powder (120 mg, 15 %).

M.p. > 260°C (dec.), ¹H NMR (500 MHz, DMSO) δ_H (ppm): 6.58 (4H, s), 4.38 – 4.34 (8H, m), 4.27-4.21 (16H, m); ¹³C NMR (500 MHz, DMSO) δ_C (ppm): 143.9, 141.1, 137.6, 112.8, 108.6, 98.7, 72.1, 65.2, 64.3, 49.9; MS/MALDI: *m/z* = 856 [M⁺]; HRMS *m/z* [M+H]⁺ 856.9972, C₃₇H₂₈O₁₂S₆ requires 856.9978; Elemental analysis found: C, 51.48; H, 2.77; S, 22.09 requires C₃₇H₂₈O₁₂S₆ C, 51.85; H, 3.29; S, 22.45 %.

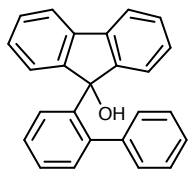
2-Iodo-1,1'-biphenyl (3.5)²²⁸



To a suspension of 2-amino-1,1'-biphenyl (15.0 g, 89 mmol) in concentrated HCl (18 mL) and water (90 mL) was added an aqueous solution of sodium nitrite (7.4 g, 193.0 mmol) over 10 min at 0 °C. The brown mixture was then stirred at 0 °C for 45 min and added slowly to an aqueous solution of KI (29.6 g, 320 mmol) over 5 min. The final solution was stirred at RT for 12 h and then extracted with diethylether. The organic layers were washed with a solution of 3 M HCl, a saturated solution of NaHCO₃, brine, water and dried over MgSO₄. The solvents were removed under vacuum to give the product as a purple oil (24.3 g, 98 %). This compound was used without any other purification.¹H

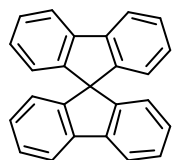
NMR (500 MHz, CDCl₃) δ_{H} (ppm): 7.98 (1H, dd, $J = 8.0$ and 1.1 Hz), 7.3–7.5 (7H, m) 7.05 (1H, td, $J = 7.85$ and 1.7 Hz).

9-(1,10-Biphenyl-2-yl)-9H-fluoren-9-ol (**3.6**)²²⁸



Magnesium (2.3 g, 93.0 mmol) was added to the 500 mL round bottom flask and purged with nitrogen. Dry ether (50 mL) was then added. Compound **3.5** (20.0 g, 71.4 mmol) was slowly added dropwise whilst the diethyl ether was gently refluxing. The mixture was heated to reflux for 90 min and then diluted with 100 mL of diethylether. The mixture was then filtered under nitrogen atmosphere using Schlenk filtration and a solution of 9-fluorenone (16.8 g, 93 mmol) dissolved in 150 mL of toluene was added dropwise. The mixture was heated to reflux for 24 h. After cooling, the solution was added to 150 g of crushed ice, diluted with 150 mL of toluene and 150 mL of concentrated HCl was added in 5 min. The solution was stirred for 3 h at RT. The two layers were separated and the aqueous layer extracted with CH₂Cl₂. The organic layers were then washed with a saturated solution of NaHCO₃, brine, and water and dried over MgSO₄. The solvents were removed under vacuum and the crude product was purified by column chromatography eluting with a gradient from hexane to dichloromethane. The first fraction was recovered 9-fluorenone, and the second was the desired product **3.6** as a white solid (8.5 g, 36%), which was used immediately without further purification. ¹H NMR (400 MHz, CDCl₃) δ_{H} (ppm): 8.47 (1H, d, $J = 8.0$ Hz), 7.54 (1H, td, $J = 7.4$ and 1.5 Hz), 7.32 (1H, td, $J = 7.5$ and 1.4 Hz), 7.23-7.13 (8H, m), 6.90 (1H, dd, $J = 7.5$ and 1.4 Hz), 6.82 (1H, m), 6.61 (2H, br t, $J = 7.6$ Hz), 6.00 (2H, dd, $J = 8.1$ and 1.0 Hz), 2.2 (1H, s).

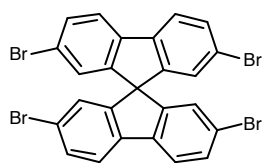
9,9'-Spirobifluorene(**3.7**)²²⁹



To a solution of 9-(2'-biphenyl)-9-fluorenol (**3.6**) (8.5 g, 25.4 mmol) in refluxing acetic acid was added concentrated hydrochloric acid (0.1 mL) and the solution heated to reflux for 40 min. The solution was cooled to room temperature, and water (50 mL) was added causing immediate precipitation. The resulting white solid was filtered and washed with water and dried *in vacuo* to afford the product **3.7** as a white solid (7.45 g, 93%).

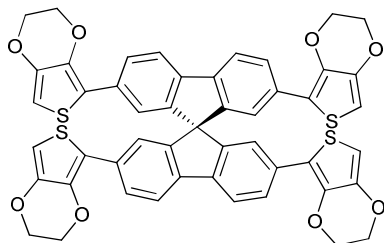
M.p. 200 – 202 °C (Lit.²³⁰206 °C); ¹H NMR (400 MHz, CDCl₃) δ_H (ppm): 7.86 (4H, d, *J* = 7.6 Hz), 7.38 (4H, td, *J* = 7.5 and 0.9 Hz), 7.08 (4H, td, *J* = 7.5 and 0.9 Hz), 6.74 (4H, d, *J* = 7.6 Hz).

2,2',7,7'-Tetrabromo-9,9'-spirobifluorene (**3.8**)²²⁹



To a solution of 9,9'-spirobifluorene **3.7** (3.0 g, 9.48 mmol) in chloroform (20 mL) at 0 °C were added FeCl₃ (77 mg, 0.47 mmol) and bromine (2 mL, 38.8 mmol). The solution was warmed to room temperature and stirred for 4 h. The resulting suspension was poured into water and washed with saturated Na₂S₂O₃ until the red colour disappeared. The aqueous layer was extracted with dichloromethane (2x) and the combined organic layers were dried over MgSO₄. The resulting crude material was purified *via* column chromatography eluting with a gradient from hexane to ethyl acetate/ hexane (1:3) to afford **3.8** as an off white crystalline powder (1.58 g, 26 %). M.p. > 340 °C, (Lit.²³¹M.p. > 320 °C); ¹H NMR (400 MHz, CDCl₃) δ_H (ppm): 7.67 (4H, d, *J* = 8.2 Hz), 7.55 (4H, dd, *J* = 8.2 and 1.8 Hz), 6.84 (4H, d, *J* = 1.7 Hz).

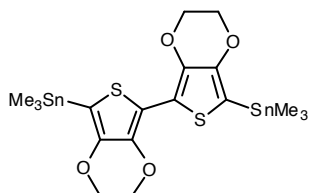
2,2',7,7'-Tetrakis(2,3-dihydrothieno[3,4-b][1,4]dioxin-5-yl)-9,9'-spirobi[fluorene] (**3.9**)



2,2',7,7'-Tetrabromo-9,9'-spirobifluorene (**3.8**) (300 mg, 0.47 mmol), 2-trimethylstannyl-3,4-ethylenedioxythiophene **3.3** (1.23 g, 2.8 mmol) and Pd(PPh₃)₄ (30 mg) were added to the microwave vial with anhydrous DMF (20 mL) and heated to 160 °C for 2 h in a microwave. The mixture was then filtered through celite and washed with CH₂Cl₂. The resulting solution was washed with water and organic layer was dried over Na₂SO₄, filtered and evaporated. The remaining DMF was removed by Kugelrohr distillation at 40 °C, 6 x 10⁻² mbarr and the resulting orange solid was purified by column chromatography in CH₂Cl₂/hexane (3/1), R_f = 0.1. The product was reprecipitated with CH₂Cl₂/hexane to yield **3.9** as a yellow powder (35 mg, 8 %).

M.p. > 340 °C; ^1H NMR (500 MHz, CDCl_3) δ_{H} (ppm): 7.82 – 7.80 (8H, m), 6.99 (4H, s), 6.18 (4H, s), 4.22 – 4.16 (8H, m), 4.18 – 4.15 (8H, m). ^{13}C NMR (125 MHz, CDCl_3) δ_{C} (ppm): 149.5, 142.2, 140.1, 138.1, 132.9, 126.0, 121.7, 120.1, 117.9, 97.6, 64.8, 64.5; MS/MALDI: $m/z = 876$ [M^+]; HRMS m/z [$\text{M}+\text{H}$] $^+$ 877.1059, $\text{C}_{49}\text{H}_{32}\text{O}_8\text{S}_4$ requires 877.1053.

5,5_-Bis(trimethylstannyl)-2,2_-bi(3,4-ethylenedioxythiophene)(3.10)²¹⁰



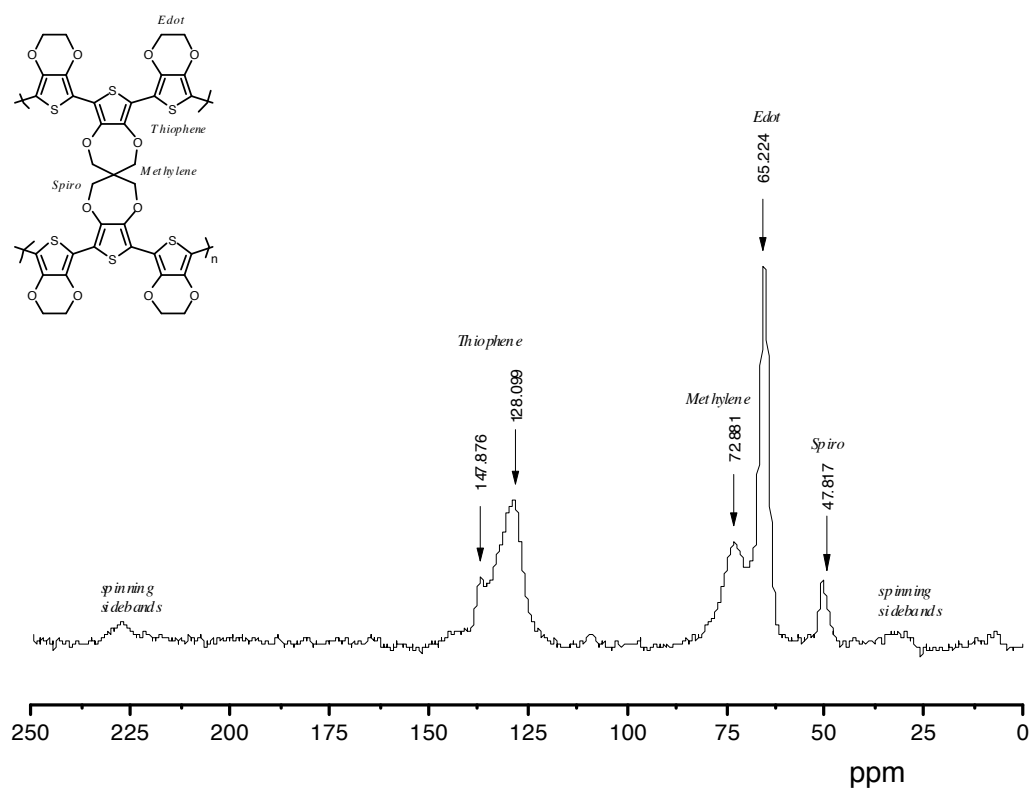
2,2-Bis(3,4-ethylenedioxythiophene) (1.5 g, 5.3 mmol) was dissolved in dry THF (50 mL) and cooled down to -78 °C and *n*-BuLi (8.8 mL, 13.2 mmol, 1.5 M in cyclohexane) was added. The mixture was stirred for 1 h whilst warming up to 0 °C and then cooled back to -78 °C. Trimethyltin chloride (13.2 mL, 13.2 mmol, 1 M in THF) was then added and the reaction was left to stir overnight. The reaction was quenched with a saturated solution of ammonium chloride, washed with water and extracted with CH_2Cl_2 . The organic layer was dried over MgSO_4 , filtered and evaporated under reduced pressure. The crude solid was recrystallised from hexane to afford desired product **3.10** (1.1 g, 35%). Although some starting material was present, this was used for the next step without further purification (more than 95 % pure). ^1H NMR (400 MHz, CDCl_3) δ_{H} (ppm): 4.32 – 4.29 (4H, m), 4.23 – 4.19 (4H, m), 0.36 (18H, s).

General synthesis of the polymers *via* Stille cross coupling

The tetrabrominated monomer (**3.2** or **3.8**) (1.0 eq) and 5,5-bis(trimethylstannyl)-2,2-bi(3,4-ethylenedioxythiophene) (**3.10**) (2.0 eq) and tetrakis(triphenylphosphine)-palladium (10 mass % of monomer) were added to a 2 neck round bottom flask and the solids were purged three times with vacuum/ nitrogen. Then, dry toluene (50 mL) was added and the mixture was refluxed for 3 days. Once no starting material observed on TLC, the reaction was cooled down and the solid was filtered and washed several times with toluene, methanol, acetone and dichloromethane before being transferred into a Soxhlet thimble extraction with toluene (24 h) and dichloromethane (24 h). The insoluble solid was then collected and dried under vacuum.

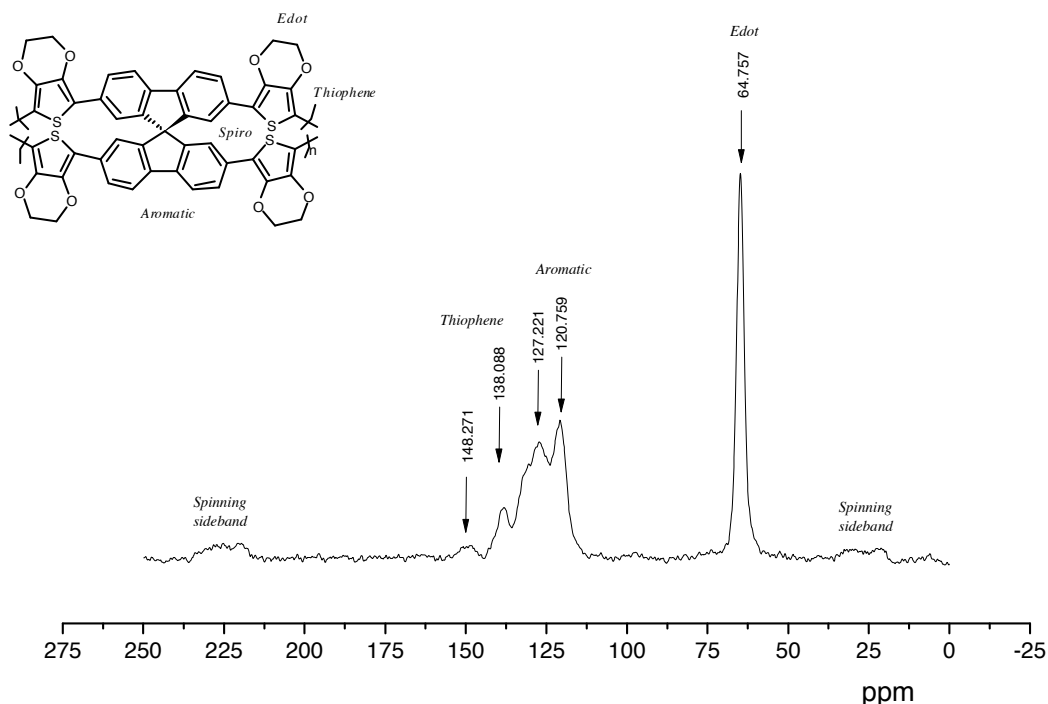
P3.11 – Compound **3.2** (300 mg, 0.490 mmol), 5,5-Bis(trimethylstannyl)-2,2-bi(3,4-ethylenedioxythiophene) **3.10** (383 mg, 0.632 mmol), tetrakis(triphenylphosphine)-palladium (30 mg). Yield 280 mg (62 %) of black powder. TGA onset 277 °C, DSC no transition observed.

CP-¹³C NMR

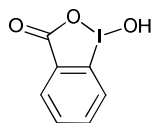


P3.12 – Compound **3.8** (200 mg, 0.316 mmol), 5,5-Bis(trimethylstannyl)-2,2-bi(3,4-ethylenedioxythiophene) **3.10** (383 mg, 0.632 mmol), tetrakis(triphenylphosphine)palladium (30 mg). Yield 210 mg of a brown solid (71 %). TGA onset 309 °C, DSC no transition observed.

CP-¹³C NMR



2-Iodosylbenzoic acid(**3.13**)²¹¹



NaIO₄ (6.7 g, 31 mmol) and 2-iodobenzoic acid (7.4 g, 30 mmol) were suspended in 30% (v:v) aq. AcOH (45 mL). The mixture was vigorously stirred and refluxed for 4 h. The reaction mixture was then diluted with cold water (120 mL) and allowed to cool to room temperature, under protection from light. After 1 h, the crude product was filtered and washed with ice cold water (3 x 30 mL) and acetone (3 x 30 mL), and air-dried in the dark to give the pure product **3.13** as a colourless solid (6.9 g, 88 %). M.p. > 260 °C (dec.), ¹H NMR (500 MHz, DMSO, δ_H (ppm)): 8.01 (1H, dd, *J* = 7.5 and 1.5 Hz), 8.01 (1H, s), 7.96 (1H, m), 7.84

(1H dd, $J = 8.1$ and 0.6 Hz), 7.70 (td, $J = 7.4$ and 0.9 Hz); ^{13}C NMR (125 MHz, DMSO) δ_{C} (ppm): 167.7, 134.4, 131.5, 131.1, 130.3, 126.3, 120.4.

Table of yield for the synthesis of 3.13

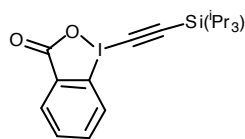
Batch Number	2-Iodobenzoic acid	NaIO ₄	AcOH/water (30 % v/v)	Yield
I	7.4 g, (30 mmol)	6.7 g, (31 mmol)	45 mL	6.9 g, 88 %
II	17.0 g, (68.5 mmol)	14.7 g, (68.5 mmol)	100 mL	17.1 g, 94 %
III	25.0 g, (0.1 mol)	21.5 g, (0.1mol)	150 mL	25.1 g, 95 %
IV	25.0 g, (0.1 mol)	21.5 g, (0.1mol)	150 mL	24.7 g, 93 %

Triisopropylsilyltrimethylsilylacetylene (3.14)²¹¹

$(\text{iPr}_3\text{Si})-\text{C}\equiv\text{C}-\text{SiMe}_3$ *n*-Butyllithium (2.22 M in hexanes, 13.2 mL, 29.9 mmol) was added dropwise to a stirred solution of ethynyltrimethylsilane (3.0 g, 30 mmol) in THF(50 mL) at -78 °C. The mixture was then warmed to 0 °C and stirred for 5 min, then cooled back to -78 °C and chlorotriisopropylsilane (6.4 mL, 30 mmol) was added dropwise. The mixture was then allowed to warm to room temperature and stirred overnight. A saturated solution of NH₄Cl (40 mL) was added and extracted with diethyl ether (2 x 100 mL). The organic layer was washed with water and brine, then dried over MgSO₄, filtered and concentrated under reduced pressure to obtain a colourless liquid which was further purified by Kugelrohr distillation (60 °C/2.2 mbar) to yield **3.14** as a colourless liquid (6.36 g, 83%). ^1H NMR (500 MHz, CDCl₃, δ_{H} (ppm): 1.08 (21H, m), 0.18 (9H, s).

Table of yield for the synthesis of 3.14

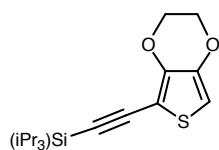
Batch Number	Ethynyltrimethylsilane	iPrSiCl	<i>n</i> -BuLi	Yield
I	3.0 g, (30.0mmol)	6.4 mL, (30.0mmol)	29.9 mmol	6.4 g, 83 %
II	6.11 g, (62.2mmol)	13.3 mL, (62.2mmol)	61.0mmol	11.5 g, 72 %
III	25.0 g, (0.26mol)	54.4 mL, (0.26mol)	0.250 mol	58.0 g, 89 %

1-[(Triisopropylsilyl)ethynyl]-1,2-benziodoxol-3(1H)-one (3.15)²¹¹

2-Iodosylbenzoic acid (**3.13**) (5.9 g, 22.5 mmol) was added to a 2-neck round bottom flask. After 3 vacuum/nitrogen cycles, anhydrous acetonitrile (160 mL) was added *via canula* and cooled to 4 °C. Trimethylsilyltriflate (4.5 mL, 24.7 mmol) was added dropwise *via* a dropping funnel over 30 min. After 15 min, (trimethylsilyl-triisopropylsilyl)acetylene (**3.14**) (6.3 g, 24.7mmol) was added dropwise over 15 min. The suspension was left to warm up to RT and after 30 min became a solution. After 10 min, pyridine (2.0 mL, 24.7mmol) was added. After 15min, the reaction mixture was transferred into a one-neck 1L flask and the solvent was evaporated under vacuum until a solid was obtained. The solid was dissolved in CH₂Cl₂ (200 mL) and washed with 1M HCl (200 mL) and the aqueous layer was extracted with CH₂Cl₂ (200mL). The organic layers were combined, washed with a saturated solution of NaHCO₃ (2 x 200 mL), dried over MgSO₄, filtered and the solvent was evaporated under reduced pressure. Recrystallization from acetonitrile (*ca.* 120 mL) afforded **3.15** as a white crystals (5.32 g, 55%). M.p > 170 °C (dec.) (Lit.²¹¹> 170 -175 °C (dec.), ¹H NMR (500 MHz, CDCl₃) δ_H (ppm): 8.43 (1H, m), 8.30 (1H, m), 7.77 (2H, m), 1.17 (21H, m).

Table of yields for synthesis of 1-[(Triisopropylsilyl)ethynyl]-1,2-benziodoxol-3(1H)-one (3.15)

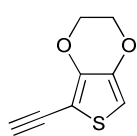
Batch Number	2-Iodosylbenzoic acid (3.13)	Trimethylsilyltriflate	Triisopropylsilyl-trimethylsilylacetylene (3.14)	Pyridine	Yield
I	5.9g (22.5mmol)	4.5 mL (24.7 mmol)	6.3g (24.7 mmol)	2.0 ml (24.7 mmol)	5.32 g, 55 %
II	10.8 g (40.7mmol)	8.1 mL (44.8 mmol)	11.4 g (44.8 mmol)	3.6 ml (44.8 mmol)	12.0 g, 69 %
III	12.3 g (46.4mmol)	9.2 mL (51.0mmol)	13.0 g (51.0mmol)	4.1 ml (51.0mmol)	17.0 g, 85 %
IV	19.2 g (72.0mmol)	13.9 mL (80.0mmol)	20.4g (80.0mmol)	6.4 ml (80.0mmol)	27.9 g, 90 %

((2,3-Dihydrothieno[3,4-b][1,4]dioxin-5-yl)ethynyl)triisopropylsilane (3.16)²¹¹

To a stirring solution of Au(I)Cl (68 mg, 0.291 mmol) in CH₃CN (30 mL) was added EDOT (2.5 g, 17.5 mmol). After 2 min, TFA (0.45 mL, 5.84 mmol) and **3.15** (2.5 g, 5.84 mmol) were added. The reaction was sealed and stirred at RT overnight. Diethyl ether (200 mL) was added and the organic layer was washed twice with 0.1 M NaOH (200 mL). The aqueous layers were combined and extracted with diethyl ether (200 mL). The organic layers were combined, washed with saturated NaHCO₃ (200 mL), brine (200 mL), dried with MgSO₄ and concentrated under reduced pressure. Purification by flash chromatography (hexane/CH₂Cl₂, 8:2) afforded **3.16** as yellow oil (0.97 mg, 52 %). ¹H NMR (500 MHz, CDCl₃) δ_H (ppm): 6.23 (1H, s), 4.29 – 4.26 (2H, m), 4.20 – 4.17 (2H, m), 1.15 (m, 21 H).

Table of yields for synthesis of 1-[(Triisopropylsilyl)ethynyl]-1,2-benziodoxol-3(1H)-one (3.16)

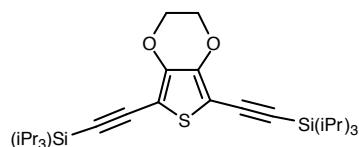
Batch Number	EDOT	3.15	Au(I)Cl	TFA	Yield
I	2.5 g, (17.5mmol)	2.5 g, (5.84 mmol)	68.0 mg, (0.29 mmol)	0.45 mL, (5.84 mmol)	0.97 g, 52 %
II	10.0 g, (70.3mmol)	10.0 g, (23.4 mmol)	200.0 mg, (0.86 mmol)	1.8 mL, (23.4mmol)	3.6 g, 48 %
III	5.0 g, (35.2mmol)	5.0 g, (11.7 mmol)	136.0 mg, (0.59mmol)	0.9 mL, (11.7mmol)	1.7 g, 45 %
IV	10.0 g, (70.3mmol)	10.0 g, (23.4 mmol)	270.0 mg, (0.12 mmol)	1.8 mL, (23.4 mmol)	1.8 g, 24 %
V	10.0 g, (70.3mmol)	10.0 g, (23.4 mmol)	200.0 g, (0.86 mmol)	1.8 mL, (23.4 mmol)	3.5 g, 46 %
VI	10.0 g, (70.3mmol)	10.0 g, (23.4 mmol)	200.0g, (0.86 mmol)	1.8 mL, (23.4 mmol)	3.8 g, 50 %

5-ethynyl-2,3-dihydrothieno[3,4-b][1,4]dioxine (3.17)²¹¹

((2,3-Dihydrothieno[3,4-b][1,4]dioxin-5-yl)ethynyl)triisopropylsilane **3.16** (0.97g, 3 mmol) was dissolved in dry THF and cooled to 0 °C. Tetrabutylammoniumhexafluorofluoride (TBAF) (3.3 mL, 3.3 mmol, 1M solution in THF) was added and mixture was stirred for 1h whilst allowing to warm to RT. The reaction was quenched with saturated aqueous NH₄Cl and diluted with diethyl ether. The organic layer was washed with brine and water, dried over MgSO₄, filtered and evaporated under reduced pressure. The crude mixture was purified twice by column chromatography, eluting CH₂Cl₂/hexane (2:8) and again CH₂Cl₂/hexane (1:1) to obtain **3.17** as a brown oil (0.76 g, 76%). ¹H NMR (400 MHz, CDCl₃) δ_H (ppm): 6.29 (1H, s), 4.32 – 4.29 (2H, m), 4.22 – 4.19 (2H, m), 3.48 (1H, s); ¹³C NMR (100 MHz, CDCl₃,) δ_C (ppm): 145.7, 140.8, 101.6, 97.5, 84.0, 74.7, 65.3, 64.5; MS (GC/CI) 167 [M+H]⁺; Elemental analysis, Found: C, 57.72; H, 3.75; S 19.07 requires: C₆H₈O₂S, C, 57.81; H, 3.75; S, 19.29 %.

Table of yields for synthesis of 5-ethynyl-2,3-dihydrothieno[3,4-b][1,4]dioxine (3.17)

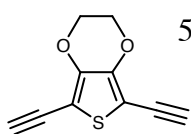
Batch Number	3.16	TBAF	Yield
I	0.97g, (3 mmol)	3.3 mL, (3.0 mmol)	0.38 g, 77 %
II	2.0 g, (6.8 mmol)	6.8 mL, (6.8 mmol)	0.76 g, 76 %
III	1.91 g, (6.8 mmol)	5.9 mL, (5.9 mmol)	0.84 g, 86 %
IV	3.1 g, (9.6 mmol)	9.6 mL, (9.6 mmol)	1.34 g, 84 %
V	3.5 g (10.8 mmol)	10.8 mL, (10.8 mmol)	1.0 g, 55 %
VI	4.0 g (12.3 mmol)	12.5 mL, (12.5 mmol)	1.6 g, 82 %

5,7-Bis((triisopropylsilyl)ethynyl)-2,3-dihydrothieno[3,4-b][1,4]dioxine (3.18)²¹¹

To a stirring solution of Au(I)Cl (41 mg, 0.18 mmol) in CH₃CN (18 mL) was added EDOT (0.5 g, 3.52 mmol). After 2 min, TFA (1.49 mL, 7.74mmol) and **3.15** (3.32 g, 7.74 mmol) were added. The reaction was sealed and stirred at RT overnight.

Diethyl ether (200 mL) was added and the organic layer was washed twice with 0.1 M NaOH (200 mL). The aqueous layers were combined and extracted with diethyl ether (200 mL). The organic layers were combined, washed with saturated NaHCO₃ (200 mL), brine (200 mL), dried with MgSO₄ and concentrated under reduced pressure. Purification by flash chromatography (hexane/CH₂Cl₂ 8:2) afforded **3.18** as yellow oil (800 mg, 70 %), which was used for next step without further purification. ¹H NMR (500 MHz, CDCl₃) δ_H (ppm): 4.25 (4 H, s), 1.11 (42 H, m).

5,7-Diethynyl-2,3-dihydrothieno[3,4-b][1,4]dioxine (3.19)



5,7-Bis((triisopropylsilyl)ethynyl)-2,3-dihydrothieno[3,4-b][1,4]dioxine **3.18** (800 mg, 2.48 mmol) was dissolved in dry THF and cooled to 0 °C. Tetrabutylammonium-hexafluorofluoride (TBAF) (2.72 mL, 2.72 mmol, 1 M solution in THF) was added and the mixture was stirred for 1 h whilst allowing to warm to RT. The reaction was quenched with saturated aqueous NH₄Cl and diluted with diethyl ether. The organic layer was washed with brine and water, dried over MgSO₄, filtered and evaporated under reduced pressure. The crude mixture was purified twice by column chromatography, eluting with CH₂Cl₂/hexane (2:8) and again with CH₂Cl₂/hexane (1:1) to obtain a white crystalline solid (150 mg, 34 %). ¹H NMR (400 MHz, CDCl₃) δ_H (ppm): 4.31 (4H, s), 3.49 (2H, s). This compound is very unstable and turns black upon standing over few hours, probably due to the rapid polymerization. Therefore it has been used immediately without further purification and analytical characterization.

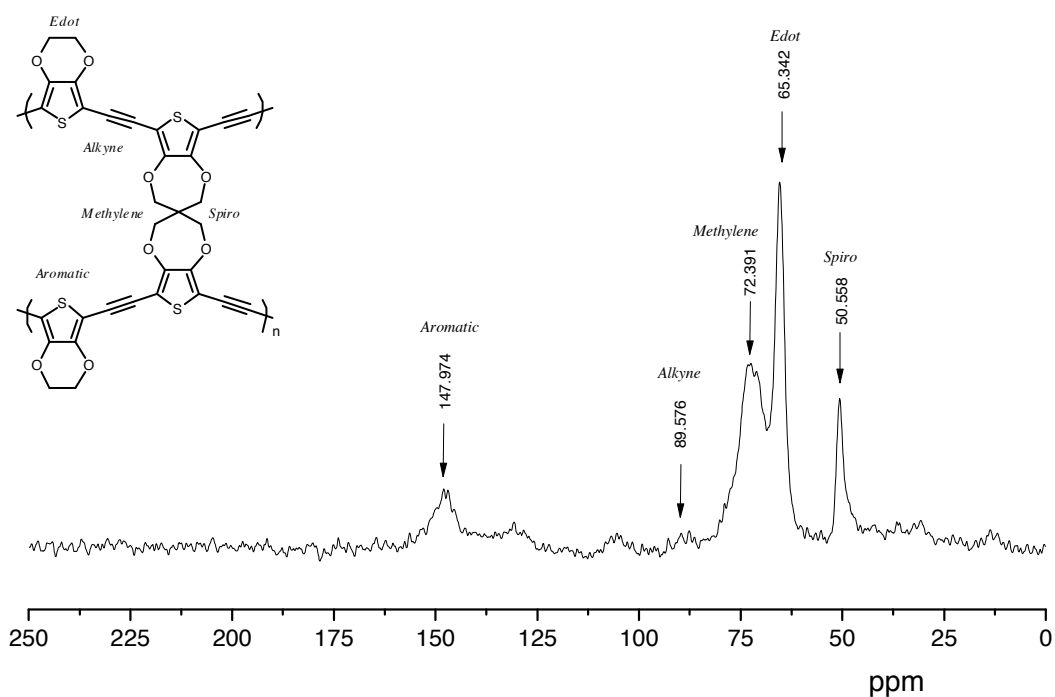
General synthesis of the polymers via Sonogashira cross coupling¹²⁷

The monomer (1 eq), dialkynyl counterpart (3 eq), tetrakis(triphenylphosphine)-palladium (10 mass % of the monomer) and copper iodide (10 % mass of the monomer) were added to the small microwave vial and the solids were purged three times with vacuum/ nitrogen. Then, dry DMF/Et₃N (1:1, 0.4 M of monomer concentration) was added. The reaction mixture was heated at 90 °C for 2.5 days. Once no starting material was observed by TLC, the reaction was cooled down and the solid was filtered and washed several times with toluene, methanol, water and

chloroform before being transferred into a Soxhlet thimble and being extracted with methanol (24h). The insoluble solid was then collected and dried under vacuum.

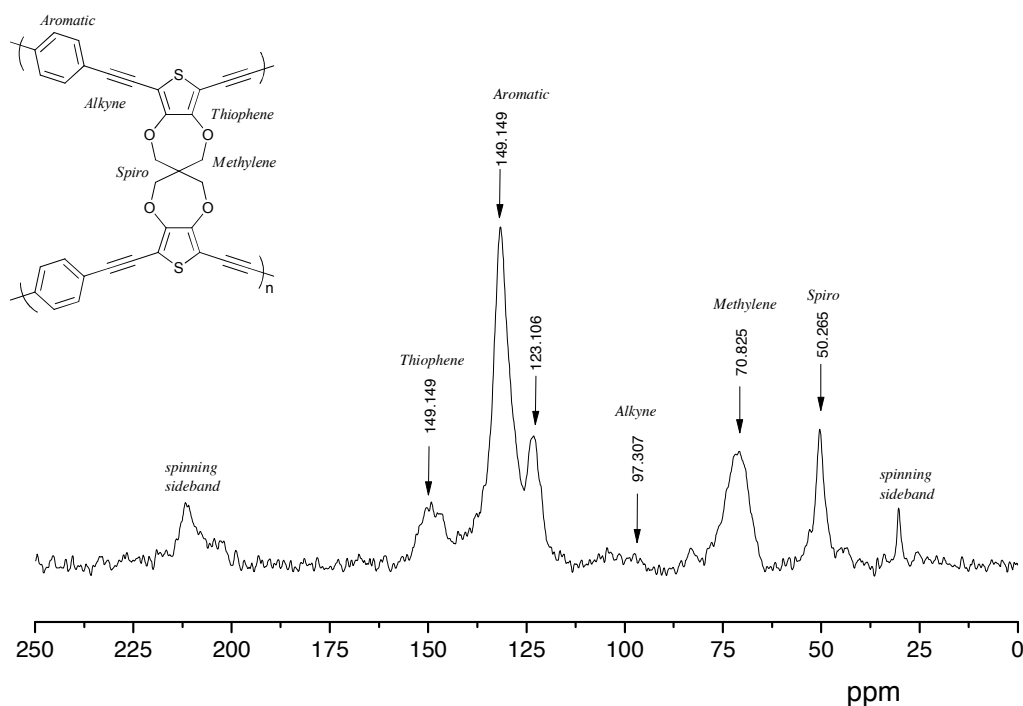
P3.20 – Compound **3.2** (75 mg, 0.123 mmol), 5,7-diethynyl-2,3-dihydrothieno[3,4-b][1,4]dioxine **3.19** (70 mg, 0.368 mmol), tetrakis(triphenylphosphine)palladium (7 mg), copper iodide (7 mg). Yield 60 mg of brown solid (73 %). TGA, onset 285 °C, DSC, no transition observed.

CP - ^{13}C NMR



P3.21 – Compound **3.2** (306 mg, 0.5 mmol), 1,4-diethynylbenzene (190 mg, 1.5 mmol), tetrakis(triphenylphosphine)palladium (15 mg), copper iodide (10 mg). Yield 180 mg of brown solid (65 %). TGA onset 353 °C, DSC, no transition observed.

CP - ^{13}C NMR



General procedure for Sonogashira cross-coupling (**3.22**, **3.23**, **3.27**, **3.30**, **3.32**, **3.37**)

Conventionally:

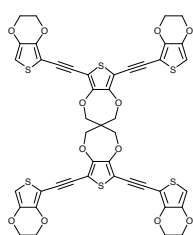
The halogenated compound (1.0eq), 5-ethynyl-2,3-dihydrothieno[3,4-b][1,4]dioxine **3.17** (1.2-1.5 eq per halogen), tetrakis(triphenylphosphine)palladium (10 mass % of the halogenated compound), copper iodide (0.3 eq) were added to a 2 neck round bottom flask and the solids were purged three times with vacuum/ nitrogen. Dry THF was then added to form a suspension. Subsequently, triethylamine (2-5 mL) was added to form a dark solution. The reaction mixture was stirred at RT until the TLC showed consumption of starting material. The reaction mixture was filtered through celite with CH_2Cl_2 and washed with saturated aqueous NH_4Cl , then water, and the aqueous layer back extracted with CH_2Cl_2 . The organic layers were

combined and dried over MgSO_4 , filtered and evaporated at reduced pressure. The resulting mixture was purified by column chromatography eluting with CH_2Cl_2 /hexane. The crude materials were precipitated from hot CH_2Cl_2 with hexane if necessary.

Microwave:

The halogenated compound (1.0 eq), 5-ethynyl-2,3-dihydrothieno[3,4-b][1,4]dioxine **3.17** (1.2 - 1.5 eq per halogen), tetrakis(triphenylphosphine)palladium (10 mass % of the halogenated compound), copper iodide (0.3 eq) and were added to a 20 mL oven dried microwave vial and the solids were purged three times with vacuum/nitrogen. Then anhydrous DMF (20 mL) and triethylamine (3-5 mL) were added. The reaction was carried out in a microwave for 2 h at 160 °C. The reaction mixture was filtered through celite with CH_2Cl_2 and washed with saturated aqueous NH_4Cl , then water, and the aqueous layer back extracted with CH_2Cl_2 . The organic layers were combined and dried over MgSO_4 , filtered and evaporated at reduced pressure. The resulting mixture was purified by column chromatography eluting CH_2Cl_2 /hexane or light petroleum ether. The crude materials were precipitated from hot CH_2Cl_2 into hexane if necessary.

6,6',8,8'-Tetrakis((2,3-dihydrothieno[3,4-b][1,4]dioxin-5-yl)ethynyl)-2,2',4,4'-tetrahydro-3,3'-spirobi[thieno[3,4-b][1,4]dioxepine] (3.22)



Conventional procedure. Spiro-bis(2,5-dibromopropylene-dioxythiophene) **3.2** (0.592 g, 0.97 mmol), 5-ethynyl-2,3-dihydrothieno[3,4-b][1,4]dioxine **3.17** (0.74 g, 4.45 mmol), tetrakis(triphenylphosphine)palladium (60 mg) copper iodide (55 mg, 0.03 mmol). Column chromatography CH_2Cl_2 /hexane 1/1.

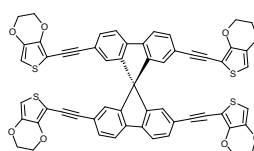
There were many different fractions containing several different products of partial coupling, but none was a desired product.

Microwave: Spiro-bis(2,5-dibromopropylene-dioxythiophene) **3.1** (0.3 g, 0.49 mmol), 5-ethynyl-2,3-dihydrothieno[3,4-b][1,4]dioxine **3.17** (0.375 g, 2.26 mmol) tetrakis(triphenylphosphine)palladium (30 mg) copper iodide (30 mg, 0.15 mmol).

Column chromatography CH₂Cl₂/ hexane, 1:1. The crude material was reprecipitated from hot chloroform with hexane to afford **3.22** as a yellow powder (300 mg, 63 %, 95 % purity).

M.p. >300 °C (dec.); ¹H NMR(400 MHz, DMSO) δ_H (ppm): 6.80 (4H, s), 4.32 – 4.30 (4H, m), 4.24(4H, s), 4.23 – 4.22 (8H, m); ¹³C NMR (100 MHz, DMSO) δ_C (ppm): 150.2, 145.6, 140.9, 103.4, 103.1, 88.1, 95.9, 88.1, 85.3, 71.4, 65.0, 64.1, 49.9, MS/MALDI: *m/z* = 954 [M+H⁺].

2,2',7,7'-tetrakis((2,3-dihydrothieno[3,4-b][1,4]dioxin-5-yl)ethynyl)-9,9'-spirobifluorene] (3.23)



Microwave: 2,2',7,7'-Tetrabromo-9,9'-spirobifluorene **3.8**

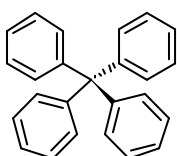
(331 mg, 0.523 mmol), 5-ethynyl-2,3-dihydrothieno[3,4-

b][1,4]dioxine **3.17** (400 mg, 2.4 mmol), tetrakis-

(triphenylphosphine)palladium (40 mg), copper iodide (30 mg, 0.15 mmol). Column chromatography CH₂Cl₂/ hexane, 1:1. The crude material was reprecipitated from hot chloroform into hexane to afford **3.23** as a yellow powder (140 mg, 28 %, 97 % purity).

M.p. > 340 °C; ¹H NMR (400 MHz, DMSO) δ_H (ppm): 8.12 (1H, d, *J* = 7.9 Hz), 7.57 (1H, dd *J* = 8.0 and 1.4 Hz), 6.73 (1H, d, *J* = 0.7 Hz), 6.67 (1H, s), 4.25 – 4.21 (2H, m), 4.18 – 4.15 (2H, m); ¹³C NMR (100 MHz, DMSO) δ_C (ppm): 147.8, 144.9, 140.8, 140.8, 131.2, 125.5, 122.1, 121.7, 102.3, 96.5, 95.1, 81.8, 64.8, 64.1, 54.9. MS/MALDI: *m/z* = 972 [M+H⁺].

Tetraphenylmethane (3.24)²¹³



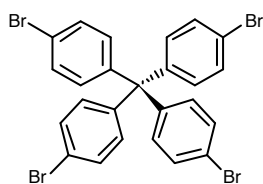
Chlorotriphenylmethane (25.0 g, 89.7 mmol) and aniline (22.0 mL, 22.5 g, 232 mmol) were added to a 1-neck round bottom flask and

heated at 190 °C under vigorous stirring with a mechanical stirrer.

After 15 min, the mixture was allowed to cool to room temperature which caused the mixture to solidify. Then, 2 M HCl (100 mL) and methanol (150 mL) were added and the mixture was heated for 30 min at 80 °C. After cooling to room temperature, the resulting solid was filtered off and pulverized by mortar and pestle, then washed

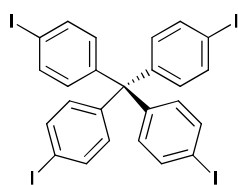
with water (250 mL) and dried in *vacuo* for 3 days to obtain a purple solid (30 g). The dry solid was suspended in DMF (250 mL) and cooled to $-15\text{ }^{\circ}\text{C}$, sulfuric acid (96%, 27.5 mL) and isoamylnitrite (19.9 mL) were added slowly and the suspension was stirred for 1 h. After this time, hypophosphoric acid (30%, 75 mL) was added dropwise. Once addition was completed, the reaction mixture was heated at $50\text{ }^{\circ}\text{C}$ until the evolution of gas had ceased. Then, the solid was filtered off and washed twice with DMF (250 mL), water (250 mL) and ethanol (250 mL). After drying in *vacuo* the tetraphenylmethane (16.2 g, 57%) was obtained as a brownish powder. Mp $238 - 239\text{ }^{\circ}\text{C}$ (Lit.²³² $236 - 238\text{ }^{\circ}\text{C}$); $^1\text{H NMR}$ (400 MHz, CDCl_3) δ_{H} (ppm): 7.28 – 7.10 (m).

Tetrakis(4-bromophenyl)methane (3.25)²¹³



Tetraphenylmethane (2.0 g, 6.24 mmol) was added in small portions to a round bottomed flask containing bromine (6.4 mL, 0.125 mol.) under vigorous stirring at RT. After the addition was completed, the resulting solution was stirred for 20 min and then cooled down to $-78\text{ }^{\circ}\text{C}$. At this temperature, ethanol (15 mL) was added slowly and the resulting suspension was allowed to warm to room temperature while stirring overnight. Then, the precipitate was filtered off and washed subsequently with an aqueous $\text{Na}_2\text{S}_2\text{O}_3$ solution (50 mL) and water (100 mL). After drying in *vacuo*, the crude solid was recrystallized from chloroform and the obtained crystals were discarded (possibly overbromination). The filtrate was evaporated to afford tetrakis(4-bromophenyl)methane 3.25 as a yellowish solid (2.8 g, 70%). M.p. $> 340\text{ }^{\circ}\text{C}$ (Lit.²³² $> 300\text{ }^{\circ}\text{C}$); $^1\text{H NMR}$ (400 MHz, CDCl_3) δ_{H} (ppm): 7.40 (8H, m), 7.01 (8H, m).

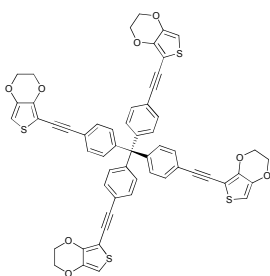
Tetrakis(4-iodophenyl)methane (3.26)²¹⁴



A suspension of tetraphenylmethane (1.25 g, 2.25 mmol), bis(trifluoroacetoxy)iodobenzene (2.95 g, 6.85 mmol), and iodine (2.1 g, 8.25 mmol) in carbon tetrachloride (20 mL) was stirred at reflux for 16 h. After cooling to RT, the suspension was filtered, and the solid residue was washed several times with dichloromethane.

After drying, **3.26** was obtained as a very light pink powder (300 mg; 16%): M.p. >320 °C; M.p. not reported; $^1\text{H NMR}$ (400 MHz, CDCl_3) δ_{H} (ppm): 7.60 (2H, d, $J = 8.8$ Hz), 6.89 (2H, d, $J = 8.8$ Hz).

Tetrakis(4-((2,3-dihydrothieno[3,4-b][1,4]dioxin-5-yl)ethynyl)phenyl)methane (3.27)

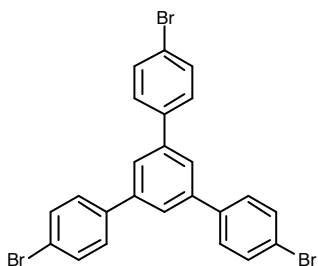


Attempt I - Microwave: Tetrakis-(4-bromophenyl)-methane **3.25** (300 mg, 0.471 mmol), 5-ethynyl-2,3-dihydrothieno[3,4-b][1,4]dioxine **3.17** (360mg, 2.17 mmol), tetrakis-(triphenylphosphine)palladium (40 mg), copper iodide (40 mg, 0.15 mmol). Column chromatography CH_2Cl_2 / hexane 2:8. The main fraction contained only the product of partial coupling, but not a desired product.

Attempt II: Conventional procedure. Tetrakis-(4-iodophenyl)-methane **3.26** (300 mg, 0.364 mmol), 5-ethynyl-2,3-dihydrothieno[3,4-b][1,4]dioxine **3.17** (363 mg, 2.18 mmol), tetrakis(triphenylphosphine)palladium (30 mg), copper iodide (30 mg, 0.15 mmol). Column chromatography CH_2Cl_2 /hexane (1:1) up to CH_2Cl_2 . Reprecipitated from hot CH_2Cl_2 with hexane. Yield 180 mg (51 %) of bright yellow solid.

M.p. > 310 °C (dec.); $^1\text{H NMR}$ (400 MHz, DMSO) δ_{H} (ppm): 7.47 (8H, d, $J = 8.6$ Hz), 7.80 (8H, d, $J = 8.6$ Hz), 6.73 (4H, s), 4.32 – 4.29 (8H, m), 4.23 – 4.20 (8H, m); $^{13}\text{C NMR}$ (100 MHz, DMSO) δ_{C} (ppm): 145.6, 145.0, 140.9, 130.73, 130.7, 120.3, 102.3, 96.6, 94.6, 81.1, 64.9, 64.1; MS/MALDI: $m/z = 977$ $[\text{M}]^+$; HRMS m/z $[\text{M}+\text{H}]^+$ 977.1384, $\text{C}_{57}\text{H}_{36}\text{O}_8\text{S}_4$, requires 977.1366; Found: C, 69.72; H, 3.30; $\text{C}_{57}\text{H}_{36}\text{O}_8\text{S}_4$ requires: C, 70.06; H, 3.71; O, 13.10; S, 13.13 %

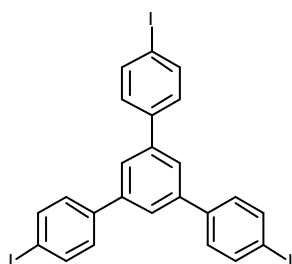
1,2,3- (4-Bromophenyl)benzene (3.28)²¹⁵



To a 15 mL two necked round bottom bottle was added 4'-bromoacetophenone (3.0 g, 15.7 mmol) *p*-toluensulfonic acid monohydrate (0.286 g, 1.57 mmol). The reaction mixture was stirred at 130 °C overnight. where all contents solidified. The solids were neutralized

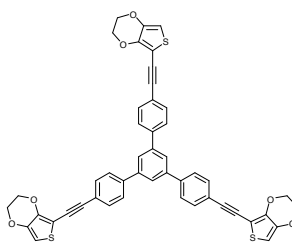
with saturated NaHCO_3 , dissolved in CH_2Cl_2 (300 mL) and extracted. The combined organic layers were dried by MgSO_4 , filtered, and concentrated in *vacuo*. The residue was purified by flash column chromatography CH_2Cl_2 /petroleum ether (2:8) to afford **3.28** as a white solid (2.1 g, 74%). M.p. 260 – 263 °C (Lit²³³ 263 °C); ^1H NMR (400 MHz, CDCl_3) δ_{H} (ppm): 7.70 (3H, s), 7.62 (6H, m), 7.55 (6H, m).

1,2,3-(4-bromophenyl)benzene (**3.29**)²¹⁵



To a 20 mL two necked round bottom flask was added 4-iodoacetophenone (3.0 g, 12.2 mmol) and *p*-toluenesulfonic acid monohydrate (0.232 g, 1.3 mmol). The reaction mixture was stirred at 130 °C overnight during which time all contents solidified. The solids were neutralized with saturated NaHCO_3 , dissolved in CH_2Cl_2 (300 mL) and extracted. The combined organic layers were dried with MgSO_4 , filtered, and concentrated in *vacuo*. The residue was purified by flash column chromatography CH_2Cl_2 /petroleum ether (2:8) to afford **3.29** as a white solid (1.74 g, 62%). M.p. 261 – 262 °C (Lit²³³ 262 – 263 °C); ^1H NMR (500 MHz, CDCl_3) δ_{H} (ppm): 7.82 (6H, m), 7.69 (3H, m), 7.41 (6H, m).

5,5'-((5'-(4-((2,3-Dihydrothieno[3,4-b][1,4]dioxin-5-yl)ethynyl)phenyl)-[1,1':3',1''-terphenyl]-4,4''-diyl)bis(ethyne-2,1-diyl))bis(2,3-dihydrothieno[3,4-b][1,4]dioxine) (**3.30**)

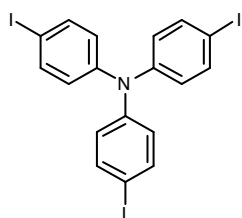


Attempt I Conventional procedure. 1,2,3-(4-Bromophenyl)benzene **3.28** (0.71 g, 1.31 mmol), 5-ethynyl-2,3-dihydrothieno[3,4-b][1,4]dioxine **3.17** (0.76 g, 4.57 mmol), tetrakis(triphenylphosphine)palladium (75 mg) and copper iodide (75 mg, 0.4 mmol). Reaction time 4 days at RT. Column chromatography with gradient elution from CH_2Cl_2 /hexane 2:8 - CH_2Cl_2 /hexane 8:2. The mixture contained many different byproducts, including partial coupling and the desired product was not found in any of the collected fractions.

Attempt II: Conventional procedure. 1,2,3-(4-iodophenyl)- benzene **3.29** (0.86 g, 1.25 mmol), 5-ethynyl-2,3-dihydrothieno[3,4-b][1,4]dioxine **3.17** (0.75 g, 4.51 mmol), tetrakis(triphenylphosphine)palladium (70 mg), copper iodide (71 mg, 0.38 mmol). Reaction time of 4 days at RT. Column chromatography with gradient elution from CH₂Cl₂/hexane 2:8 - CH₂Cl₂/hexane 1:1. Yield 200 mg (20 %) of yellow solid.

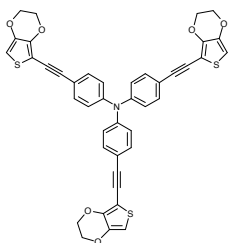
M.p. > 180 °C (dec.); ¹H NMR (400 MHz, CDCl₃) δ_H (ppm): 7.80 (1H, s), 7.66 (4H, m), 6.35 (1H, s), 4.36 – 4.33 (2H, m), 4.26 – 4.22 (2H, m); ¹³C NMR (125 MHz, CDCl₃) δ_C (ppm): 144.4, 141.9, 141.1, 140.7, 132.1, 127.3, 125.2, 122.6, 101.5, 98.9, 95.7, 81.2, 65.3, 64.6; MS/MALDI: *m/z* = 798 [M⁺]; HRMS *m/z* [M⁺] 798.1193, C₄₈H₃₀O₆S₃ requires 793.1199.

Tris-(4-iodophenyl)amine (**3.31**)²³⁴



A mixture of triphenylamine (3.0 g, 12 mmol), HgO (12.18 g, 56 mmol), and I₂ (15.24 g, 60 mmol) in ethanol (150 mL) was stirred overnight at RT. The solvent was removed, and the product was separated from the mercuric salts with boiling toluene. The solution was filtered through a short column of Al₂O₃ and the solvent was evaporated. The product was precipitated from hot toluene with MeOH to afford product **3.31** as an off-white solid (6.33 g, 84%). M.p. 181-182 °C (Lit.²³⁵ 182 -184 °C); ¹H NMR (500 MHz, CDCl₃) δ_H (ppm): 7.55 (6H, d, *J* = 8.8 Hz), 6.82 (6H, d, *J* = 8.8 Hz).

Tris(4-((2,3-dihydrothieno[3,4-b][1,4]dioxin-5-yl)ethynyl)phenyl)amine (**3.32**)



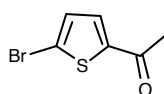
Conventional procedure. Tris-(4-iodophenyl)amine **3.31** (0.398 g, 0.64 mmol), 5-ethynyl-2,3-dihydrothieno[3,4-b][1,4]dioxine **3.17** (0.383 g, 2.3 mmol), tetrakis(triphenylphosphine)palladium (40 mg), copper iodide (10 mg, 0.02 mmol). Column chromatography CH₂Cl₂/light petroleum ether, 1:1. Reprecipitated from hot CH₂Cl₂ with hexane. Yield 312 mg (66 %) of bright yellow solid.

Table of yields for the synthesis of **3.32**

Batch Number	3.31	3.17	Et ₃ N	Pd-(PPh ₃) ₄	CuI	Conditions	Yield
I	398 mg (0.64 mmol)	0.383 g (2.3 mmol)	3 mL	40 mg	10 mg	Conventionally	312 mg, 66 %
II	2 x 300 mg (0.481 mmol)	2 x 288 mg (1.73 mmol)	2 x 3 mL	2 x 30 mg	2 x 10 mg	2 x μ w vial combined for work up	Impurity of the same R _f
III	300 mg (0.481 mmol)	288 mg (1.73 mmol)	3 mL	30 mg	10 mg	Conventionally	70 mg, 20 %
IV	500 mg (0.803 mmol)	466 mg (2.81 mmol)	5 mL	30 mg	10 mg	Conventionally	30 mg, 5 %
V	650 mg (1.03 mmol)	771 mg (4.63 mmol)	5 mL	70 mg	40 mg	Conventionally Everything freshly repurified	680 mg, 89 %

M.p. > 130 °C (dec.); ¹H NMR (500 MHz, CDCl₃) δ _H (ppm): 7.41 (2H, d, *J* = 8.7 Hz), 7.03 (2H, d, *J* = 8.7 Hz), 6.31 (1H, s), 4.32 – 4.29 (2H, m), 4.22 – 4.20 (2H, m); ¹³C NMR (125 MHz, CDCl₃) δ _C (ppm): 146.7, 144.2, 141.0, 132.8, 124.1, 117.9, 101.2, 99.1, 95.7, 80.1, 65.2, 64.5; MS/MALDI: *m/z* = 736.5 [M⁺]; HRMS *m/z* [M+H]⁺ 738.1057, C₄₂H₂₇NO₆S₃ requires 738.1073.

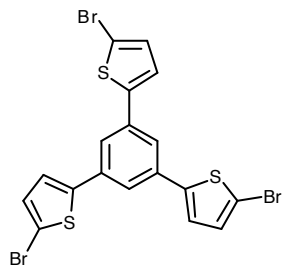
5-Acetyl-2-bromothiophene (**3.33**)²¹⁷



2,5-dibromothiophene (2.42 g, 10.0 mmol) was dissolved in dry diethyl ether (100 mL) and the solution was cooled down to -10 °C, *n*-BuLi (4.43 mL, 10 mmol, 2.26 M solution in hexane) was added. The solution was stirred for 1h and then *N,N*-dimethylacetamide (0.93 mL, 10.0 mmol) was added. The mixture was stirred for 2h at RT and subsequently hydrolyzed with water (50 mL) and extracted with CH₂Cl₂ (2 x 100 mL). The organic layer was dried over Na₂SO₄, filtered and evaporated under reduced pressure to afford an orange solid which was further purified by column chromatography eluting with CH₂Cl₂ to obtain **3.33** as a white solid (0.9 g, 44 %). M.p. 93 – 95 °C (Lit.²³⁶95 °C); ¹H NMR (500

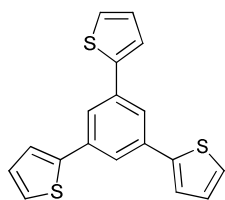
MHz, CDCl₃) δ_{H} (ppm): 7.45 (1H, d, $J = 4.0$ Hz), 7.11 (1H, d, $J = 4.0$ Hz), 2.52 (3H, s).

1,3,5-Tris[2-(5-bromo)-thiophene]benzene (3.34)



Attempt I²¹⁷: 5-acetyl-2-bromothiophene **3.33** (0.9 g, 4.39 mmol) was dissolved in 20 mL of anhydrous mixture of toluene/ethanol (1:1) and tetrachlorosilane (2.5 mL, 21.9 mmol) was added under vigorous stirring. The mixture was stirred under nitrogen for a further 18 h. Then the mixture was carefully poured into water and extracted with CH₂Cl₂. The organic layer was dried over Na₂SO₄, filtered and evaporated under reduced pressure. The resulting mixture was purified by column chromatography, eluting with CH₂Cl₂/light petroleum ether (2:8), and the resulting material was precipitated from CH₂Cl₂ with hexane. ¹H NMR spectrum confirmed the presence of the product ¹H NMR (500 MHz, CDCl₃) δ_{H} (ppm): 7.52 (1H, s), 7.14 (2H, d, $J = 3.9$ Hz), 7.13 (1H, d, $J = 3.9$ Hz) but also identified impurity of the same R_f. Further attempts to purify the product has been made *via* reprecipitation, recrystallisation or column chromatography with various solvent mixtures, but none was successful.

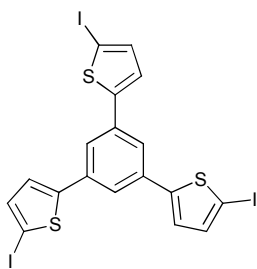
1,3,5-Tris(2-thienyl)benzene (3.35)



Attempt II²¹⁷: 2-acetylthiophene (5.0 g, 39.6 mmol) was dissolved in 12 mL of anhydrous mixture of toluene/ethanol (1:1) and tetrachlorosilane (23.0 mL, 198.0 mmol) was added slowly under vigorous stirring. The mixture was stirred under nitrogen at RT overnight. Then the mixture was carefully poured into water and extracted with CH₂Cl₂. The organic layer was dried over Na₂SO₄ filtered and evaporated under reduced pressure. The resulting mixture was purified by column chromatography eluting with CH₂Cl₂/light petroleum ether (8:2) to afford **3.35** in less than 3 % yield. NMR shows presence of the product: ¹H NMR (400 MHz, CDCl₃) δ_{H} (ppm): 7.76 (3H, s), 7.42 (3H, dd, $J = 1.1$ and 3.6 Hz), 7.35 (3H, dd, $J = 1.1$ and 5.1 Hz), 7.14 (3H, dd, $J = 3.6$ and 5.0 Hz), but further purification was required.

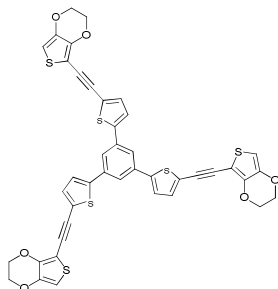
Attempt III: Stille coupling 1,3,5 –Tribromobenzene (300 mg, 0.95 mmol), tributylstannylthiophene (1.6 g, 42.8 mmol) and tetrakis(triphenylphosphine)-palladium (30 mg) were added to three 20 mL oven dried microwave vial and the solids were purged three times vacuum/ nitrogen. Then anhydrous DMF (20 mL) was added. The reactions were carried out in a microwave for 2 h at 160 °C and then combined together for work up. The reaction mixture was filtered through celite with CH₂Cl₂ and washed with saturated aqueous NH₄Cl, then water, and the aqueous layer back extracted with CH₂Cl₂. The organic layers were combined and dried over MgSO₄, filtered and evaporated at reduced pressure. The resulting mixture was purified by column chromatography eluting with CH₂Cl₂/hexane (2:8) to afford **3.35** as a white solid (0.6 g, 66 %). M.p. 156 – 158 °C (Lit²³³ 155 – 156 °C); ¹H NMR (400 MHz, CDCl₃) δ_H (ppm): 7.76 (3H, s), 7.42 (3H, dd, *J* = 1.1 and 3.6 Hz), 7.35 (3H, dd, *J* = 1.1 and 5.1 Hz) 7.14 (3H, dd, *J* = 3.6 and 5.0 Hz).

1,3,5-tris(5-iodothiophen-2-yl)benzene (**3.36**)²¹⁸



A stirred suspension of the 1,3,5-tris(2-thienyl)benzene (**3.35**) (0.5 g, 1.5 mmol) in HOAc/CHCl₃ (1:4, 25 mL) was treated with *N*-iodosuccinimide (1.1 g, 4.85 mmol). The reaction mixture was then heated under reflux conditions to 90 °C for 10 min and all of the NIS dissolved. The crude products precipitated from solution upon cooling. The precipitate was filtered and reprecipitated from hot CH₂Cl₂ with hexane to afford **3.36** as a grey fluffy solid (550 mg, 52 %). This product was used for next step immediately without further purification. ¹H NMR (400 MHz, DMSO) δ_H (ppm): 7.68 (3H, d), 7.46 (3H, d, *J* = 3.0 Hz), 7.42 (3H, *J* = 3.0 Hz), ¹³C NMR (100 MHz, DMSO) δ_C (ppm): 147.6, 138.1, 134.6, 127.0, 121.3, 76.8.

1,3,5-tris(5-((2,3-dihydrothieno[3,4-b][1,4]dioxin-5-yl)ethynyl)thiophen-2-yl)benzene (3.37)



Conventional procedure. 1,3,5-tris(5-iodothiophen-2-yl)benzene **3.36** (600 mg, 0.854 mmol), 5-ethynyl-2,3-dihydrothieno[3,4-b][1,4]dioxine **3.17** (640 g, 3.84 mmol), tetrakis(triphenylphosphine)palladium (60 mg), copper iodide (50 mg, 0.3 mmol). Column chromatography CH₂Cl₂/hexane (1:1) up to CH₂Cl₂. Reprecipitated from hot CH₂Cl₂ with hexane. Yield 480 mg (69%) of bright yellow solid.

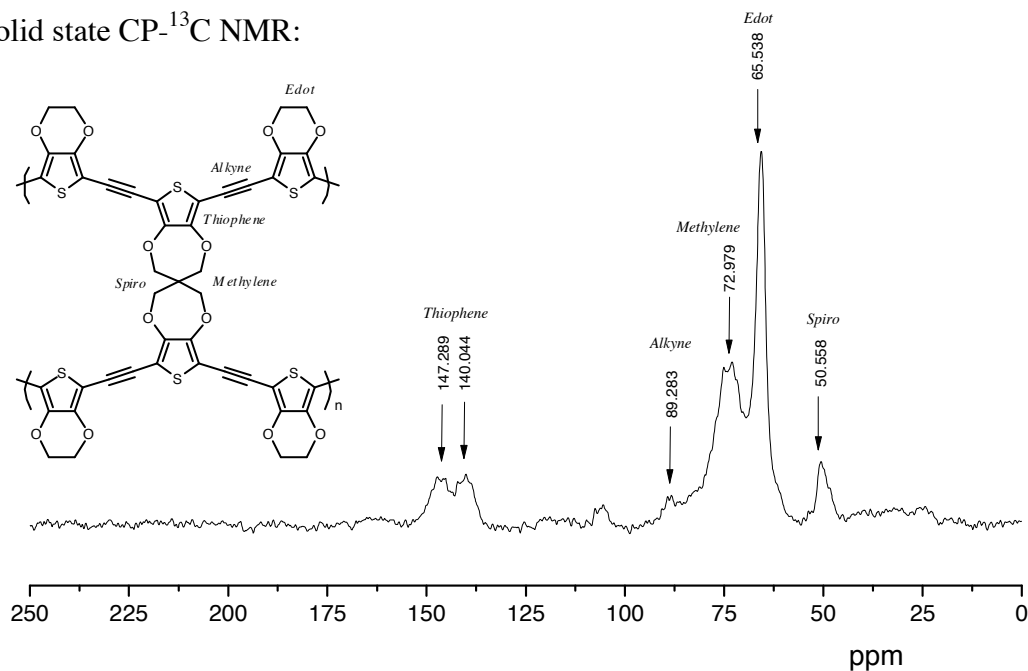
M.p. > 225 °C (dec.); ¹H NMR (400 MHz, DMSO) δ_H (ppm): 7.87 (1H, s), 7.80 (1H, d, *J* = 3.9 Hz), 7.47 (1H, d, *J* = 3.9 Hz), 6.81 (1H, s), 6.67 (1H, s), 4.35 – 4.32 (2H, m), 4.26 – 4.23 (2H, m); ¹³C NMR (100 MHz, DMSO) δ_C (ppm): 145.4, 143.7, 140.9, 134.7, 133.8, 126.0, 122.1, 121.9, 103.1, 96.1, 88.1, 85.6, 65.0, 64.2; MS/MALDI: *m/z* = 817 [M]⁺; HRMS *m/z* [M⁺] 815.9901, C₄₂H₂₄O₆S₆ requires 816.9892, Elemental analysis, Found: C, 61.26; H, 2.81; C₄₂H₂₄O₆S₆ requires: C, 61.74; H, 2.96 %.

General synthesis of the polymers via oxidative polymerization

NOBF₄ (min 3.0 eq) was weighed out into a round bottom flask in a glove box and a then transferred to a manifold in a fume-hood under nitrogen. 1,2-Dichloroethane (10 mL) was added to form a suspension which was cooled down to 0°C. Solution of the monomer in 1,2-dichloroethane was slowly added. The mixture turned black after the first few drops were added. The reaction mixture was left to stir overnight at RT. The polymer formed was then filtered if possible, or if the powder was too fine, the solvent was evaporated at reduced pressure and the black polymer collected from the flask and transferred to a Soxhlet thimble. The polymer was purified by Soxhlet extraction with chloroform for 24 h. Then, the black polymer was suspended in chloroform and N₂H₄·H₂O (3-5 ml) was added. The mixture was refluxed overnight whilst the powder turned brown. The polymer was collected by filtration, transferred to a Soxhlet thimble and purified *via* Soxhlet extraction, first with methanol for 24 h and then with chloroform for 24 hours.

P3.22 – Compound **3.22** (100 mg, 0.105 mmol), NOBF₄ (55 mg, 0.47 mmol). Yield 95 mg (95%) of brown solid. TGA, onset 334 °C. No transition observed in DSC.

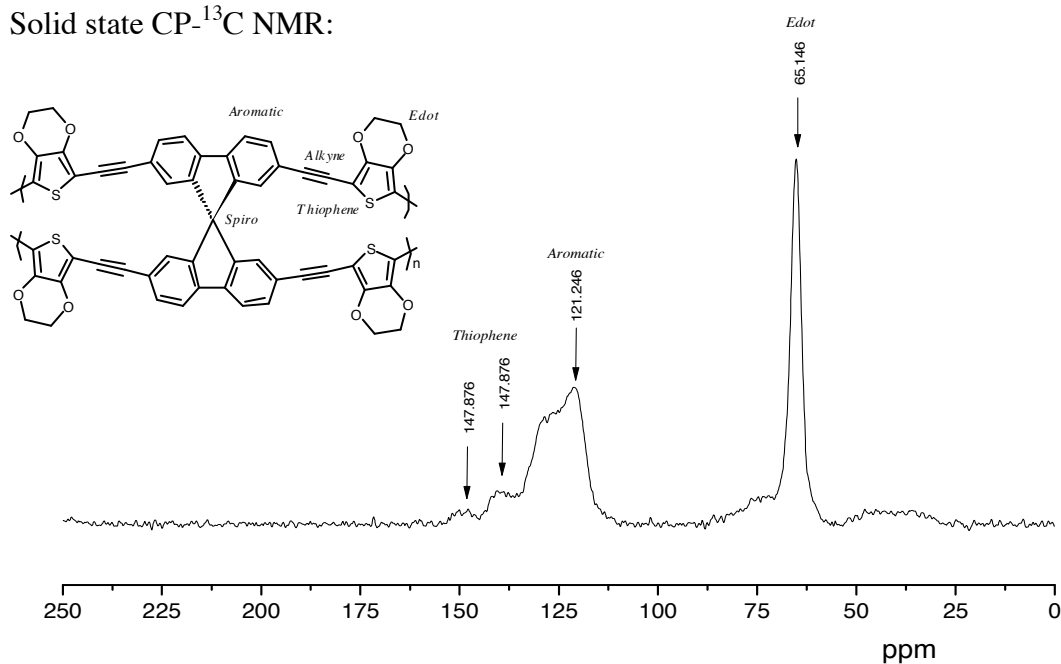
Solid state CP-¹³C NMR:



The emerging peaks at *ca.* 110 ppm might be associated with end-capping alkyne units within the polymer backbone.

P3.23 – **3.23** (150 mg, 0.154 mmol), NOBF₄ (75 mg, 0.64 mmol), yielded 135 mg (91%) of brown solid. TGA onset – 366 °C. No transition observed in DSC.

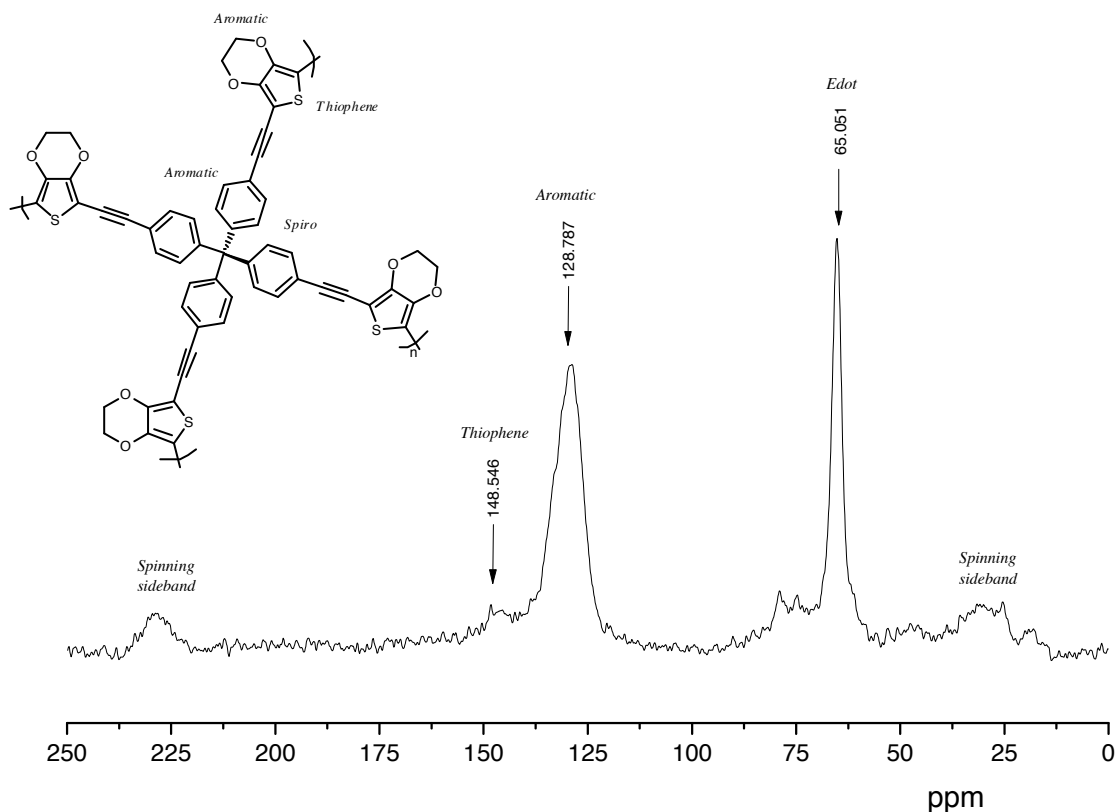
Solid state CP-¹³C NMR:



The peak associated with spiro carbon is not clearly visible but would be expected around 50 ppm.

P3.27 – Compound **3.27** (100 mg, 0.102 mmol), NOBF₄ (80 mg, 0.68 mmol); Yield 98 mg (98 %) of a brown solid. TGA onset 336 °C. No transition observed in DSC.

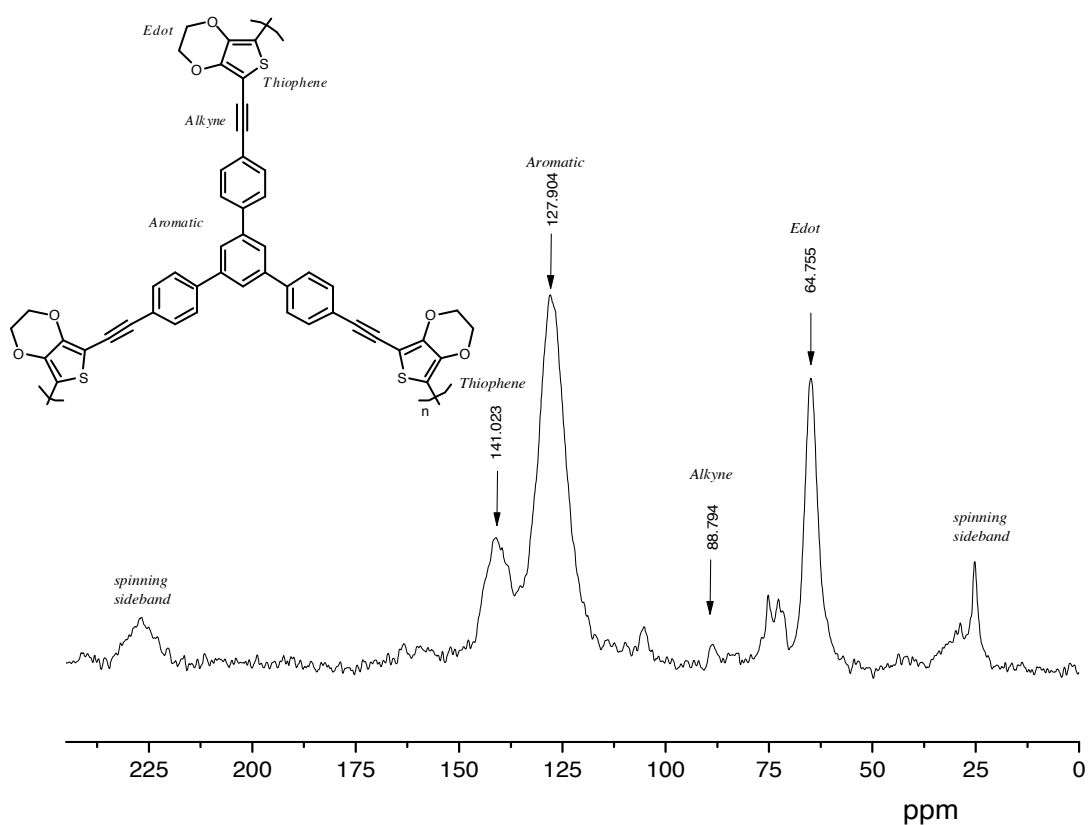
Solid state CP-¹³C NMR:



The peak associated with spiro carbon and alkyne units are not clearly visible but would be expected around 50 and 90 ppm, respectively. The emerging peaks at *ca.* 75 ppm might be associated with end-capping EDOT units within the polymer backbone.

P3.30 – Compound **3.30** (150 mg, 0.188 mmol), NOBF₄ (80 mg, 0.68 mmol), yielded 128 mg (85 %) of brown solid. TGA onset 184 °C. No transition observed in DSC.

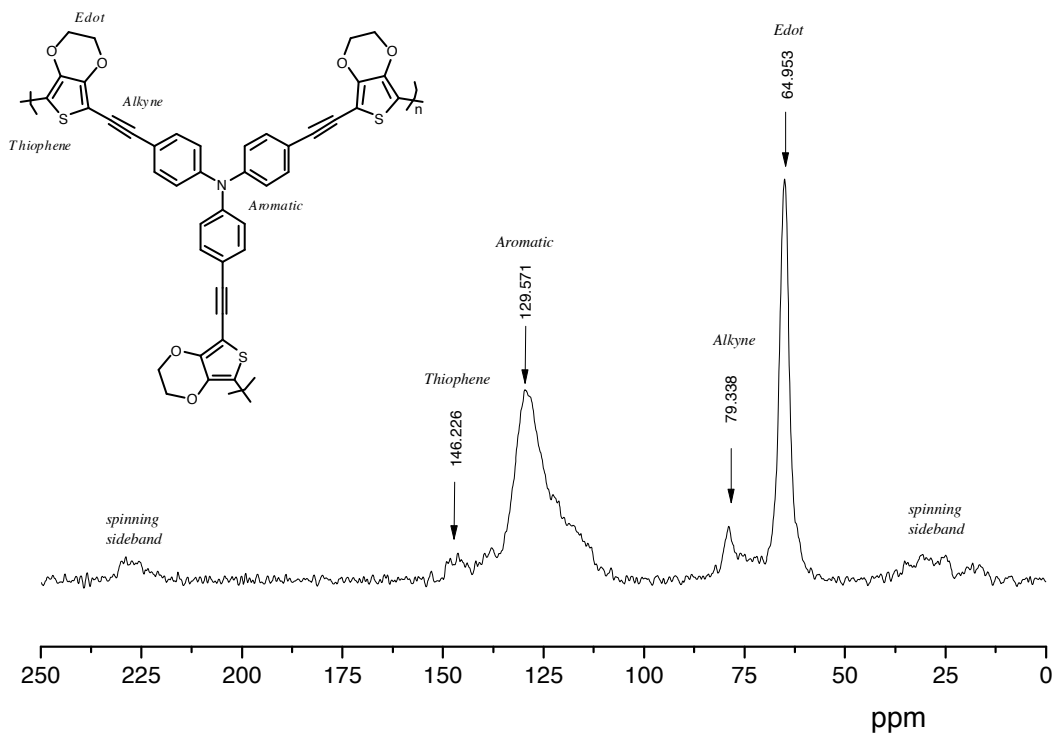
Solid state CP-¹³C NMR:



The small peaks at *ca.* 75 and 110 ppm might be associated with end-capping EDOT and end-capping alkyne units within the polymer backbone, respectively. The peak at *ca.* 25 ppm might belong to trapped impurities.

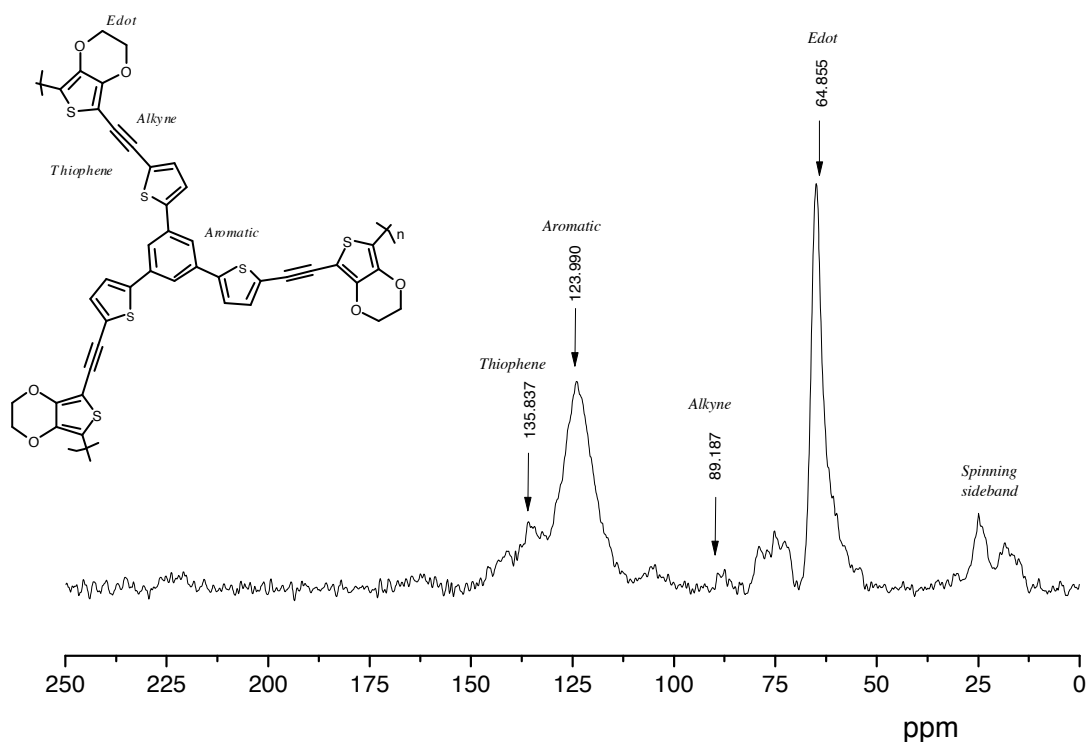
P3.32 – Compound **3.32** (350 mg, 0.474 mmol), NOBF_4 (244 mg, 2.1 mmol). Yield 340 mg (98 %) of brown solid. TGA onset 388 °C. No transition observed in DSC.

Solid state CP- ^{13}C NMR:



P3.37 – Compound **3.37** (300 mg, 0.367 mmol), NOBF_4 (180 mg, 1.5 mmol). Yield 260 mg (87%) of brown solid. TGA onset 340 °C. No transition observed in DSC.

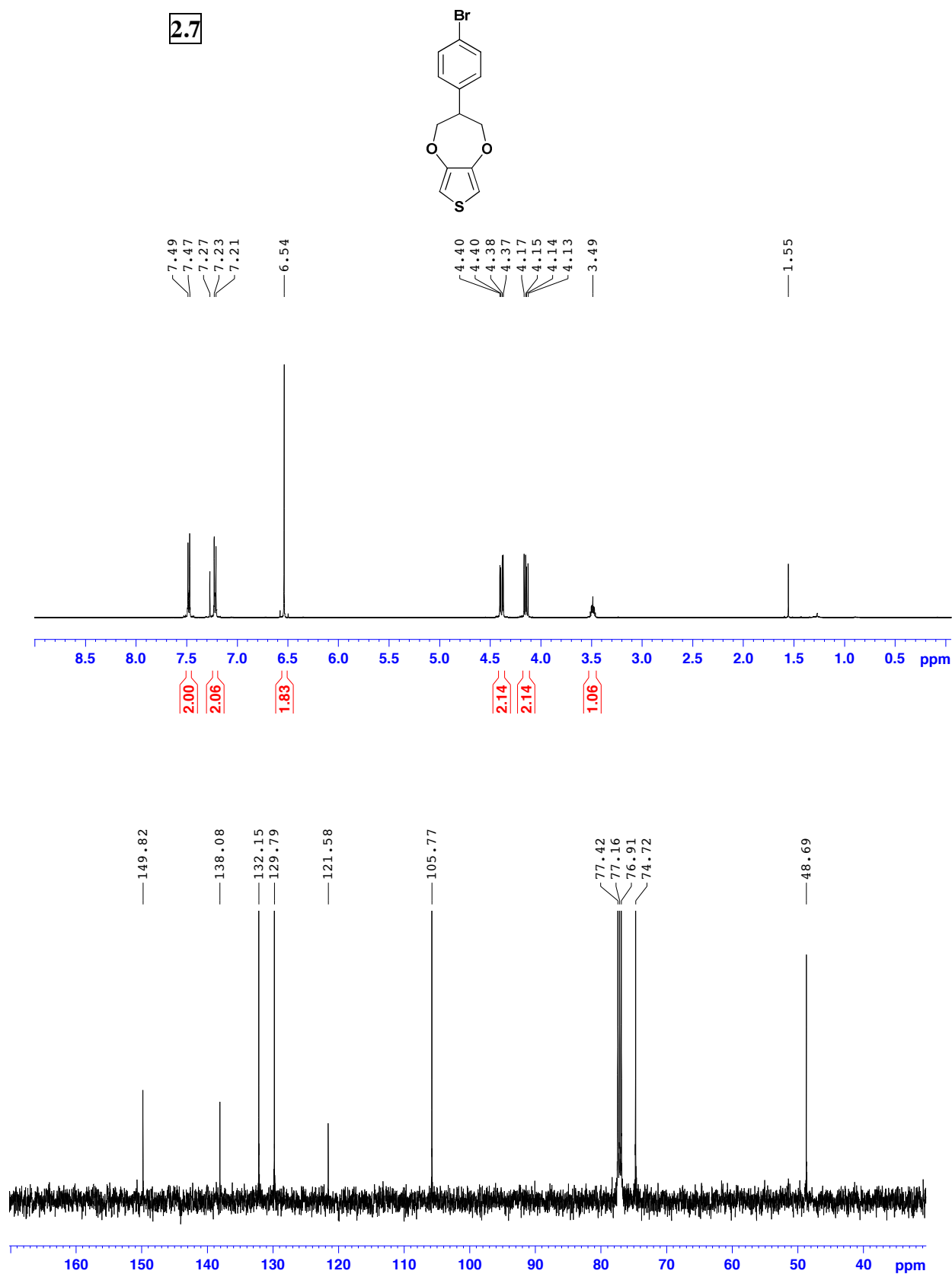
Solid state CP - ^{13}C NMR:

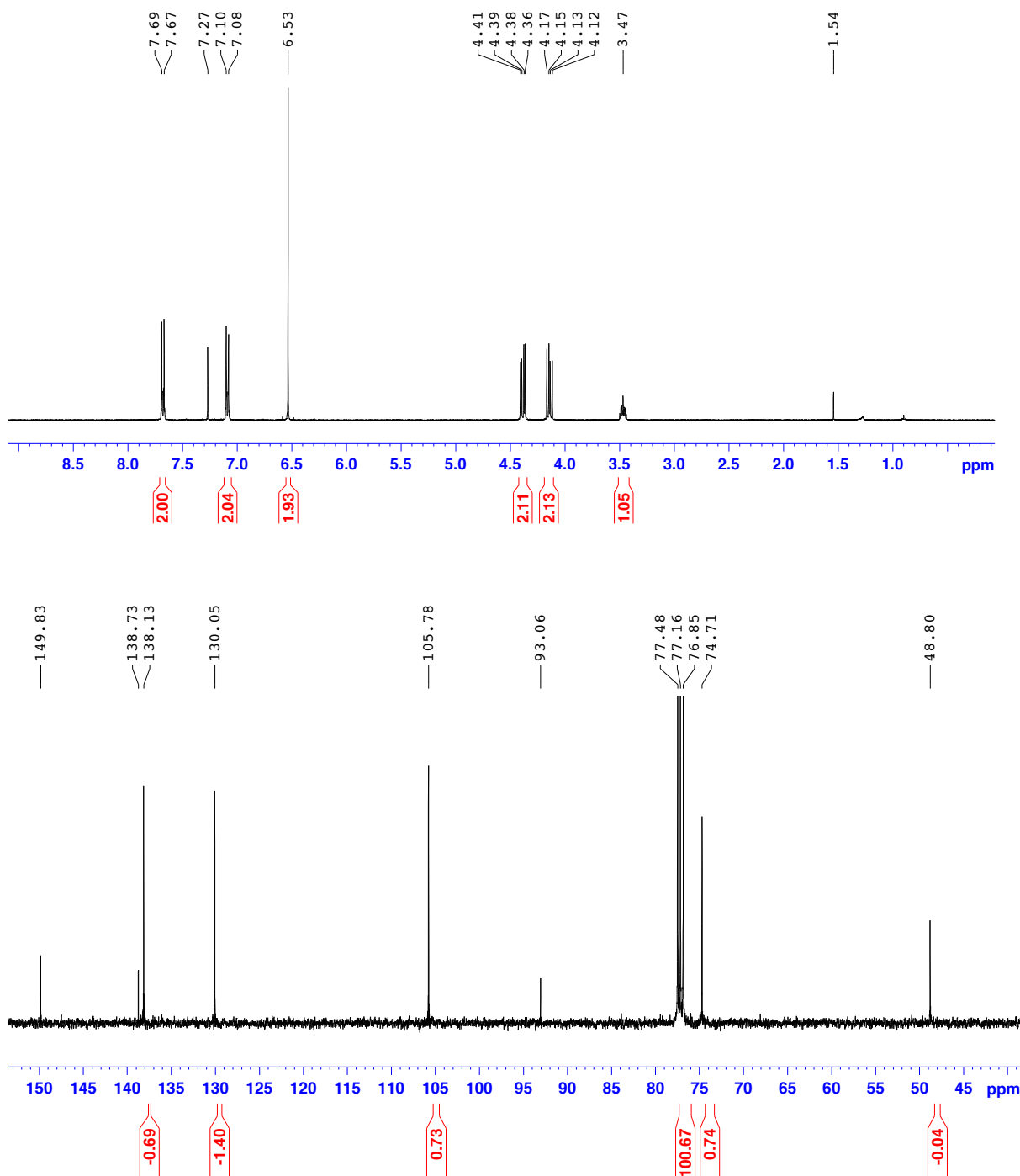
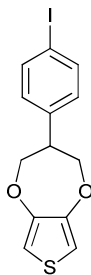


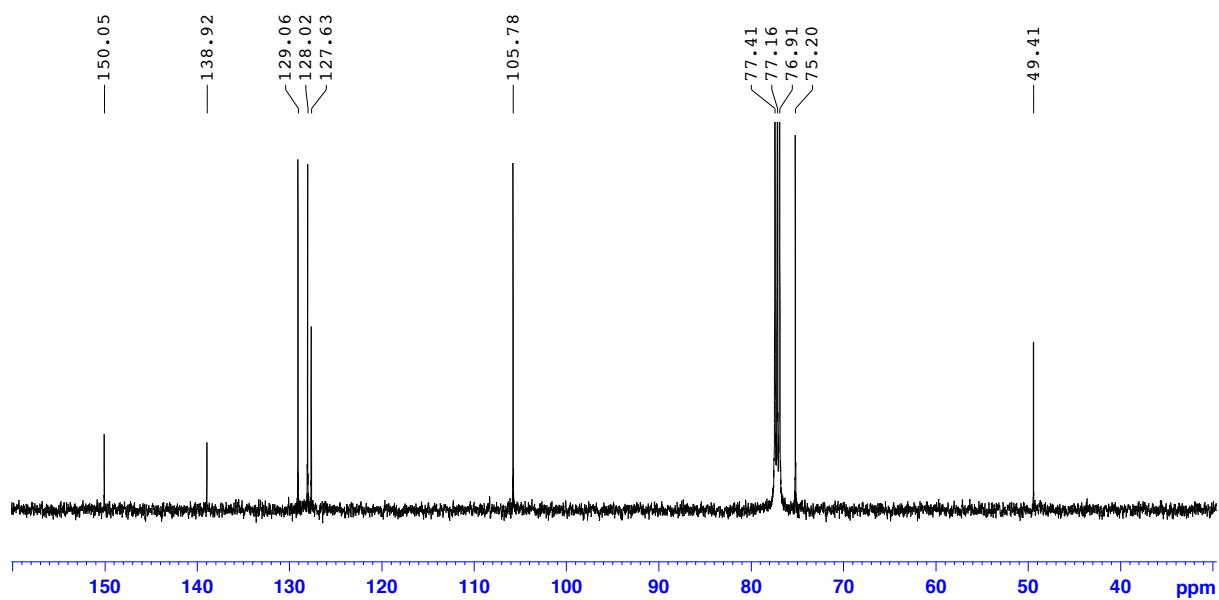
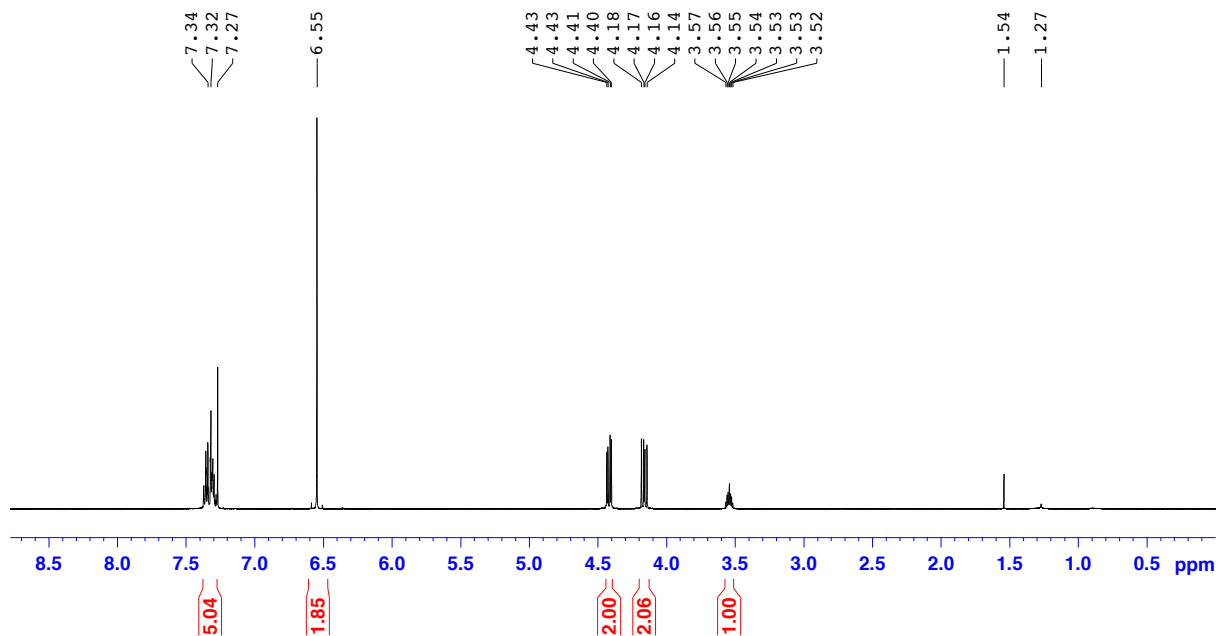
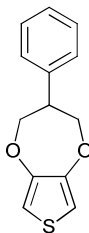
The small peaks at *ca.* 75 and 110 ppm might be associated with end-capping EDOT and end-capping alkynyl units within the polymer backbone, respectively. The peak at *ca.* 25 ppm might belong to trapped impurities.

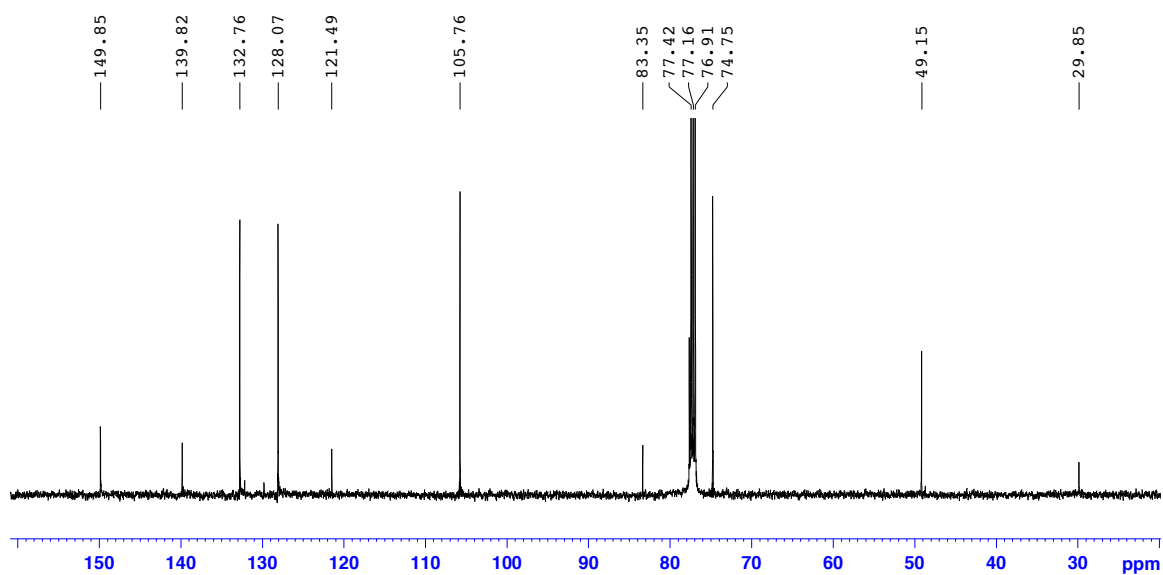
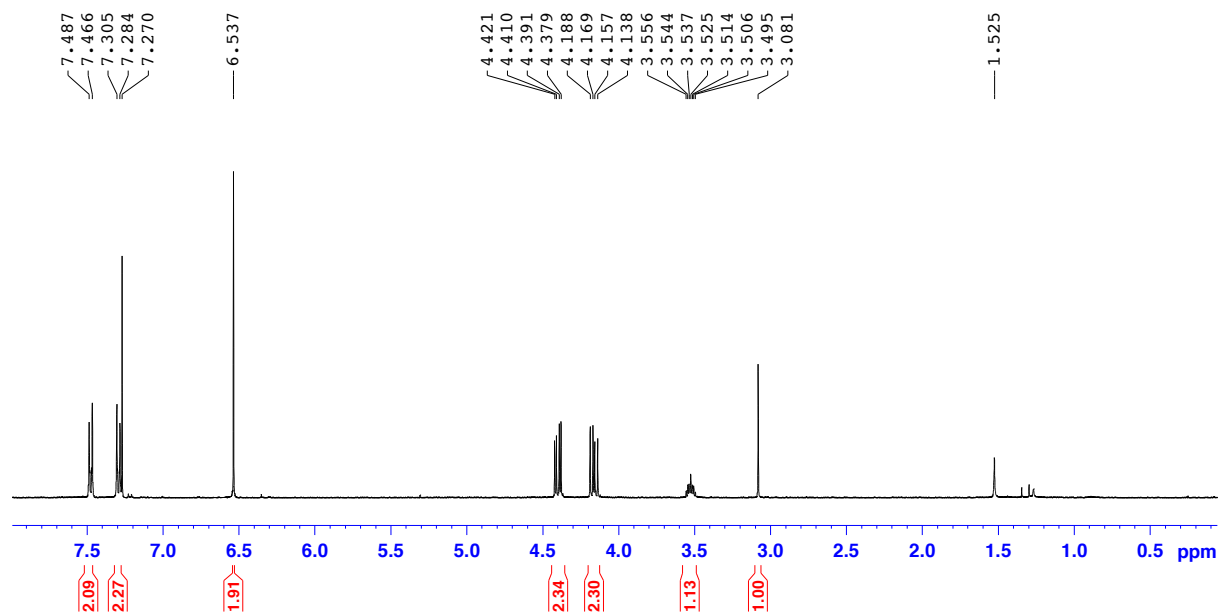
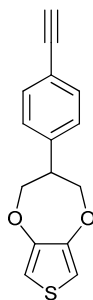
6 APPENDIX

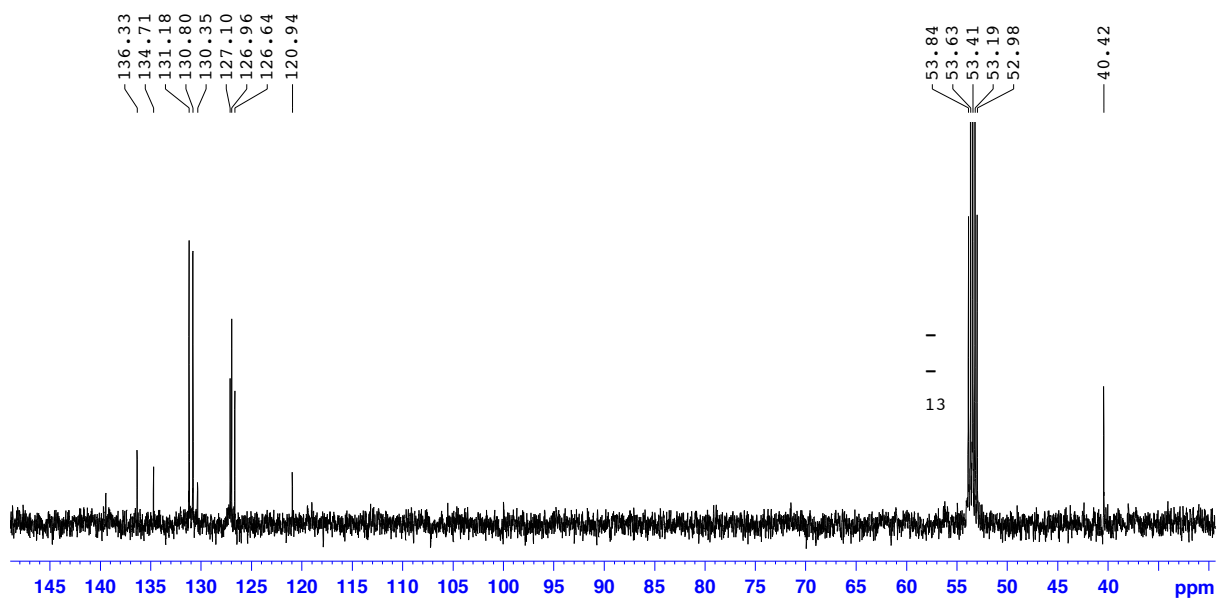
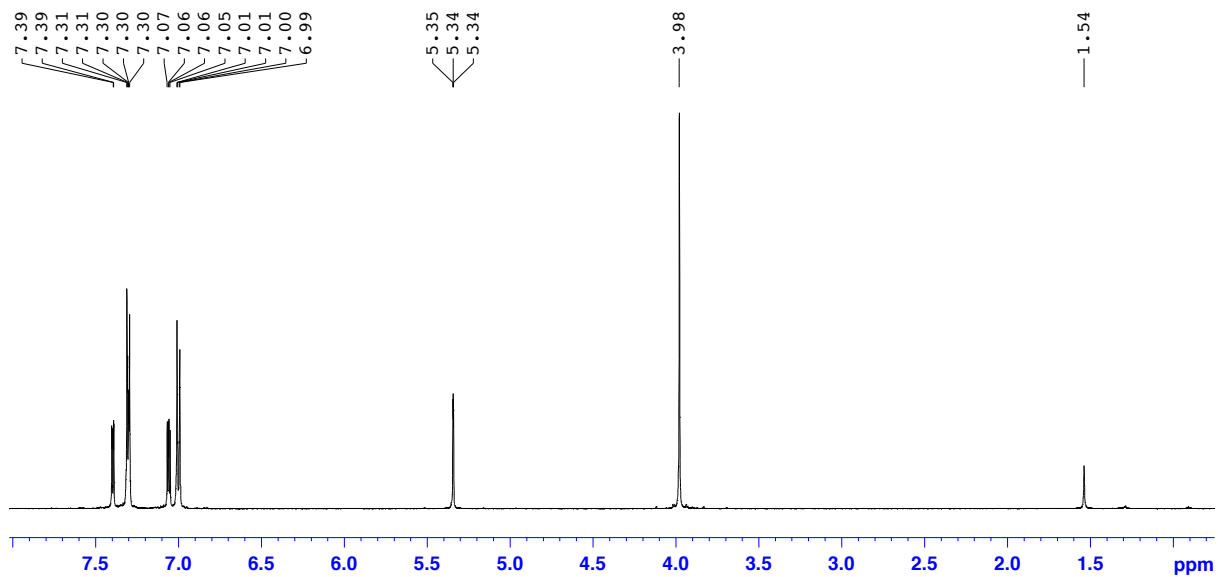
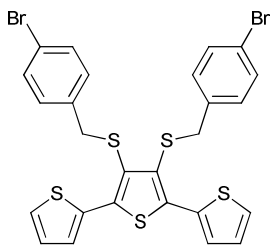
^1H and ^{13}C NMR spectra of novel compounds **2.7**, **2.8**, **2.10**, **2.12**, **2.19**, **2.20**, **3.4**, **3.9**, **3.17**, **3.22**, **3.23**, **3.27**, **3.30**, **3.32** and **3.37**.

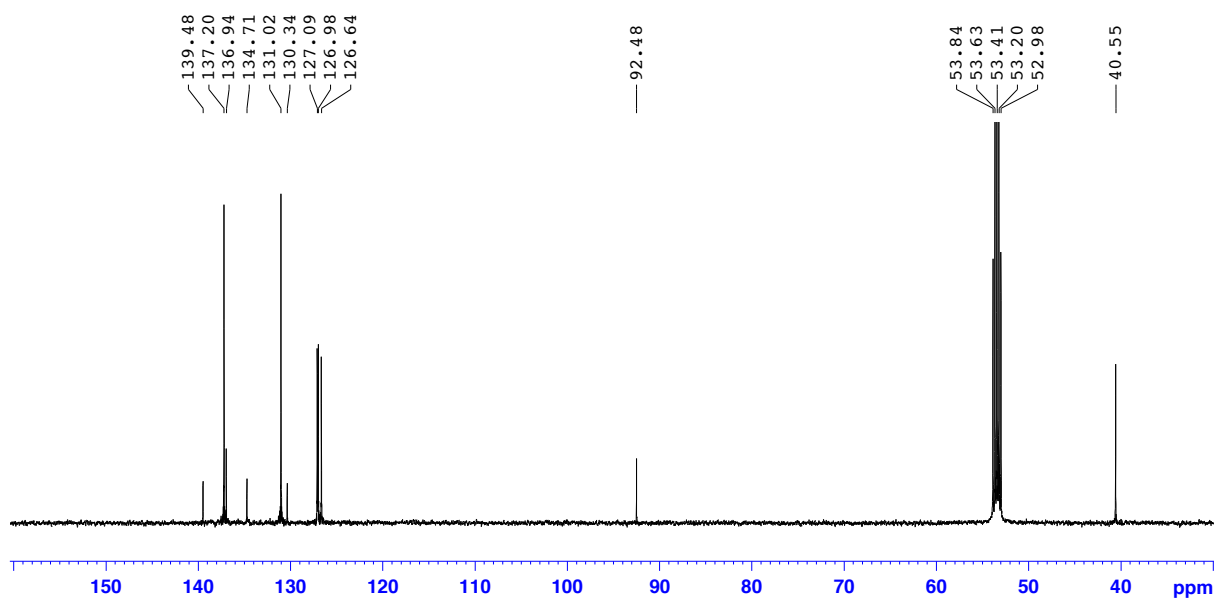
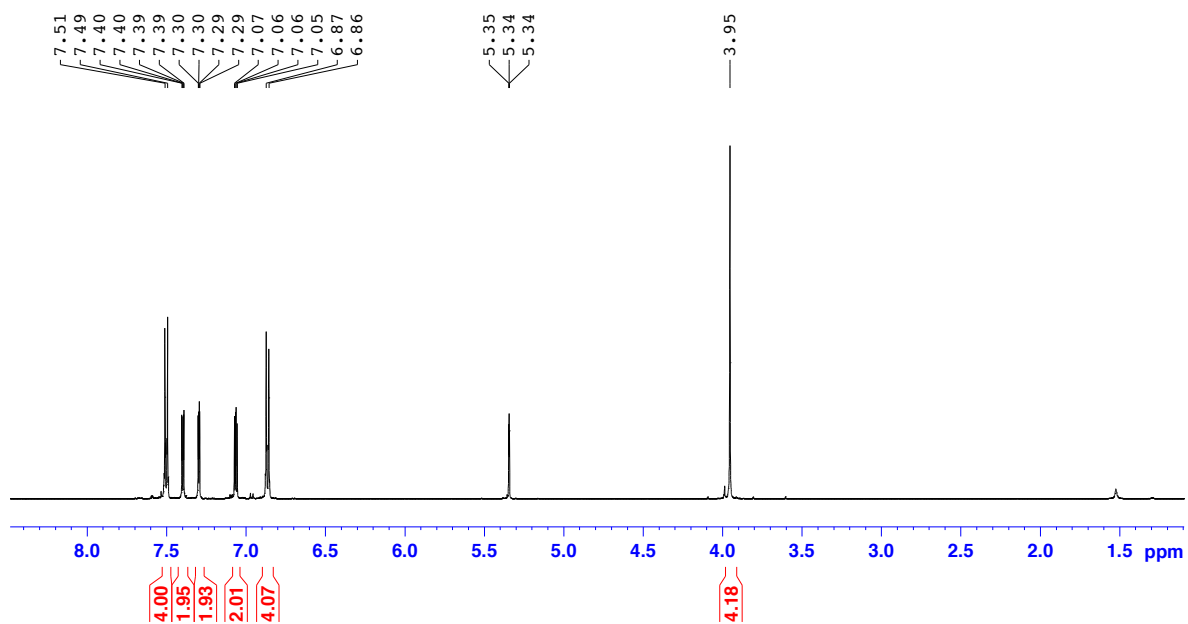
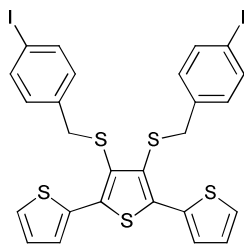


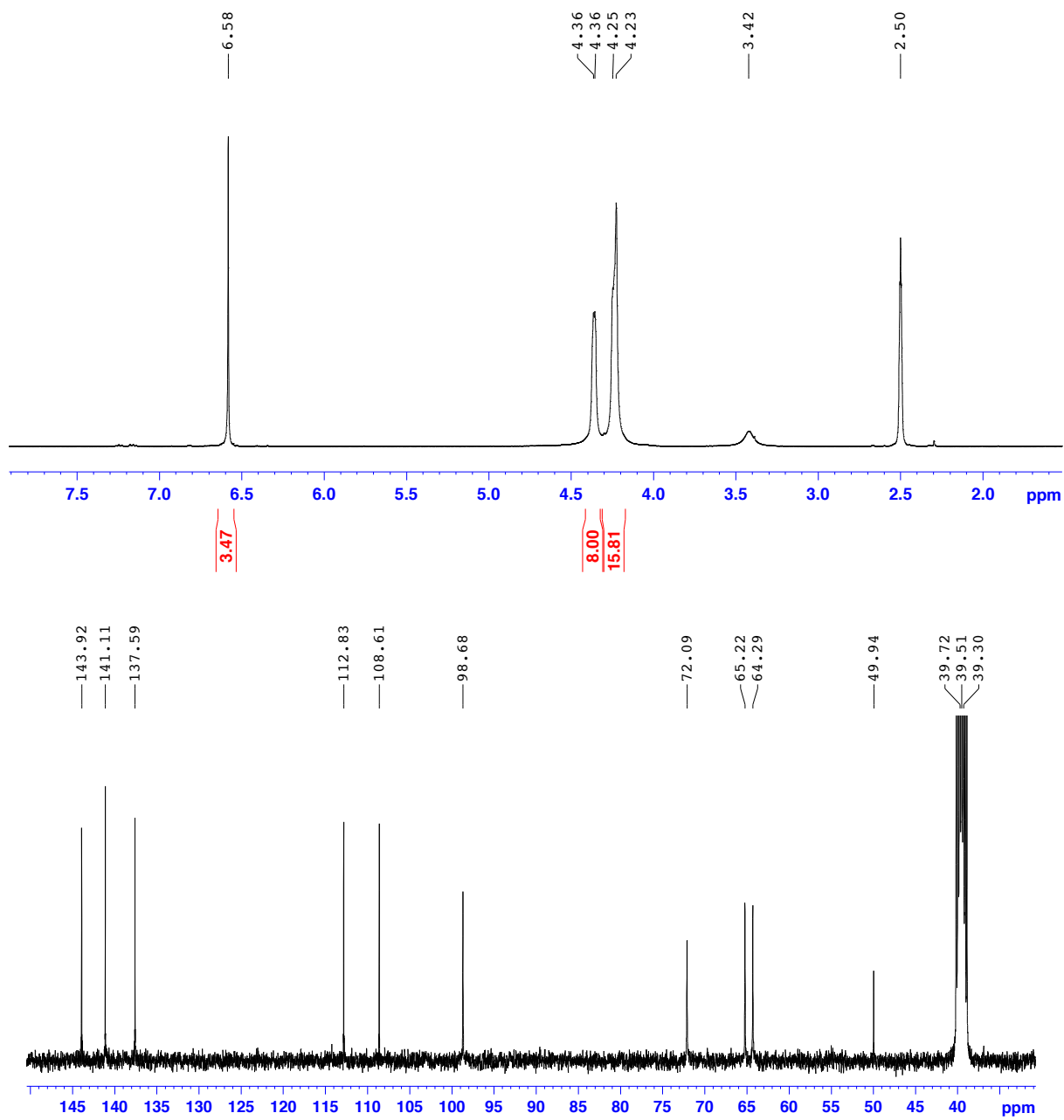
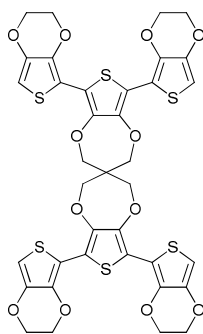
2.8

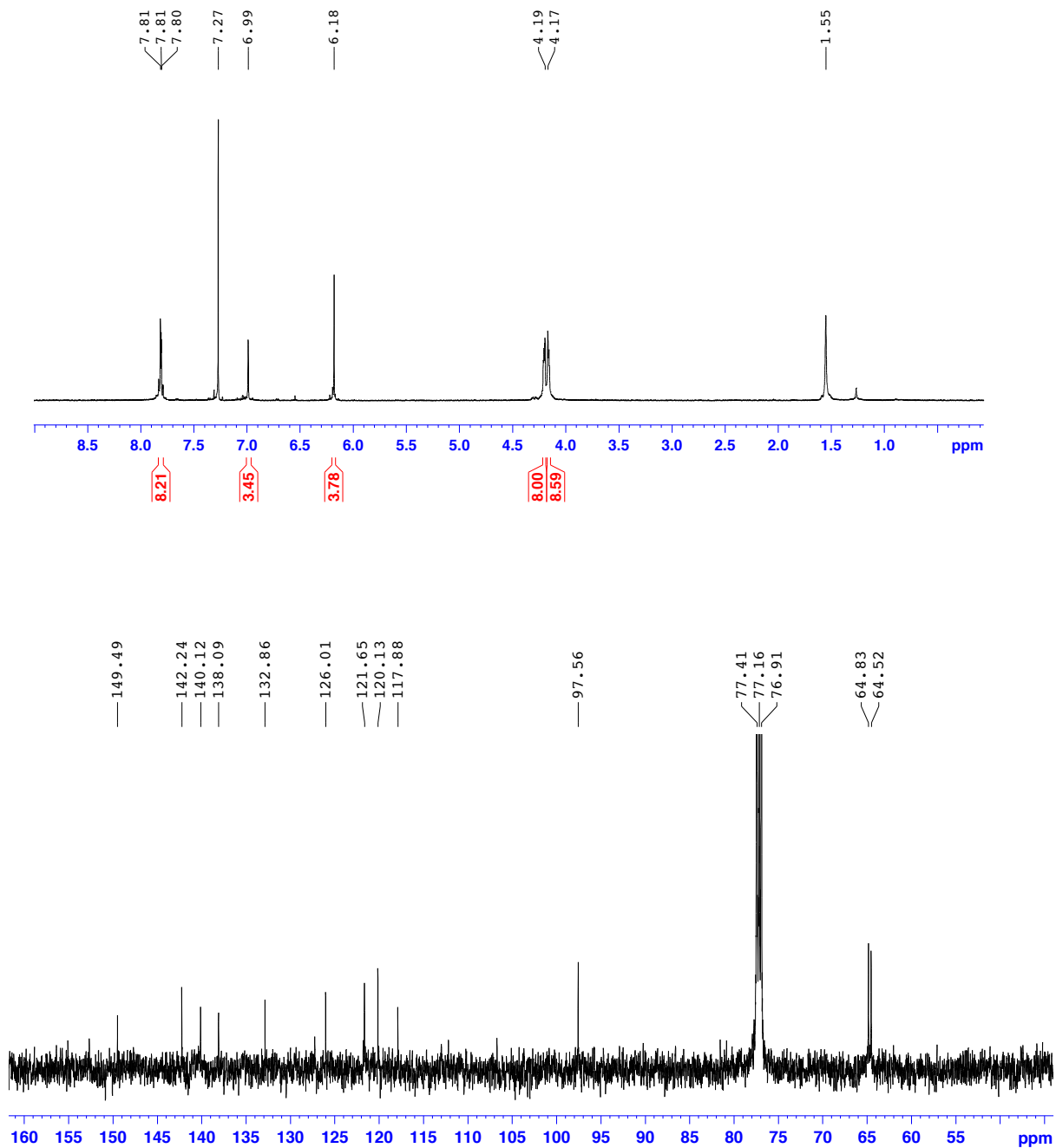
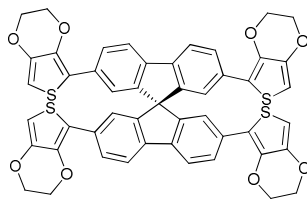
2.10

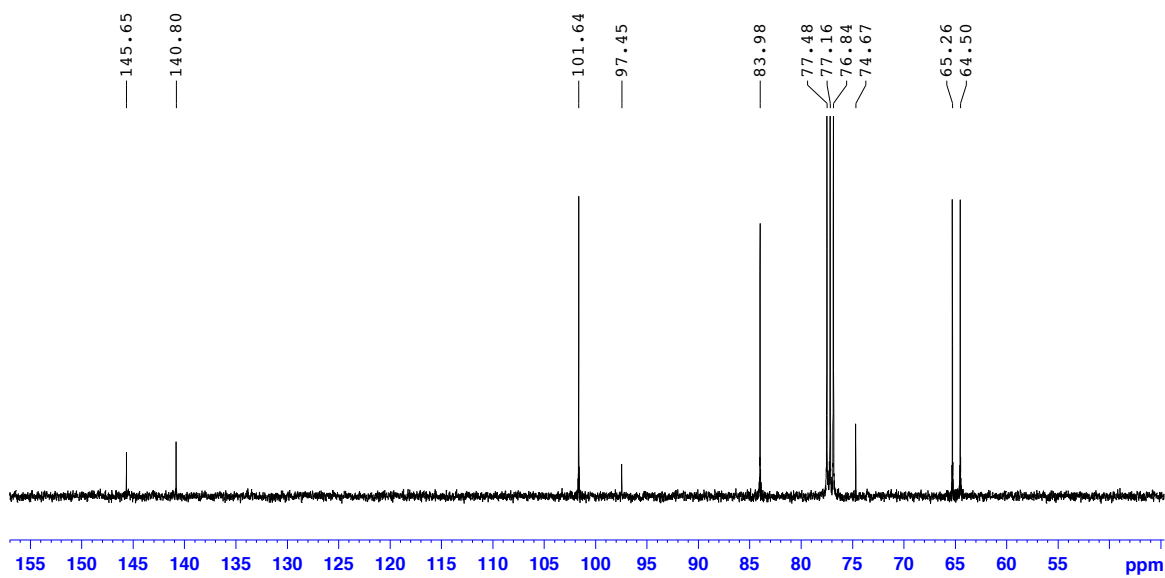
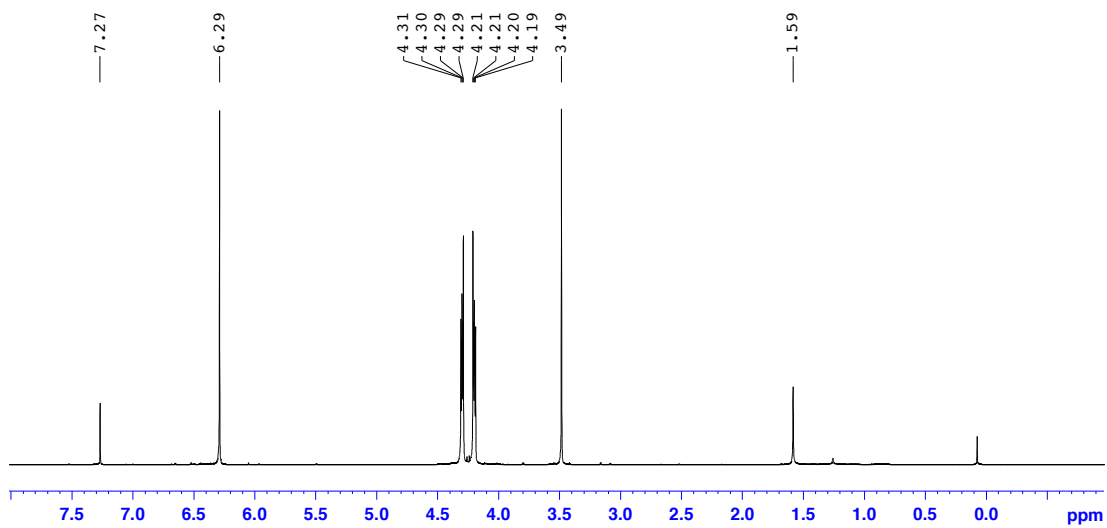
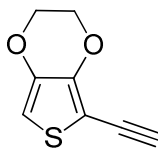
2.12

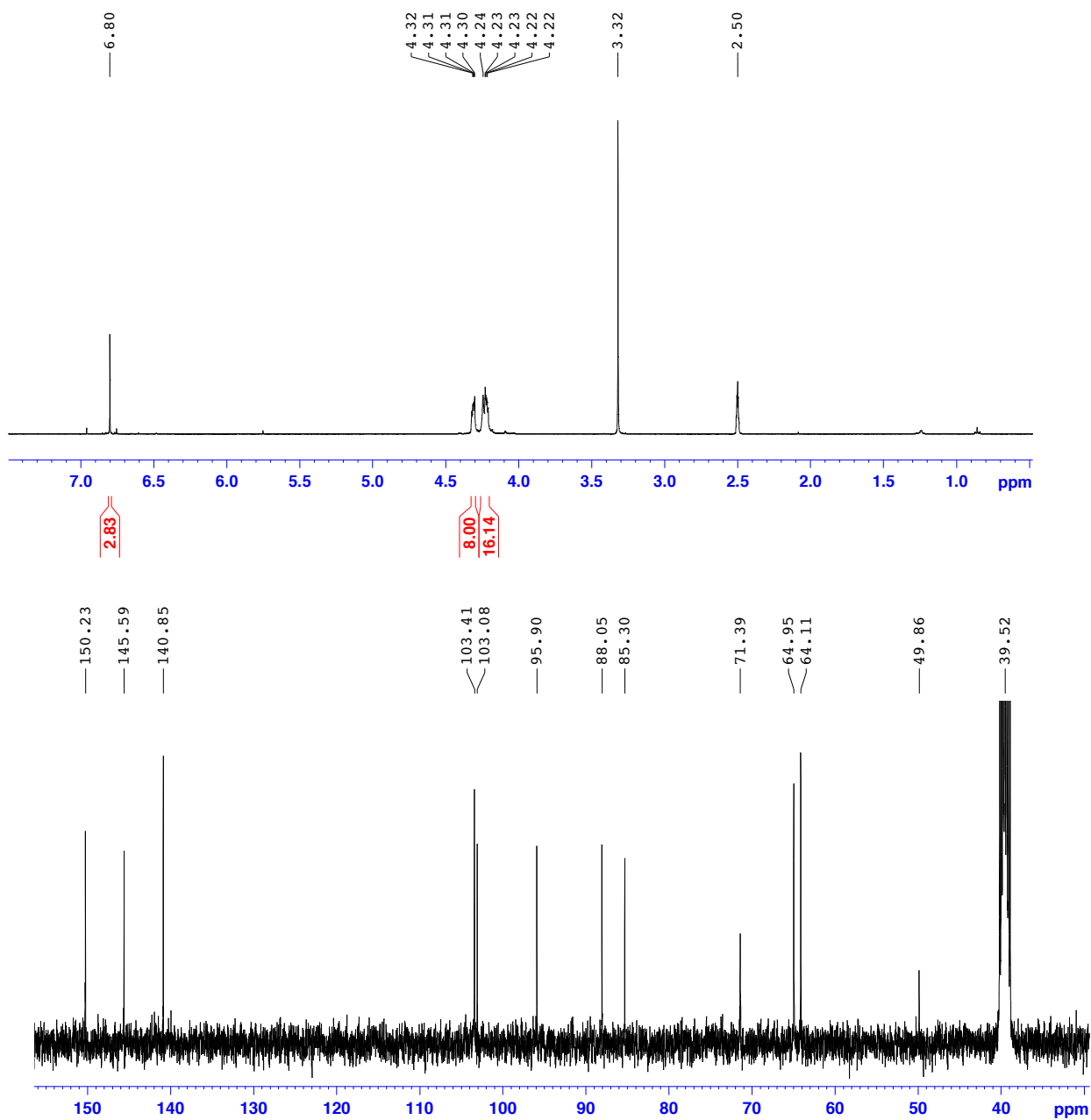
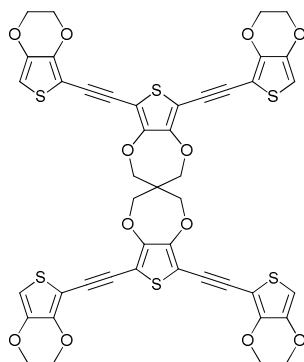
2.19

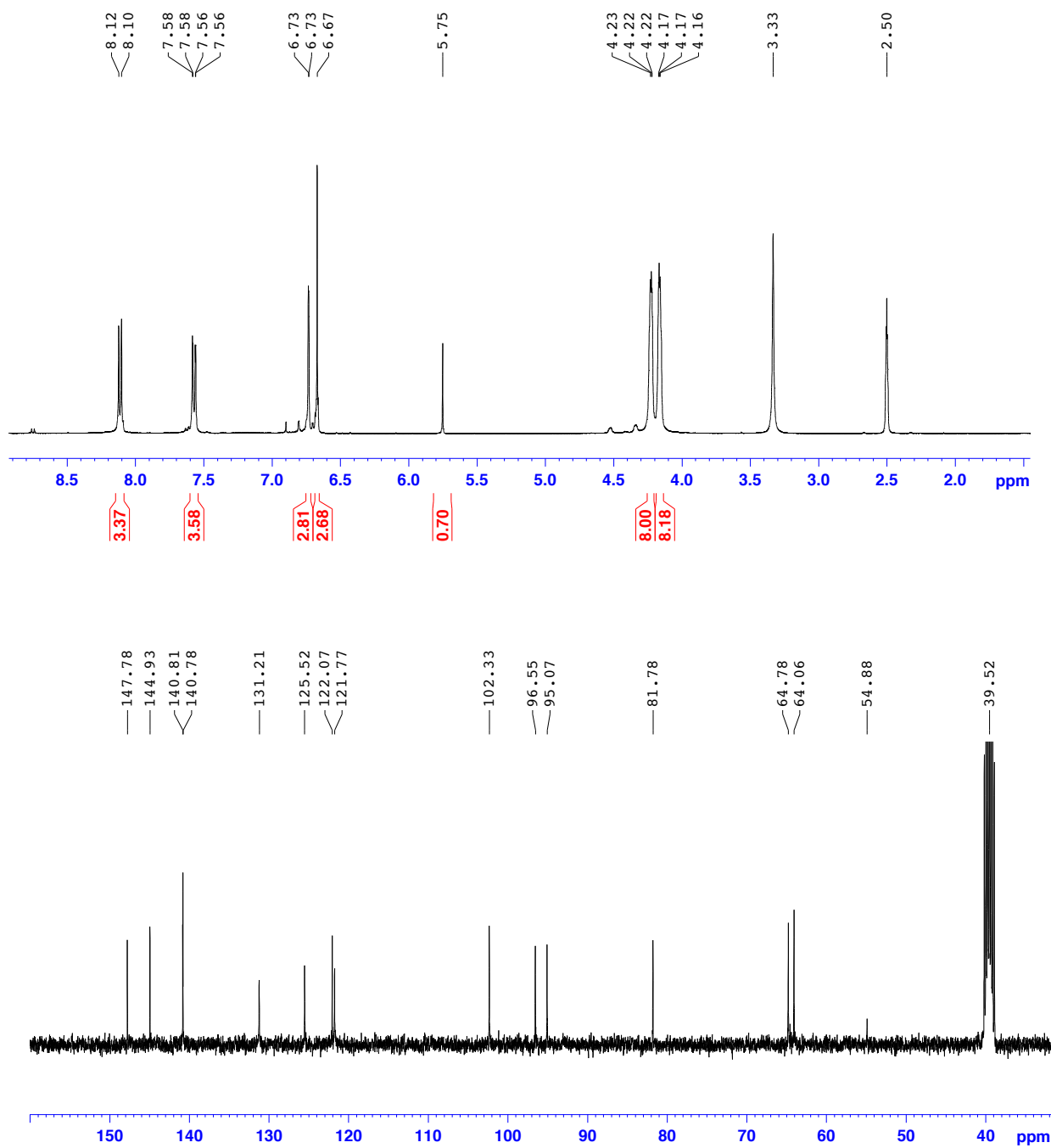
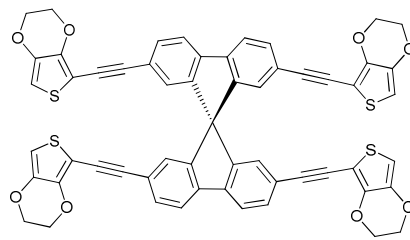
2.20

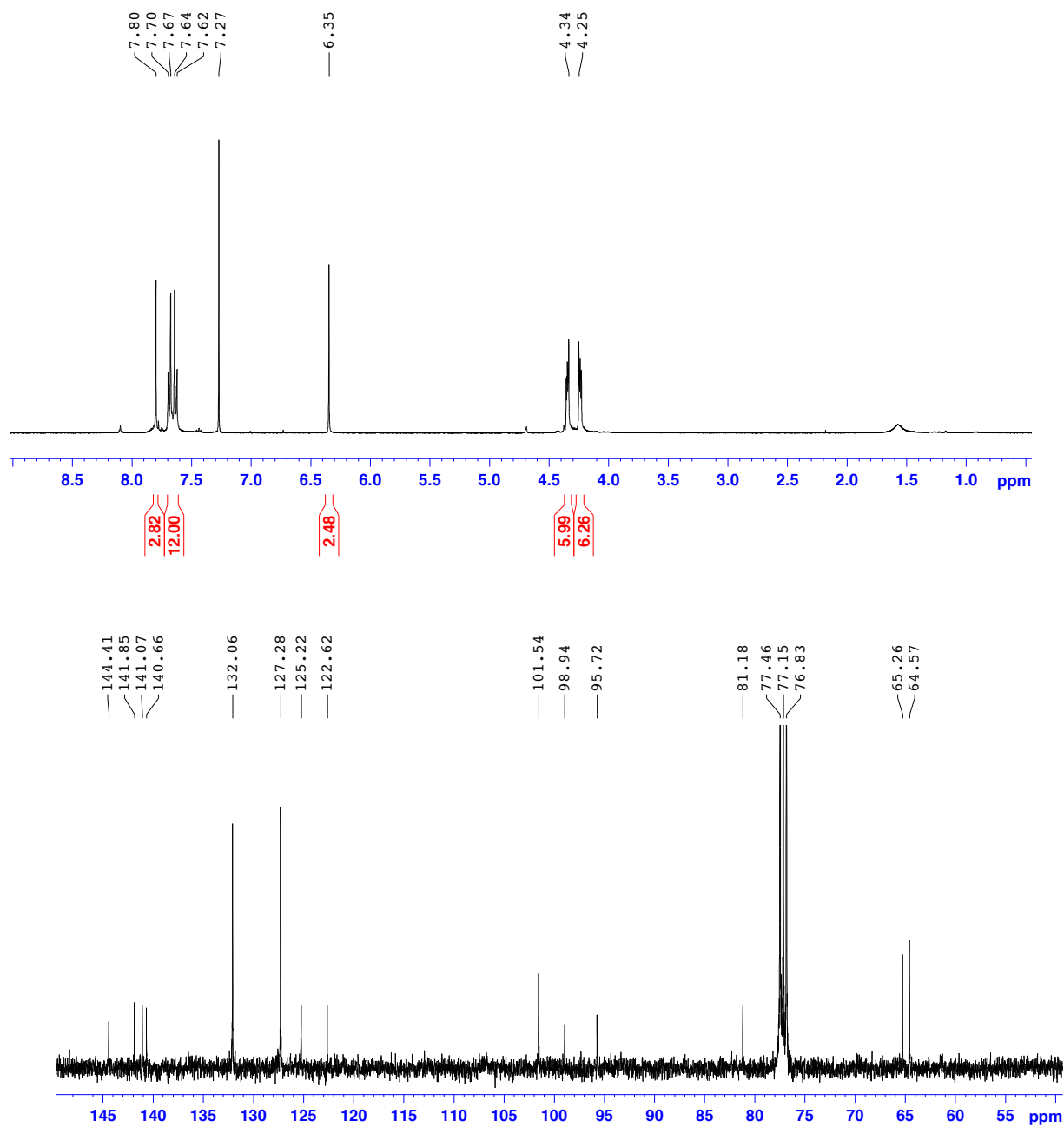
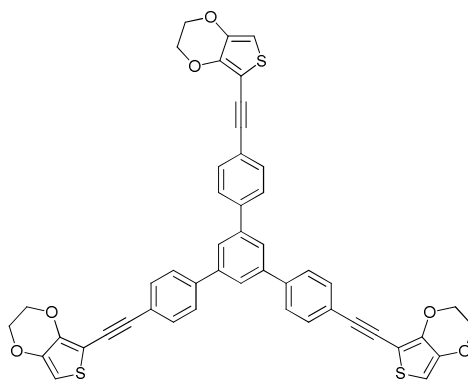
3.4

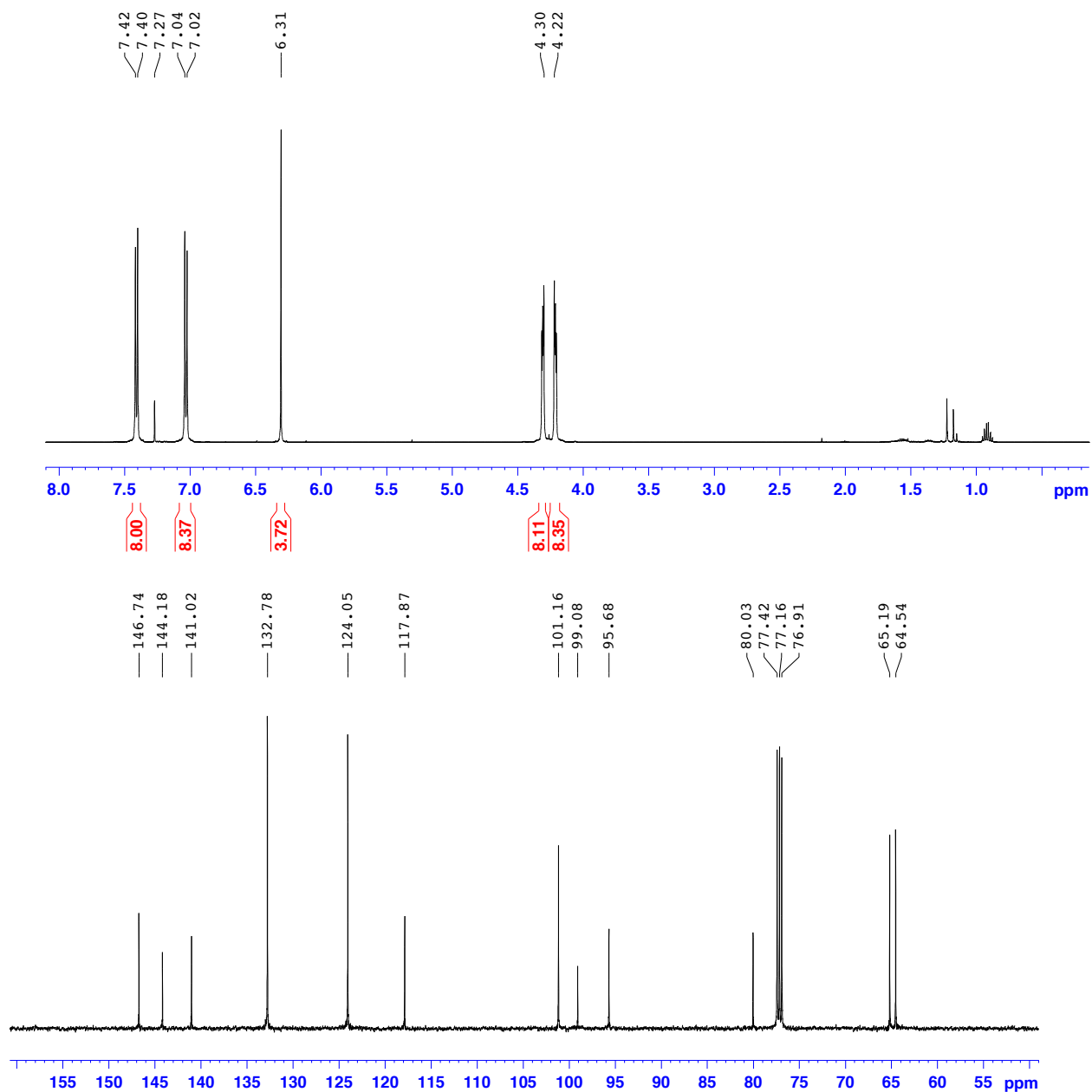
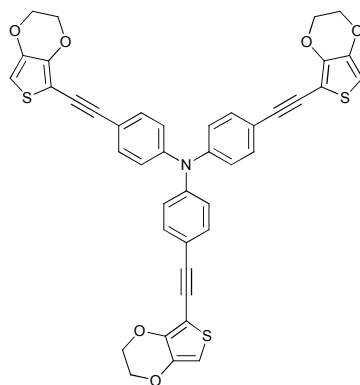
3.9

3.17

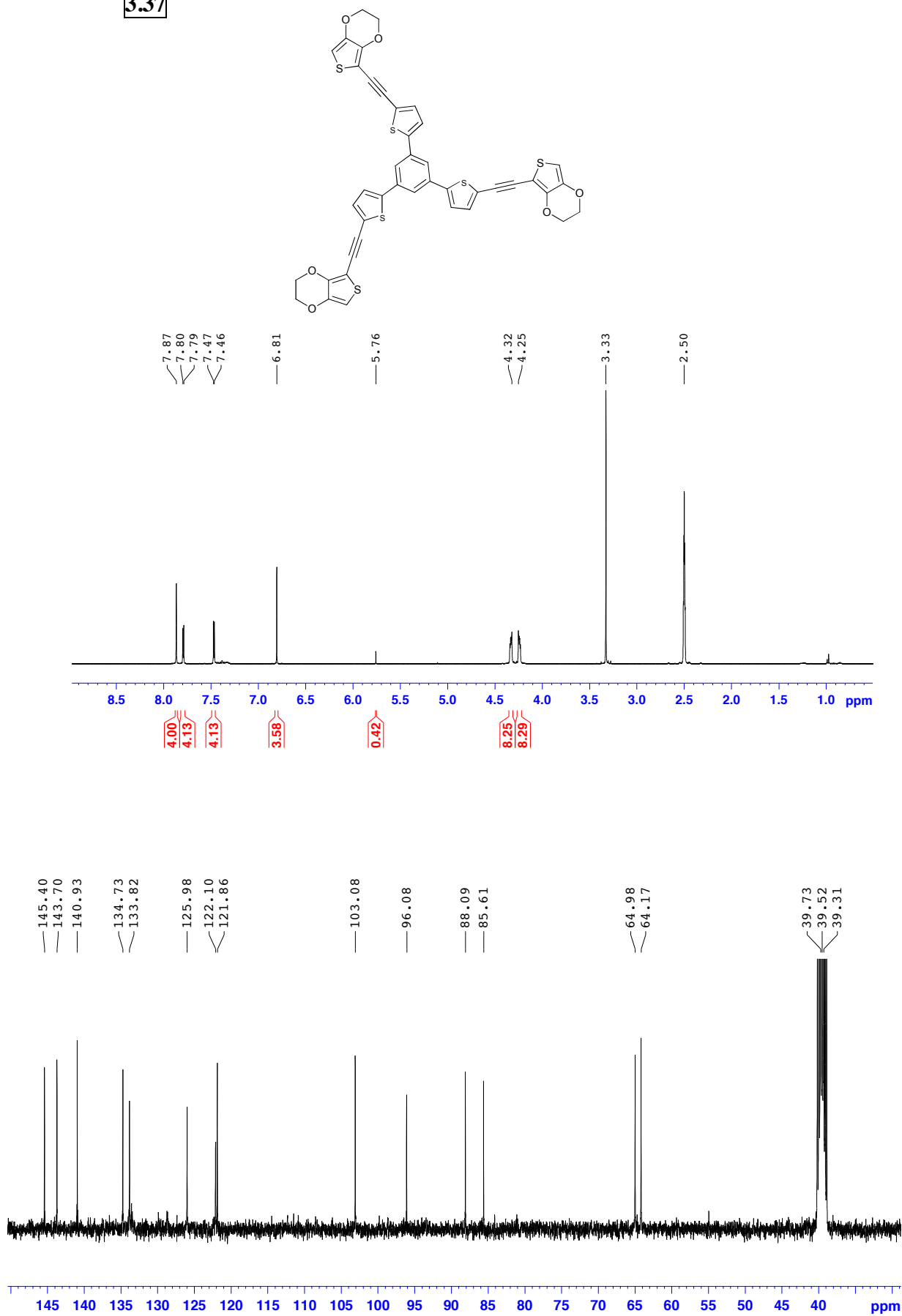
3.22

3.23

3.30

3.32

3.37



7 REFERENCES

1. N. R. Armstrong, W. Wang, D. M. Alloway, D. Placencia, E. Ratcliff and M. Brumbach, *Macromol. Rapid Commun.*, **2009**, *30*, 717.
2. I. Botiz and S. B. Darling, *Mater. Today*, **2010**, *13*, 42.
3. C. J. Brabec, S. Gowrisanker, J. J. M. Halls, D. Laird, S. Jia and S. P. Williams, *Adv. Mater.*, **2010**, *22*, 3839.
4. J.-T. Chen and C.-S. Hsu, *Polym. Chem.*, **2011**, *2*, 2707.
5. W. Wu, Y. Liu and D. Zhu, *Chem. Soc. Rev.*, **2010**, *39*, 1489.
6. T. Someya, A. Dodabalapur, J. Huang, K. C. See and H. E. Katz, *Adv. Mater.*, **2010**, *22*, 3799.
7. A. Rockett, *The Materials Science of Semiconductors*, Springer Science+Business Media, LLC, New York, **2008**.
8. V. Coropceanu, J. Cornil, D. A. da Silva Filho, Y. Olivier, R. Silbey and J.-L. Brédas, *Chem. Rev.*, **2007**, *107*, 926.
9. A. R. Murphy and J. M. J. Fréchet, *Chem. Rev.*, **2007**, *107*, 1066.
10. Y. Shirota and H. Kageyama, *Chem. Rev.*, **2007**, *107*, 953.
11. J.-i. Yamada, H. Akutsu, H. Nishikawa and K. Kikuchi, *Chem. Rev.*, **2004**, *104*, 5057.
12. M. Turbiez, P. Frère, M. Allain, C. Videlot, J. Ackermann and J. Roncali, *Chem. Eur. J.*, **2005**, *11*, 3742.
13. P. Atkins and J. d. Paula, *Atkins Physical Chemistry*, Oxford University Press, Oxford, **2006**.
14. L. E. Smart and E. A. Moore, *Solid state chemistry*, 2nd edn., CRC Press Taylor & Francis Group, Boca Ranton, **2005**.
15. M. R. Bryce, *Chem. Soc. Rev.*, **1991**, *20*, 355.
16. A. J. Bard and L. R. Faulkner, *Electrochemical Methodes: Fundamentals and Applications*, JOHN WILEY & SONS, INC., Hamilton, **2001**.
17. W. Barford, *Electronic and optical properties of conjugated polymers: International Series of Monographs on Physics No. 129*, Oxford University Press, GB, **2005**.
18. M. S. Freund and B. Deore, *Self-doped conducting polymers*, John Wiley & Sons Ltd, GB, **2007**.
19. Y. Liu, Y. Liu and X. Zhan, *Macromol. Chem. Phys.*, **2011**, *212*, 428.
20. X. Zhao and X. Zhan, *Chem. Soc. Rev.*, **2011**, *40*, 3728.
21. J. Roncali, *Chem. Rev.*, **1992**, *92*, 711.
22. L.-H. Xie, C.-R. Yin, W.-Y. Lai, Q.-L. Fan and W. Huang, *Prog. Polym. Sci.*, **2012**, *37*, 1192.
23. C. G. Zoski, *Handbook of electrochemistry*, Elsevier, New Mexico, USA, **2007**.
24. F. A. Settle, *Handbook of Instrumental Techniques for Analytical Chemistry*, Prentice Hall PTR (ECS Professional), Arlington, Virginia, **1997**.
25. G. Gritzner and J. Kuta, *Pure Appl. Chem.*, **1984**, *56*, 461.
26. J. Heinze, *Angew. Chem. Int. Ed.*, **1984**, *23*, 831.
27. C. H. Hamann, A. Hamnett and M. Vielstich, *Electrochemistry* Second edn., WILEY-VCH, **2007**.
28. R. J. Waltman and J. Bargon, *Tetrahedron*, **1984**, *40*, 3963.
29. R. J. Waltman and J. Bargon, *Can. J. Chem.*, **1986**, *64*, 76.
30. M. A. d. V. M. Romero, R. del Río, F. R. Díaz, F. Armijo, *Int. J. Electrochem. Sci.*, **2012**, *7*, 10132

31. K. Teshima, K. Yamada, N. Kobayashi and R. Hirohashi, *J. Electroanal. Chem.*, **1997**, 426, 97.
32. R. G. Nuzzo and D. L. Allara, *J. Am. Chem. Soc.*, **1983**, 105, 4481.
33. P. Klouda, *Moderní analytické metody*, Second edn., Pavel Klouda, Ostrava, Czech Republic, **2003**.
34. G. Tranter, J. Holmes and J. Lindon, *Encyclopedia of Spectroscopy and Spectrometry*, Elsevier, London, UK, **2000**.
35. D. H. Williams and I. Fleming, *Spectroscopic Methods in Organic Chemistry*, Fifth edn., McGraw-Hill, **1995**.
36. J. Roncali, *Chem. Rev.*, **1997**, 97, 173.
37. L. Groenendaal, F. Jonas, D. Freitag, H. Pielartzik and J. R. Reynolds, *Adv. Mater.*, **2000**, 12, 481.
38. A. Hulanicki, S. Geab and F. Ingman, *Pure Appl. Chem.*, **1991**, 63, 1247.
39. B. Adhikari and S. Majumdar, *Prog. Polym. Sci.*, **2004**, 29, 699.
40. J. Janata and A. Bezegh, *Anal. Chem.*, **1988**, 60, 62R.
41. G. F. Fine, L. M. Cavanagh, A. Afonja and R. Binions, *Sensors*, **2010**, 10, 5469.
42. N. Yamazoe, J. Hisamoto, N. Miura and S. Kuwata, *Sens. Actuators*, **1987**, 12, 415.
43. J. Janata and M. Josowicz, *Nat Mater*, **2003**, 2, 19.
44. X. Liu, Y. Xu and D. Jiang, *J. Am. Chem. Soc.*, **2012**, 134, 8738.
45. M. C. Lonergan, E. J. Severin, B. J. Doleman, S. A. Beaber, R. H. Grubbs and N. S. Lewis, *Chem. Mater.*, **1996**, 8, 2298.
46. T. E. Mlsna, S. Cemalovic, M. Warburton, S. T. Hobson, D. A. Mlsna and S. V. Patel, *Sens. Actuators, B*, **2006**, 116, 192.
47. S. V. Patel, T. E. Mlsna, B. Fruhberger, E. Klaassen, S. Cemalovic and D. R. Baselt, *Sens. Actuators, B*, **2003**, 96, 541.
48. F. M. Battiston, J. P. Ramseyer, H. P. Lang, M. K. Baller, C. Gerber, J. K. Gimzewski, E. Meyer and H. J. Güntherodt, *Sens. Actuators, B*, **2001**, 77, 122.
49. A. Hierlemann, D. Lange, C. Hagleitner, N. Kerness, A. Koll, O. Brand and H. Baltes, *Sens. Actuators, B*, **2000**, 70, 2.
50. F. I. Bohrer, E. Covington, C. a. Kurdak and E. T. Zellers, *Anal. Chem.*, **2011**, 83, 3687.
51. R. E. Shaffer, S. L. Rose-Pehrsson and R. A. McGill, *Anal. Chim. Acta*, **1999**, 384, 305.
52. A. Bermak, S. B. Belhouari, M. Shi and D. Martinez, *Encyclopedia of Sensors*, American Scientific Publishers, Pennsylvania, USA, **2006**.
53. H. Bai and G. Shi, *Sensors*, **2007**, 7, 267.
54. R. A. Potyrailo, C. Surman, N. Nagraj and A. Burns, *Chem. Rev.*, **2011**, 111, 7315.
55. C. Ge, N. R. Armstrong and S. S. Saavedra, *Anal. Chem.*, **2007**, 79, 1401.
56. S. de Marcos and O. S. Wolfbeis, *Anal. Chim. Acta*, **1996**, 334, 149.
57. L. Zhang, M. E. Langmuir, M. Bai and W. Rudolf Seitz, *Talanta*, **1997**, 44, 1691.
58. B. R. Panda and A. Chattopadhyay, *J. Colloid Interface Sci.*, **2007**, 316, 962.
59. K. Kim and H. Minamitani, *Opt. Rev.*, **2000**, 7, 152.
60. F. Li and A. Stein, *Chem. Mater.*, **2010**, 22, 3790.
61. J. Bobacka, *Electroanal.*, **2006**, 18, 7.
62. Z. Chen and C. Lu, *Sens. Lett.*, **2005**, 3, 274.
63. L. Li, F. Vilela, J. Forgie, P. J. Skabara and D. Uttamchandani, *Micro & Nano Letters, IET*, **2009**, 4, 84.
64. H. Supriyatno, K. Nakagawa and Y. Sadaoka, *Sens. Actuators, B*, **2001**, 76, 36.
65. F. Mizutani, S. Yabuki, T. Sawaguchi, Y. Hirata, Y. Sato and S. Iijima, *Sens. Actuators, B*, **2001**, 76, 489.
66. G. Shi, M. Luo, J. Xue, Y. Xian, L. Jin and J.-Y. Jin, *Talanta*, **2001**, 55, 241.

67. W. H. Christensen, D. N. Sinha and S. F. Agnew, *Sens. Actuators, B*, **1993**, *10*, 149.
68. A. Ciszewski and G. Milczarek, *Talanta*, **2003**, *61*, 11.
69. T. Lang, T. Hirsch, C. Fenzl, F. Brandl and O. S. Wolfbeis, *Anal. Chem.*, **2012**, *84*, 9085.
70. J. M. Slater and E. J. Watt, *Analyst*, **1991**, *116*, 1125.
71. C. K. Chiang, Y. W. Park, A. J. Heeger, H. Shirakawa, E. J. Louis and A. G. MacDiarmid, *J. Chem. Phys.*, **1978**, *69*, 5098.
72. A. MacLean, C. Moran, W. Johnstone, B. Culshaw, D. Marsh and P. Parker, *Sens. Actuators, A*, **2003**, *109*, 60.
73. B.-S. Joo, J.-S. Huh and D.-D. Lee, *Sens. Actuators, B*, **2007**, *121*, 47.
74. T. A. Betts, C. A. Tipple, M. J. Sepaniak and P. G. Datskos, *Anal. Chim. Acta*, **2000**, *422*, 89.
75. E. T. Zellers and M. Han, *Anal. Chem.*, **1996**, *68*, 2409.
76. S. Miwa and T. Arakawa, *Thin Solid Films*, **1996**, *281–282*, 466.
77. F. Chu, L. Ye, J. Yang and J. Wang, *Opt. Commun.*, **2012**, *285*, 1171.
78. S. T. McGovern, G. M. Spinks and G. G. Wallace, *Sens. Actuators, B*, **2005**, *107*, 657.
79. K. Norrman, A. Ghanbari-Siahkali and N. B. Larsen, *Annual Reports Section "C" (Physical Chemistry)*, **2005**, *101*, 174.
80. K. Holmberg, D. O. Shah and M. J. Schwuger, *Handbook of applied surface and colloid chemistry*, Wiley, **2002**.
81. N. E. Agbor, M. C. Petty and A. P. Monkman, *Sens. Actuators, B*, **1995**, *28*, 173.
82. D. Li, Y. Jiang, Z. Wu, X. Chen and Y. Li, *Sens. Actuators, B*, **2000**, *66*, 125.
83. R. Nohria, R. K. Khillan, Y. Su, R. Dikshit, Y. Lvov and K. Varahramyan, *Sens. Actuators, B*, **2006**, *114*, 218.
84. J. H. Park and T. S. Sudarshan, *Chemical Vapor Deposition (Surface Engineering Series, Vol. 2)*, Asm International, **2000**.
85. E. Tekin, P. J. Smith and U. S. Schubert, *Soft Matter*, **2008**, *4*, 703.
86. W. Storr, www.Electronics-Tutorials.ws.
87. I. S. Board, *IEEE Std 211-1997*, **1998**, i.
88. J. Bird, *Electrical and electronic principles and technology*, 4th edn., Elsevier, Oxford, UK, **2010**.
89. Z. Zou, J. Kai, M. J. Rust, J. Han and C. H. Ahn, *Sens. Actuators, A*, **2007**, *136*, 518.
90. D. L. McCorkle, R. J. Warmack, S. V. Patel, T. Mlsna, S. R. Hunter and T. L. Ferrell, *Sens. Actuators, B*, **2005**, *107*, 892.
91. R. Blue, Z. Vobecka, P. J. Skabara and D. Uttamchandani, *Sens. Actuators, B*, **2013**, *176*, 534.
92. A. S. Abu-Abed and R. S. Lindquist, *Prog. Electromagn. Res.*, **2008**, *7*, 75.
93. S. Cosnier and A. Karyakin, *Electropolymerization: Concepts, Materials and Applications*, Wiley, Weinheim, Germany, **2010**.
94. Z. Vobecka, R. Blue, F. Vilela, P. J. Skabara and D. Uttamchandani, *Micro & Nano Letters, IET*, **2012**, *7*, 962.
95. B. J. Holliday, T. B. Stanford and T. M. Swager, *Chem. Mater.*, **2006**, *18*, 5649.
96. A. Kros, R. J. M. Nolte and N. A. J. M. Sommerdijk, *J. Polym. Sci., Part A: Polym. Chem.*, **2002**, *40*, 738.
97. Q. Hao, X. Wang, L. Lu, X. Yang and V. M. Mirsky, *Macromol. Rapid Commun.*, **2005**, *26*, 1099.
98. P. N. Bartlett and S. K. Ling-Chung, *Sens. Actuators*, **1989**, *20*, 287.
99. A. L. Kukla, A. S. Pavluchenko, Y. M. Shirshov, N. V. Konoshchuk and O. Y. Posudievsky, *Sens. Actuators, B*, **2009**, *135*, 541.

100. A. Guadarrama, M. L. Rodríguez-Méndez and J. A. de Saja, *Sens. Actuators, B*, **2004**, *100*, 60.
101. J. Akhavan, *Chemistry of explosives*, 2nd edn., The Royal Society of Chemistry, Cornwall, **2004**.
102. S. Singh, *J. Hazard. Mater.*, **2007**, *144*, 15.
103. S. J. Toal and W. C. Trogler, *J. Mater. Chem.*, **2006**, *16*, 2871.
104. J. Wang, *Electroanal.*, **2007**, *19*, 415.
105. L. Senesac and T. G. Thundat, *Mater. Today*, **2008**, *11*, 28.
106. W. D. Won, L. H. DiSalvo and J. Ng, *Appl. Environ. Microb.*, **1976**, *31*, 576.
107. M. E. Germain and M. J. Knapp, *Chem. Soc. Rev.*, **2009**, *38*, 2543.
108. J. S. Caygill, F. Davis and S. P. J. Higson, *Talanta*, **2012**, *88*, 14.
109. J. Weber and A. Thomas, *J. Am. Chem. Soc.*, **2008**, *130*, 6334.
110. R. J. Harper, J. R. Almirall and K. G. Furton, *Talanta*, **2005**, *67*, 313.
111. S. Singh, *J. Hazard. Mater.*, **2007**, *144*, 15.
112. S. W. Thomas, G. D. Joly and T. M. Swager, *Chem. Rev.*, **2007**, *107*, 1339.
113. A. T. Nimal, U. Mittal, M. Singh, M. Khaneja, G. K. Kannan, J. C. Kapoor, V. Dubey, P. K. Gutch, G. Lal, K. D. Vyas and D. C. Gupta, *Sens. Actuators, B*, **2009**, *135*, 399.
114. F. G. Bosco, M. Bache, E. T. Hwu, C. H. Chen, S. S. Andersen, K. A. Nielsen, S. S. Keller, J. O. Jeppesen, I. S. Hwang and A. Boisen, *Sens. Actuators, B*, **2012**, *171–172*, 1054.
115. E. J. Houser, T. E. Mlsna, V. K. Nguyen, R. Chung, R. L. Mowery and R. Andrew McGill, *Talanta*, **2001**, *54*, 469.
116. L. A. Pinnaduwege, V. Boiadjev, J. E. Hawk and T. Thundat, *Appl. Phys. Lett.*, **2003**, *83*, 1471.
117. L. A. Pinnaduwege, A. Wig, D. L. Hedden, A. Gehl, D. Yi, T. Thundat and R. T. Lareau, *J. Appl. Phys.*, **2004**, *95*, 5871.
118. U. Willer and W. Schade, *Anal. Bioanal. Chem.*, **2009**, *395*, 275.
119. A. Díaz Aguilar, E. S. Forzani, M. Leright, F. Tsow, A. Cagan, R. A. Iglesias, L. A. Nagahara, I. Amlani, R. Tsui and N. J. Tao, *Nano Lett.*, **2009**, *10*, 380.
120. G. Bunte, J. Hürttlen, H. Pontius, K. Hartlieb and H. Krause, *Anal. Chim. Acta*, **2007**, *591*, 49.
121. K. Bratin, P. T. Kissinger, R. C. Briner and C. S. Bruntlett, *Anal. Chim. Acta*, **1981**, *130*, 295.
122. D. Lu, A. Cagan, R. A. A. Munoz, T. Tangkuaram and J. Wang, *Analyst*, **2006**, *131*, 1279.
123. J. Wang, R. K. Bhada, J. Lu and D. MacDonald, *Anal. Chim. Acta*, **1998**, *361*, 85.
124. J. Wang, S. Thongngamdee and A. Kumar, *Electroanal.*, **2004**, *16*, 1232.
125. K. S. W. Sing, D. H. Everett, R. A. W. Haul, L. Moscou, R. A. Pierotti, J. Rouquerol and T. Siemieniowska, *Pure Appl. Chem.*, **1985**, *57*, 603.
126. D. Wu, F. Xu, B. Sun, R. Fu, H. He and K. Matyjaszewski, *Chem. Rev.*, **2012**, *112*, 3959.
127. J.-X. Jiang, A. Laybourn, R. Clowes, Y. Z. Khimyak, J. Bacsá, S. J. Higgins, D. J. Adams and A. I. Cooper, *Macromolecules*, **2010**, *43*, 7577.
128. S. Yuan, S. Kirklin, B. Dorney, D.-J. Liu and L. Yu, *Macromolecules*, **2009**, *42*, 1554.
129. J.-X. Jiang, F. Su, A. Trewin, C. D. Wood, H. Niu, J. T. A. Jones, Y. Z. Khimyak and A. I. Cooper, *J. Am. Chem. Soc.*, **2008**, *130*, 7710.
130. T. Ben, H. Ren, S. Ma, D. Cao, J. Lan, X. Jing, W. Wang, J. Xu, F. Deng, J. M. Simmons, S. Qiu and G. Zhu, *Angew. Chem.*, **2009**, *121*, 9621.
131. M. P. Tsyurupa and V. A. Davankov, *React. Funct. Polym.*, **2006**, *66*, 768.

132. X. Liu and A. Basu, *J. Am. Chem. Soc.*, **2009**, *131*, 5718.
133. A. R. Millward and O. M. Yaghi, *J. Am. Chem. Soc.*, **2005**, *127*, 17998.
134. P. Kuhn, M. Antonietti and A. Thomas, *Angew. Chem. Int. Ed.*, **2008**, *47*, 3450.
135. A. I. Cooper, *Adv. Mater.*, **2009**, *21*, 1291.
136. R. Dawson, A. I. Cooper and D. J. Adams, *Prog. Polym. Sci.*, **2012**, *37*, 530.
137. S. Yuan, B. Dorney, D. White, S. Kirklin, P. Zapol, L. Yu and D.-J. Liu, *Chem. Commun.*, **2010**, *46*, 4547.
138. C. Zhao, E. Danish, N. R. Cameron and R. Katakya, *J. Mater. Chem.*, **2007**, *17*, 2446.
139. M. S. Silverstein, H. Tai, A. Sergienko, Y. Lumelsky and S. Pavlovsky, *Polymer*, **2005**, *46*, 6682.
140. Z. Wang, S. Yuan, A. Mason, B. Repogle, D.-J. Liu and L. Yu, *Macromolecules*, **2012**, *45*, 7413.
141. G. E. Pollock, D. O'Hara and O. L. Hollis, *J Chromatogr Sci*, **1984**, *22*, 343.
142. Y.-L. Zhang, S. Liu, S. Liu, F. Liu, H. Zhang, Y. He and F.-S. Xiao, *Catal. Commun.*, **2011**, *12*, 1212.
143. F. Vilela, K. Zhang and M. Antonietti, *Energy Environ.Sci.*, **2012**, *5*, 7819.
144. X. Yang, L. Chen, B. Huang, F. Bai and X. Yang, *Polymer*, **2009**, *50*, 3556.
145. M. R. Abidian, D. H. Kim and D. C. Martin, *Adv. Mater.*, **2006**, *18*, 405.
146. F. Schacher, M. Ulbricht and A. H. E. Müller, *Adv. Funct. Mater.*, **2009**, *19*, 1040.
147. X. Wang, S. M. Husson, X. Qian and S. R. Wickramasinghe, *J. Membr. Sci.*, **2010**, *365*, 302.
148. A. B. Fuertes, M. Sevilla, S. Alvarez and T. Valdes-Solís, *Microporous Mesoporous Mater.*, **2008**, *112*, 319.
149. C. Pevida, C. E. Snape and T. C. Drage, *Energy Procedia*, **2009**, *1*, 869.
150. D. Kowalski and P. Schmuki, *Chem. Commun.*, **2010**, *46*, 8585.
151. Y. Wan, Y. Shi and D. Zhao, *Chem. Mater.*, **2007**, *20*, 932.
152. D. A. Olson, L. Chen and M. A. Hillmyer, *Chem. Mater.*, **2007**, *20*, 869.
153. B. D. Reeves, B. C. Thompson, K. A. Abboud, B. E. Smart and J. R. Reynolds, *Adv. Mater.*, **2002**, *14*, 717.
154. J. Schmidt, J. Weber, J. D. Epping, M. Antonietti and A. Thomas, *Adv. Mater.*, **2009**, *21*, 702.
155. K. Severin, *Dalton Trans.*, **2009**, *0*, 5254.
156. A. P. Côté, A. I. Benin, N. W. Ockwig, M. O'Keeffe, A. J. Matzger and O. M. Yaghi, *Science*, **2005**, *310*, 1166.
157. H. M. El-Kaderi, J. R. Hunt, J. L. Mendoza-Cortés, A. P. Côté, R. E. Taylor, M. O'Keeffe and O. M. Yaghi, *Science*, **2007**, *316*, 268.
158. N. B. McKeown, S. Makhseed and P. M. Budd, *Chem. Commun.*, **2002**, *0*, 2780.
159. N. B. McKeown, S. Hanif, K. Msayib, C. E. Tattershall and P. M. Budd, *Chem. Commun.*, **2002**, *0*, 2782.
160. P. M. Budd, E. S. Elabas, B. S. Ghanem, S. Makhseed, N. B. McKeown, K. J. Msayib, C. E. Tattershall and D. Wang, *Adv. Mater.*, **2004**, *16*, 456.
161. B. S. Ghanem, M. Hashem, K. D. M. Harris, K. J. Msayib, M. Xu, P. M. Budd, N. Chaukura, D. Book, S. Tedds, A. Walton and N. B. McKeown, *Macromolecules*, **2010**, *43*, 5287.
162. J.-H. Ahn, J.-E. Jang, C.-G. Oh, S.-K. Ihm, J. Cortez and D. C. Sherrington, *Macromolecules*, **2005**, *39*, 627.
163. J.-X. Jiang, F. Su, A. Trewin, C. D. Wood, N. L. Campbell, H. Niu, C. Dickinson, A. Y. Ganin, M. J. Rosseinsky, Y. Z. Khimyak and A. I. Cooper, *Angew. Chem. Int. Ed.*, **2007**, *46*, 8574.

164. R. Dawson, A. Laybourn, R. Clowes, Y. Z. Khimyak, D. J. Adams and A. I. Cooper, *Macromolecules*, **2009**, *42*, 8809.
165. R. Dawson, A. Laybourn, Y. Z. Khimyak, D. J. Adams and A. I. Cooper, *Macromolecules*, **2010**, *43*, 8524.
166. J. Brandt, J. Schmidt, A. Thomas, J. D. Epping and J. Weber, *Polym. Chem.*, **2011**, *2*, 1950.
167. J. Schmidt, M. Werner and A. Thomas, *Macromolecules*, **2009**, *42*, 4426.
168. H. Ren, T. Ben, F. Sun, M. Guo, X. Jing, H. Ma, K. Cai, S. Qiu and G. Zhu, *J. Mater. Chem.*, **2011**, *21*, 10348.
169. T. Ben, H. Ren, S. Ma, D. Cao, J. Lan, X. Jing, W. Wang, J. Xu, F. Deng, J. M. Simmons, S. Qiu and G. Zhu, *Angew. Chem. Int. Ed.*, **2009**, *48*, 9457.
170. D. Yuan, W. Lu, D. Zhao and H.-C. Zhou, *Adv. Mater.*, **2011**, *23*, 3723.
171. J. M. Oyarzum, *Pigment processing: Physico-Chemical Principles*, Druckerei Hubert & Co., Hannover, Germany, **2000**.
172. R. Aveyard and D. A. Haydon, *An introduction to the principles of surface chemistry*, Cambridge University Press, London, **1973**.
173. S. J. Gregg and K. S. W. Sing, *Adsorption, surface area and porosity*, Academic Press Inc. (London) Ltd, London, New York, **1967**.
174. S. Brunauer, P. H. Emmett and E. Teller, *J. Am. Chem. Soc.*, **1938**, *60*, 309.
175. S. Lowell and J. E. Shield, *Powder Surface Area and Porosity*, 3rd edn., Chapman and Hall Ltd, London, **1991**.
176. N. A. Lange and J. A. Dean, *Lange's handbook of chemistry* 14th edn., McGraw-Hill New York, **1992**.
177. J. Roncali, P. Blanchard and P. Frere, *J. Mater. Chem.*, **2005**, *15*, 1589.
178. H. J. Spencer, P. J. Skabara, M. Giles, I. McCulloch, S. J. Coles and M. B. Hursthouse, *J. Mater. Chem.*, **2005**, *15*, 4783.
179. H. J. Lee, J. Lee and S.-M. Park, *J. Phys. Chem. B*, **2010**, *114*, 2660.
180. G. Zotti, S. Zecchin, G. Schiavon, F. Louwet, L. Groenendaal, X. Crispin, W. Osikowicz, W. Salaneck and M. Fahlman, *Macromolecules*, **2003**, *36*, 3337.
181. J. C. Forgie, P. J. Skabara, I. Stibor, F. Vilela and Z. Vobecká, *Chem. Mater.*, **2009**, *21*, 1784.
182. B. Somboonsub, S. Srisuwan, M. A. Invernale, S. Thongyai, P. Praserttham, D. A. Scola and G. A. Sotzing, *Polymer*, **2010**, *51*, 4472.
183. M. Dietrich, J. Heinze, G. Heywang and F. Jonas, *J. Electroanal. Chem.*, **1994**, *369*, 87.
184. S.-C. Shiu, J.-J. Chao, S.-C. Hung, C.-L. Yeh and C.-F. Lin, *Chem. Mater.*, **2010**, *22*, 3108.
185. H. W. Heuer, R. Wehrmann and S. Kirchmeyer, *Adv. Funct. Mater.*, **2002**, *12*, 89.
186. F. H. Allen, J. P. M. Lommerse, V. J. Hoy, J. A. K. Howard and G. R. Desiraju, *Acta Cryst. B*, **1997**, *53*, 1006.
187. F. H. Allen, B. S. Goud, V. J. Hoy, J. A. K. Howard and G. R. Desiraju, *J. Chem. Soc., Chem. Commun.*, **1994**, 2729.
188. J. M. A. Robinson, D. Philp, K. D. M. Harris and B. M. Kariuki, *New J. Chem.*, **2000**, *24*, 799.
189. A. Kumar, D. M. Welsh, M. C. Morvant, F. Piroux, K. A. Abboud and J. R. Reynolds, *Chem. Mater.*, **1998**, *10*, 896.
190. S. P. Mishra, R. Sahoo, A. V. Ambade, A. Q. Contractor and A. Kumar, *J. Mater. Chem.*, **2004**, *14*, 1896.

191. C. L. Gaupp, D. M. Welsh and J. R. Reynolds, *Macromol. Rapid Commun.*, **2002**, *23*, 885.
192. R. C. Shallcross, G. D. D'Ambruoso, B. D. Korth, H. K. Hall, Z. Zheng, J. Pyun and N. R. Armstrong, *J. Am. Chem. Soc.*, **2007**, *129*, 11310.
193. A. S. Sarac, H.-D. Gilsing, A. Gencturk and B. Schulz, *Prog. Org. Coat.*, **2007**, *60*, 281.
194. D. M. Welsh, A. Kumar, E. W. Meijer and J. R. Reynolds, *Adv. Mater.*, **1999**, *11*, 1379.
195. E. Ertas and T. Ozturk, *Tetrahedron Lett.*, **2004**, *45*, 3405.
196. F. Goldoni, B. M. W. Langeveld-Voss and E. W. Meijer, *Synth. Commun.*, **1998**, *28*, 2237.
197. C. E. Katz and J. Aubé, *J. Am. Chem. Soc.*, **2003**, *125*, 13948.
198. A. Klapars and S. L. Buchwald, *J. Am. Chem. Soc.*, **2002**, *124*, 14844.
199. A. Ranganathan, B. C. Heisen, I. Dix and F. Meyer, *Chem. Commun.*, **2007**, 3637.
200. C. Pozo-Gonzalo, T. Khan, J. J. W. McDouall, P. J. Skabara, D. M. Roberts, M. E. Light, S. J. Coles, M. B. Hursthouse, H. Neugebauer, A. Cravino and N. S. Sariciftci, *J. Mater. Chem.*, **2002**, *12*, 500.
201. F. S. Guziec, J. M. Russo, F. F. Torres, G. C. Long and M. R. Tellez, *J. Chem. Soc., Perkin Trans. 1*, **1989**, 1068.
202. P. J. Skabara, I. M. Serebryakov, D. M. Roberts, I. F. Perepichka, S. J. Coles and M. B. Hursthouse, *J. Org. Chem.*, **1999**, *64*, 6418.
203. D. Mackay, W. Y. Shiu, K.-C. Ma and S. C. Lee, *Physical-Chemical Properties and Environmental Fate for Organic Chemicals*, 2nd edn., CRC Press, Taylor & Francis Group, Boca Raton, Florida, **2006**.
204. S. Yun and J. Kim, *Sens. Actuators, B*, **2010**, *150*, 308.
205. S. D. Hersee and J. M. Ballingall, *J. Vac. Sci. Technol. A*, **1990**, *8*, 800.
206. Y. S. Kim, S.-C. Ha, H. Yang and Y. T. Kim, *Sens. Actuators, B*, **2007**, *122*, 211.
207. S. J. Lue, W. W. Chen, S. Y. Wu, L. D. Wang and C. H. Kuo, *J. Membr. Sci.*, **2008**, *311*, 380.
208. W. R. Vieth, *Diffusion in and through polymers, principles and applications*, Carl Hanser Verlag, Oxford University Press, Munich, Vienna, New York, Barcelona, **1991**.
209. H. Pang, P. J. Skabara, D. J. Crouch, W. Duffy, M. Heeney, I. McCulloch, S. J. Coles, P. N. Horton and M. B. Hursthouse, *Macromolecules*, **2007**, *40*, 6585.
210. J. J. Apperloo, L. B. Groenendaal, H. Verheyen, M. Jayakannan, R. A. J. Janssen, A. Dkhissi, D. Beljonne, R. Lazzaroni and J.-L. Brédas, *Chem. Eur. J.*, **2002**, *8*, 2384.
211. J. P. Brand and J. Waser, *Angew. Chem. Int. Ed.*, **2010**, *49*, 7304.
212. J.-X. Jiang, A. Trewin, F. Su, C. D. Wood, H. Niu, J. T. A. Jones, Y. Z. Khimyak and A. I. Cooper, *Macromolecules*, **2009**, *42*, 2658.
213. O. Plietzsch, C. I. Schilling, M. Tolev, M. Nieger, C. Richert, T. Muller and S. Brase, *Org. Biomol. Chem.*, **2009**, *7*, 4734.
214. I. Aujard, J.-P. Baltaze, J.-B. Baudin, E. Cogné, F. Ferrage, L. Jullien, É. Perez, V. Prévost, L. M. Qian and O. Ruel, *J. Am. Chem. Soc.*, **2001**, *123*, 8177.
215. Y. Zhao, J. Li, C. Li, K. Yin, D. Ye and X. Jia, *Green Chem.*, **2010**, *12*, 1370.
216. R. Chinchilla and C. Nájera, *Chem. Rev.*, **2007**, *107*, 874.
217. F. Cherioux and L. Guyard, *Adv. Funct. Mater.*, **2001**, *11*, 305.
218. M. Hemgesberg, D. M. Ohlmann, Y. Schmitt, M. R. Wolfe, M. K. Müller, B. Erb, Y. Sun, L. J. Gooßen, M. Gerhards and W. R. Thiel, *Eur. J. Org. Chem.*, **2012**, *2012*, 2142.

219. M. R. Andersson, D. Selse, M. Berggren, H. Jaervinen, T. Hjertberg, O. Inganaes, O. Wennerstroem and J. E. Oesterholm, *Macromolecules*, **1994**, *27*, 6503.
220. M. S. A. Abdou, X. Lu, Z. W. Xie, F. Orfino, M. J. Deen and S. Holdcroft, *Chem. Mater.*, **1995**, *7*, 631.
221. T. Cai, Y. Zhou, E. Wang, S. Hellström, F. Zhang, S. Xu, O. Inganäs and M. R. Andersson, *Sol. Energy Mater. Sol. Cells*, **2010**, *94*, 1275.
222. G. Koßmehl and G. Chatzitheodorou, *Macromol. Rapid. Commun.*, **1983**, *4*, 639.
223. G. Kossmehl and J. Hocker, *Germany Pat.*, **1986**, 4611032.
224. M. B. Zaman and D. F. Perepichka, *Chem. Commun.*, **2005**, 4187.
225. E. Bosch and J. K. Kochi, *J. Org. Chem.*, **1994**, *59*, 5573.
226. A. Vaitiekunas and F. F. Nord, *J. Am. Chem. Soc.*, **1953**, *75*, 1764.
227. N. Ríos-Lombardía, E. Busto, V. Gotor-Fernández and V. Gotor, *Eur. J. Org. Chem.*, **2010**, *2010*, 484.
228. C. Poriel, Y. Ferrand, S. Juillard, P. Le Maux and G. Simonneaux, *Tetrahedron*, **2004**, *60*, 145.
229. R. Wu, J. S. Schumm, D. L. Pearson and J. M. Tour, *J. Org. Chem.*, **1996**, *61*, 6906.
230. D. H. Hey, J. A. Leonard and C. W. Rees, *J. Chem. Soc.*, **1963**, 3125.
231. W.-F. Jiang, *Synth. Commun.*, **2008**, *38*, 1888.
232. M. C. C. Ng, D. J. Craig, J. B. Harper, L. van-Eijck and J. A. Stride, *Chem. Eur. J.*, **2009**, *15*, 6569.
233. S. Kotha, D. Kashinath, K. Lahiri and Raghavan B. Sunoj, *Eur. J. Org. Chem.*, **2004**, *2004*, 4003.
234. O. P. Varnavski, J. C. Ostrowski, L. Sukhomlinova, R. J. Twieg, G. C. Bazan and T. Goodson, *J. Am. Chem. Soc.*, **2002**, *124*, 1736.
235. N. Niamnont, W. Siripornnoppakhun, P. Rashatasakhon and M. Sukwattanasinitt, *Org. Lett.*, **2009**, *11*, 2768.
236. E. Campaigne and J. L. Diedrich, *J. Am. Chem. Soc.*, **1951**, *73*, 5240.